Johannes Peterleithner, Dipl.-Ing.

Interferometric Vibrometry for Combustion Dynamics

DISSERTATION

zur Erlangung des akademischen Grades

Doktor der technischen Wissenschaften

eingereicht an der

Technischen Universität Graz

Betreuer und erster Gutachter:

Jakob Woisetschläger, ao.Univ.-Prof. Dipl.-Ing. Dr.techn.

Institute for Thermal Turbomachinery and Machine Dynamics

zweiter Gutachter

Giuliani, Fabrice, Dipl.-Ing. Dr.techn. Priv.-Doz.

Graz, Mai 2016

Gefördert durch den FWF, Projekt P24096-N24

The reasonable man adapts himself to the world;

the unreasonable one persists in trying to adapt the world to himself.

Therefore all progress depends on the unreasonable man.

George Bernard Shaw

EIDESSTATTLICHE ERKLÄRUNG

Ich erkläre an Eides statt, dass ich die vorliegende Arbeit selbstständig verfasst, andere als die angegebenen Quellen/Hilfsmittel nicht benutzt, und die den benutzten Quellen wörtlich und inhaltlich entnommenen Stellen als solche kenntlich gemacht habe. Das in TUGRAZonline hochgeladene Textdokument ist mit der vorliegenden Dissertation identisch.

……. …….

Datum Unterschrift

Vorwort

Die vorliegende Arbeit ist am Institut für Thermische Turbomaschinen und Maschinendynamik der Technischen Universität Graz entstanden und wurde durch den FWF im Rahmen des Projektes P 24096-N24 - Interferometric Detection of Thermoacoustic Oscillations in Flames – finanziert.

Für die Unterstützung bedanke ich mich sehr bei meinem Betreuer Ao.Univ.-Prof. Dipl.-Ing. Jakob Woisetschläger, der neben der fachlichen Hilfestellung vor allem als Motivator in schwierigen Stunden, zum Beispiel Freitags um 21:00 Uhr abends mit 'Komm, schalt den Brenner nochmal ein, das müss ma jetzt genau wissen!' behilflich war. Weiters erinnere ich mich an viele gesellschaftspolitische Diskussionen mit Ihm und den einen oder anderen guten Rat für das private Leben. Nur die Assimilation zu einem Trekkie hat nicht geklappt.

Bei Univ.-Prof. Dr.-Ing. Franz Heitmeir bedanke ich mich, der einerseits den wissenschaftlichen Freiraum seiner Mitarbeiter gewährleistete und andererseits die Einrichtung des neuen Thermoakustikmessraumes ermöglichte.

Bei Dipl.-Ing. Dr.techn. Priv.-Doz. Fabrice Giuliani möchte ich mich für die Übernahme der Zweitbegutachtung bedanken.

Prof. Dr. Thomas Sattelmayer hat mir im Rahmen einer Messkampagne einen Einblick in die Arbeit am renommierten Lehrstuhl für Thermodynamik der TU München gewährt. Ausserdem stand mir Prof. Sattelmayer regelmäßig mit fachlicher Hilfestellung zur Seite.

Dipl.-Ing. Nicolai Stadlmair ebenfalls vom Lehrstuhl für Thermodynamik der TU München danke ich für die engagierte Zusammenarbeit.

Bei PD Dr.-Ing. habil. Andreas Fischer und Dipl.-Phys. Raimund Schlüßler der TU Dresden bedanke ich mich für die erfolgreiche Messkampagne.

Bei unserem Akustikexperten Dipl.-Ing. Dr.techn. Andreas Marn bedanke ich mich für die vielen investierten Stunden und anregenden Diskussionen die ausschlaggebend für den Erfolg dieser Arbeit waren.

Weiters möchte ich Riccardo Basso (M.Eng.) und Dipl.-Ing Florian Salcher erwähnen, die im Rahmen ihrer Diplomarbeit viele experimentelle Untersuchungen durchführten und somit eine große Stütze für mich waren.

Vor allem bedanke ich mich bei meiner Verlobten Callie, die mich jederzeit unterstützt hat und großes Verständnis für meine Arbeit zeigte.

Johannes Peterleithner

Wels im. Mai 2016

Kurzfassung

Die westliche Gesellschaft hängt stark von schnellen Transportmitteln wie dem Flugzeug sowie von permanenter Verfügbarkeit von elektrischer Energie ab, deswegen hat die Forschung auf dem Gebiet der Verbrennung in Turbomaschinen einen starken Einfluss auf die Gesellschaft.

Um die heutigen strengen Schadstoffvorschriften die der Gesetzgeber vorschreibt, zu erfüllen, haben Turbomaschinenhersteller die Entwicklung von emissionsarmen Magerverbrennungskonzepten vorangetrieben. Diese Systeme neigen allerdings verstärkt zu Verbrennungsinstabilitäten. Wärmefreisetzungsschwankungen verursachen Schallabstrahlung und im Falle von thermoakustischer Kopplung kann dies zu großen Druckamplituden führen, welche die Integrität des Brenners beeinträchtigen und bis hin zur Zerstörung des gesammten Turbinensatzes führen können. In Flammen kann die schwankende Wärmefreisetzung über eine geeignete Kopplungsbeziehung mit den Dichteschwankungen, genauer mit der zeitlichen Ableitung der Dichteschwankungen in Verbindung gebracht warden.

Das so genannte Laser Vibrometer, ein Interferometer, ursprünglich in der Oberflächenschwingungsdiagnostik angewandt, kann die Zeitableitungen von Dichteschwankungen in Flammen direkt aufzeichnen. Das Ziel dieser Arbeit war die Möglichkeiten und Grenzen dieses Systems in experimentellen Flammen sowie in gasturbinenrelevanten Brennern zu erforschen. Dies ist eine innovative Anwendung in der Verbrennungsdiagnostik, einem Gebiet, wo Techniken zur Messung von Wärmefreisetzung rar sind.

In dieser Arbeit war der Fokus auf der Anwendung des Systems auf vorgemischte turbulente Flammen wie sie in Industrieanwendungen üblich sind. Getestet wurde die Robustheit der Kupplungsbeziehung, die die Dichteschwankungen mit dem Parameter von Interesse verbindet, nämlich der dynamischen Wärmefreisetzungsrate.

In einem zweiten Teil der Arbeit wurde die Möglichkeit untersucht, das akustische Fernfeld mittels messung der Dichteschwankungen in der Flamme vorherzusagen. Die zugrunde liegende Hypothese behauptet, dass aus den lokalen Laser Vibrometer Aufnahmen innerhalb der Verbrennungszone, die akustische Strahlung einer Flamme vorhergesagt werden kann, da Laser Vibrometer quantitativ die erste zeitliche Ableitung von Dichteschwankungen detektieren können. Mit der gleichzeitig experimentellen Aufnahme des akustischen Feldes wurde diese Annahme getestet.

Eine solche quantitative Vorhersage des abgestrahlten Lärmes durch interferometrische Detektion von Fluktuationen innerhalb der Flamme stellt einen innovativen Aspekt für experimentelle Forschung in der Thermoakustik dar.

Abstract

Western society strongly depends on fast transportation such as air traffic and permanent availability of electric energy, thus research in the field of combustion in turbomachinery has a strong impact on society.

In order to meet the stringent pollutant regulations set by governments, low-emission concepts of combustion systems in turbomachinery have been developed. As a drawback, lean combustion systems have a strong tendency towards combustion instabilities. Unsteady heat release will cause sound radiation and in case of thermoacoustic coupling can lead to large amplitudes and compromise the integrity of the combustor leading to engine failure. The unsteady heat release can be related to the density fluctuations in the flame, or to be more precise, to the time derivative of density fluctuations.

The so-called laser vibrometer – an interferometer used in engineering for surface vibration detection – can directly record the time derivatives of density fluctuations in flames. To explore the capabilities and boundaries of this system in experimental flames as well as in engine relevant burners was the goal of this thesis. This is an innovative application in combustion diagnostics, a field where heat release-measurement techniques are scarce.

In this thesis the focus was on the application of the system to turbulent premixed flames, as common in industry applications. Tested was the robustness of the coupling equation which links density fluctuations to the real parameter of interest – the dynamic heat release rate.

Secondly, far-field sound prediction by detection of density fluctuations in the flame was investigated. The underlying hypothesis claims that from the local laser vibrometer recordings in the combustion zone, the acoustic radiation of a flame can be predicted, since laser vibrometers can detect the first time derivative of density fluctuations quantitatively. With the simultaneously, experimentally recorded acoustic power distribution in the far-field of the flame, this assumption can be tested.

Such a quantitative prediction of the radiated noise around the flame by interferometric detection of fluctuations in the flame provides an innovative aspect for experimental thermoacoustic research.

Table of contents

List of Figures

List of Tables

Nomenclature

a	-	general variable
A_{meas}	M^2	measurement area
AOM	-	acousto-optical modulator
c	M/s	speed of sound
CAEP	Hz	Committee on Aviation Environmental Protection
CCPP	Hz	combined cycle power plants
C(f)	Hz	cross power spectrum
CO	-	carbon monoxide
c_p	J/Kg/K	heat capacity at constant pressure
CPS	W	cross power spectrum
CPSD	W/Hz	cross power spectral density
ENBW	Hz	equivalent noise band width
f_B	Hz	frequency of the Bragg cell
f_{meas}	Hz	frequency to measure
f_{Ny}	Hz	Nyquist-frequency
FDF	-	flame describing function
FTF	-	flame transfer function
G	m^3/kg	Gladstone-Dale constant
H	J/kg	enthalpy
HC	-	hydro-carbons
I_{LIV}	W/m^2	intensity at detector
$\vec{I}$	W/m^2	sound Intensity
ICAO	-	International Civil Aviation Organization
Im	-	imaginary part
K	m/s/V	vibrometer calibration constant
LIV	-	laser interferometric vibrometry
MMM	-	multi-microphone-method
MP	-	measurement point
no_{av}	-	number of blocks to average (FFT)
N	-	refractive index
NO	-	nitrogen oxide
P	Pa	pressure
PLL	-	phase lock loop
P(f)	-	power of a signal at a certain frequency range
P_{far}	W	acoustic power in the far field
q_V	J/m^3	volumetric heat release
$\dot{Q}$	W	total heat release rate
$\dot{Q}$	W	total heat release rate
r	m	radial distance
R	J/kg/K	specific gas constant
SARP	-	Standards and Recommended Practices
spls	-	samples
SL	-	sample length
SR	-	sample rate
T	K	temperature
t	S	time
u, v, w	m/s	velocities in coordinate direction
U	V	voltage
UN	-	United Nations
x, y, z	-	cartesian coordinates

Φ_{dis}	W/kg	energy dissipation rate
Δf	Hz	frequency resolution
κ	-	ratio of specific heats
ρ	kg/m³	density
ζ	m	length of laser beam
χ	m/s	speed of light
λ	m	wavelength of light

1 Introduction

Gas turbines have been a major contributor to electricity generation from their first industrial application in 1939 onwards [1]. Today, in combined cycle power plants (CCPP) they reach efficiencies of beyond 60% and emissions for NOX and CO as low as 25 ppm and 10 ppm respectively [2]. Although a mature technology, they find new grounds of application in the environment of solar and wind power, where they play the role of a backup power with a minimum off-to-peak-production time (Figure 1). This also requires the new challenge part load capability.

As a second application, aviation relies almost exclusively on gas turbines. They are the unquestioned number one choice for powering civil and military long distance air transportation. Although alternative technologies such as battery or hydrogen driven airplanes are investigated, all ideas struggle with the power-density of the fuel, storage and the overall power-to-weight ratio including the motor. For those parameters, the combination of burning hydrocarbon fuel in jet engines is unsurpassed and will be the number one choice for short- and medium-term perspectives. In contrast to pure hydrogen, the relevant hydrocarbons such as Kerosene are liquid at standard conditions. This dramatically simplifies the handling and causes indirect weight reduction due to fuel being stored in the wings, instead of heavy pressure tanks.

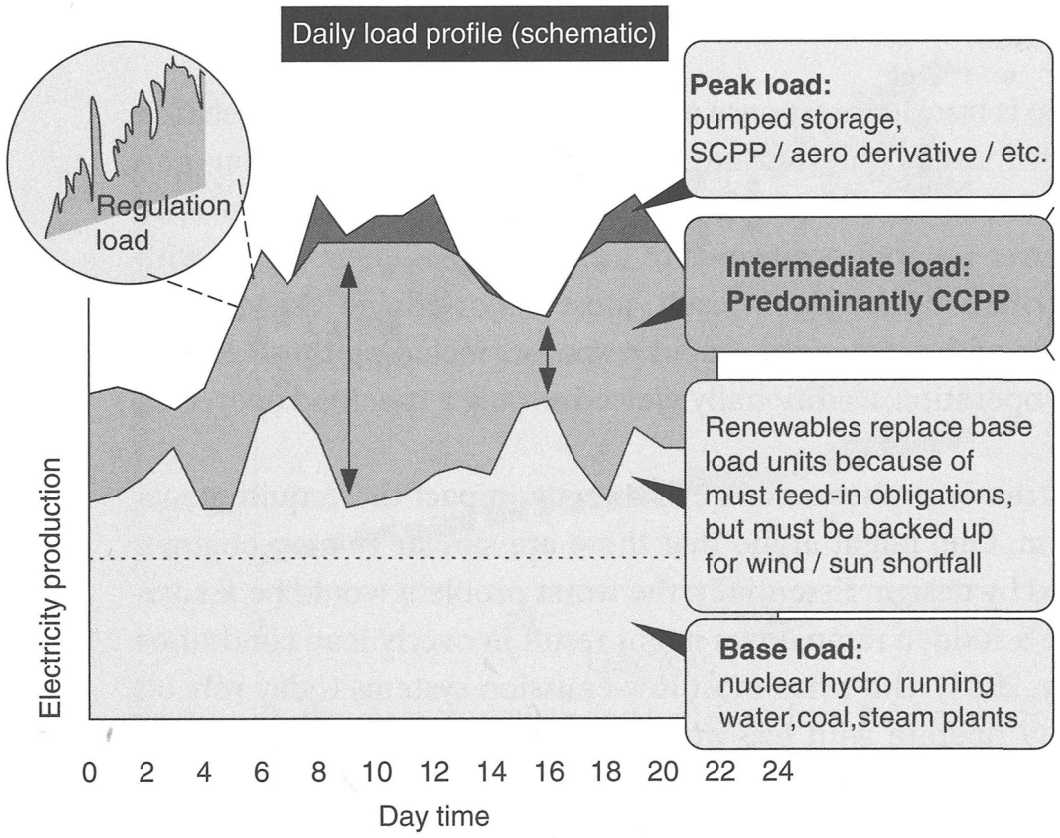

Figure 1: Typical daily distribution of electricity demand (image courtesy: Balling [3]).

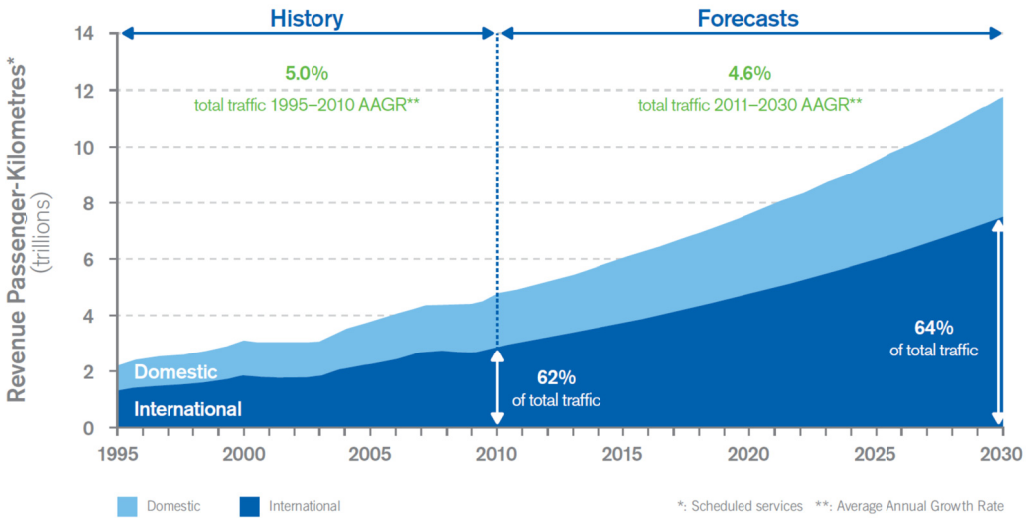

Figure 2: Prediction of air traffic increase by the ICAO [4].

Because of all the advantages of hydrocarbons as a propellant, society puts up with its major drawback: emissions.

Air traffic will increase dramatically according to the International Civil Aviation Organization (ICAO) as shown in Figure 2. The ICAO predicts an increase of 4.6% p.a. in revenue passenger-kilometers [4]. With current technology, this would mean a dramatic increase of fuel consumption and consequently emission. Air traffic in the European Union contributes to the overall greenhouse gas emission with as much as 3% [5]. This is the most important driver for the legislator issuing stricter emission restrictions.

On a global scale, aviation generates 2,6% of the equivalent CO2 emissions, the aviation growth forecast predicts this figure to possibly move up to 4,9% by 2035 according to the “most probable” CO2 scenarios [6].

1.1 Emissions

Burning jet fuel in a turbine not only converts chemical energy to thermal energy, it also produces a range of chemical products, mainly carbon dioxide and water. Since those are final products, it is difficult to reduce them. Additional emissions are not necessarily final products and can nowadays be largely but not totally avoided if the combustion process is controlled in a smart way. Below and in Figure 3 an overview of those emissions is given.

Carbon dioxide has no toxic influence on the human body but it is known to be the main cause of man-made global warming [7, 8]. The production of CO_2 cannot be avoided, however by increasing the thermodynamic efficiency of the engine, the level can be reduced.

Water (H_2O) is also an inevitable final product of complete combustion. It has no toxic influence either. However it is also known to have a warming influence on the climate when emitted in high altitudes [9].

Nitrogen oxide (NO_x) on the other side is harmful on several levels. First, for the human body it is highly toxic in direct contact causing inflammation of airways (e.g. pulmonary edema) by forming Nitric acid (HNO3) when in contact with the water in the respiratory system. Second, it indirectly enables the generation of ozone at ground level which also has direct negative effects on the human body [11]. Finally at high altitude, it also enables the generation of ozone but there, the latter is a greenhouse gas. NOx reduction can be achieved by reducing the combustion temperature and residence time.

Carbon monoxide (CO) is highly toxic for the organism. This colorless, odorless, and tasteless gas combines with hemoglobin and renders it incapable to deliver oxygen to the bodily tissue. It is produced by incomplete oxidation of carbon but can be avoided by ensuring complete combustion.

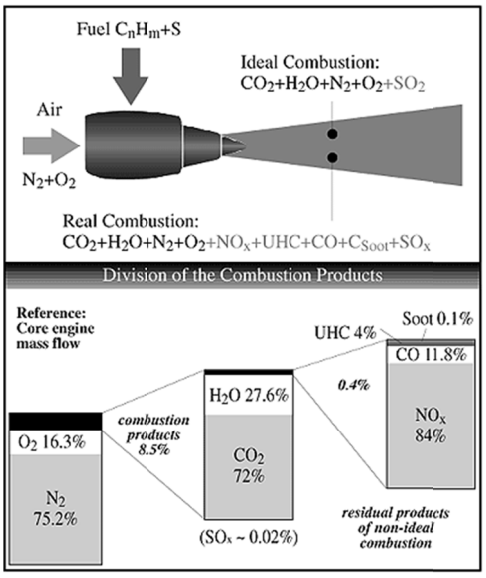

Figure 3:Pollutant emissions issued from an aero engine (Source: [10]).

Figure 4: B 52 at takeoff with water injection. Soot plumes can be seen behind the engines (image courtesy: US Air Force).

Unburned hydro carbons (uHC) can form ground-level ozone in the vicinity of NOx. Some are toxic on their own, with the potential to cause cancer [12]. Reduction of uHC's can be achieved by complete combustion.

Soot, also called smoke, is a non-volatile particulate matter. It is generated by incomplete combustion at rich conditions and can easily be identified by optical analysis. At the beginning of jet engine aviation, high levels of soot were generated at takeoff (Figure 4). Nowadays, in typical gas turbine combustion this carbonaceous material consists of single particles in the range of 10 to 80 nanometers [3]. Even after agglomeration they are often below 10 micrometers, which is small enough to enter the lungs and consequently the bloodstream of the human body. Not volatile by itself, but due to its extremely high surface area, it often acts as a carrier of volatile substances, which condense on the surface of the soot particles and are transported into the respiratory systems – or even into the blood vessels, the circulatory system of the human body. The reduction of soot is achieved by avoiding high fuel to air ratios.

1.1.1 Emission Regulations

Regulation of pollutants is carried out by states independently. However, the ICAO, which is a specialized agency of the United Nations (UN), establishes and issues international civil aviation Standards and Recommended Practices (SARPs), developed and formulated by its Committee on Aviation Environmental Protection (CAEP). Many countries use these recommendations as a basis for their

legislation [13]. Current ICAO Standards for engine emissions contained in Annex 16, Volume II [14] cover:

- Nitrogen oxides (NO_x),
- Carbon monoxide (CO),
- Unburned hydro carbons (uHC) and
- Soot.

Due to its impact on global warming [7, 8]

- Carbon Dioxide (CO_2)

is expected to be covered soon in the new Standard Annex 16 Volume III [15].

1.2 Combustor Technologies

In order to achieve ICAO certification in the future, the limits of old technologies are pushed and new technologies are introduced. Currently, two major trends can be found. The increase of the ratio between combustor pressure and ambient pressure in order to increase efficiency and reduce CO_2 emissions is applied to classic combustor technologies. Additionally, the change towards lean combustion concepts in order to reduce NO_x emissions is on its way.

For a given fuel, CO_2 cannot be influenced easily by better control of the combustion process, since complete combustion will always lead to carbon dioxide production as a final product of combustion. The only possibility to reduce the CO_2 production is by increasing the overall efficiency of the engine and airplane [16].

Alternatively it is possible to increase the heat value of the fuel by increasing the H/C ratio of the fuel. For example in a preceding EU project at TU Graz (Alfa-Bird) a synthetic liquid jet fuel was investigated which had a 5% higher heating value than jet A1.

For the engineer, particularly the increased efficiency demand is critical, although many parts of the machine can contribute to reduce loss, the only parameter increasing the thermodynamic efficiency is an increased pressure ratio [16]. Modern engines in service get close to a ratio of 60 and near future projects are expected to exceed 70 [17]. The resulting power densities are in the region of decaMW per liter volume, where it gets very difficult to maintain stable combustion.

The increased efficiency of course has the convenient side effect of reduced fuel consumption and consequently fuel costs. The German airline industry for example, averages on below 4 liters of kerosene per person per hundred kilometers for long range airplanes. Additionally, due to the high competition of the industry, engine designers are expected to improve the units with respect to:

- lower down time

which can be achieved by longer service intervals and

- longer range capability

which is manifested in the so called Extended Operations (ETOPS) certification. It certifies twin-engine airplanes to be capable of continuing their flight in cruise conditions for a certain time period before it has to land, once one engine fails. The new Airbus A350 for example features an ETOPS 370 certification, so it can stay in the air for another 370 minutes after one engine failed, offering a virtually unrestricted route choice for the airline. Currently the longest scheduled non-stop flight from Dubai to Auckland covers a distance of 14,162 kilometers. The expected features mentioned above demand more reliable and at the same time more efficient technologies from engine manufacturers.

Besides increased pressure ratios for classic combustor technologies, the trend goes to lean combustion in order to reduce NO_x emissions. While piston engines for automobile applications nowadays reduce NO_x emissions by means of a catalyst, this is not possible for aero turbines due to weight restrictions and a dramatically higher volume flow rate. Achieving low NO_x without any after treatment is particularly challenging, because a considerable amount of NO_x called thermal NO_x is produced with high temperatures. In combustion, the highest temperatures are achieved near stoichiometric conditions because the lowest amount of gas has to be heated by the exothermal reaction (Figure 5).

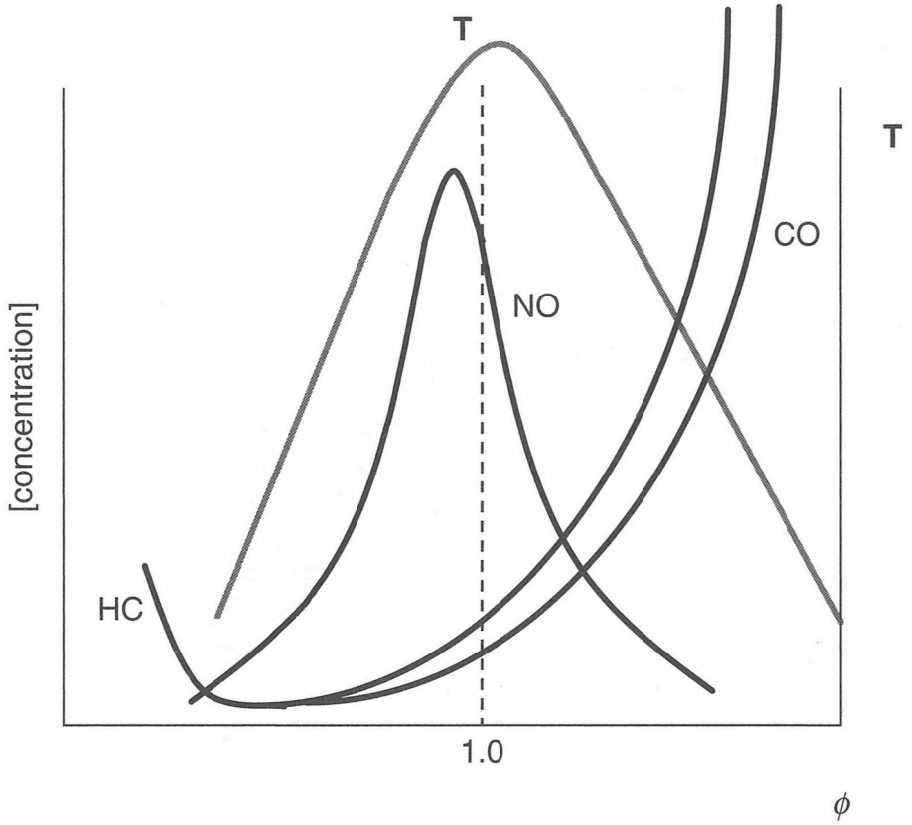

Figure 5: Nitrogen oxide (NO), unburned Hydro carbons (HC) and Carbon Monoxide (CO) emissions and Temperature (T) of a typical hydro carbon combustion as a function of local equivalence ratio (image courtesy: Lieuwen [13]).

In order to keep the NOx emissions low, this high-temperature regime must be avoided. Equivalence ratios beyond unity would give rise to carbon monoxide due to a lack of oxygen and increase fuel burn without additional power output. Therefore, the only operational regime left, is one at low equivalence ratios. This region however is challenging, because the combustion process is less stable, threatened by lean-blow-out (LBO).

When such a typical dry low NO_x combustor operates at low equivalence ratios, more air takes part in the main combustion process, allowing the flame to burn 'cooler'. As a consequence, after the primary reaction zone, less dilution air is needed to cool down the fluid to a temperature acceptable for the turbines first stage. In order to reduce the mass flow of cooling air through the liner, the number of cooling holes must be reduced, which has the inconvenient side effect of less acoustical damping (Figure 6).

The described constellation of a highly instationary combustion process combined with less damping in the combustor makes this upcoming technology prone to combustion instabilities, where combustor

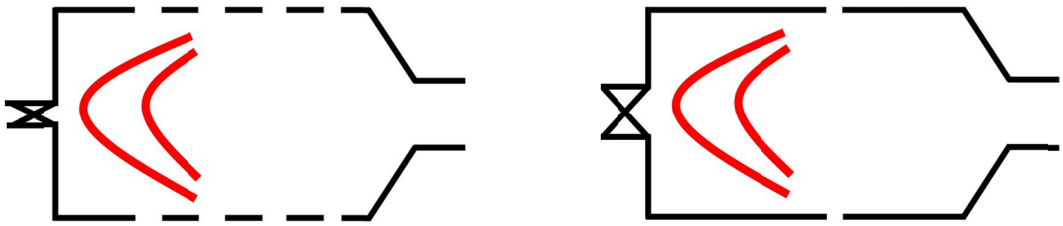

Figure 6: Conventional combustion chamber (left) and lean premixed combustor (right).

acoustics and combustion dynamics strongly interact with each other. The successful suppression of combustion instabilities can only be achieved by understanding the underlying mechanisms and dynamics as well as the combustion noise emitted by the flame.

1.3 Measurement Technology

While numerical methods have vastly improved in recent years, experimental work is still necessary for validation. The common characterizing parameters of instationary fluids, such as velocity and pressure, can be accurately quantified with classic approaches such as laser-Doppler-anemometry and piezo-pressure transducers. Those systems are generally applicable for combustion analysis if precautions are taken: Pressure transducers must be water- or nitrogen cooled. For velocity measurements, proper seeding must be chosen and optical accessibility ensured. Tools, recording temperature and heat release in the flame, on the other side, are scarce. While temperature can be acquired with Raman spectroscopy, for the acquisition of heat release, so far only chemiluminescence has been used. There, the light emitted by the flame at certain wavelengths is considered proportional to transfer from chemical to thermal energy in the flame (combustion process). This simple and easy to use system is popular but has drawbacks when used in the environment of equivalence ratio fluctuations and in the presence of strain rates [18]. Given those circumstances, an alternative technique is welcome in the scientific community. Here laser interferometric technologies come into play. They rely on the fact, that monofrequent light can be described as waves, and those waves can interfere with each other. When they are superimposed, the resulting wave has smaller, the same or greater amplitude as the original waves. In this work the so called laser interferometric vibrometry (LIV) is applied, where interference between a reference beam and a measuring beam is detected [19]. The measurement beam, exposed to a changing refractive index in the measurement section detects a change of speed of light. In gasses a change of refractive index can be directly linked to its density via the Gladstone-Dale constant [20, 21]. The physical measurand is then the time derivative of the density (ρ) in the measurement area (A_{meas}) integrated over the laser-beam length (ζ):

$$\int_{\zeta} \frac{\partial \rho'}{\partial t}(A_{meas}, \zeta, t) d\zeta = \frac{k}{2G} U(t) \tag{1}$$

with the Gladstone-Dale constant (G), the calibration constant (k), and the output voltage of the LIV (U). When investigating reacting gases, not so much the density fluctuation but the heat release is of interest, since it takes part in the fundamental coupling mechanism [22] and is used for stability analysis [23]. With the appropriate theoretical frame work heat release can be assessed qualitatively and quantitatively, as described by Dowling [24]:

$$\frac{d\rho}{dt} = \frac{1}{c^2}\frac{dp}{dt} - \frac{\kappa - 1}{c^2}\frac{dq_V}{dt} \tag{2}$$

with the pressure (p), the speed of sound (c), the ratio of specific heats (κ) and the volumetric heat release (q_v). The LIV system measures the density fluctuations integrated along the line-of-sight with a time resolution of more than 100,000 samples per second. Additionally, 2D- traversing provides lateral resolution, and the integration over those measurement points provides the entire density fluctuations and consequently the entire volumetric heat release of the flame.

1.3.1 History

Interferometric methods have been used for a wide range of investigations in engineering and science for decades. Among them were fluid flow investigations (e.g. shearography) and surface vibration investigations (e.g. holography). Those methods relied on a sophisticated setup operated by highly trained personnel.

It was not until the 1990's when Polytec, a Germany based company, developed a Laser interferometric vibrometer system (Figure 7), a compact application of interferometry which detects surface vibration of moving objects (Figure 8 top) [19]. This gave engineers the opportunity to assess structural vibrations of mechanical parts without restrictions in material or shape. The measurement tool can be set up and ready to measure in several minutes. The setup consists of a sensing head including all optical parts and a processor evaluating the information. Those systems are compact and fairly easy to use. The biggest advantage is that they are highly accurate and non-intrusive. The only drawback in surface vibration recording is a slight dependency of the signal on refractive index changes of the medium (air) between the sensing head and the test object (e.g. sound waves).

In the research presented in this thesis such a drawback however can be exploited in order to measure the refractive index fluctuations and consequently the density fluctuations of the gas in front of the object only. For this the background surface which reflects the laser beam must be kept as rigid as possible (Figure 8 bottom). This new application of LIV has - for the first time – been tested at Graz University of Technology in 2000. Subsequently, several projects have been successfully completed in order to understand the capabilities and restrictions of the method. This started off with the proof of concept and the quantification of density fluctuations in a first project, funded by the Austrian Science Fund (FWF). In a second project the focus moved to the application in reacting flows. Finally, for this project, the necessary theoretical framework was discussed in order to quantify heat release from vibrometer measurements, not only in laminar but also in turbulent flames, providing a parameter of interest to combustion industry. Thus, the use of laser vibrometers proved to be

Figure 7: Laser vibrometer sensing head and processor (image courtesy: Polytec).

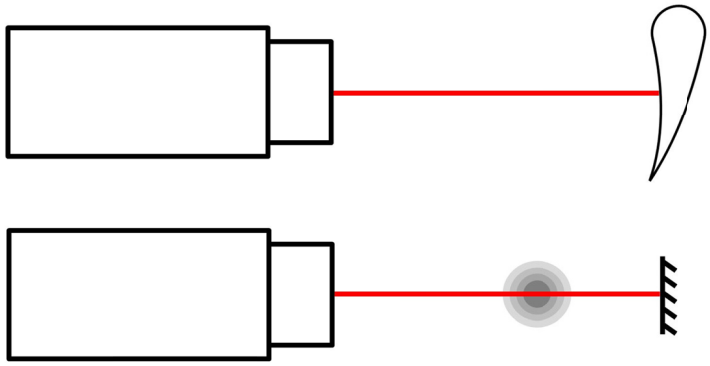

Figure 8: Laser Vibrometer setup for surface vibration- (top) and density fluctuation measurements (bottom).

useful for the investigation of density fluctuations in unsteady non-reacting and reacting flows [25, 26, 27], periodic flows through turbomachinery [21, 28] and reacting flows [29, 30, 31, 32, 33, 34]. Furthermore, this technique has also been used by a number of other authors to investigate flow and sound fields [35, 36, 37, 38, 39, 40, 41].

1.3.2 Relevant Preceding Work at TU Graz

FWF Y0057-TEC START – proof of concept (Non-Intrusive Optical Diagnostics of Turbulent Flows in Turbomachinery)

Mayrhofer et al. [27] used the laser interferometric vibrometry for the first time in order to detect density fluctuations caused by vortex shedding in the wake of a turbine blade. This periodic effect was used in order to trigger a laser Doppler velocimeter.

In 2001 Mayrhofer et al. [21] demonstrated that density fluctuations of a free jet can be compared to the velocity field of constant temperature anemometry. Turbulent energy spectra were compared and an error analysis was given.

Hampel et al. [42] demonstrated local density fluctuation measurements with dual laser vibrometry in a non-reacting flow. Two crossing beams and a correlation technique in the frequency domain reveal local density fluctuations rather than line-of-sight integrated information. By rotating the setup, artefacts were successfully identified and eliminated. For local quantitative measurements, the effective measurement area must be known. This was found to be challenging to identify.

FWF P 19955-N19 - Experimental Investigation of Flame-Flame Interaction in a Gas-Turbine Model Combustor with Forced Flow Instabilities

This project was submitted to the Austrian Science fund in December 2006. Underlying hypothesis was the relation between density fluctuations, pressure and heat release fluctuations given by Dowling in [24]. In order to prepare this proposal first feasibility tests were performed by Fabrice Giuliani,

Bernhard Wagner, Jakob Woisetschläger and Franz Heitmeir [43]. This was the very first time, the LIV system was applied to reacting flows. Fabrice Giuliani – at that time Head of the Combustion Division at the Institute for Thermal Turbomachinery and Machine Dynamics - provided his experience in the design and testing of combustion chambers with forced instabilities. The publication served as a proof of concept, and revealed promising insight into flame dynamics.

Köberl et al. [33] applied the LIV to an unconfined laminar methane fired diffusion flame of 7.5kw thermal power. Dual-LIV measurements matched with differential interferometry data. In a second step, a premixed swirl stabilized flame of 17.5kW thermal power was investigated at atmospheric conditions. By means of Dual-LIV, the time derivative of density fluctuations was compared to tomographic reconstruction of chemiluminescence measurements. Similar trends were found for both measurement techniques. In a combustion chamber, the same burner was operated in a three flame configuration with natural gas at a total power of 27kW. The time derivative of local density fluctuations was compared to chemiluminescence measurements with matching trends. Flame-flame interaction and self-excited combustion oscillation were visualized using dual-LIV.

Funded by EU-project NEWAC (”New Aero-engine Core Concepts”, AIP5-CT-2006-030876) and organized as a cooperation between TU Graz (Fabrice Giuliani) and École Centrale Paris (Thierry Schuller), Leitgeb et al. [29] employed the link in eq. 2 in order to conclude on heat release fluctuations excited by acoustic modulation of the feedline and quantitatively draw a comparison between LIV and chemiluminescence. For this, an unconfined laminar premixed flame was used and acoustically excited. Additionally, the sound emitted by the perturbed flame was detected by means of LIV and compared to microphone measurements. For the first time, results of LIV have been quantified in laminar flames.

FWF P 24096-N24 - Interferometric Detection of Thermoacoustic Oscillations in Flames

As a logical consequence to preceding projects, in this work, **heat release of turbulent combustion had to be quantified** by means of LIV according to $\int d\rho/dt \approx \dot{Q}$. In order to validate the system it was necessary to compare time resolved heat release fluctuations recorded by LIV with established techniques such as chemiluminescence and microphone methods within their limits of validity. For this, confined and unconfined flames had to be investigated in the range of 4 kW to 50 kW of thermal power at rich and lean conditions, from equivalence ratios of $\varphi = 0.71$ to $\varphi = 1.43$. In terms of flame dynamics, a comparison between measurement techniques had to be drawn for natural spectra, as well as for excited flames. For this, the feedline flow had to be modulated by a siren. For validation, local as well as global heat release was studied. Furthermore, it was necessary to investigate the influence of the speed of sound on the link between density fluctuations and heat release as described in Equation **(2)**. Additionally, a more detailed study on signal correlation between two laser vibrometers was performed. This led to velocity recordings without the need of tracer particles and spatial correlations (structural decay).

Additionally, an **industry relevant application** had to be evaluated. To measure the flame transfer function is a well-established approach to quantify the stability behavior of a flame. Here integral-LIV recordings were compared to the classical OH-chemiluminescence technique.

The second part of the project was devoted to the **prediction of combustion noise by means of LIV**. Sound emitted by a flame can be predicted by measured density fluctuations ($\int d^2\rho/dt^2 \sim p'$ in far-field)

as derived by Strahle [44]. Although an old theory, it has never been experimentally proven. This proof was the second goal of this project. For this, the sound intensity in a spherical surface around the flame was measured and compared with the density fluctuation data acquired by two-dimensional traversing of the LIV-system. For these experiments, a model combustor of 4kW thermal power was used. This variable geometry burner was originally designed by Leitgeb and Giuliani in a preceding project ”New Aero-engine Core Concepts” (NEWAC, AIP5-CT-2006-030876). The design and validation is well documented [45, 46, 47]. This initial burner was then further improved and redesigned with retrospect to the validation of measurement technologies. The new design now provides rotational symmetry of the flame and sufficient cooling air for operation within a combustion chamber. This new burner was characterized including the spatially and time resolved flow field, temperature field and acoustic spectrum. To facilitate acoustic measurements, a new laboratory had to be built at the institute which included a low reflective environment around the flame. For the high power flame of industrial relevance a test rig at Technische Univeristät München was available during a measurement campaign.

2 Theoretical Background

In this chapter, a brief overview of the most relevant theories related to 'interferometric detection of heat release rate' is given. The setup of the Laser Interferometric Vibrometer (LIV) is explained including the basic principles. Since dynamic processes are investigated, spectral analysis is an important tool in order to reduce the sheer amount of data to a comprehendible set of plots and diagrams. An overview of spectral analysis, including a practical step-by-step guide of the Fourier transform is presented. Since one of the strengths of LIV is its high acquisition rate, dynamic aspects of combustion are investigated in this thesis. For the detection of heat release rate fluctuations though, it is necessary to understand the nature and occurrence of combustion fluctuations. As a comparison, in this thesis, OH*-Chemiluminescence is used and therefore presented next. Finally combustion noise theory is presented briefly. All of the chapters mentioned here, have the intent to provide the reader with the most important facts of the particular topic, for a complete reading, additional literature is suggested. Besides a measurement campaign at TU Dresden, Dresden, Germany and TU München, München, Germany, the majority of experiments have been performed at the Institute of Thermal Turbomachinery and Machine Dynamics at TU Graz, Graz, Austria (Figure 9).

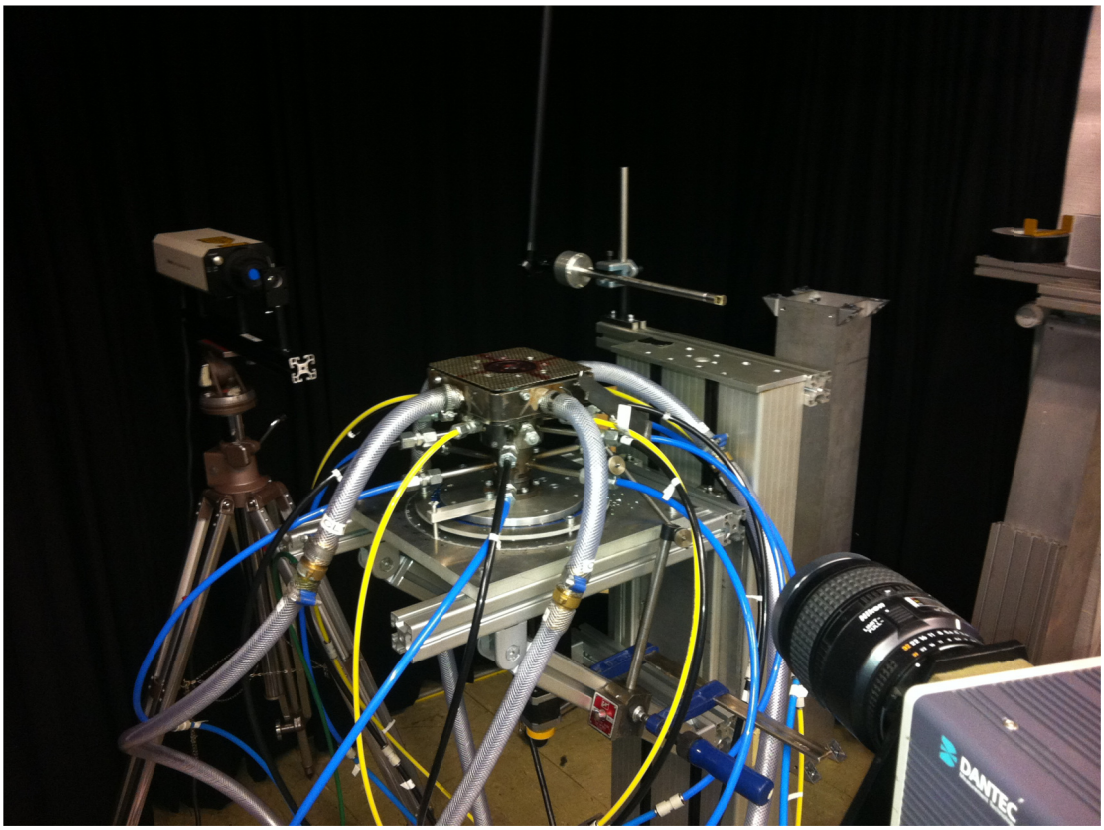

Figure 9: Variable geometry burner with PIV and LIV setup in the 'Thermoakustik-Messraum' in the basement of the Institute, where most of the experiments have been performed.

2.1 Working Principle of the Vibrometer

In contrast to the introduction where the relevance of vibrometry is explained and the actual measurand and its link to combustion is discussed within this chapter the fundamental principle of vibrometry is presented.

Laser vibrometers are widely used to detect surface vibrations of machinery. For best results the laser beam must be focused on the object. In the present work however - when density fluctuations are measured - it is important to ensure a parallel laser beam. For this, the setup includes the sensing head itself, a concave focus lens and a rigidly fixed mirror. The measurement beam is collimated at a desired diameter by means of the internal optics (Figure 10) and the concave focus lens. The beam passes the measurement region and is then reflected back into the sensing head by a rigidly fixed mirror (Figure 11).

The lenses are slightly tilted in order to avoid its reflection from hitting the sensing head. This ensures that the vibrations of the lens mount do not corrupt the signal. Vibrations of the mirror on the other hand are always detected by the system. To receive meaningful results, the vibration of the mirror must be reduced to a minimum and shifted outside the frequency band of interest. Thus, the surface mirror was bonded to a massive steel box filled with sand. This ensures damping of the mirror and its high mass pulls the Eigen frequency of the mirror to a value below 10 Hz. Such low frequencies can then be easily separated from the frequencies of the density fluctuations typical for industrial flames. In the measurement section, the speed of light χ_{meas} is a function of the refractive index of the medium n_{meas}. The refractive index (n) is defined as follows:

$$n_{meas}(t) = \frac{\chi_{vac}(t)}{\chi_{meas}(t)} \tag{3}$$

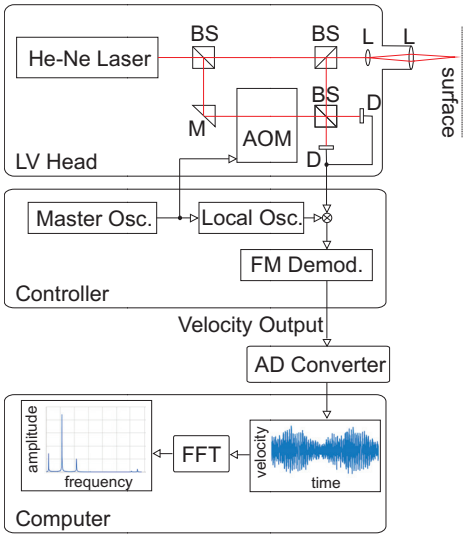

Figure 10: Internal optical and electronical arrangement of the Laser Interferometer.

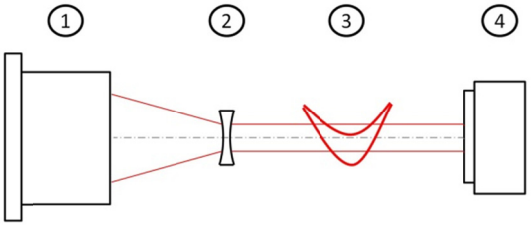

Figure 11: Setup of the Laser Interferometer for combustion diagnostics with the sensing head (1), the collimating lens (2), the flame (3) and the mirror (4).

with the speed of light in vacuum χ_{vac}. As soon as the refractive index of the medium changes over time, the frequency of the speed of light is modulated by the frequency of the change in refractive index f_{meas}:

$$\frac{1}{\lambda}\int_{\zeta}\frac{\partial n'}{\partial t}(A_{meas},\zeta,t)d\zeta = f_{meas} \tag{4}$$

with the wavelength of light (λ). This superimposed information can then be detected by the detector. The vibrometer itself consists of a laser light source feeding into a Mach-Zehnder interferometer, shown in Figure 10. The laser beam is split into a measuring beam and a reference beam. This reference beam passes an acousto-optical modulator (Bragg cell), which constantly shifts the laser light frequency of the reference beam by the Bragg frequency f_b. As soon as both beams are superimposed, the intensity at the detector I_{LIV} results in a beat between the Bragg frequency and the frequency of the refractive index fluctuation.

$$\frac{I_{LIV}}{I_{LIV0}} = 1 + \cos(2\pi(f_n + f_B)t) \tag{5}$$

By adding this acousto-optical modulator (AOM) to the system, negative and positive frequencies can now be distinguished. Consequently, positive and negative gradients of the refractive index can be identified. By means of a phase lock loop (PLL) a change of input frequency at the photodetector results in a change of output voltage U(t) of the decoder unit. When the known Bragg frequency is filtered and the wavelength of the laser light is known, the frequency of refractive index is directly linked to the output current by the calibration constant (k) (e.g. 5mm/s/V).

$$\lambda f_n = \frac{k}{2} U(t) \tag{6}$$

Combining equation (4) and (6) then results in:

$$\int_{\zeta} \frac{\partial n'}{\partial t}(A_{meas}, \zeta, t) d\zeta = \frac{k}{2} U(t) \tag{7}$$

If the test medium is gaseous, the refractive index changes with density. The parameters are linked via the Gladstone-Dale constant (G) as follows:

$$n - 1 = G\rho \tag{8}$$

The Gladstone-Dale constant is a function of the wavelength of the light source used and the chemical composition of the gas investigated. It can be derived from dispersion relations [48, 20]. The line-of-sight integral density fluctuations dρ'/dt per measurement area A_{meas} in the test volume are then linked to the output voltage by combining equation (7) and (8):

$$\int_{\zeta} \frac{\partial \rho'}{\partial t}(A_{meas}, \zeta, t) d\zeta = \frac{k}{2G} U(t) \tag{9}$$

A factor of two is due to the laser beam passing the cylindrical measurement volume twice.

2.2 Spectral Analysis – A Pragmatic Approach

In scientific applications, spectral analysis is used when dynamic systems are investigated. Very often these systems are highly complex and analyzation tends to be easier when isolating single frequencies or with the aid of spectral analysis in order to comprehend the entire scope of frequencies.

Most signals in physics are continuous. Nevertheless, electronic recording of signals is only possible at discrete time steps. The sampling rate defines how many samples are recorded per second. In the following example signal analysis is carried out step by step with a pure sinus of 4 Hz. Using a sample rate (SR) of 64 samples (spls) per second (1/64 seconds time intervals) means that one period is described by 16 samples recorded at constant time intervals for 1 second (Figure 12). In a frequency spectrum (Figure 13), this signal is described by three values: signal amplitude, frequency and phase (relative to a signal reference). With this information, the entire time signal can be reproduced and dynamic behavior can be assessed quickly. A complete frequency spectrum consists of one plot of amplitude over frequency and one phase-plot over frequency. Since data storage space can become a cost factor, particularly with complex investigations, the sampling rate cannot be increased indefinitely. Nevertheless, for a given signal it must be high enough in order to reproduce the original data correctly.

Increasing the frequency of the sinusoidal signal above from 4 Hz to 32 Hz, and further to 40 Hz, reveals that only up to a certain point, the sample rate of 64Hz is sufficient in order to obtain correct information (Figure 14). Among others, Harry Nyquist discovered and Claude Shannon mathematically formulated that only frequencies below half the sample rate can be reproduced correctly. This is expressed in the so called Nyquist-Shannon theorem with f_{Ny} the Nyquist frequency:

$$f_{max} \leq \frac{SR}{2} = f_{Ny} \tag{10}$$

or in words: the highest frequency which can be reconstructed from the sample (f_{max}) must be smaller or equal than the so called Nyquist-frequency (f_{Ny}), which is half of the sampling rate.

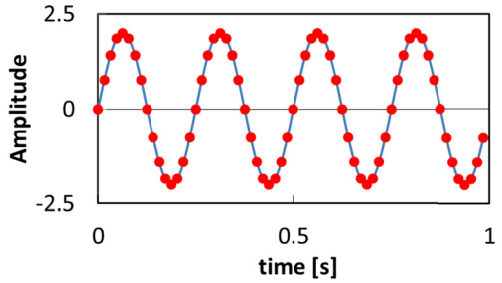

Figure 12: Continuous time signal of 4 Hz sinus of amplitude 2. Recorded with 64 samples per second.

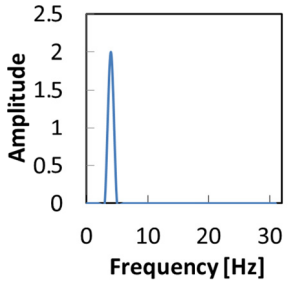

Figure 13: Amplitude and phase spectra of 4 Hz sinus with amplitude of two.

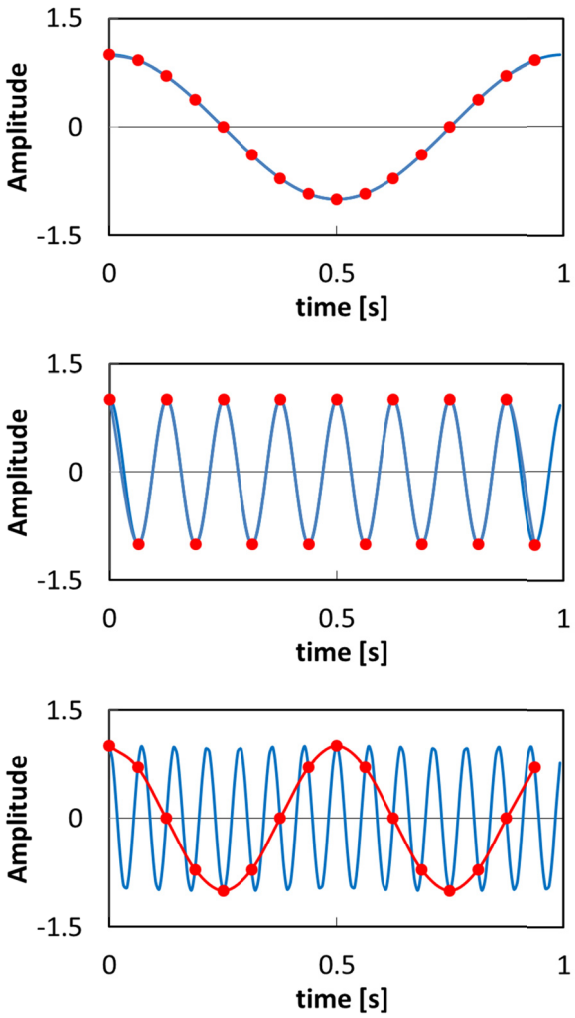

Figure 14: Different frequencies sampled at the same sample rate of 64 spls/sec. They are over sampled (top), sampled according to Nyquist-Shannon theorem (middle) and under sampled (bottom).

2.2.1 Fourier Transform

For spectral analysis, the Fourier transform is the most popular tool for frequency analysis of a given time signal. Most scripting languages used in academia and industry, such as Matlab, provide a built in application of the Fourier transform. With a time signal of equidistant time steps, a frequency spectrum can be calculated quickly. It is a more difficult task to obtain correct amplitude and phase of a noisy signal which contains unknown frequencies. The aim of the following subchapter is to provide a procedure to obtain correct amplitudes and frequencies.

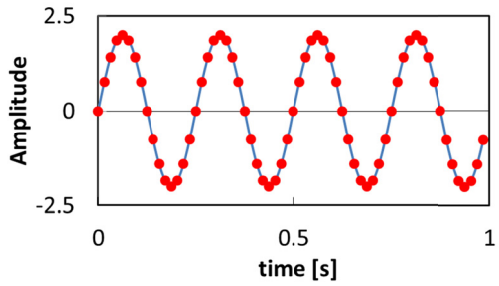

Figure 15: Time domain: 4Hz Signal, Amplitude 2 at SR=64.

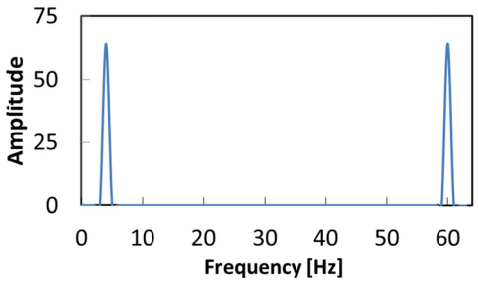

Figure 16: Double-sided raw spectrum: 4Hz Signal at SL=SR=64, no Division by SL jet.

2.2.2 Sample Rate, Sample Length and Nyquist-Shannon Theorem

In the above example a pure sinusoidal wave of 4 Hz frequency without noise was acquired with 64 samples per second (SR) for a recording length of one second. This gives a total number of 64 samples for one period. These 64 samples are also called sample length (SL). In the Matlab application of the Fourier transform, the resulting spectrum for a given sample with sample length SL and sample rate SR has as many frequency bins as the original time signal has time steps (SL). This result is a so called double-sided spectrum mirrored around the Nyquist frequency with a preliminary (wrong) amplitude (Figure 15 and Figure 16).

The first bin or 0 Hz represents the mean value of the time signal and the bin number SL/2+1 (here the 33rd bin) is the Nyquist frequency (32Hz) from eq. 1. To the left and right of that frequency, the frequency bins are distributed evenly with $\frac{SL-2}{2} = \text{bins above Nyq} = \text{bins below Nyq}$. In the above example, 64 entries minus the bin for 0 Hz and the one for the Nyquist frequency divided by two makes 31 frequency entries above and below the Nyquist Frequency. The frequencies between 0 Hz and the Nyquist frequency are the so called real frequencies. In Matlab the part above Nyquist does not contain any additional information. Those are just the real frequencies mirrored around Nyquist. In order to reveal correct amplitude – in a first step for most implementations of the Fourier transform - the entire spectrum must be divided by the value of the sample length (Figure 17).

Since the information above Nyquist is redundant, usually only single-sided spectra are plotted. Preserving the energy in the spectrum, the double-sided spectrum can be transformed into a single-sided one by mirroring the part above Nyquist which is the same as just leaving the mirroring away and multiplying the real frequencies by a factor of two. Now the correct amplitude is revealed. In the double-sided spectrum, the mean value and the Nyquist frequency appear only once, therefore those two bins are not multiplied by two when changing to a single-sided spectrum (Figure 18).

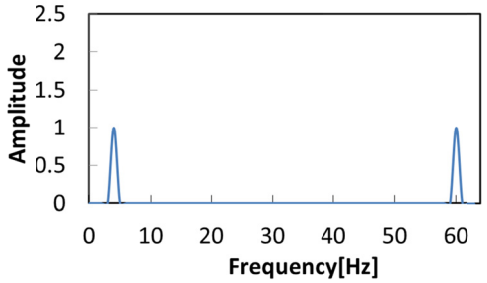

Figure 17: Double-sided spectrum: 4Hz Signal at SL=SR=64. The amplitude is divided by the sample length.

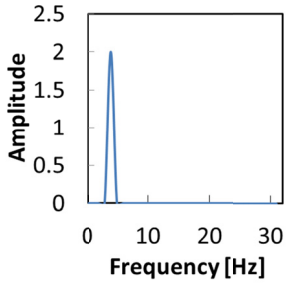

Figure 18: Single-sided spectrum: 4Hz Signal at SL=SR=64. The spectrum above f_{Ny} is mirrored back.

2.2.3 Aliasing

Given that any frequency is mirrored around Nyquist, the theorem itself reveals an additional problem. Frequencies above Nyquist cannot be reconstructed correctly (undersampling). If the data contains information above the Nyquist frequency, the spectrum at lower frequencies is corrupted. Recording a signal with frequency information higher than Nyquist shows that low frequency signals can be introduced that stem from the undersampled data. Now even a spectrum with otherwise low noise can be misleading. Looking at the undersampled time signal of a pure sine wave of 40 Hz in (Figure 14 bottom) a Fourier transform shows that the frequency is correctly shown in the double-sided spectrum. This is in addition to one mirrored around Nyquist, as expected (Figure 16). It is not possible to identify which one of the two is the real signal and which one is just the reflection around the Nyquist frequency (Figure 19). When calculating the single-sided spectrum, we only see a frequency of 24 Hz (Figure 20). Without additional information, there is no possibility of knowing whether this frequency is correct or a 'ghost' frequency. Therefore, we can not only not detect these frequencies above the Nyquist frequency, but they also corrupt the spectrum below the maximum frequency.

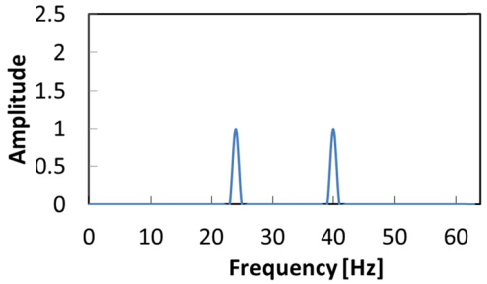

Figure 19: Double-sided spectrum: 40Hz, which is above Nyquist when sampled at SL=SR=64.

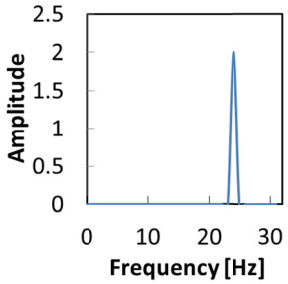

Figure 20: Single-sided spectrum: 40Hz Signal at SL=SR=64 gives a 'ghost' frequency.

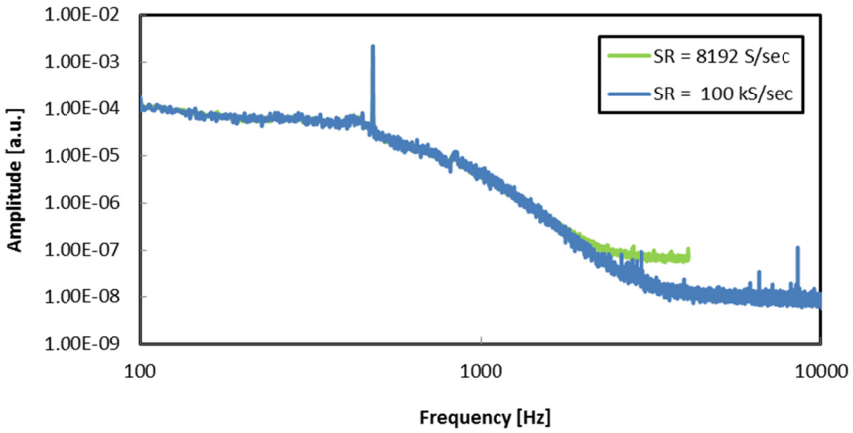

Figure 21: Heat release of turbulent combustion. Measurements with 8192 spls/sec (green, under-sampled) and 100 kspls/sec (green).

In Figure 21, the amplitude of heat release of a combustion process is shown. The sample rate of the initial measurement was not high enough to reproduce the correct amplitude of the turbulence in the combustion at higher frequencies, The correct level can be detected with an increased sample rate.

2.2.4 Frequency Resolution

Since the Fourier transform produces a spectrum with a finite number of bins, a frequency resolution (Δf) can be defined. The frequency resolution of a spectrum depends on the sampling rate and the sample length and is not necessarily one Hz. When the frequency bins are evenly distributed, the first bin is zero, and the last one in the single-sided spectrum is the Nyquist frequency. We then divide the Nyquist frequency by the number of gaps between bins below Nyquist. As a resolution, we then have:

$$\frac{F_{Ny}}{Bins_{0-F_{Ny}}} = \frac{SR/2}{SL/2} = \Delta f \tag{11}$$

Whenever the sample length is different to the sample rate, the frequency resolution differs from one. In order to calculate the frequency resolution from the experimental sample one proceeds as follows. With a sample rate (SR) of 64 samples per seconds and 64 samples sample rate, the signal is sampled for 1 second. The lowest frequency that fits in this sample length is 1Hz. Therefore, the frequency resolution is one Hertz. By increasing the sample length at the same SR, the frequency resolution gets smaller (e.g. 128 samples equals 0.5 Hz at same SR). Considering that in a noisy, turbulent flame a high number of frequency spectra must be averaged (several hundreds), the recording time for each position recorded might extend into the 10 minute range.

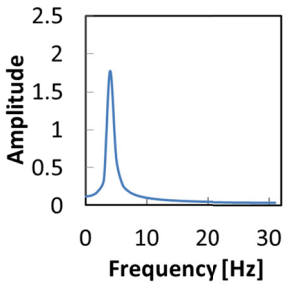

Figure 22: Single-sided spectrum: 4.25Hz Signal at SL=SR=64, Δf=1Hz

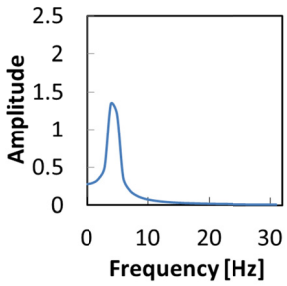

Figure 23: Single-sided spectrum: 4.5Hz Signal at SL=SR=64, Δf=1Hz

2.2.5 Scalloping Loss

All of the above examples were chosen, so the frequencies of interest were exactly a multiple of the frequency resolution. In real engineering problems, quite often this is not possible. Generally, frequencies do not match a frequency bin in the spectrum exactly. The energy of those frequencies is distributed between neighboring bins, causing a so called 'scalloping loss' which in worst case can be up to 36% in amplitude. In Figure 18 the spectrum of the 4 Hz sine with an amplitude of two is shown at SL = SR = 64. By increasing the frequency stepwise, without altering the amplitude of the input signal, the amplitude of the spectrum is heavily dampened (Figure 22) with the strongest deviation exactly in between two frequency bins (Figure 23).

There are some methods in spectral analysis to retrieve the correct amplitude. It is easiest but often costly to increase the sample length. This does not necessarily work for purely monofrequent signals, but works for physical signals that usually have a statistic distribution around one peak. One example

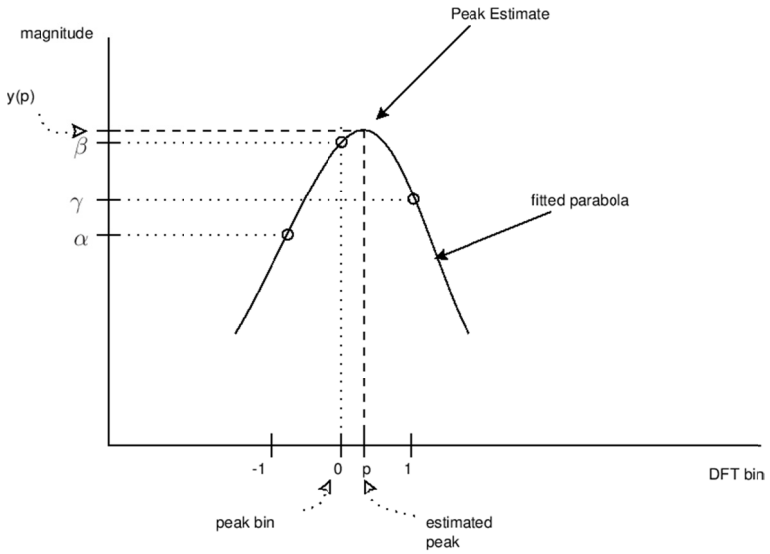

Figure 24: Quadratic interpolation of spectral peaks [49].

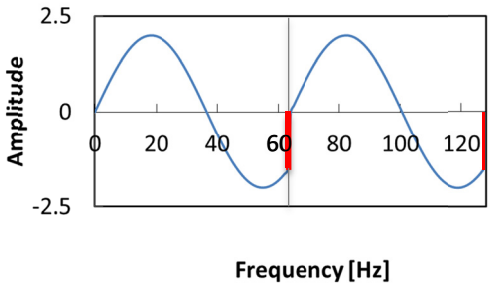

Figure 25: Visualization of Discontinuity. The Fourier transform assumes periodicity, and therefore repeats the given sample, causing a discontinuity.

is a combustor resonance, where small temperature fluctuations or feedline fluctuations alter the cavity resonance slightly over time. The result is a somewhat smeared amplitude. Alternatively it is possible to apply a peak detection technique. Then, for example, a quadratic interpolation of a certain amount of neighboring bins can estimate the amplitude (Figure 24). A better option is to apply filters, as described below.

2.2.6 Discontinuity

The most common approach however is to apply a filter to the sampling window [50]. This approach tries to correct the fact that the Fourier transform assumes a periodic signal, which means that the signal repeats itself indefinitely. If the frequency however does not fit into the sample length exactly, repeating the signal introduces a discontinuity and causes the energy of that frequency to spread over the spectrum (Figure 25).

A window function is a vector of the same length as the sample length of the time signal. This vector is then multiplied with the time sample length before the Fourier transform is performed. Most window functions are close to or zero at the borders (Figure 26). This way they suppress the discontinuity (Figure 27). Ideally, the correct amplitude can be retrieved. The drawback is that the stronger the filter, the more the peak spreads over several bins. And therefore, it is difficult to identify the exact frequency. This is not a problem if the frequencies of interest are known, and the focus of the investigation lies on the amplitude itself. A flame excited by a siren with defined frequency would be such an example.

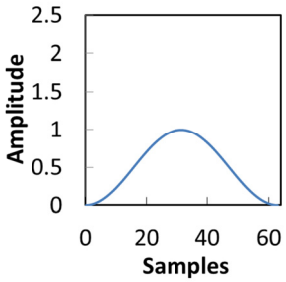

Figure 26: Filter with zero at borders, here a Hanning window.

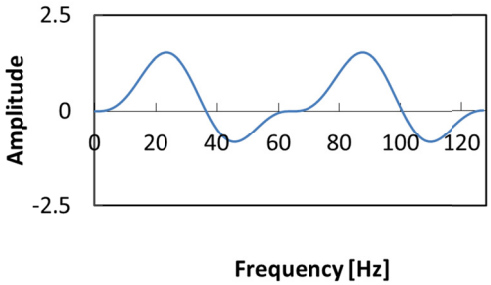

Figure 27: Continuity after applying a filter.

The signal obtained should also be of monofrequent character and peaks in the spectrum should be well apart from each other in order to be identified. The most common window functions are briefly described below.

The rectangular filter has a value of unity over the entire sample length, and therefore is the same as not using a filter at all. The rectangular filter reaches highest spectral resolution, but has the highest scalloping loss of all filters with up to 36% if the frequency is exactly between two bins.

Flattop windowing is a family of different filters that have the lowest possible scalloping loss, with the tradeoff of low spectral resolution. They are most common in calibration applications, where noise is generally low, pure harmonic or a combination of harmonic signals is investigated and where it is significant to know the exact amplitude of a signal. Since they have very bad frequency resolution, they are not appropriate for broad band signals or when frequencies are not separated well in the spectrum.

In engineering most people use a Blacksmith, Hamming, Hanning or Butterworth filter, since those filters represent a good balance between spectral resolution and scalloping loss. Generally the tradeoff between the window-functions is that they are either very good at frequency resolution (rectangular window) or correct amplitude caption (flattop window), or average to good at both (Hamming, Hanning). Note: For window functions, the sample block has to be normalized by a value other than the sample length. For a detailed application guide of window functions, Heinzel et al [51] is recommended. One property of filters is, the stronger the filter is, the more time signal bins it suppresses on the edges of the window, and consequently information is lost. This drawback can be circumnavigated by employing window overlapping which is described below.

2.2.7 Window-Averaging

So far examples were considered where the sample rate, the sample length, and the total number of samples were equal. In environments where the signal-to-noise ratio is low, as generally in turbulent combustion measurements, it is necessary to repeat measurements and average the result in order to reduce stochastic noise and compensate for fluctuations in the point of operation. This can be done by increasing the total number of samples without changing sample length or sample rate. Then the total sample with length $spls_{tot}$ is split into sampling block of length SL. If used the window-function is applied (Figure 28) and the Fourier transform is performed for each of those blocks individually. The total number of samples divided by the sample length of the Fourier transform then results in the number of blocks to average (no_{av}).

$$no_{av} = \frac{Spls_{tot}}{SL} \tag{12}$$

When using this procedure, noise is reduced and a cleaner spectrum is the result. Figure 28 shows that the window function is close to zero at the edges. If the time signal is multiplied by the window function, it is heavily dampened there. If a window function is applied, it is therefore beneficial to let the sample blocks overlap in order to retrieve otherwise lost information at the edges of the sample blocks (Figure 29).

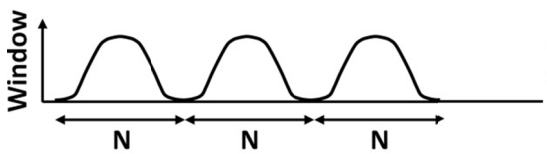

Figure 28: Several sample blocks with SL=N without overlapping.

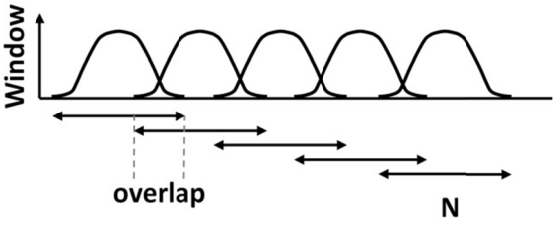

Figure 29: Several sample blocks with SL=N with overlapping.

So far only the amplitude was considered. As mentioned above, the Fourier transform also provides information about the phase of harmonic signals. Care must be taken when several sample blocks are averaged. If, as generally the case, the frequency of interest is not a multiple of the frequency resolution, the phase is not meaningful since the starting phase differs for each sampling block. Thus averaging results in a wrong phase.

2.2.8 Cross Correlation

In order to obtain a correct phase from Fourier transforms with several averaged blocks, it is necessary to perform a cross correlation with a reference signal before the averaging process takes place. For this the amplitude and phase spectrum of both signals are necessary. Complex numbers are used to describe amplitude and phase for ease of computation. The correlation power spectrum C(f) can be calculated from two signals F1(f) and F2(f) using the convolution theorem.

$$\overline{C(f)} = \overline{FT[c_{12}(\tau)]} = \overline{F_1(f) * F_2^*(f)} \quad (13)$$

The overbar indicates the averaged quantities. The asterisk denotes the conjugated complex values.

2.2.9 Auto Correlation

In order to evaluate the energy or power of a spectrum, the power spectrum P(f) must be calculated from the amplitude and phase spectrum or, easier, the complex spectrum. This is achieved by computing the auto correlation of the signal, which is calculated by the complex signal times the conjugated complex of the same signal.

$$\overline{P(f)} = \overline{FT[c_{11}(\tau)]} = \overline{F_1(f) * F_1^*(f)} \quad (14)$$

2.3 Combustion Theory

2.3.1 Flame Dynamics

For a continuous combustion process to take place air and fuel must flow into the combustion region. Often the turbulent feedline flow generates periodic disturbances such as vortex shedding off edges. In gas turbines the set of compressor stages represent an additional source of disruptions of vorticity and acoustics. While vorticity can only travel downstream, acoustic modes can travel up- and downstream. When they hit the fuel feed line at the injector, two situations can occur:

In real engines where a low loss-design is favored, the pressure drop over the fuel feed line is low. A small change in pressure of the airstream then alters the injector-pressure drop and consequently alters the fuel mass flow. Here, the acoustic wave in the air supply modulates the fuel flow. When this fluctuating fuel flow hits the combustion region, the heat release starts to fluctuate and at the same time, the equivalence ratio changes (Figure 30). This situation is difficult to investigate since some measurement techniques are sensitive to both heat release and equivalence ratios and consequently these effects cannot be isolated from each other.

Sometimes in experimental model combustors, where efficiency is not important, a large pressure drop over the injector makes it relatively insensitive to acoustic waves. The heat release rate is fairly constant, but the alternating air mass flow still generates equivalence ratio waves. Finally, a third setup is possible where air and fuel are premixed far upstream (Figure 31). When a homogenous mixture is achieved, flow modulations cannot cause equivalence ratio waves anymore. In this setup, only heat release fluctuations are possible. This is the preferred setup for investigations of heat release fluctuations because the uncertainty of equivalence ratio waves is eliminated.

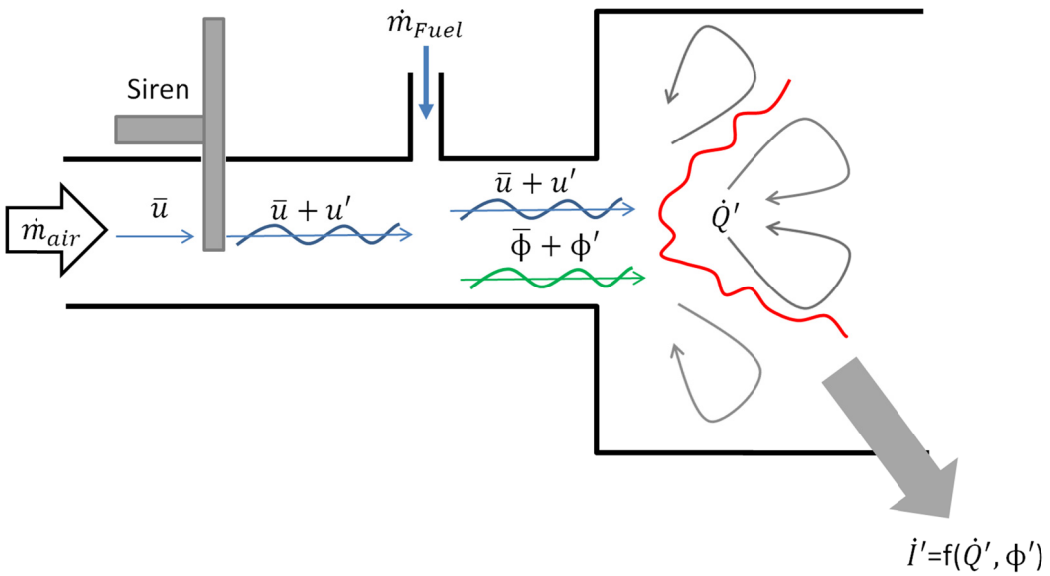

Figure 30: Industrial burner with low feedline impedance.

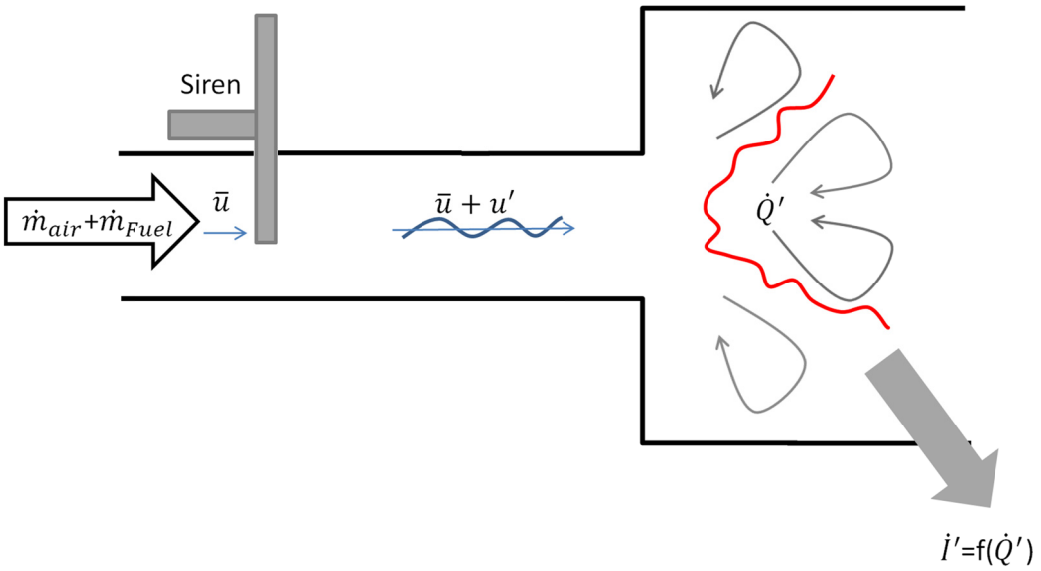

Figure 31: Perfectly premixed setup without equivalence ratio waves.

2.3.2 Thermoacoustic Coupling

In the previous chapter it was shown that the heat release can be influenced by the acoustics of a burner. The flame itself exhibits noise and usually attenuates certain frequencies while it dampens others. When the acoustic waves exhibited by the flame travel downwards and hit the combustor exit they are reflected to a certain degree. The reflected wave travels upwards and eventually passes the injector. If the geometrical properties of the burner are right, and the upwards traveling wave is in phase with the initial disruption (e.g. from the compressor rotor-blade), excitation of the instability takes place and amplitudes of pressure and heat release grow until acoustic dampening limits the process. If dampening in the system is low, amplitudes of pressure caused by thermoacoustic coupling can rise until structural integrity is compromised. The feedback loop of such a confined flame does not necessarily need to be closed via the fuel injector, several coupling mechanisms are known. Generally the stability of a combustion process was formulated by Rayleigh and is known as the stability criterion [22]:

$$\int_0^\tau \int_0^V p'(x,t)q'(x,t)dVdt > \int_0^\tau \int_0^V \phi_{dis}(x,t)dVdt \qquad (15)$$

It states, that if the integral of the local product of pressure fluctuation p' and heat release fluctuation q' exceeds the integral dampening (energy dissipation) Φ_{dis}, the coupling can turn into an acoustic instability. Where p‘ and q‘ are unsteady pressure and heat release, respectively, τ is the period of oscillation and V is the combustor volume (control volume). The driving potential gets a maximum if pressure and heat release fluctuations are in phase. For a thermoacoustic coupling, a feedback mechanism is necessary. This can, for example, happen in the following manner. Consider a flame which is disrupted by an incoming velocity disturbance of a certain frequency (Figure 32). If the flame is receptive to this frequency, it starts to fluctuate itself, radiating acoustic waves (pressure).

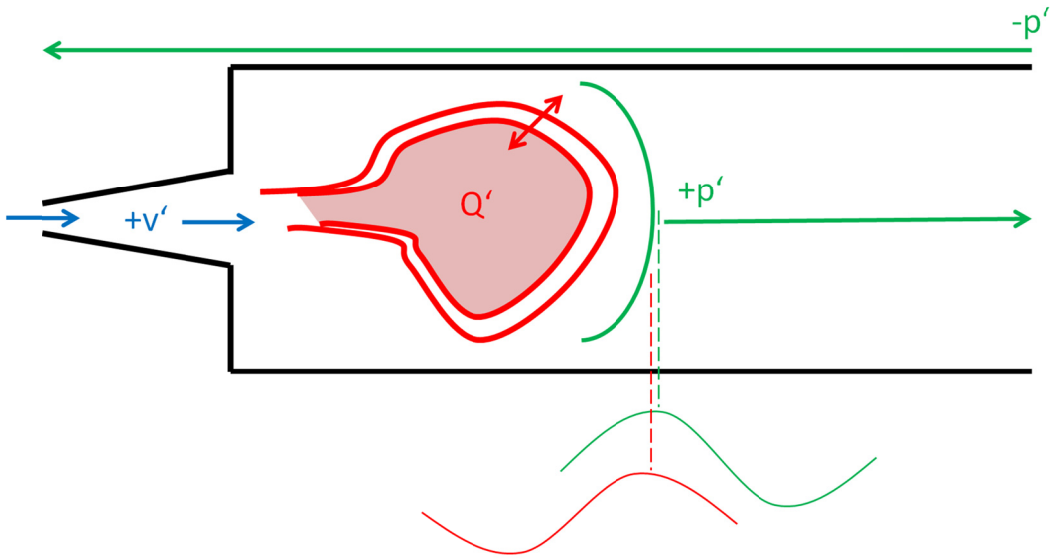

Figure 32: Heat-release-pressure-coupling in a combustor.

Depending on the design of the combustor exit, it may reflect the pressure wave to a certain degree in the form of a negative or positive pressure wave, traveling upstream. If this pressure wave interacts with the fluid upstream of the flame, for example at the fuel injector, it may modulate the mass flow and velocity at this point. If such a fluctuation is in phase with the original velocity fluctuation, excitation of the whole system can occur and can lead to large amplitudes which finally damage the equipment.

Lean combustion systems as developed in recent years for industry application are particularly susceptible to thermoacoustic coupling. At constant thermal power - for lean combustion – more air is required in the primary combustion zone, which then causes a cooler reaction. Consequently, less air is necessary to be injected in the downstream area of the liner in order to reach an appropriate turbine inlet temperature. In conventional combustion systems cooling air was usually injected through bores of different diameters in downstream section of the liner. As a side effect, those burners had a high level of acoustic dampening, which widely suppressed thermoacoustic coupling. With less cooling holes in modern burners where thermoacoustic coupling is less likely to be suppressed, combustion instabilities can arise.

2.3.3 Chemiluminescence

The reaction of oxygen and typical hydrocarbons in gas turbine combustion is highly exothermic. Most of the released energy is represented by the heat that increases the temperature of the reaction products. Additionally, a small fraction of the energy of that reaction is released in the form of electromagnetic waves.

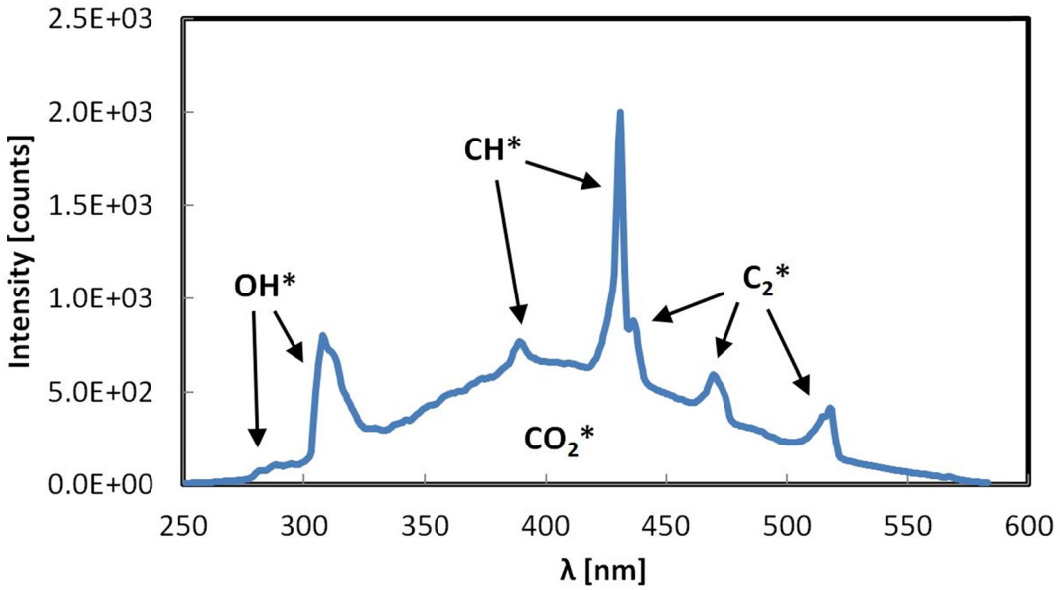

Figure 33: Typical spectrum of the chemiluminescence emitted by a methane air flame.

The light of the CO2 emission is distributed over the whole visible spectrum. Additionally radicals release light at distinct frequencies (Figure 33). OH*, CH* and C2* are the most dominant ones. While CO2 is a final product, CH* and OH* radicals are present in the very vicinity of the flame front or downstream of it and are therefore often used to visualize flames. With restrictions, proportionality exists between the light exhibited by certain radicals and the total energy released by the reaction. This link is often exploited in order to detect heat release by measuring the chemiluminescence of CH* and OH* radicals. Unfortunately the chemiluminescence intensity is also sensitive to equivalence ratio and strain rate. As shown in the experimental data from Lauer [18] (Figure 34), heat release monotonically increases with increasing equivalence ratios until unity. With increasing equivalence ratio OH*- and CH*-chemiluminescence increases as well. In contrast to the heat release however, the function is initially shaped concave and after an inflection point at around φ=0.8 the curve starts to be shaped convex. Therefore the trend is given with some restrictions in accuracy.

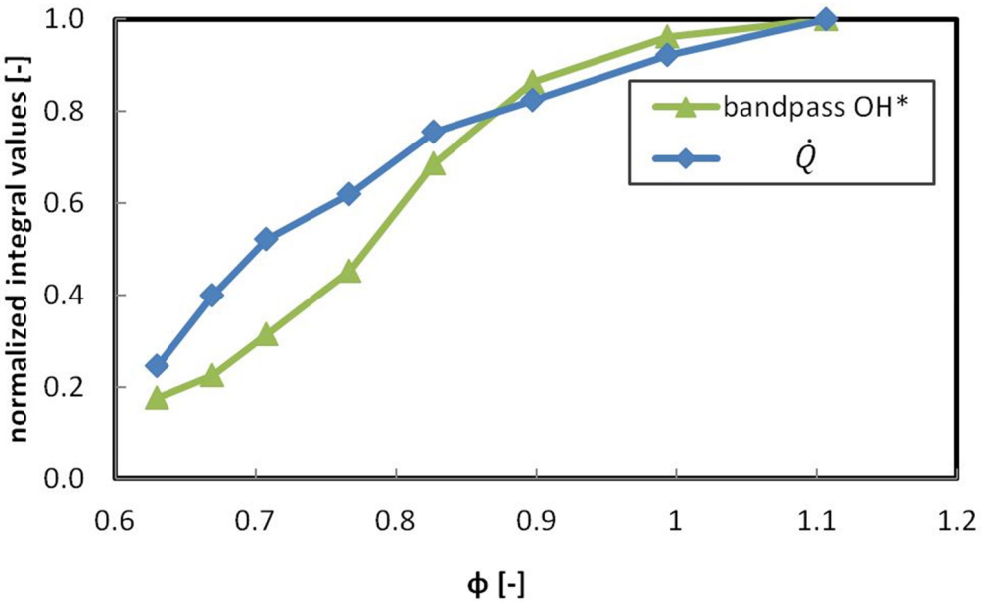

Figure 34: OH*-chemiluminescence and heat release rate as a function of equivalence ratio (data from Lauer [18]).

Additionally, the equivalence ratio is a function of strain rate, which can vary in the flame. This introduces an additional uncertainty as shown in (Figure 35). The strain rate is a measure of how much the flame front is stretched by velocity gradients in the flow. In contrast to heat release - where chemiluminescence can be misleading - for equivalence ratio measurements the quotient of OH* and CH* is a very robust measure [18]. OH* and CH* chemiluminescence

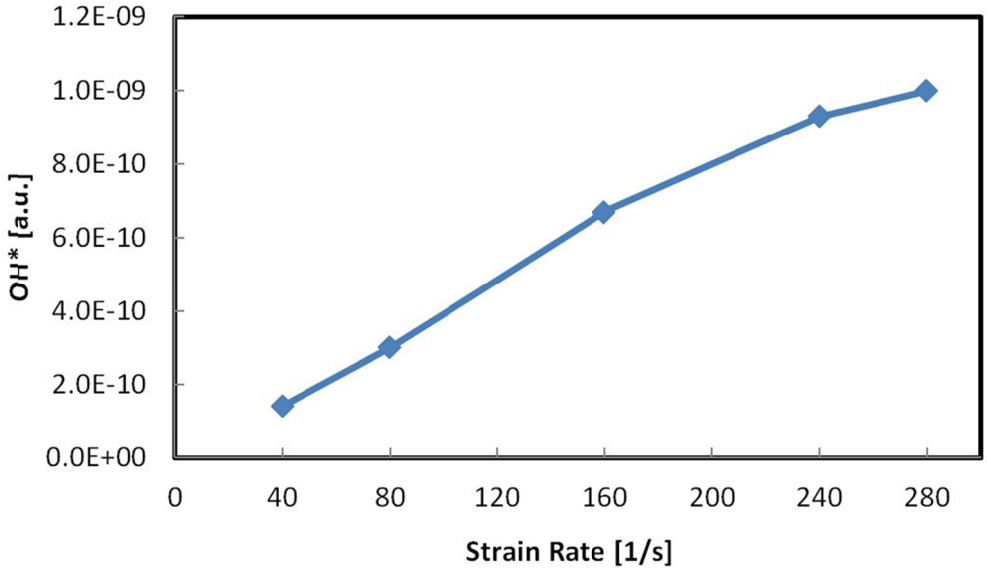

Figure 35: OH*-chemiluminescence as a function of strain rate (data taken from Panoutsos [52]).

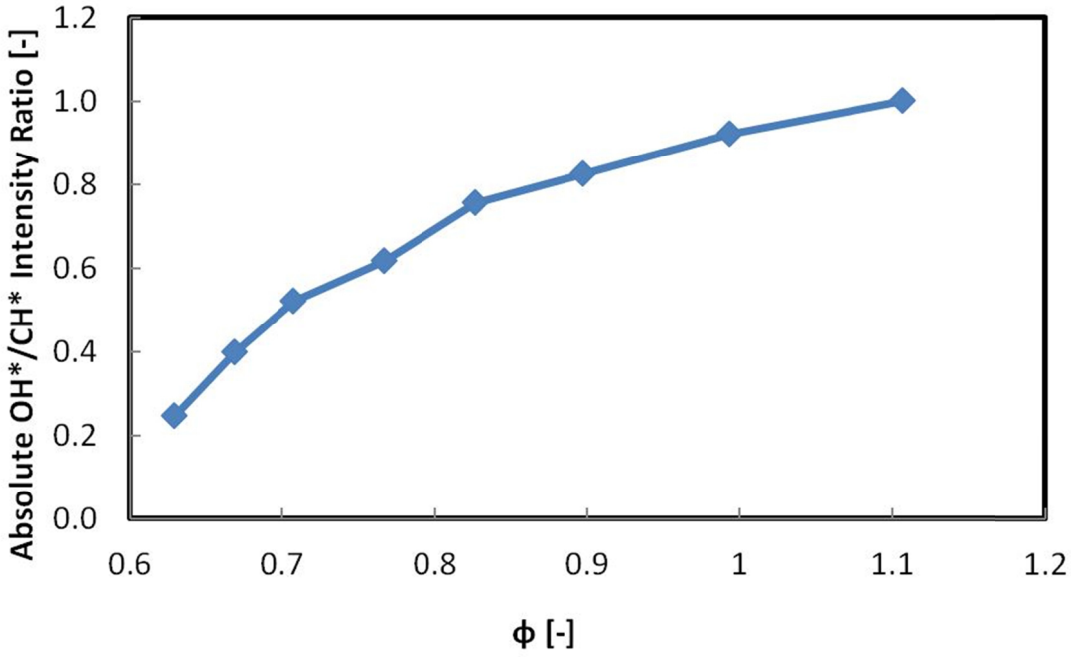

Figure 36: Ratio of OH*/CH*-intensity over equivalence ratio (data taken from Panoutsos [52])

depend on heat release in a similar manner. The quotient of both is a reliable parameter proportional to equivalence ratio only as shown in Figure 36.

2.3.4 Flame Transfer Function

For stability analysis tools which are quick and easy to use are preferred by industry in order to assess a large set of configurations and points of operation. One of these tools is the so called flame transfer function (FTF), which physically correlates the total heat release fluctuation Q' in the flame to the velocity fluctuation at the burner exit u'. Both are normalized by their mean values. Amplitude and phase are recorded as a function of excitation frequency. The FTF is generally defined by the following equation:

$$\mathrm{FTF} = \frac{\dot{Q}'/\bar{\dot{Q}}}{u'/\bar{u}} \tag{16}$$

The information of the FTF is a key input to network models, which can predict gas turbine stability. Network models were originally used in system dynamics analysis. In the model the flame remains a 'black box'. The flame is described as a single input single output block measured by the FTF. The flame transfer function can only account for the linear behavior of the flame. This is important when absolute amplitudes are investigated rather than the trend of the FTF. A variety of methods for the measurement of flame transfer functions in research combustors are in use. Measuring the chemiluminescence from OH* or CH* in the flame as the measure for heat release rate is widely applied. Velocity fluctuations at the burner exit are obtained either directly from hot wire anemometry or laser Doppler anemometry. On this basis, direct measurements of the FTF are only possible in flames, which

exhibit a proportionality between the heat release fluctuations flame chemiluminescence (OH* and/or CH*). This is the case in adiabatic flames with low strain rates and constant equivalence ratio, such as perfectly premixed flames [18]. On the other hand, an error is introduced in technically premixed combustion systems, where a linearity between OH* and CH* can no longer be assumed.

2.3.5 Coupling Mechanism Between dρ/dt and Q'

Although the rate of change of density fluctuations dρ/dt is an interesting quantity in combustion analysis, information about heat release is more sought-after by the engineer, since it describes the flame dynamics and the stability behavior more directly. Thus, in the following, a link between density fluctuations and heat release is established. Additionally, the limitations of this approach are discussed. Ideal gas is assumed and exposed to heat addition as usual in thermoacoustics studies. In differential form, the density fluctuations are related to the pressure (p) and temperature (T) fluctuations as follows:

$$d\rho = \left.\frac{\partial\rho}{\partial p}\right|_T dp + \left.\frac{\partial\rho}{\partial T}\right|_p dT \tag{17}$$

Elimination of dT from this equation using the first law of thermodynamics gives:

$$dq + \frac{dp}{\rho} = dh = c_p dT \tag{18}$$

with the heat release (q), enthalpy (h) and heat capacity at constant pressure (c_p). Combination with the ideal gas law

$$p = \rho RT \tag{19}$$

with the gas constant (R), leads to

$$d\rho = \left(\frac{1}{RT} - \frac{p}{RT^2}\frac{1}{\rho c_p}\right)dp - \frac{p}{RT^2}\frac{1}{c_p}dq \tag{20}$$

using

$$c_p = \frac{\kappa R}{\kappa - 1} \tag{21}$$

with the ratio of heat capacities κ and the relation between sound velocity c and temperature

$$c = \sqrt{\kappa R T} \tag{22}$$

results in:

$$\frac{d\rho}{dt} = \frac{1}{c^2}\frac{dp}{dt} - \frac{\kappa - 1}{c^2}\frac{dq_V}{dt} \tag{23}$$

This is the most general solution used and discussed by several authors [24, 29]. The time derivatives in Equation (23) express the fluctuation components of density, pressure and heat release. It is common practice to replace the material derivatives by partial derivatives when studying thermoacoustic low Mach numbers problems. With the link between the material derivatives of a general variable (a) and partial derivatives for time t, and the space coordinates x, y, z:

$$\begin{aligned} \frac{d}{dt}a(x,y,z,t) \; &= \frac{\partial}{\partial t}a(x,y,z,t) \\ &+ \frac{\partial}{\partial x}a(x,y,z,t)\frac{\partial x}{\partial t} \\ &+ \frac{\partial}{\partial y}a(x,y,z,t)\frac{\partial y}{\partial t} \\ &+ \frac{\partial}{\partial z}a(x,y,z,t)\;\frac{\partial z}{\partial t} \end{aligned} \tag{24}$$

This gives:

$$\frac{\partial \rho'}{\partial t} = \frac{1}{c^2}\frac{\partial p'}{\partial t} - \frac{\kappa - 1}{c^2}\frac{\partial q_V{}'}{\partial t} \tag{25}$$

This implies the assumption that the convective transport of the heat release fluctuations has no effect on the driving potential of thermoacoustic instabilities. The use of partial derivatives allows the treatment of wave propagation separate from the heat release in e.g. hybrid field methods using the inhomogeneous wave equation [53], Acoustic Perturbation Equations (APE) [54] as well as Linearized Euler Equations (LEE) and Linearized Navier Stokes Equations (LNSE) (e.g. [55]). In isothermal flows, the heat input is zero and the density fluctuations represent the change of pressure in the system:

$$\frac{\partial \rho'}{\partial t} = \frac{1}{c^2}\frac{\partial p'}{\partial t} \tag{26}$$

then e.g. acoustic waves can be detected with the aid of density fluctuations as done by [29, 36]. In reacting flows on the other hand, where heat input is considerable, it can be shown that the pressure

term can be neglected in the combustion zone (flame) because it is at least an order of magnitude smaller than the other terms in Equation (25) [24, 56]. This finally leads to:

$$\frac{\partial \rho'}{\partial t} = -\frac{\kappa - 1}{c^2}\frac{\partial {q_V}'}{\partial t} \tag{27}$$

Equation (27) reveals a proportionality between the time derivatives of density fluctuation recorded by vibrometers and the heat release fluctuations in the flame front [29]. It is of particular interest to experimentally investigate whether the local and global proportionality between density fluctuations and fluctuating heat release rate in the flame exists in reality. As shown later, this is not always the case (a.) because for not fully adiabatic conditions density fluctuations also occur outside the flame front and (b.) because changes in density are present in the products, which is both the case for combustion with spatially or temporal varying equivalence ratio.

2.3.6 Influence of the Speed of Sound

As shown in equation (27), the link between density gradients and heat release includes the speed of sound. Therefore, to quantify the heat release exactly, it is necessary to detect the temperature for a given gas in the system. As an alternative, if pressure fluctuations are not present, the heat release can be expressed as a function of absolute density and density gradients only. Starting off with the coupling equation without pressure (eq. (27).) and substituting the speed of sound results in:

$$\frac{d\rho'}{dt} = -\frac{\kappa - 1}{\kappa R T}\frac{d{q_V}'}{dt} \tag{28}$$

and employing the ideal gas equation gives

$$\frac{d\rho'}{dt} = -\frac{\rho(\kappa - 1)}{p\kappa}\frac{d{q_V}'}{dt} \tag{29}$$

since pressure fluctuations are already assumed to be small in the flame, the mean pressure can be assumed without including an additional error, as it is necessary to detect absolute density. This can be carried out with methods such as shearography.

$$\frac{1}{\rho}\frac{d\rho'}{dt} = -\frac{(\kappa - 1)}{p\kappa}\frac{d{q_V}'}{dt} \tag{30}$$

2.4 Combustion Noise

The combustion process in laminar flames as seen in candles is almost silent, while turbulent combustion as predominantly applied in industrial burners can be very violent and exhibit high amplitudes of noise. This noise can be particularly severe when the reaction takes place at elevated pressure. Combustion generated noise has been a topic for many years in industrial applications where reacting flows are predominantly turbulent. Especially the prediction, and consequently the reduction of correlated and stochastic sound radiation of flames have been investigated intensively [57, 58]. Early theories as well as experimental validations suggest that the far-field sound pressure is proportional to fluctuations of heat release in the flame [59]. For measurability, many publications supported the use of the time derivative of OH*-Chemiluminescence [60]. However, the density distribution in the flame had to be assumed. Alternatively, early work [44] suggested the use of density fluctuations in the flame (ρ'_T) integrated over the flame volume (V) in order to estimate density fluctuations in the far-field (ρ') and consequently combustion noise:

$$\rho'(r) = \frac{1}{4\pi c_0^2 r}\frac{\partial^2}{\partial t^2}\int_V \rho'_T\left(r_0, t - \frac{r}{c_0}\right) dV(r_0) \qquad (31)$$

with (c_0) speed of sound in the far-field , radial distance (r) of observer and radius (r_0) of the flame. Since time resolved density fluctuations were difficult to measure, an adaption of the equation with application of OH*-chemiluminescence estimating the mean density in the flame was often preferred [58]. The development of the LIV technique and experimental work enabled accurate measurements of time resolved line-of-sight and local density fluctuations in turbulent jets [21, 42] and in laminar [29, 31] and turbulent flames [30]. With this basis, it is possible to prove Strahle's assumption directly. In the following, sound power as a function of sound intensity and consequently of $\partial\rho'_T/\partial t$ is derived. Comparing sound power has the advantage that this number does not depend on the distance of the observer (microphone) in contrast to sound intensity. It has the same significance as comparing density fluctuations since in the far-field sound power is a direct function of the density fluctuation. Additional information about the pp-probe is provided in appendix C. This is necessary because in a laboratory environment the far-field condition for low frequencies is usually not fulfilled and flames have a low pass characteristic. This means that combustion noise is of rather low frequencies because high frequencies of feedline modulation are filtered by the flame.

2.4.1 Calculation of Sound Power from $\partial\rho'_T/\partial t$

In the far-field where sound pressure p' and particle velocity are in phase, sound power P_{far} can be calculated from density fluctuations as follows.

$$P_{far} = 4\pi r^2 \frac{p'^2}{\rho_0 c_0} = 4\pi r^2 \frac{(c_0^2\rho')^2}{\rho_0 c_0} \qquad (32)$$

with the mean density in the far-field ρ_0. A sphere is defined as the detection surface. Combining Equation (31) and Equation (32) results in the sound power as a function of density fluctuations:

$$P_{far} = \frac{1}{4\pi\rho_0 c_0}\left(\frac{\partial^2}{\partial t^2}\int_V \rho'_T\left(r_0, -\frac{r}{c_0}\right)dV(r_0)\right)^2 \quad (33)$$

with radius r of the surface. After performing a fast Fourier transform (FFT) - now in the frequency domain - the time derivative of a variable is simply the variable times the angular frequency with a time lag of pi/2:

$$FFT\left(\frac{\partial \rho'_T}{\partial t}\right) = 2\pi f * FFT(\rho'_T, angle - 90°) \quad (34)$$

Replacing the integral by the sum of all measurement points (MP) times the measurement volume, the power can be calculated as follows (in the frequency domain):

$$\mathrm{P_{far}(f)} = \frac{1}{4\pi\rho_0 c_0}\left(2\pi \mathrm{f}\sum_{\mathrm{MP=1}}^{\mathrm{n}}\frac{4}{\pi}\mathrm{A_{meas}}\zeta\frac{\partial \rho'_{\mathrm{T}}}{\partial \mathrm{t}}_{\mathrm{A}}(\mathrm{phas}-90°)\left(\mathrm{r_0}, \mathrm{t}-\frac{\mathrm{r}}{\mathrm{c_0}}, \mathrm{f}\right)\right)^2 \quad (35)$$

with A_{meas} * ζ the measurement area times the measurement length. The factor 4/π corrects the measurement area for a circular laser beam in a rectangular measurement grid. For the total sound power the sum over all frequencies is

$$\sum_f P_{far}(f) = \sum_f \frac{1}{4\pi\rho_0 c_0}\left(2\pi f\sum_{MP=1}^{n}\frac{4}{\pi}A_{meas}\zeta\frac{\partial \rho'_T}{\partial t}(phase-90°)\left(r_0, t-\frac{r}{c_0}\right)\right)^2 \quad (36)$$

2.4.2 Calculation of Sound Power from PP-Probe

In the near field where sound pressure p' and particle velocity $\vec{v}$ are not in phase, sound power P can be calculated via sound intensity $\vec{I}$:

$$P = \int_A \vec{I}dA \int_A p'\vec{v}dA \quad (37)$$

Pressure is far easier to measure than particle velocity, therefore, the Euler equation is often used to estimate the particle velocity:

$$\frac{\partial v}{\partial t} = -\frac{1}{\rho_0}\frac{\partial p}{\partial r} \quad (38)$$

The velocity along one dimension can then be expressed as a function of the pressure at two different positions:

$$v = -\frac{1}{\rho_0}\int_t \frac{p_{r+\Delta r} - p_r}{\Delta r}\,dt \tag{39}$$

As a consequence, the sound intensity can be calculated by

$$I = pv = -\frac{p_{r+\Delta r} + p_r}{2}\frac{1}{\rho_0}\int_{At} \frac{p_{r+\Delta r} - p_r}{\Delta r}\,dt \tag{40}$$

For spectral analysis this equation can be expressed as a function of the imaginary part of the cross spectral density of the complex pressures (CPSD):

$$I = pv = -\frac{1}{\rho_0 2\pi f \Delta r} Im(CPSD) \tag{41}$$

The cross power spectral density in the frequency domain can then be calculated from the cross power spectrum (CPS) divided by the equivalent nose band width (ENBW) [51]. The ENBW is constant for a constant frequency resolution Δf and a given window function. The CPS is the complex conjugated multiplication of the individual complex amplitudes:

$$CPSD = \frac{CPS}{ENBW} = \frac{FFT(p_{r+\Delta r)} \times FFT(p_{r)}}{ENBW} = \frac{FFT(p_{r+\Delta r)} * FFT(p_{r)}^{*}}{ENBW} \tag{42}$$

The equation holds true if the flame diameter is small compared to the wavelength and distance to the observer. If the flame diameter is large the spatial distribution of coherent heat release cannot be neglected anymore. Extinction and amplification of pressure waves from local heat release (density) fluctuations would depend on the position of the source in the flame. For small flames the noise is proportional to the total heat release [44].

3 Results and Discussion

The results obtained during this research are discussed by means of selected publications (Table 1) in the following chapter. The results are organized into three sections. In the fundamentals section limitations of the system are analyzed and validation is performed. In the second section of the results, the application of the system and usability with respect to thermo-acoustics is discussed. In the final section it is shown that combustion noise can be predicted by means of LIV measurements.

Table 1: Selected publications on LIV in combustion.

Title	Journal/Conference	Abbreviation
LASER VIBROMETRY FOR COMBUSTION DIAGNOSTICS IN THERMOACOUSTIC RESEARCH	J. Peterleithner and J. Woisetschläger, Technisches Messen, vol. 82, no. 11, pp. 549-555, 2015.	Peterleithner et al. 2015 A [61]
ANALYSIS OF MEASURED FLAME TRANSFER FUNCTIONS WITH LOCALLY RESOLVED DENSITY FLUCTUATION AND OH-CHEMILUMINESCENCE DATA	J. Peterleithner, N. V. Stadlmair, J. Woisetschläger and T. Sattelmayer, Journal of Engineering for Gas Turbines and Power, vol. 138, no. 3, 2016.	Peterleithner et al. 2015 B [30]
INTERFEROMETRIC INVESTIGATION OF THE THERMO-ACOUSTICS IN A SWIRL STABILIZED METHANE FLAME	J. Peterleithner, A. Marn and J. Woisetschläger, in Proceedings of the ASME Turbo Expo, 2015.	Peterleithner et al. 2015 C [62]
COMPARISON OF FLAME TRANSFER FUNCTIONS ACQUIRED BY CHEMILUMINESCENCE AND DENSITY FLUCTUATION	J. Peterleithner, R. Basso, F. Heitmeir, J. Woisetschläger, Schlüßler. R., Czarske. J. and A. Fischer, in Proc. ASME Turbo Expo, 2016.	Peterleithner et al. 2016 A [63]
ANALYSIS OF COMBUSTION NOISE USING LOCALLY RESOLVED DENSITY FLUCTUATIONS AND A MICROPHONE ARRAY	Johannes Peterleithner, Stefan Zerobin, Jakob Woisetschläger in Proc. ASME Turbo Expo, 2016.	Peterleithner et al. 2016 B [64]

Contribution of co-authors to the publications:

In order of appearance, for all Publications listed above ao.Univ.-Prof. Dipl.-Ing. Dr.techn. Woisetschläger contributed significantly to this work not only passively as a supervisor but also by providing support with a range of sophisticated optical measurement techniques as well as by initiating discussions triggering new directions of investigation.
For ‘Peterleithner et al. 2015 B’ [30], Dipl.-Ing. Nicolai Stadlmair and Prof. Dr. Thomas Sattelmayer from TU München enabled measurements at their combustion test rig which features a down scaled close-to-industry burner with a well-controlled flame. They also provided substantial combustion knowledge leading to this paper.

For ‘Peterleithner et al. 2015 C’ [62], Dipl.-Ing. Dr.techn. Andreas Marn contributed by performing the CFD calculations of the burner-plenum and with several discussions providing technical input.
For ‘Peterleithner et al. 2016 A’ [63] Mr. Basso measured and post processed the chemiluminescence images. Univ.-Prof. Dr.-Ing. Franz Heitmeir is head of the Institut for Thermal Turbomachinery and Machine Dynamics, TU Graz and contributed to the new test rig and laboratory.
Dipl.-Phys. Raimund Schlüßler, Prof. Czarske and PD Dr.-Ing. habil. Andreas Fischer provided the FM-DGV system as well as the necessary know-how in order to acquire and post process the velocity fields of the flame.
For ‘Peterleithner et al. 2016 B’, Dipl.-Ing. Stefan Zerobin provided support with the installation of the microphone setup and the acquisition routines.

3.1 Fundamentals and Uncertainties

3.1.1 Uncertainty Analysis of Heat Measurements - Speed of Sound

When applied to combustion research, LIV reveals some uncertainties. They must be considered in order to receive meaningful results. In the first paper of this chapter (PETERLEITHNER ET AL. 2015 A) a comprehensive overview of the measurement technique is given. Limits of the coupling relation (resonance) as well as in the detection of pressure fluctuation in the combustor are demonstrated by the example of an experimental burner. The variable geometry burner used in this investigation uses swirl-stabilization for flame anchoring. The swirl strength is set by the ratio between axial and tangential air without changing the overall air-fuel-ratio. The burner was combined with an optically accessible combustion chamber at atmospheric pressure. As point of operation a power of 3.4 kW, a global equivalence ratio of 0.68 and a swirl number of 0.65 were set. The first characterization of the burner was performed using OH*-chemiluminescence which showed mean values of heat release and a 'brightest-pixel' technique of schlieren visualization which showed the regions of strongest density fluctuations. Those techniques were used as a confidence check and to validate the vibrometry technique. One influence found, was the distortion of heat release results due to a varying speed of sound in the combustor. Although traditionally assumed to be constant [24], changing temperature varies the speed of sound and consequently alters the heat release distribution. When correcting the local speed of sound for mean values of temperature, absolute values of heat release change but the relative distribution of heat release experience only minor differences. Shown below (Figure 37), the real region of heat release is slightly shifted compared to the one without temperature correction. The peak value is dampened due to the high values of heat release which are usually accompanied by higher values of temperature. The region outside the flame is of minor importance since there, density fluctuations are close to zero.

In the second part of PETERLEITHNER ET AL. 2015 A the velocity of convective heat above the flame is detected by measuring the phase difference between the two vibrometers.

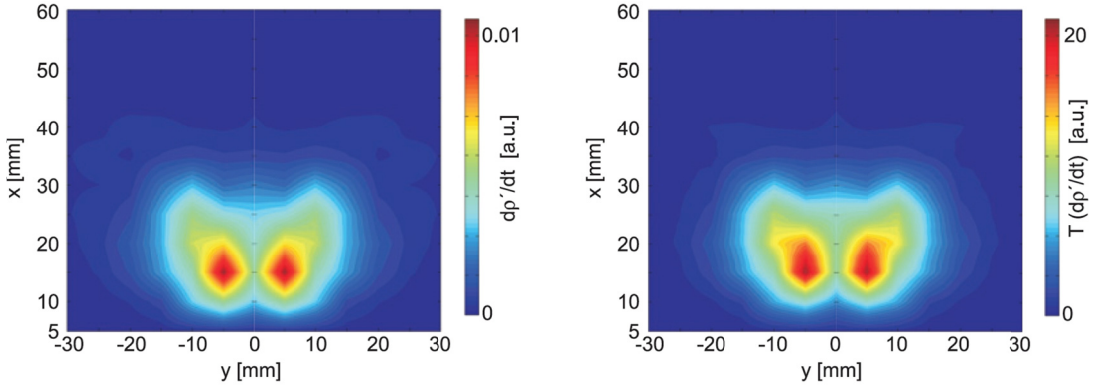

Figure 37: Density-gradient fluctuations with (left) and without (right) temperature correction.

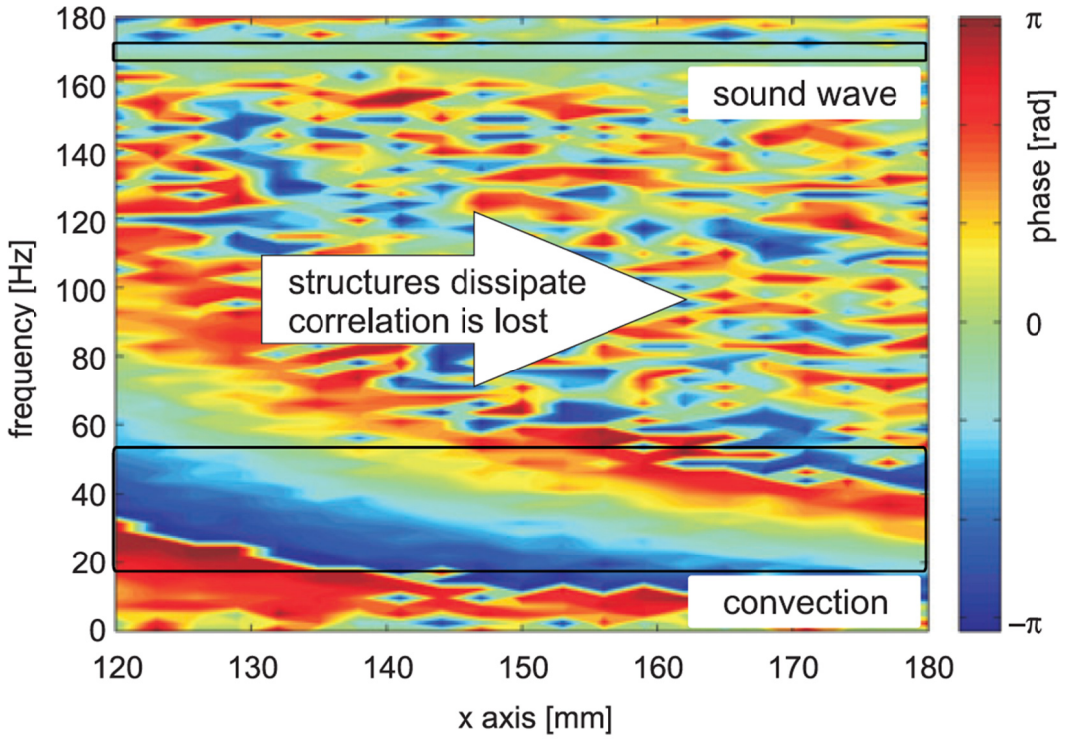

Figure 38: Phase difference between two vibrometers above the flame as a function of the distance between the two measurement beams.

This is done by means of two vibrometers and a correlation technique. One of the vibrometers was traversed and one set up at a fixed position. It was found that for good correlations long measurement times are necessary. The dissipation of convective structures was visualized as shown below (Figure 38). The fact that the correlation between the two signals is lost is interpreted as the dissipation of the structures. Smaller structures at higher frequencies dissipate quicker than big structures at low frequencies. The region of coherent structures (bottom left) shows a continuous change of phase. In contrast to this, the phase changes randomly for higher frequencies and with increasing distance between the vibrometers. Then only noise is detected. On the very top of the plot at app. 170 Hz the phase does not change with increasing distance between the vibrometers. This almost identical phase can only be caused by structures of high velocity. For low Mach number flow problems such as many combustion applications, these structures can only be sound waves. They can be easily distinguished from entropy fluctuations which travel with the speed of the bulk flow.

3.1.2 Uncertainty of Density Measurements – Refractive Index and Gladstone-Dale Constant

Density fluctuations are derived from the refractive index of a gas via dispersion relations using the Gladstone-Dale constant as shown above. Thus, the refractive index and Gladstone-Dale constant vary with the type of gas. The flames investigated in this work comprise mainly oxygen, nitrogen, methane, carbon dioxide and steam. Values can be found for those gases in Table 2. At the vibrometers wave-

length of 633 nm the variation of refractive indices is below .2 per mill. [65]. Therefore in case of mixture-inhomogeneity, the uncertainty of refractive index can be disregarded.

Table 2: The refractive index and the Gladstone-Dale constant for different gases at 633nm according to Loria and Gardiner [20, 65].

Gas	O_2	N_2	CH_4	CO_2	Steam
n	1.0002513	1.0002977	1.0004414	1.0004477	-
G	1.89E-04	2.39E-04	6.17E-04	2.26E-04	3.12E-04

The Gladstone dale constant on the other hand, significantly changes with gas composition and must therefore be analyzed in detail. As shown in Figure 39, there is a discrepancy between products and reactants. For both, the Gladstone Dale constant increases continuously with richer mixtures. G of the reactants increases linearly with the equivalence ratio. In contrast to this, for the products, G increases on a gentle slope until an equivalence ratio of unity. From then on it is characterized by a steep slope, where a small change of equivalence ratio causes a rather big variation in the Gladstone dale constant. Thus the difference between products and reactants gradually increases. As a consequence lean mixtures provide a smaller variation between reactants and products. Due to the fact that during the measurement, there is no easy way to distinguish between products and reactants, this variation cannot be avoided and will cause a loss of accuracy. For equivalence ratios below 1.16 the error is smaller than 2% as shown in Figure 39. On the other hand, equivalence ratios beyond 1.16 introduce a higher uncertainty which even increases gradually with the equivalence ratio.

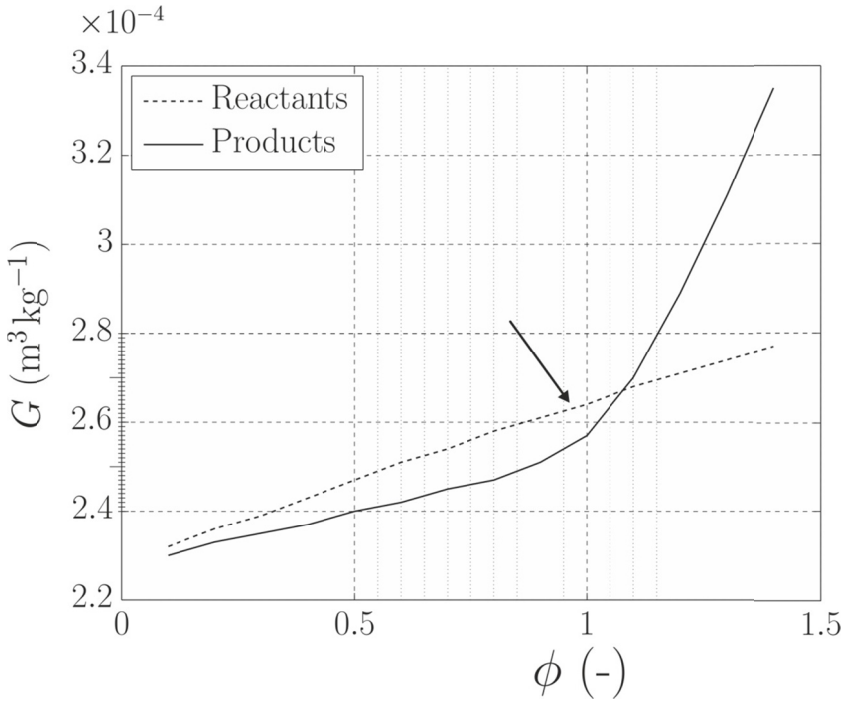

Figure 39: The Gladstone dale constant of a methane-air flame as a function of equivalence ratio (data taken from Leitgeb et al. [29]).

This is mainly because of methane having a high value of G and being only partly consumed at rich conditions. In contrast to this, for lean conditions oxygen - with the lowest G in the reaction - is less consumed by the reaction.

Beside the theoretical analysis of uncertainties, it is of interest for the combustion diagnosis community, to compare the system with other techniques in a turbulent large scale flame. This was done in Peterleithner et al. 2015 B. There LIV was benchmarked against chemiluminescence and the so-called multi-microphone-method (MMM). In this research the flame investigated is typical for gas turbine combustion with a mean equivalence ratio of 0.7. When the fresh gases are perfectly premixed, the Gladstone Dale constant is calculated as the mean value of products and reactants which gives a mean value of 2.495e-4 with an uncertainty of +- 0.045e-4 or +-1.6%. On the other hand technically premixed flames, common in industry, can introduce fluctuations of equivalence ratio as described in the theory chapter. With appearance of those mixture inhomogeneities, the Gladstone-Dale constant would ideally have to be adapted accordingly in order to provide a correct value of density fluctuations. Then, the instantaneous local gas composition would have to be known which is experimentally challenging. Assuming a mean Gladstone-Dale constant on the other hand distorts the resulting density fluctuations, but dramatically simplifies the procedure. Since these local and periodic changes are unknown, the accuracy of the measurement suffers. Equivalence ratio waves were intentionally introduced in Peterleithner et al. 2015 B in order to quantify the accuracy of the LIV measurement technique with respect to varying G. The fluctuations of Φ are shown in Figure 40 as a function of axial position in the flame and in

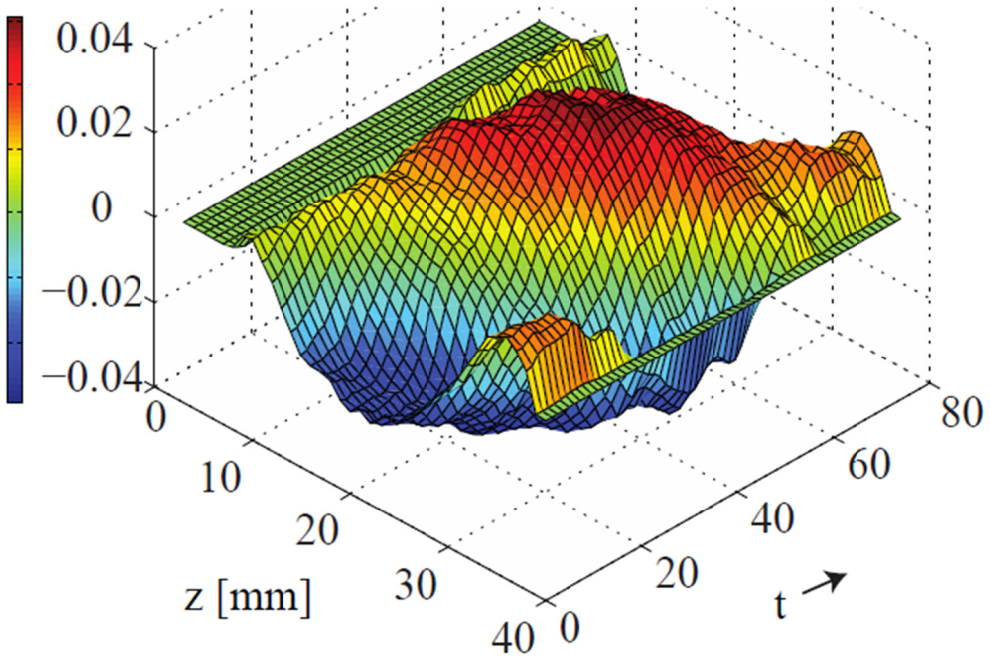

Figure 40: Equivalence ratio waves detected by OH*/CH*-ratio measurements.

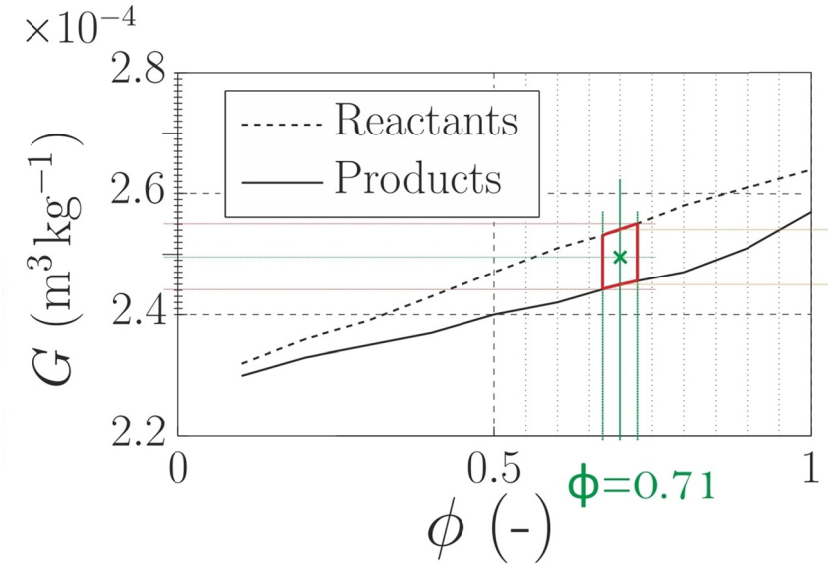

Figure 41: Gladstone Dale constant of uncertainties of mixture variation (data taken from Leitgeb et al. [29]).

one period of excitation. For this flame, the equivalence ratio fluctuations were around 4%. Consequently, the equivalence ratio varies between 0.672 and 0.728 (Figure 40). This increases the uncertainty of the Gladstone Dale constant, including the mixture uncertainty, to a total value of +-2.2 %. The uncertainties are shown in Table 3.

Table 3: Error estimation for a methane flame of Φ = 0.7, considering the uncertainty from Figure 41.

	error
reaction uncertainty	+-1.6%
reaction + Φ'-uncertainty	+-2.2%

The above error estimation was carried out for the flame investigated in [30] where time resolved experimental data for the equivalence ratio waves was available. The values of Table 3 do represent errors for this flame. For different flames the uncertainty can change.

The above error analysis was carried out on the hypothesis that the equivalence ratio is homogenous and its value is modulated by the siren. Effects at a high degree of unmixedness of the gases due to violent fluctuations are not considered. To quantify this in detail, remains an open field of research. The worst case scenario observed in our studies with the variable geometry burner was a change of equivalence ratio due to the mixing with ambient air on the side of the flame. This has been documented in [66] were the local equivalence ratio varied within the flame volume by 30%. In case the Gladstone-Dale constant would not be adapted to these local variations, a worst case systematic error of ±5% would result from above considerations. This error is still relatively low because the curve of reactants and products in Figure 41 is rather flat-angled. This systematic error can be reduced by local or temporal OH*/CH* recordings estimating the variations in the Gladstone-Dale constant.

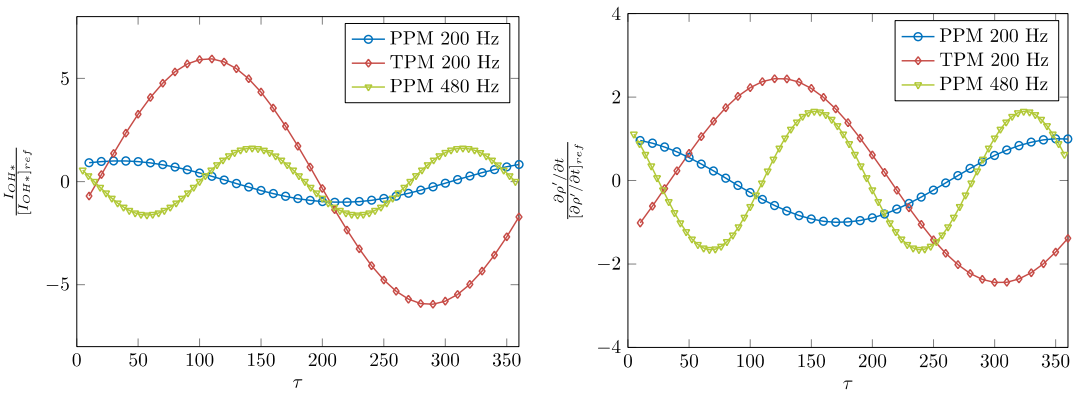

Figure 42: Heat release fluctuations detected by OH*(left) and LIV (right).

3.1.3 Comparison of LIV and OH*-Chemiluminescence

On basis of the previously stated uncertainty analysis, in the paper Peterleithner et al. 2015 B, the focus is specifically on the validation of the technique in a gas turbine relevant combustor at atmospheric conditions. This is the first publication to draw a quantitative comparison of heat release measured by LIV in a turbulent flame. The heat release detected from laser vibrometry was compared to the conventional technique of recording OH*-chemiluminescence. Due to the low errors found above and the comparably strong influence of the equivalence ratio onto chemiluminescence [26, 18] the expectation was to find more accurate results for heat release by measuring the density fluctuations rather than light intensity fluctuations. Secondly, the integral heat release fluctuations were compared to a purely acoustical method, called multi-microphone-method (MMM), which is also independent of the equivalence ratio. The results were integrated over the combustion region. On an integral level, LIV matched the MMM better than the OH*-Chemiluminescence did. For technically premixed flames, the OH*-chemiluminescence showed a significant overshoot caused by equivalence ratio waves (Figure 42). Perfectly premixed flames were in good agreement for all three measurement techniques.

3.1.4 Reviewed articles on Fundamentals and Uncertainties:

- PETERLEITHNER ET AL. 2015 A

J. Peterleithner and J. Woisetschläger, "Laser vibrometry for combustion diagnostics in thermoacoustic research," Technisches Messen, vol. 82, no. 11, pp. 549-555, 2015.

- Peterleithner et al. 2015 B.

J. Peterleithner, N. V. Stadlmair, J. Woisetschläger and T. Sattelmayer, "Analysis of measured flame transfer functions with locally resolved density fluctuation and OH-Chemiluminescence Data," Journal of Engineering for Gas Turbines and Power, vol. 138, no. 3, 2016.

Beiträge

Johannes Peterleithner and Jakob Woisetschläger*

Laser vibrometry for combustion diagnostics in thermoacoustic research

Untersuchung thermoakustischer Oszillationen mittels Laservibrometer

DOI 10.1515/teme-2015-0072
Received August 17, 2015; accepted September 9, 2015

Abstract: A novel technique for time- and space-resolved measurement of density fluctuation is presented. It is non-intrusive and based on laser Doppler vibrometry. The density fluctuations reveal information on dynamic heat release and fluid velocity. The significance of this technique is proven by recording thermo-acoustic oscillations in a model combustor.

Keywords: Interferometry, laser vibrometry, thermoacoustics, combustion diagnostics.

Zusammenfassung: Es wird ein neuartiges Verfahren zur frequenz- und ortsaufgelösten Messung von Dichteschwankungen vorgestellt, welches berührungslos arbeitet und auf der interferometrischen Laser-Doppler-Vibrometrie beruht. Sowohl die Schwankungen der Wärmefreisetzung in Flammen als auch die Strömungsgeschwindigkeit lassen sich mit diesem Verfahren bestimmen. Die Aussagekraft dieser neuen Messmethode wurde mit der Untersuchung von thermoakustischen Oszillationen einer Methanflamme unter Beweis gestellt.

Schlüsselwörter: Interferometrie, Laser Vibrometer, Thermoakustik, Verbrennungsdiagnostik.

1 Introduction

State-of-the-art technology in industrial gas turbines for power generation uses lean-premixed combustion for high combustion efficiency and low emissions. High power densities and lean combustion increase the susceptibility to thermoacoustic oscillations. These instabilities arise from the positive coupling between the fluctuations of pressure and heat release [1], cause combustion noise and can damage the machine during operation. High temperatures, high turbulence and the need for local data name only few of the challenges experienced in such arrangements of powerful burners in the order of 1 MW of power each. Techniques to prevent thermo-acoustic oscillations are not only relevant in lean-premixed gas turbine combustors but also in mobile heaters, industrial furnaces boilers and lately aero-engines.

A number of sophisticated measurement techniques are currently used to tackle these problems including microphone arrays, pressure and temperature sensors, high-speed intensified cameras, chemiluminescence, schlieren technique, Rayleigh and Raman scattering, particle image velocimetry, Doppler global velocimetry and laser velocimetry. All these currently used techniques lack either the necessary time resolution, do not provide local data or need tracer particles added to the flow.

On the other hand, in designing new machinery with reduced noise emission from surface vibrations heterodyne interferometric methods are a powerful tool to provide local frequency spectra of vibration. Currently, one of the most used technologies in vibration detection is laser vibrometry. In this work presented here we give all information needed to record local and global heat release fluctuations from flames using commercially available laser vibrometers whenever optical access is granted to the combustion zone. It is also shown that by correlating the time signals from two laser vibrometers velocities can be recorded without the need for additional tracer particles or mechanically probing the test section.

2 Background

Laser vibrometers (LV) are interferometric systems widely used to detect surface vibrations from machinery. With an acousto-optic modulator as frequency modulator these in-

***Corresponding author: Jakob Woisetschläger,** Technische Universität Graz, e-mail: jakob.woisetschlaeger@tugraz.at
Johannes Peterleithner: Technische Universität Graz

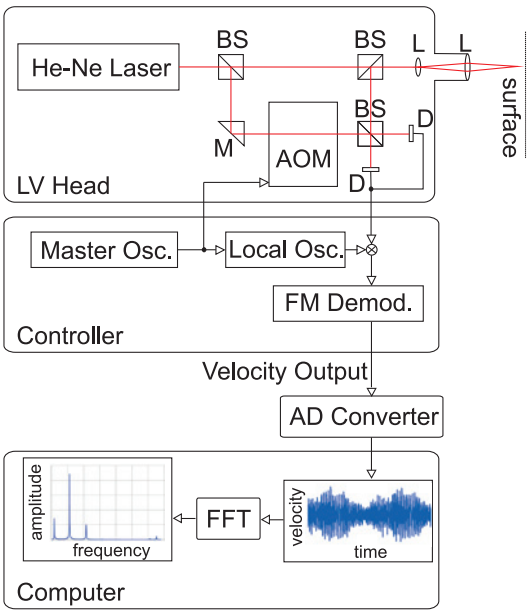

Figure 1: Setup of a laser vibrometer for surface vibration recording [2]. BS beam splitter, M mirror, L lens, AOM acousto-optic modulator.

terferometers record vibration velocity rather than vibration amplitude. The basic principle of such a system is shown in Figure 1 as provided by [2]. Using interferometric techniques these powerful commercially available systems can detect vibrations without mechanical contact to the surface, and provide sub-nanometer resolution at wide frequency ranges.

In combustion research at TU Graz such systems are used to detect density fluctuations with fixed geometry in the optical path because LV then directly record the time derivative of density fluctuations [3–7]. Generally the changes in density occur through changes of pressure p or entropy s. Employing the first law of thermodynamics and assuming perfect gas [8] leads to

$$\frac{d\rho}{dt} = \frac{1}{c^2}\frac{dp}{dt} - \frac{(\kappa-1)}{c^2}\dot{q}_V, \tag{1}$$

with $\dot{q}_V$ the heat release rate per unit volume, p pressure, c speed of sound, κ ratio of the specific heat capacities and t time. It can be shown that the pressure term can be neglected in flames, because it is at least one order of magnitude smaller than the other terms in Equation (1) [8, 9]. This proportionality between the time derivatives of density recorded by LV and the desired heat release rate in the flame was first used by [4] and proven by [5]. The time derivatives in Equation (1) express the contributions of pressure and heat release to the density fluctuations recorded. Under the assumption that the LV records data only in the flame where pressure fluctuations can be neglected we get

$$\frac{d\rho}{dt} = -\frac{(\kappa-1)}{c^2}\frac{dq_V}{dt}. \tag{2}$$

By Fourier transform of the recorded density fluctuations the frequency spectra of the heat release fluctuations can be plotted. Only at the cavity resonance frequency of the combustion chamber the pressure term cannot be neglected.

While all other techniques exhibit problems in the determination of local heat release rates [10], LV can be used to either provide heat release rates $\dot{Q}$ globally within the entire combustion volume, or locally $\dot{q}$. While interferometric line-of-sight data need tomographic reconstruction to obtain local values – or Abel-inversion in case of objects with cylindrical symmetry – the dual-LV technique provides this local data in one recording [11, 12].

In non-reacting flows, LV are used to characterize the pressure field (e. g. sound field). In such applications only the first term in Equation (1) is of interest [13–17].

Replacing the materials derivatives in Equations (1) and (2) by partial derivatives and using Reynold's definition of mean and fluctuating components convective terms will appear, with dash denoting the fluctuating components. These convective terms include density gradients, gradients in heat release and velocities, as well as, the respective fluctuating components. With velocities and velocity fluctuations small compared to the speed of sound (low Mach number problems) the convective transport of heat release is small (see [18] for a more detailed discussion). Then the amplitude is only slightly above the background noise, but the phase can clearly visualize the flow pattern of the convective heat. First studies revealed that two LV with parallel or crossed beams can detect flow velocities in flames using the phase lag whenever a density structure first passes through beam 1, then through beam 2 [4, 12].

3 Experimental setup: The methane/air burner

This work and previous work [6, 19] used a swirl-stabilised methane/air flame at atmospheric pressure conditions. The variable geometry burner used in this investigation is seen in Figure 2 colour coding the most important parts. The swirl strength is set by the ratio between axial (gray) and tangential air (yellow) without changing the overall air-fuel-ratio. The burner was combined with an optically accessible liner at atmospheric pressure. In Figure 2 the

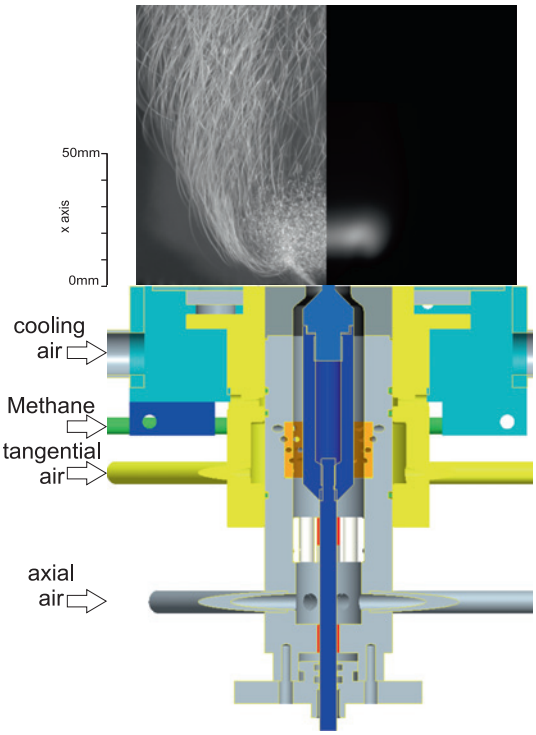

Figure 2: Variable geometry burner used to investigate thermo-acoustic oscillations in a swirl-stabilized methane flame.

schematics of the burner are shown together with a line-of sight integrated schlieren visualisation on the left side of the image and the spectral emittance at 430 nm (CH*) on the right side. For schlieren visualisation 700 frames were recorded with the brightest 10 percent of each pixel accounted for an averaging process. Such procedure generates streamlines around the combustion zone and shows small turbulent combustion structures in the combustion zone. OH* and CH* line-of-sight time-averaged chemiluminescence was recorded using a TECHSPEC band-pass-filter for 310 and 430 nm (both Edmund Optics, Barrington, NJ, USA) together with an ICCD camera (NanoStar, 1280 × 1024 pixel, LaVision, Göttingen, Germany) and a UV lens (105 mm, $f/4.5$, Nikon, Tokio, Japan). For the results shown in this publication, the burner was operated at 3.37 kW power, $0.9\dot{m}_{tan}/\dot{m}_{ax}$ (tangential to axial mass flows), a global equivalence ratio of 0.68, and a swirl number of 0.65.

4 Experimental setup: The laser vibrometer

For the investigations two laser vibrometers were used (interferometer head OFV-353, velocity decoder OFV-3001, calibration factor 5 mm/s/V, 20 kHz bandwidth, no filters, Polytec, Waldbronn, Germany). The basic setup to record heat release fluctuations is shown in Figure 3. An additional lens with −40 mm focal length was used to collimate the beam to a certain diameter. The scanning width depended on the beam diameter and e. g. was 3 mm for a 3 mm beam diameter. An optical access must be granted to apply this technique – here two quartz glass windows with 220 × 90 mm^2 were used when a liner (combustion chamber) was mounted on top of the flame. To scan the field, the combustor was mounted on a DANTEC lightweight traverse (DANTEC Dynamics, Roskilde, Denmark), while the vibrometer was fixed. Analog input modules NI-91215 (National Instruments, Austin, Texas) and Labview 8.6 software were used for data recording. Each scanned position was sampled with 245760 samples at a sample rate of 4096 S/s. Together with the vibrometer voltage a microphone signal was recorded (KECG2738PBJ-A, miniature electret condenser microphone, omni-directional, −40 dB, 2.8 mm diameter, Kingstate Electronics Corp, New Taipei City, Taiwan). For the phase shift $\varphi(t)$ between

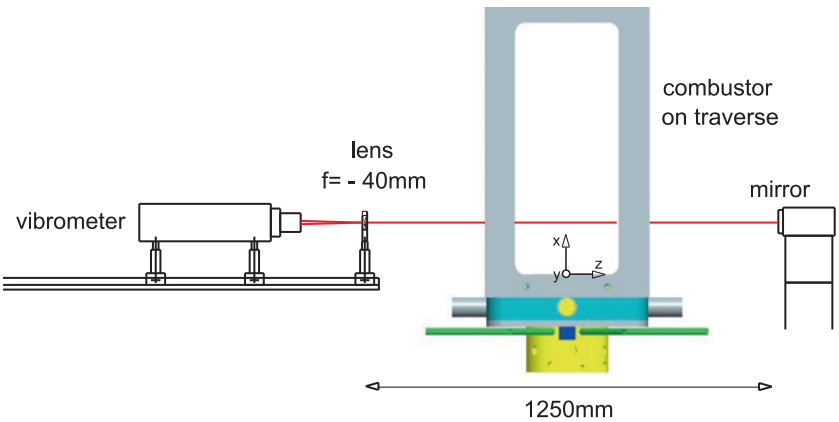

Figure 3: Setup of the laser vibrometer used to detect heat release fluctuations in flames.

reference and object wave in the interferometer (and thus the optical path difference ΔL) we find

$$\frac{\partial}{\partial t}\varphi(t) = \frac{2\pi}{\lambda}\frac{\partial}{\partial t}\Delta L(t) = \frac{2\pi}{\lambda}G\int_z \frac{\partial \rho'(z,t)}{\partial t}dz$$

$$= \frac{2\pi}{\lambda}k_{\text{vib}}U(t), \tag{3}$$

using G the Gladstone–Dale constant for the given equivalence ratio [20], $\rho'(z,t)$ the density fluctuations along the optical axis, k_{vib} the calibration constant of the vibrometer, here 5 mm/s/V, and $U(t)$ the vibrometer output voltage. z is the coordinate along the optical axis of the LV. The integral expresses the line-of-sight character of the measurement. In case of two or more uncorrelated density fluctuations along the light beam the interferometer averages on these structures thus leading to a decrease in standard deviation by the square root of the fluctuations number [13]. With a few events observed in the low frequency range this systematic error is not significant here. The Gladstone dale constant depends on the local equivalence ratios along the laser beam. Under technically premixed conditions the systematic error can be in the order of 1%, while in the perfectly premixed flame used here there is no systematic error. Recording frequency spectra or power spectra $S(f)$ by a Fast-Fourier-Transform FT the time derivative of density fluctuations along the beam path can be transformed into the density fluctuation by using the $2\pi f$ conversion factor at the given frequencies f

$$S(f) = \text{FT}^2\left[\int \rho'(t)\,dz\right] = \frac{1}{4\pi^2 f^2}\,\text{FT}^2\left[\int \frac{\partial \rho'}{\partial t}(t)\,dz\right]$$

$$= \frac{1}{4\pi^2 f^2}\,\text{FT}^2\left[\frac{k_{vib}U(t)}{G}\right]. \tag{4}$$

When two laser vibrometers are used, local density fluctuations can be recorded by correlating signals from the two intersecting laser beams [11, 12]. For this dual laser vibrometry either one, or both vibrometers can be traversed horizontally, in order to get radial profiles of density fluctuations at certain frequencies or frequency bands with the vibrometers fixed. Another possibility is to scan the flow in axial direction with only one laser vibrometer, while the second vibrometer and the burner are fixed [4, 12]. Considering a streamline within a flame, a density fluctuation now firstly crosses laser beam 1, secondly beam 2, a phase delay is recorded, depending on the convective flow velocity of this structure in axial direction. Whenever such a structure decays while moving in axial direction, or leaves the test volume due to tangential motion, the correlation will be lost. This will provide information on structural decay and velocity. The cross-correlation $c_{12}(t)$ between two functions $f_1(t)$ and $f_2(t)$ is given by

$$c_{12}(\tau) = \frac{1}{T}\int_0^T f_1^*(t) f_2(t+\tau)dt. \tag{5}$$

Using the convolution theorem the correlation power spectrum $C(f)$ can be calculated from two laser vibrometer frequency spectra $F_1(f)$ and $F_2(f)$. Due to the turbulent nature of combustion, a high number of single spectra must be averaged to obtain meaningful results

$$\overline{C(f)} = \overline{\text{FT}[c_{12}(\tau)]} = \overline{F_1(f)\cdot F_2^*(f)}. \tag{6}$$

The overbar indicates the averaged quantities. For this correlation technique up to 2000 complex cross-spectra were averaged since the accuracy depends on the square root of the number of sampled spectra [11].

5 Results and discussion

In this model combustor thermo-acoustic oscillations have been observed and documented in earlier works [7, 12]. LV can scan the flow field to record frequency spectra of heat release fluctuations. These line-of-sight data can be used to record local data by Abel inversion or tomographic algorithms. Local data can also be recorded directly by dual-LV using correlation methods [11]. Figure 4 shows the easy-to-read line-of-sight results providing deep insights in thermo-acoustics. Figure 4 plots the resulting frequency spectra of a line scan (3 mm steps with 3 mm beam diameter) through the flame with and without liner at different scanning heights. When discussing the spectra of the flame without liner first, we observe a periodic phenomenon at 230 Hz with a higher harmonic at 460 Hz, suggesting a non-sinusoidal signal. With the liner in place an additional acoustic wave is excited at a frequency of 200 Hz in the cavity. This periodic instability is observed when the burner excites a standing wave in the liner cavity. At this 200 Hz frequency strong amplitudes can be seen in the flame and lower amplitudes in the non-reacting areas outside the flame. It is important to learn that the pressure term in Equation (1) can not necessarily be neglected when a combustion chamber resonance is observed. When the line scan is performed above the combustion zone, as shown in the right plot in Figure 4, the amplitude at the chamber resonance frequency has its maximum beyond a radial extend of 20 mm. Comparing this finding with the schlieren image in Figure 2 indicates that in this region mixing with colder air takes place. While in the centre the hot gases from the combustion flow downstream,

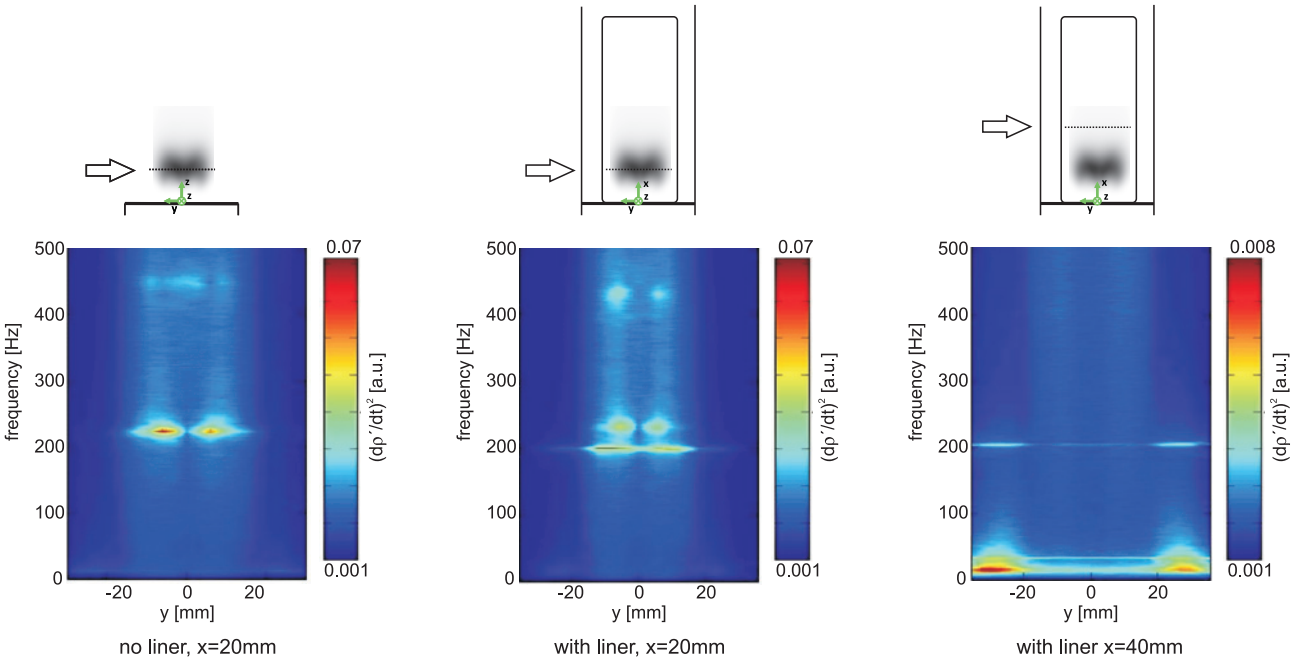

Figure 4: Density fluctuation frequency spectra recorded by laser vibrometry. The laser beam is scanned through the flame for two different heights with and without liner at resonant conditions.

the colder cooling gases in the outside seem to have just the correct temperature to particularly enable the standing pressure wave, thus the higher resonance amplitude in this region. In the scans at 40 mm height (Figure 4, right plot) the contributions from heat release are already small compared to the resonant pressure term. Also strong amplitudes were detected at the lower frequencies at 15 Hz and at 30 Hz across the whole section of the burner. The 30 Hz signal is constant at all positions scanned, indicating a structural vibration of the test rig (traverse). In contrast, the 15 Hz frequency is not of uniform amplitude along the cross-section of the combustion chamber and slowly decays towards higher frequencies, indicating a convective-aerodynamic effect. In this region hot strains from the flame rise next to cooling air along the windows. This convective transport of heat was already expected by analyzing the Schlieren image.

One important fact from Equations (1) and (2) is the temperature dependency of the speed of sound. While in hydrocarbon combustion the ratio of specific heat capacities depends only slightly on temperature, the speed of sound is sensitive to temperature changes. In order to record the fluctuations of heat release rate at a given frequency or for a given frequency interval correctly, the temperature distribution in the flame must be known to record the heat release fluctuations form Equation (2) cor-

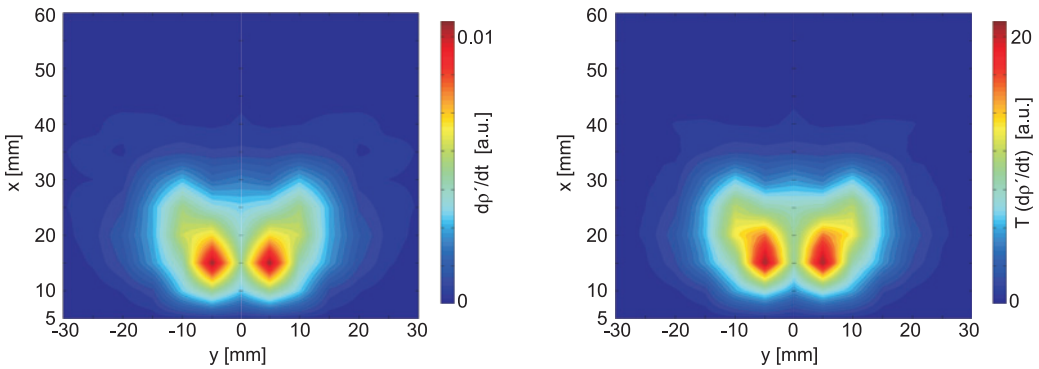

Figure 5: Density fluctuations within 230–260 Hz as recorded by the LV are shown left, while the temperature corrected values in the right image present the heat release fluctuations in this frequency range.

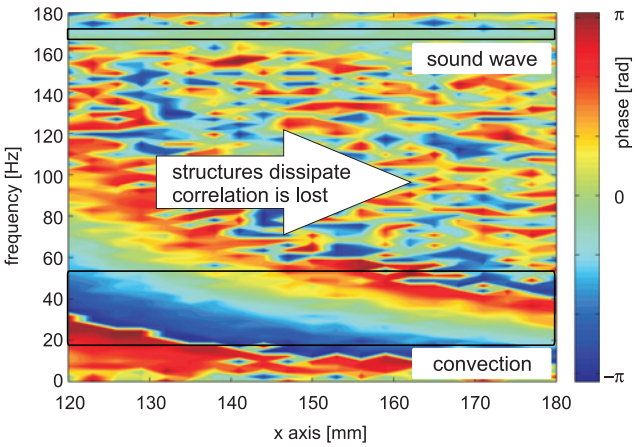

Figure 6: Recording the convective heat transport velocity using phase correlation from dual laser vibrometry above the nozzle ($y = 0$ mm).

rectly. Assuming perfect gas and using the gas law, this temperature field can be acquired by measuring the density distribution for example with shearography, a spatial correlation technique interferometrically comparing the wavefront with its sheared counterpart. Here a shearographic technique was used allowing for independent alignment of shear (sensitivity) and carrier fringe system [4, 21]. The influence of the local temperature distribution on the result is shown in Figure 5 for fluctuations within 230–260 Hz as recorded by the LV. While the overall fluctuation-pattern does not change much, in regions of strong temperature gradients, it does change significantly.

In order to assess the velocity of convective structures two vibrometers can be aligned above each other. When a density fluctuation crosses laser beam 1 first, then beam 2, a phase delay is recorded, depending on the axial velocity of this structure. By traversing one vibrometer, the evolution of the flow and the decay of the structures can be visualized. Whenever such a structure decays while moving in axial direction, or leaves the test volume due to tangential motion, the correlation will be lost. Such a scan for density fluctuations for two LV with perpendicular laser beams is shown in Figure 6 for frequencies between 0 and 180 Hz with a cavity resonance at 165 Hz. This change in resonance frequency compared to the results presented in Figure 4 was caused by a slightly different point of operation. Shown is the phase lag observed by scanning one LV, while the other one is fixed. The data processing was done according to Equation (6) by a cross-correlation procedure with a high number of samples due to the high level of turbulence in this flow. The first vibrometer was set up at $x = 80$ mm, and the second vibrometer's starting height was at $x = 120$ mm above the burner nozzle. The second LV was traversed in axial direction up to a height of 180 mm (perpendicular laser beams). In the lower frequency range the convective heat transport is observed. From the phase lag $\Delta\varphi(x)$ in x-direction, the known scanning distance Δx, and the frequency f, the axial velocity v_{ax} can be obtained by

$$v_{ax} = \frac{2\pi}{\Delta\varphi(x)} \cdot \Delta x \cdot f. \tag{7}$$

This procedure resulted in an axial velocity of 2.5 m/s, which is in good agreement with laser-optical velocity measurements performed in this setup [7]. At higher frequencies a loss of coherence between the two LV signal is observed, due to a structural decay at these frequencies. This decay can also be seen from the correlation amplitude spectra not presented here. Another possibility for this loss of coherence is the strong tangential movement in this swirl-stabilized flame. At about 165 Hz the field in the liner is dominated by the cavity resonance. No significant phase delay between the LV positions can be observed at this frequency due to the high speed of sound. The standing acoustic wave (pressure wave) dominates the phase in this spatio-temporal correlation at 165 Hz.

6 Summary and outlook

The laser vibrometer is a powerful tool for combustion diagnostics. Based on Equations (1) to (7) amplitude and phase of density-fluctuation frequency-spectra can be recorded in a non-intrusive way with high frequency and spatial resolutions. These spectra can then be used to classify the flame and discuss thermo-acoustic oscillations whenever optical access is granted to the combustion zone. By correlating the time signals from two laser vibrometers velocities can be recorded without the need for additional tracer particles or mechanically probing the test section. For further flame characterization, flame transfer functions (FTF) can be detected by LV, since it was shown recently [18] that the fluctuations in global heat release rate $\dot{Q}'$ recorded in perfectly premixed flame by LV do agree with data recorded by OH*-chemiluminescence. Data from measurements using a high number of LV beams, maybe even from multiple directions, could provide local spatio-temporal correlations and deeper insides into combustion processes.

Acknowledgement: This research was funded by the Austrian Science Fund FWF within grant FWF-24096-N24 "Interferometric Detection of Thermoacoustic Oscillations in Flames". The authors would like to thank Dr. Andreas

Marn for his kind support and the ongoing discussion on thermo-acoustics.

References

1. J. W. S. Rayleigh, "The Explanation of Certain Acoustical Phenomena", Nature, 18(4): 319–321, 1878.
2. A. Lewin, F. Mohr and H. Selbach, "Heterodyn-Interferometer zur Vibrationsanalyse", Tech. Mess., 57: 335–345, 1990.
3. F. Giuliani, T. Leitgeb, A. Lang and J. Woisetschläger, "Mapping the density fluctuations in a pulsed air-methane flame using laser-vibrometry", ASME J. Eng. Gas Turbines Power, 132: 031603, 2010.
4. S. Köberl, F. Fontaneto, F. Giuliani and J. Woisetschläger, "Frequency resolved interferometric measurement of local density fluctuations for turbulent combustion analysis", Meas. Sci. Technol., 21: 035302 (10 pp), 2010.
5. T. Leitgeb, T. Schuller, D. Durox, F. Giuliani, S. Köberl and J. Woisetschläger, "Interferometric determination of heat release rate in a pulsated flame", Combustion and Flame, 160: 589–600, 2013.
6. A. Fischer, J. König, J. Czarske, J. Peterleithner, J. Woisetschläger and T. Leitgeb, "Analysis of flow and density oscillations in a swirl-stabilised flame employing highly resolving optical measurement techniques", Experiments in Fluids, 54: 1622 (18 pp), 2013.
7. J. Peterleithner, A. Marn and J. Woisetschläger, "Interferometric Investigation of the thermoacoustics in a swirl stabilized methane flame", Proceedings of the ASME Turbo Expo 2015: GT2015, June 15–19, 2015, Montréal, Canada, GT2015-42743, 2015.
8. A. P. Dowling and A. S. Morgans, "Feedback control of combustion oscillations", Annu. Rev. Fluid Mech., 37: 151–182, 2005.
9. A. P. Dowling, "The Calculation of Thermo-acoustic Oscillations", Journal of Sound and Vibration, 180(4): 557–581, 1995.
10. M. R. W. Lauer, "Determination of the Heat Release Distribution in Turbulent Flames by Chemiluminescence Imaging", Dissertation, Technische Universität München, 2011.
11. B. Hampel and J. Woisetschläger, "Frequency- and space-resolved measurement of local density fluctuations in air by laser vibrometry", Meas. Sci. Technol., 17: 2835–42, 2006.
12. J. Peterleithner, F. Salcher and J. Woisetschläger, "Frequency resolved interferometric detection of local density fluctuations in flames", Proc. 17th International Symposium on Application of Laser Techniques to Fluid Mechanics, Lisbon, paper 04.7_1_53, 2014.
13. N. Mayrhofer, H. Lang and J. Woisetschläger, "Experimental Investigation of Turbine Wake Flow by Interferometrically Triggered LDV-Measurements", Proc. 10th International Symposium on Application of Laser Techniques to Fluid Mechanics, Lisbon, paper 28.1, 2000.
14. L. Zipser, S. Lindner and R. Behrendt, "Interferometrische Messung und Visualisierung von Schallwellen und Turbulenzen", Tech. Mess., 69: 275–81, 2002.
15. J. Woisetschläger, N. Mayrhofer, B. Hampel, H. Lang and W. Sanz, "Laser-optical investigation of turbine wake flow", Exp. Fluids, 34: 371–378, 2003.
16. P. Gren, K. Tatar, J. Granström, N. E. Molin and E. V. Jansson, "Laser vibrometry measurements of vibration and sound fields of a bowed violin", Meas. Sci. Technol., 17: 635–644, 2006.
17. M. Martarelli, P. Castellini and E. P. Tomasini, "Subsonic jet pressure fluctuation characterization by tomographic laser interferometry", Experiments in Fluids, 54: 1626 (13 pp), 2013.
18. J. Peterleithner, N. V. Stadlmair, J. Woisetschläger and T. Sattelmayer, "Analysis of measured flame transfer functions with locally resolved density fluctuations and OH-chemiluminescence data", Proceedings of the ASME Turbo Expo 2015: GT2015, June 15–19, 2015, Montréal, Canada, GT2015-42745, 2015.
19. F. Giuliani, J. Woisetschläger and T. Leitgeb, "Design and validation of a burner with variable geometry for extended combustion range", Proceedings of ASME Turbo Expo 2012, GT2012, June 11–15, 2012, Copenhagen, Denmark, GT2012-68236, 2012.
20. W. C. Gardiner, Y. jr. Hidaka and T. Tanzawa, "Refractivity of combustion gases", Combustion and Flame, 40: 213–219, 1981.
21. G. Pretzler, H. Jäger and T. Neger, "High-accuracy differential interferometry for the investigation of phase objects", Meas. Sci. Technol., 4: 649–658, 1993.

Bionotes

Dipl.-Ing. Johannes Peterleithner
Institut für Thermische Turbomaschinen und Maschinendynamik, Technische Universität Graz, Inffeldgasse 25A, 8010 Graz, Österreich
johannes.peterleithner@tugraz.at

Johannes Peterleithner ist seit 2012 wissenschaftlicher Mitarbeiter der Arbeitsgruppe „Messung in Turbomaschinen – laseroptische Messtechnik" des Instituts für Thermische Turbomaschinen und Maschinendynamik. Arbeitsgebiete sind Verbrennungsdiagnostik und Thermoakustik.

Ao. Univ.-Prof. Dipl.-Ing. Dr.techn. Jakob Woisetschläger
Institut für Thermische Turbomaschinen und Maschinendynamik, Technische Universität Graz, Inffeldgasse 25A, 8010 Graz, Österreich
jakob.woisetschlaeger@tugraz.at

Jakob Woisetschläger ist seit 2002 Leiter der Arbeitsgruppe „Messung in Turbomaschinen – laseroptische Messtechnik" des Instituts für Thermische Turbomaschinen und Maschinendynamik. Hauptarbeitsgebiete sind Entwicklung und Anwendung optischer Messverfahren zur Strömungs- und Schwingungsuntersuchung mit einem Schwerpunkt auf turbulenten transsonischen Strömungen, Thermoakustik, Zweiphasenströmungen und elektrohydrodynamischen Strömungen.

Johannes Peterleithner
Institute for Thermal Turbomachinery
and Machine Dynamics,
Graz University of Technology,
Inffeldgasse 25/a,
Graz 8010, Austria
e-mail: Johannes.peterleithner@tugraz.at

Nicolai V. Stadlmair
Lehrstuhl für Thermodynamik,
Technische Universität München,
Garching 85748, Germany

Jakob Woisetschläger
Institute for Thermal Turbomachinery
and Machine Dynamics,
Graz University of Technology,
Graz 8010, Austria

Thomas Sattelmayer
Lehrstuhl für Thermodynamik,
Technische Universität München,
Garching 85748, Germany

Analysis of Measured Flame Transfer Functions With Locally Resolved Density Fluctuation and OH-Chemiluminescence Data

The goal of this study is to analyze flame transfer functions (FTFs) locally by quantifying the heat release rate with OH-chemiluminescence and density fluctuation measurements using laser vibrometry. In this study, both techniques are applied to a swirl burner configuration with known FTFs acquired by multimicrophone-method (MMM) measurements for perfectly premixed and partially premixed cases. The planar fields of the quantities are compared to the FTFs in order to improve the understanding regarding the specific amplitude and phase values. On the global scale values of heat release expected from the MMM are satisfactorily reproduced by both methods for the premixed cases, whereas OH*-chemiluminescence data cannot be used as indicator for heat release in the partially premixed case, where equivalence ratio fluctuations are present. Vibrometry is not affected by fluctuations of equivalence ratio but additionally reveals the periodic oscillation of the conical annular jet of the cold reactants in the combustor filled with hot products.* [DOI: 10.1115/1.4031346]

Introduction

State-of-the-art technology in industrial gas turbines for power generation predominantly uses lean-premixed combustion to achieve high combustion efficiency and low emissions. High power densities and reduced damping capabilities of the combustor increase the susceptibility to thermoacoustic oscillations. These instabilities arise from the positive coupling between the fluctuations of pressure and heat release [1]. Modeling and prediction of instabilities is often accomplished by analyzing the FTF, which relates the unsteady heat release of the flame to perturbations of acoustic velocity at the burner exit.

In the past, a variety of methods for the measurement of FTFs in research combustors have been published. A method widely used for determining the FTF is measuring the chemiluminescence from OH* within the flame as the measure for heat release. Velocity fluctuations at the burner exit are obtained either directly from hot wire anemometry or from dynamic pressure measurements with the multimicrophone-method [2,3]. Whereas all approaches relying on chemiluminescence are only applicable for adiabatic flames with low strain rates and constant equivalence ratio [4], this method is not applicable to technically premixed combustion systems. For this case, fluctuations of the equivalence ratio provide additional contribution to the heat release fluctuations and thus the FTF cannot be determined from the integral OH*-chemiluminescence [5]. Alternatively, the FTF can be obtained with the multimicrophone-method (MMM). This technique is free of these restrictions, as it is entirely based on dynamic pressure measurements and allows obtaining FTFs, which represent the flame dynamics in form of the frequency dependent amplitudes and phase for a wide range of flames. It can be applied to combustion processes with heat losses, high strain rates and partially premixed flames with equivalence ratio fluctuations or sprays. Conversely, this implies that no direct information regarding local phenomena can be captured, as the flame is treated as a "black-box" system. To overcome this shortfall, it is common practice to use physically based fit functions, which may indirectly lead to information on the effects governing flame dynamics [6,7]. In some cases, Abel-de-convoluted flame images of OH*-chemiluminescence from a high-speed camera can be used to obtain local information for further analysis of the flame dynamics. However, Lauer [4] showed that turbulence has a remarkable impact on the chemiluminescence intensity in highly turbulent flames. In such cases, discrepancies in the spatial distributions of chemiluminescence emission and heat release rate must be expected.

Experimental Setup

Test Rig. The measurements presented in this study have been carried out on the single burner test rig with a modular swirl burner system (33 mm exit diameter) for lean-premixed operation shown in Fig. 1 [8,9]. The main airflow is preheated by an electrical preheater to $T_c = 300\,^{\circ}\mathrm{C}$ before it enters the cylindrical plenum chamber with a diameter of 124 mm. Acoustic excitation is provided by two sirens positioned at two different locations. One siren is placed far upstream of the burner and modulates the main airflow, the second one is located downstream of the combustor. Transfer matrix measurements can be accomplished with this test rig using the two source-location method [3]. For perfectly premixed mode (PPM) operation, natural gas is supplied to the inlet of the plenum chamber to avoid fluctuations of the equivalence ratio. When operating in technically premixed mode (TPM), the fuel is directly injected through tangential holes in the swirler. In this case, an equivalence ratio wave is generated, if the flow is forced. A conical mixing tube attached to the swirler produces a convective time delay between the fluctuations of swirl and axial velocity at the burner exit. The combustor has a cross-sectional area of 150×150 mm and is optically accessible from two sides. An acoustically low-reflective end is attached to the combustor exit.

Measuring Techniques. Acoustic pressure fluctuations are measured by PCB 106B piezoelectric sensors. Three of these are located in the plenum chamber and three in the combustor. Simultaneous data acquisition is achieved by a personal computer equipped with a National Instruments PCI-4472 card. The phase signal of the siren excitation is provided by rotational speed

Contributed by the Combustion and Fuels Committee of ASME for publication in the Journal of Engineering for Gas Turbines and Power. Manuscript received July 14, 2015; final manuscript received August 6, 2015; published online September 22, 2015. Editor: David Wisler.

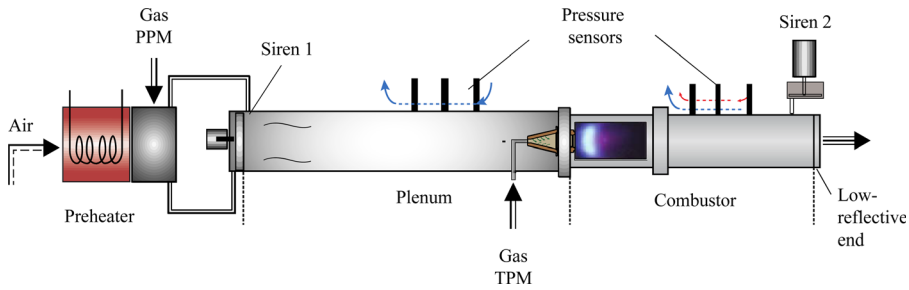

Fig. 1 Schematic of the single burner test rig with modular swirl burner system

sensors. The integral OH*-chemiluminescence intensity emitted by the flame is acquired using an UV filtered photomultiplier. The sensor consists of a photo diode and a narrow-band interference filter of 308 nm.

Phase-resolved flame images are obtained by an image intensified Photron Fastcam APX I2 high-speed camera. The OH*-chemiluminescence intensity of the flame is recorded using a narrow-band interference filter with a maximum transmission of 16.17% at a characteristic wavelength of 308.52 nm and a bandwidth of 10 nm. CH* chemiluminescence intensity is obtained by filtering at a characteristic wavelength of 431 ± 10 nm and a maximum transmission of 48%. All images are taken with a recording frequency of 12.5 kHz and a resolution of 512 × 256 pixels. Dynamic pressure data, siren phase, and trigger signal of the image intensifier are acquired simultaneously.

After calibration for thermal noise, a set of 32,768 images at a recording rate of 12,500 images per second was acquired for CH* and OH*. For post processing, the frames of 512 × 256 pixels were then split into 6 × 6 pixel subframes corresponding to 4 mm^2 in the flame cross section.

On the basis of the ratio between OH*- and CH*-chemiluminescence, the global and local equivalence ratio can be determined [10]. Fluctuations of equivalence ratio are calculated from the images obtained by the high-speed camera after sorting them according to their phase with respect to the excitation

$$\frac{\phi'(\alpha)_{xz}}{\bar{\phi}_{ij}{}^{\alpha}} = \frac{\dfrac{I_{OH*}(\alpha)_{xz}}{I_{CH*}(\alpha)_{xz}}}{\overline{\left(\dfrac{I_{OH*xz}}{I_{CH*xz}}\right)}^{\alpha}} - 1 \tag{1}$$

For the comparison on the global level, the time-series of each subframe was Fourier analyzed, resulting in local fluctuation amplitudes for the siren frequencies.

For the 2D image series plotted below, the images were sorted according to the phase to the sirens trigger. An example is shown in Figs. 2(*b*) and 2(*c*). Finally, an Abel inversion was performed to gain local data. In case of rotational symmetry of the flame, a single projection can be used. For this purpose, the software package IDEA 1.7.31 was used, developed at Graz University of Technology [11,12]. A *f*-interpolation technique was use to obtain local data from line-of-sight data by Abel inversion from radially symmetric data [13].

Abel inversion was performed on the single frames within the time-series in order to preserve the phase throughout the image processing.

Laser vibrometers (LVs) consisting of a Mach–Zehnder interferometer are widely used to detect surface vibrations from machinery. With an acoustic-optical modulator, these interferometers record vibration velocity rather than surface amplitude increasing the spectral signal by a factor of 2πf. In combustion research, these systems are used to detect density fluctuations with fixed geometrical changes in the optical path.

In this study, a single LV was used (interferometer head OFV-353, velocity decoder OFV-3001, calibration factor 5 mm/s/V, 20 kHz bandwidth, Polytec, Waldbronn, Germany). The LV was equipped with a 40 mm lens to collimate the laser beam to 2 mm diameter. To scan the field, the vibrometer was mounted on a DANTEC lightweight traverse (DANTEC Dynamics, Roskilde, Denmark). Data were acquired with analog input modules NI-91215 (National Instruments, Austin, TX) and LABVIEW 8.6 software. For each of the positions scanned at 200 Hz 6×10^6 samples were taken with a sample rate of 100 kS/s. In the 480 Hz experiments 491,520 samples at 8192 S/s were taken and the signals were filtered with a 5 kHz low pass. Together with the vibrometer voltage, the microphone signal and the siren excitation signal were recorded for all scanned positions to have a phase reference. For one single position in the field LV, microphone and photomultiplier signal (OH*) were recorded. All cross-correlations and Fourier transforms were done by a MATLAB routine providing frequency spectra (amplitude and phase) for each position scanned. Sample lengths of 50 kS (experiments with 200 Hz excitation) and 4096 S (experiments with 480 Hz excitation), respectively, were used.

Using the LV, the combustion field was scanned in 150 positions in the upper half-plane as indicated in Fig. 2. Since the LV records changes of the optical path length $L(t)$, the output voltage $U(t)$ must be related to the density fluctuations by

$$k_{vib}U(t) = \frac{d}{dt}L(t) = G\int \frac{d}{dt}\rho(t)\ dy \tag{2}$$

With the calibration factor k_{vib} (5 mm/s/V) for the LV and the Gladstone–Dale constant G, relating refractive index with density. Since the Gladstone–Dale constant for air is about 2.4×10^{-4} m^3/kg, but 6×10^{-4} m^3/kg for Methane, a slight influence of equivalence ratio fluctuations is evident.

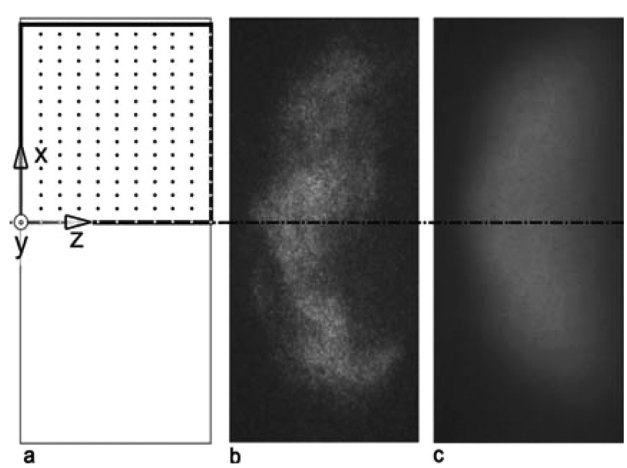

Fig. 2 Coordinate system used for the vibrometer measurements and measurement points at an area of 75 × 70 mm (*a*). A single shot (*b*) and a time averaged OH* image (*c*) of chemiluminescence.

The evaluation procedure for the LV data was identical to the procedure performed on the chemiluminescence flame images, resulting in line-of-sight plots for the density fluctuations and integral fluctuations for the field of view.

In order to derive the relationship between the density fluctuations and heat release fluctuations, we consider an ideal gas exposed to heat addition as usual in thermoacoustics studies. In differential form, the density fluctuations are related to the pressure and temperature fluctuations as follows:

$$d\rho = \left.\frac{\partial \rho}{\partial p}\right|_T dp + \left.\frac{\partial \rho}{\partial T}\right|_p dT \tag{3}$$

We eliminate dT from this equation using the first law of thermodynamics

$$dq + \frac{dp}{\rho} = dh = c_p dT \tag{4}$$

With the ideal gas law $p = \rho \mathrm{RT}$, this leads to

$$d\rho = \left(\frac{1}{RT} - \frac{p}{RT^2}\frac{1}{\rho c_p}\right)dp - \frac{p}{RT^2}\frac{1}{c_p}dq \tag{5}$$

Using $c_p = \kappa R/\kappa - 1$ and the relation between sound velocity and temperature $\mathrm{c} = \sqrt{\kappa \mathrm{RT}}$, we obtain

$$\frac{d\rho}{dt} = \frac{1}{c^2}\frac{dp}{dt} - \frac{\kappa - 1}{c^2}\frac{dq_V}{dt} \tag{6}$$

The time derivatives in Eq. (6) express the fluctuation components of density, pressure, and heat release. It is common practice to replace the material derivatives in Eq. (6) by partial derivatives when studying thermoacoustic low Mach numbers problems. This implies the assumption that the convective transport of the heat release fluctuations has no effect on the driving potential of thermoacoustic instabilities. The use of partial derivatives allows the treatment of wave propagation separate from the heat release in, e.g., hybrid field methods using the inhomogeneous wave equation [14], acoustic perturbation equations [15], as well as linearized Euler equations and linearized Navier–Stokes equations (e.g., Ref. [16]). It can be shown that the pressure term can be neglected in flames, because it is at least an order of magnitude smaller than the other terms in Eq. (4) [17,18]. This finally leads to

$$\frac{\partial \rho'}{\partial t} = -\frac{\kappa - 1}{c^2}\frac{\partial q_V{}'}{\partial t} \tag{7}$$

Equation (7) reveals a proportionality between the time derivatives of density fluctuation recorded by vibrometers and the heat release fluctuations in the flame front [19]. It is of particular interest to experimentally investigate whether the local and global proportionality between density fluctuations and fluctuating heat release rate in the flame exists in reality. As shown later, this is not always the case (a) because for not fully adiabatic conditions density fluctuations also occur outside the flame front, (b) because changes in density are present in the products, which is both the case for combustion with spatially or temporal varying equivalence ratio, and (c) because additional density fluctuations are generated at the interface between reactants and products, if these interfaces oscillate.

In the study presented below, a new approach based on the combination of line-of-sight OH*-chemiluminescence and density fluctuation data will be employed for analyzing FTFs. Both measuring techniques should give access to the heat release fluctuations of the flame independent of one another. This is achieved by acquiring OH*-chemiluminescence with an intensified camera, while density fluctuations are measured with a vibrometer on a two axis traverse. After integration over the field of view, these data can be compared with the FTF results obtained by the MMM. In the first phase, investigations are carried out for perfectly premixed conditions, whereas in the second phase the case with equivalence ratio waves is considered. These are generated when operating the burner in TPM with fuel injection in the swirler.

Flame Properties and Flow Field

Stationary Flame Behavior. In the following, the steady flame properties of the lean premixed, aerodynamically stabilized flame will be briefly described. Figure 3 shows the flow field of the flame without reaction and the reaction zone is visible from line-of-sight OH*-chemiluminescence intensity [20]. A stable and well-defined bubble-shaped recirculation zone is generated approximately 0.5D downstream of the burner outlet. In the reacting case, the bubble end is located at 1.5D–2D. The vortex breakdown is induced by the sudden change in the cross section between burner and combustor. Flame stabilization is accomplished inside the core flow at the tip of the recirculation zone. The flame propagates through the inner shear layer whereas no reaction takes place in the outer shear layer due to heat loss and strain. Further information on the aerodynamic properties of the burner is available in Ref. [20].

Flame Transfer Functions. Physically, the FTF correlates the heat release fluctuations $\dot{Q}'$ in the flame to the velocity fluctuations at the burner exit u'_b. The FTF is generally defined by the following equation:

$$\mathrm{FTF} = \frac{\dot{Q}'/\bar{\dot{Q}}}{u'/\bar{u}} \tag{8}$$

On this basis, direct measurements of the FTF are only possible in flames, which exhibit a proportionality between the heat release fluctuations and flame chemiluminescence (OH* and/or CH*).

In this study, the FTFs are determined with the fully acoustic approach as the premise of a constant equivalence ratio is not met for all investigated cases. For this purpose, the burner transfer matrices (BTM) and the burner and flame transfer matrices (BFTM) are measured with source-location method. In the next step, the flame transfer matrix (FTM) is calculated for each excitation frequency

$$\mathrm{FTM} = \mathrm{BFTM} \cdot \mathrm{BTM}^{-1} \tag{9}$$

Provided, the temperatures before (T_c) and after the flame (T_h) are known, the FTF can be calculated from the element (2,2) of the FTM from the Rankine–Hugoniot relations

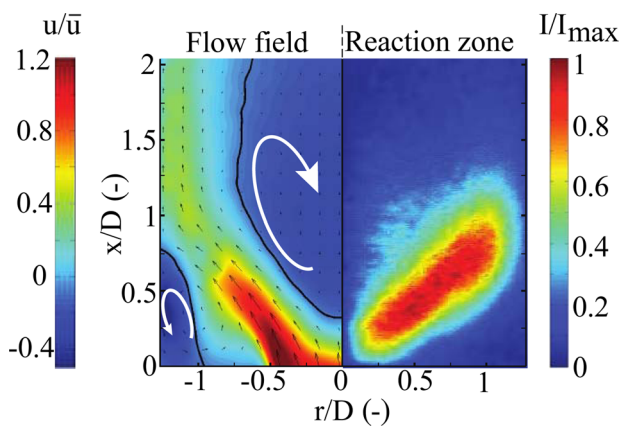

Fig. 3 Flow field (nonreacting case) and reaction zone from line-of-sight OH*-chemiluminescence in the combustor [20]

$$\mathrm{FTF}(\omega) = \frac{\mathrm{FTM}_{2,2} - 1}{1 + \frac{T_h}{T_c}} \tag{10}$$

The given FTFPPM show a clearly visible minimum at approximately 200 Hz, followed by a maximum, and finally the amplitude decreases slightly toward higher frequencies (Fig. 4). The phase is plotted with the velocity as reference, continuously decreasing with increasing frequency, representing the convective time delay between velocity fluctuations and the flame response with unsteady heat release. In contrast to that, the lowest amplitude of the FTFTPM is shifted toward lower frequencies. Maximal amplitudes are higher than in the perfectly premixed case. With increasing frequency, amplitudes of both perfect premixing and technical mixing converge, which suggests a vanishing influence of the fluctuations of equivalence ratio. The phase of the FTFTPM decreases steeper than for the PPM case. Both slopes converge toward higher frequencies [8]. Based on these results, we have chosen 200 Hz for the first excitation frequency. In this case, the amplitude of FTFPPM reaches its minimum, whereas the amplitude of FTFTPM is large. In the latter case, we expect an overprediction of the amplitude by the chemiluminescence intensity compared to the pure acoustic method. We are thus expecting the oscillations of heat release obtained from the density fluctuations to be lower compared to the chemiluminescence method when equivalence ratio waves are present.

Second, the excitation at 480 Hz is of particular interest at which the FTFPPM reveals its maximum amplitude. Using the original definition of the FTF in Eq. (8), the normalized heat release fluctuations can directly be obtained from multiplying the FTF with the normalized velocity fluctuations at the burner exit. Consequently, the influence of the velocity perturbations can be eliminated. This allows direct comparison of OH*-chemiluminescence intensity and density fluctuations. The normalized global heat release fluctuations $Q'/\bar{Q}$ obtained from the MMM for both premixing modes are plotted in Fig. 5. Considering only the amplitude behavior, it becomes clear that the deviations between the FTFPPM and FTFTPM in the low frequency range are mainly caused by the fluctuating heat release rate, which is remarkably higher in the TPM case. This contribution diminishes toward higher frequencies where the FTF amplitude is dominated by the decreasing amplitudes of the velocity perturbations. Amplitudes and phase slopes of the velocity fluctuations for both premix modes do not differ substantially from one another. For that reason the phase lag between the FTFPPM and FTFTPM for low frequencies is caused by the contribution of the heat release fluctuations alone.

Operating Conditions. The operating conditions of the single burner test rig employed in this study have been chosen identically to the configuration previously used in Refs. [8,9] for transfer matrix measurements. An overview of the operating conditions and its corresponding amplitude and phase values are shown in Table 1.

This allows comparisons to be drawn across different measurement techniques and utilization of existing data. Investigations conducted in this study have been accomplished for a fixed global equivalence ratio of $\phi = 0.71$ at constant thermal power of $P_{\mathrm{th}} = 50$ kW. Swirl strength and mixing tube length were kept constant for all experiments.

Results

Below the global OH*-chemiluminescence data acquired with a photomultiplier will be discussed first. Then the planar line-of-sight chemiluminescence and density fluctuation data acquired with the intensified camera and the vibrometer, respectively, will be presented. On this basis, the reasons for the amplitudes of the heat release fluctuations measured with the MMM for the three operating points will be analyzed. In addition, consistency checks between all three methods will be made. And finally all line-of-sight data will be deconvoluted to generate pseudo-local data, which reveal additional insight in the spatial distribution of OH*-chemiluminescence and density fluctuations.

Global Data. During experiments, the integral chemiluminescence signal was permanently monitored with a photomultiplier and a narrow-band interference filter at the OH*-emission line.

The broadband combustion noise spectra for the three operating points shown in Fig. 6 exhibit the decay of amplitude toward higher frequencies typical for turbulent flames. At 430 Hz and above 800 Hz, the eigenfrequencies of the combustor configuration lead to amplification of the heat release fluctuations due to

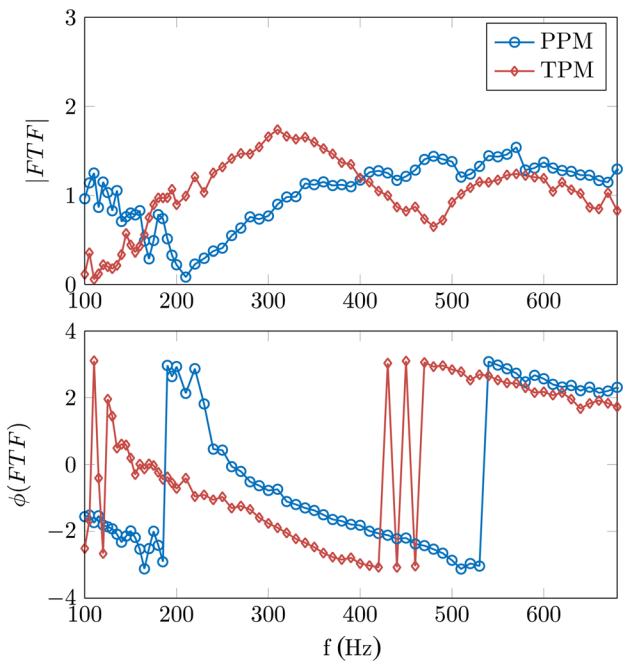

Fig. 4 Flame transfer function FTFs measured with the multi-microphone method

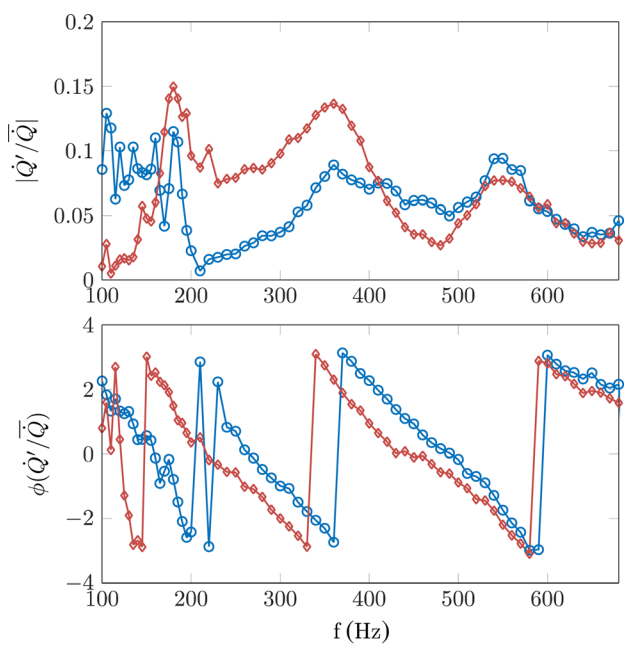

Fig. 5 Normalized heat release fluctuations extracted from the FTF

Table 1 Investigated operating modes, amplitude, and phase values are referenced to the PPM200 Hz case

Operating mode (Hz)	$\|FTF\|_{rel}$	$\varnothing(FTF)_{rel}$ (rad)	$\|\dot{Q}'\|_{rel}$	$\varnothing(\dot{Q}')_{rel}$ (rad)
PPM200	1	0	1	0
PPM480	6.51	−5.47	2.41	2.58
TPM200	4.05	−3.65	4.24	2.78

turbulent noise. However, this effect is very low, because the acoustic design of the test rig with the lowly reflecting end plate provides strong damping. At the forcing frequencies distinct peaks are present, which are approximately one order of magnitude higher than the background from turbulent noise. This shows that the siren excitation is powerful enough to provide well-correlated phase information, which is required for the generation of time series from the data (see below).

A closer look on the peak heights of OH*-Chemiluminescence in Fig. 6 delivers estimates for the ratios between fluctuation amplitudes from integral OH* emission for different operating points. For the two operating points with forcing at 200 Hz, we obtain a value of TPM200:PPM200 = 5.7 and for the two perfectly premixed cases the ratio is PPM480:PPM200 = 1.5. Within the measurement uncertainty, the latter ratio corresponds to the expectations based on the measurements with the MMM. Table 1 shows that both methods deliver consistent results for PPM. On the other hand, the amplitude measured with the photomultiplier for the TPM is significantly higher than the expected value. This indicates that the heat release fluctuations are lower than the OH*-chemiluminescence fluctuations recorded by the photomultiplier. Obviously, the equivalence ratio fluctuations generated by the fuel injection in the swirler (TPM200) are not fully dissipated during convection into the flame zone and part of the OH*-chemiluminescence fluctuations are the result of the sensitivity of OH*-chemiluminescence on the equivalence ratio.

Line-of-Sight Data. In Fig. 7, the line-of-sight integrated data are presented for the three investigated operating points. The image sequence of each figure shows the OH*-chemiluminescence and below, the sequence of density fluctuations. Please note that the full color scale has been used in each image sequence and that the scales differ when comparing the image sequences of the three operating points with each other.

According to the derivation in the introduction, the OH*-chemiluminescence and the density fluctuation image sequence should be identical or at least almost very similar for the premixed operating points PPM200 and PPM480. However, the sequences in Fig. 7 show that this is not the case. Potential reasons for the observed differences have been mentioned in the introduction and will be analyzed below.

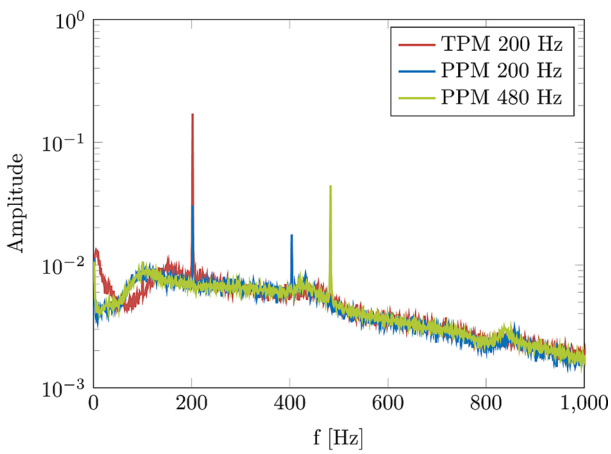

Fig. 6 Integral OH*-chemiluminescence OH* detected by the photomultiplier

The OH*-chemiluminescence image sequence for PPM200 (Fig. 7, upper section) indicates that in the premixed case a zone with periodic heat release overshoot (red) and heat release deficit (blue) is generated at the burner exit, which is convected downstream along the inner shear layer of the conical annular jet of reactants. Apparently, this convective process ends with the formation of a fluctuating flat reaction zone, but it would be difficult to identify a reason for the flat shape on the basis of the analysis of the flow (Fig. 3). The analysis of the deconvoluted images presented below will show that the flat shape of that downstream zone originates from the line-of-sight integration and that the observed flat reaction zone in fact does not exist.

According to the MMM, the amplitude of the heat release is low for PPM200. The reason for the low gain is clearly visible in the OH*- chemiluminescence image sequence: At each phase angle the zones with heat release overshoot and heat release deficit are in almost perfect balance.

The density fluctuation image sequence (Fig. 7, upper section) also shows the formation of a zone with periodic heat release fluctuations near the burner exit. However, the convective processes are almost invisible in the vibrometer measurements of PPM200. Instead a conical structure in the outer shear layer is visible, which oscillates in phase.

This structure cannot be linked to heat release because the reaction is quenched in the outer shear layer (see above). This leads to the conclusion that the density fluctuations due to the temperature difference of reactants and products, which can coexist in the outer shear layer, are measured by the vibrometer. The deconvoluted images presented below will provide more information regarding the underlying effects. In the center structures with complex shapes are measured which are difficult to understand, because they may again result from line-of-sight integration.

The OH*-chemiluminescence image sequence for TPM200 (Fig. 7, middle section) shows fundamentally different patterns. A huge flat pulsating zone is created at the burner exit, which spreads radially outward first, before it is convected in axial direction and finally vanishes. Since flame stabilization and flame propagation follow the same principles and are not specific to the method of fuel injection and premixing, the observed fundamental change of the pattern of fluctuation cannot be primarily linked to the heat release in the flame. This leads to the conclusion that the observed fluctuations to a large extend are caused by the temperature dependency of OH*chemiluminescence, which plays a role when equivalence ratio waves are convectively transported through the flame zone. This is the case shown in Fig. 8, where the axial distribution of the equivalence ratio ϕ over the phase angle is shown for TPM200. In order to illustrate the axial convection more clearly, data have been integrated over the x-axis, which is perpendicular to the main flow. Each plotted data series corresponds to a certain time step. Starting with the first data series, we see that the highest equivalence ratio is found near the downstream end of the flame. With increasing time step, this peak decreases, and a new wave starts at the beginning of the flame. This wave is then convectively transported through the flame.

Since Fig. 8 shows a significant level of fluctuation of the equivalence ratio, it cannot be expected that meaningful data regarding the heat release distribution can be extracted from the OH*-chemiluminescence image sequence shown in Fig. 7 (middle section). It is expected that the pulsation amplitude calculated on the basis of OH*-chemiluminescence is by far to high.

The density fluctuation image sequence in Fig. 7 (middle section) confirms that the reaction patterns of PPM200 and TPM200 are much less different than to be expected on the basis of the OH*-chemiluminescence image sequences for both operating points. Although the maximum amplitude in the time series plots is the same for PPM200 and TPM200, areas of high amplitude are significantly larger in the technically premixed case. This leads to a higher amplitude for TPM200.

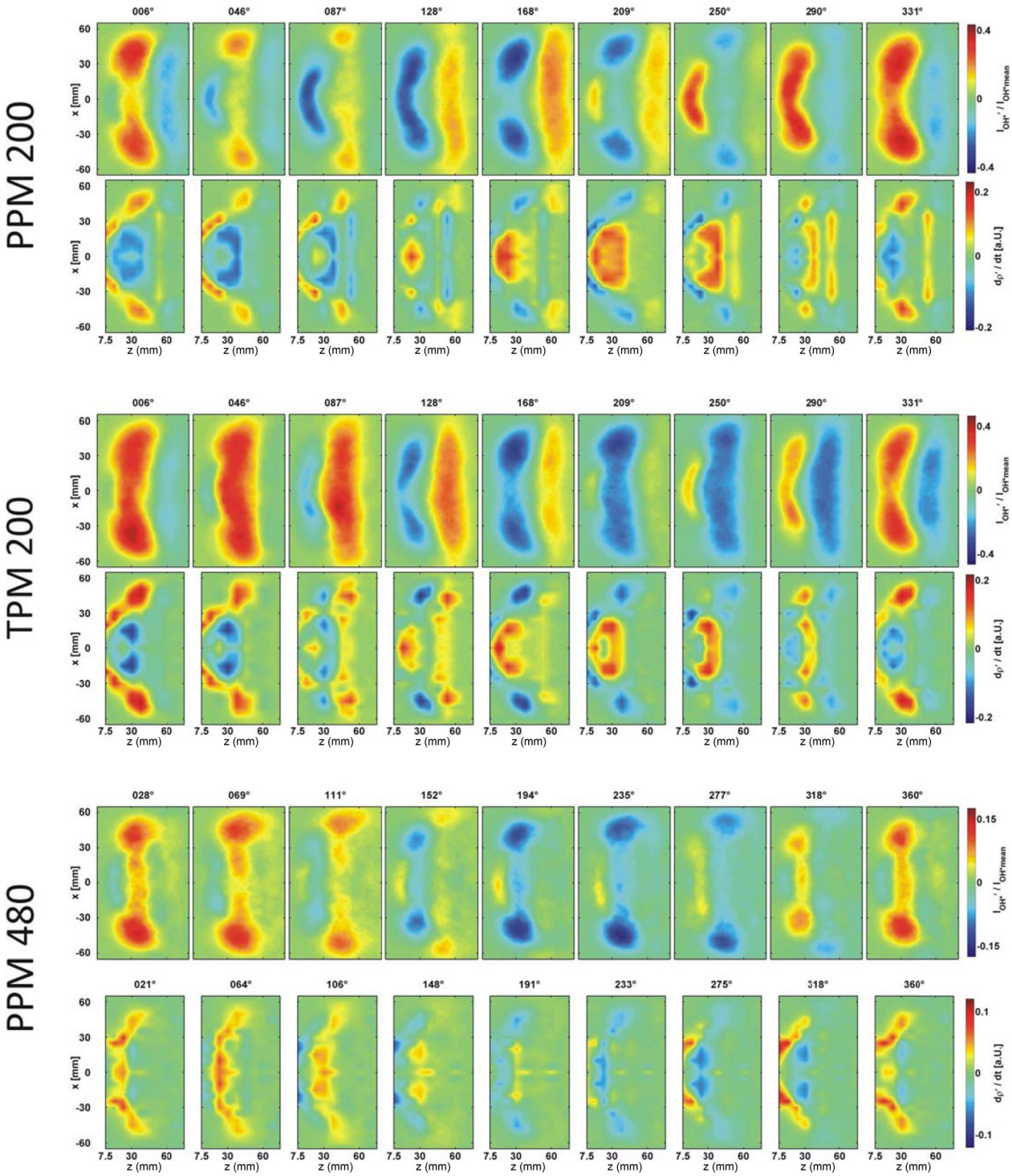

Fig. 7 Phase-resolved OH*-chemiluminescence and density fluctuations, line-of-sight data

Qualitatively, the OH*-chemiluminescence image sequence for PPM480 (Fig. 7, lower section) shows the same effects as the image sequence for PPM200. The bone-shape of the zones of heat release overshoot (red) and heat release deficit (blue) visible in Fig. 7 (lower section) are again the result of line-of-sight integration as will be shown later, when the deconvoluted images are discussed. However, the red and blue zones are no longer in balance over the cycle. Overshoot zones clearly dominate between 330 and 150 deg and deficit zones in between. The reason for that difference is the ratio of time scales: Whereas the convective time scale is independent of the forcing frequency the formation of overshoot and deficit zones is proportional to it. In line with the expectation from the measurements with the MMM the OH*-chemiluminescence image sequence also provides evidence for a high global amplitude of the heat release fluctuations.

The density fluctuation image sequence for PPM480 (Fig. 7, lower section) shows the same basic effects as the image sequence for PPM200 but it also shows the imbalance between overshoot and deficit zones over the pulsation cycle.

Spatially Integrated Line-of-Sight Data. If the data presented in the last section, Line-of-Sight Data, are integrated in x- and in z-direction, global values for the OH*-chemiluminescence and the

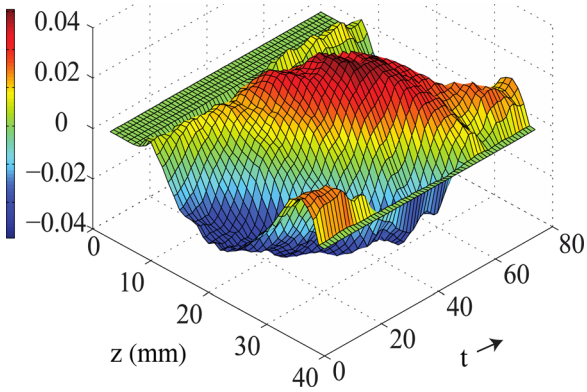

Fig. 8 Convectively transported equivalence ratio wave at 200 Hz, (TPM200), line-of-sight data with Φ' calculated according to Eq. (1)

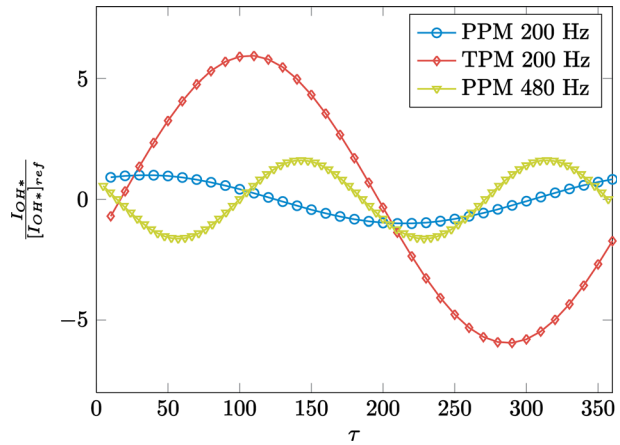

Fig. 9 Global OH*-chemiluminiescence fluctuations. The fluctuations are normalized by the PPM200 fluctuation amplitude.

density fluctuations are obtained, which reveal amplitude and phase information regarding flame dynamics like the MMM. This allows a comparison of both methods on the global scale, and in addition, the results from OH*-chemiluminescence can be compared with the data from the photomultiplier.

Figure 9 shows the normalized intensity of OH*-chemiluminescence integrated over the entire image of a time series acquired by fast Fourier transform. Considering amplitude, the technically premixed case shows by far the highest value as expected on the basis of the MMM measurements. TPM200 is about 5.9 times higher than PPM200. In further agreement, the PPM480 case exhibits 1.6 times higher fluctuations than the PPM200, although not as much higher as expected (see Table 1 for comparison). For 200 Hz the technically premixed case lags in phase. This is in agreement with the MMM measurements as well, but again, does not match the values exactly. The deviation in phase may be due to the steep gradients in gain and the sudden phase change around 200 Hz.

In analogy to Fig. 9, the line-of-sight results from the vibrometer measurement are also integrated in x- and z-direction (Fig. 10). A similar phase lag as observed for OH* is found for the technically premixed operating point, but major differences are found in the amplitudes. PPM480 still shows higher amplitude than PPM200, which exhibits the lowest value of the three operating points considered.

Most interesting is the amplitude of TPM200. Although it is still the highest of all three, it is considerably lower than the values extracted from OH*-chemiluminescence and this value corresponds better to the expectations based on the measurements with the MMM. A clear advantage of the vibrometer is that the time derivatives of density fluctuations, measured are not influenced by equivalence ratio waves like OH*-chemiluminescence.

The ratios of fluctuation amplitudes recorded by the LV are TPM200:PPM200 = 2.5 and PPM480:PPM200 = 1.6. These match the fluctuation ratios obtained by the multimicrophone method better than the OH*-chemiluminescence data. Using the LV to record the density fluctuations, the TPM200 fluctuations in heat release rate are no longer overestimated. Also a phase-shift between TPM200 and PPM200 becomes visible in the LV time-series expected from multimicrophone data.

Pseudo-local Data. Finally, the line-of sight data presented earlier are deconvoluted to provide pseudo-local data, which are free from artifacts originating from line-of-sight integration.

The OH*-chemiluminescence image sequence for PPM200 (Fig. 11, upper section) indicates that the fluctuating flat reaction zone seen in the line-of-sight data does not exist in reality. Instead, the zones with heat release overshoot or deficit are recirculated in the vortex breakdown bubble and finally reach the stagnation zone where they have been initially created before they are completely dissipated.

In the density fluctuation image sequence, two conical structures are visible which represent the inner and the outer shear layer in between the conical annular jet of reactants flowing into the combustor filled with hot combustion products. Each of them oscillates in phase but both oscillate with a phase difference of 180 deg relative to each other. This indicates a flapping motion of the annular jet, which is driven by the pulsation of the flow. The interesting finding is that the vibrometer records the density fluctuations due to the temperature difference of reactants and products in addition to the time derivatives of density fluctuations originating from combustion. Due to the oscillation of both shear layers with opposite phase, the net effect may be small after spatial integration, but it dominates the pseudo-local data. This explains the finding that the vibrometer delivers reasonable global results regarding the integral heat release fluctuation in the flame.

The OH*-chemiluminescence image sequence for TPM200 (Fig. 11, middle section) shows that the flat structure of the heat release overshoot and deficit zones does not exist in reality. The deconvoluted images once again show the strong recirculation of these zones toward the stagnation point. That implies that a significant oscillation of the equivalence ratio in the vortex breakdown bubble is present and that well mixed conditions cannot be assumed.

The density fluctuation image sequence reveals the two conical structures again. As expected, these similarly appear for both fuel injection methods.

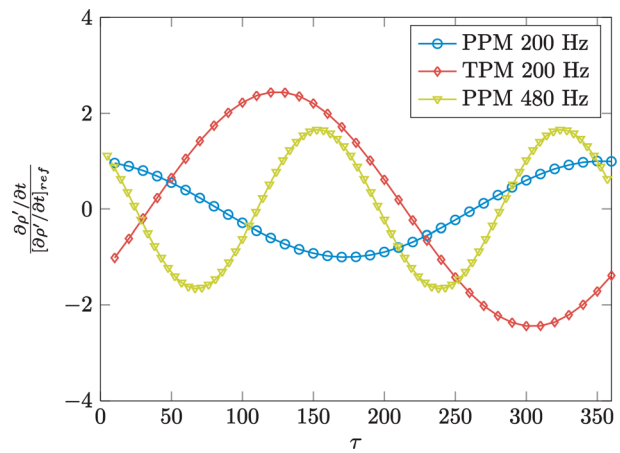

Fig. 10 Global density fluctuations. The fluctuations are normalized by the PPM200 fluctuation amplitude.

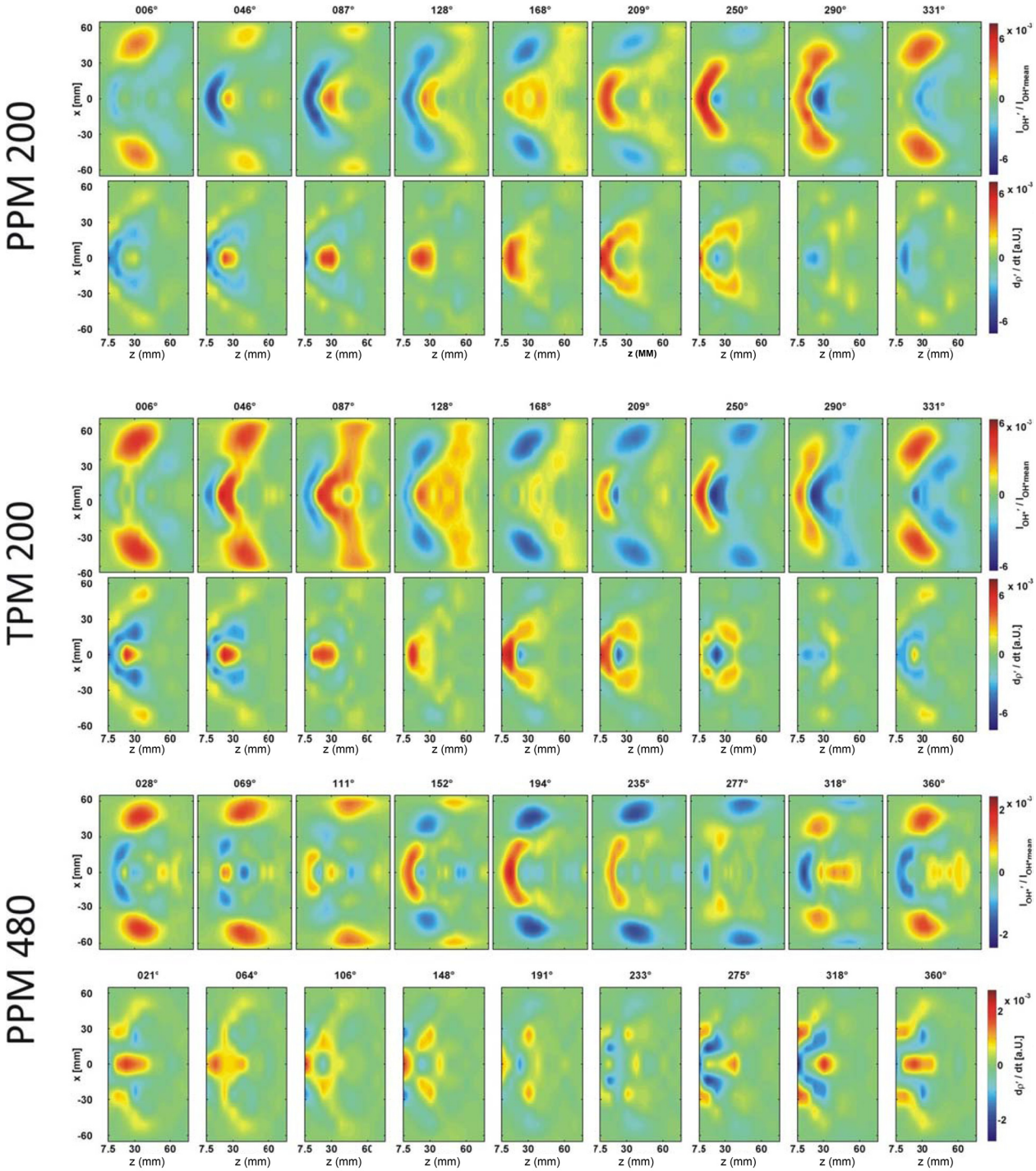

Fig. 11 Phase-resolved OH*-chemiluminiescence and density fluctuations, Abel-deconvoluted data

The OH*-chemiluminescence image sequence for PPM480 shown in the lower section of Fig. 11 proves that the bone-shape of the zones of heat release overshoot (red) and heat release deficit (blue) visible in figure Fig. 7 (lower section) do not exist in reality. Instead, these zones are generated at the burner exit and propagate radially outward during convection downstream before they are dissipated.

The density fluctuation image sequence for PPM480 does not provide additional insight compared to PPM200.

Conclusions

The focus of the study was the improvement of the understanding of FTFs measured with the MMM. In that context, a LV was used in addition to OH*-chemiluminescence imaging with an intensified camera and with a photomultiplier. The test object was a single modular swirl burner, allowing operation in perfectly premixed mode (PPM) and operation with fuel injection in the swirler (TPM) as well.

Following standard approaches in thermoacoustics research, it was shown that local density fluctuations should be proportional to the local heat release fluctuation, which can be acquired by OH*-chemiluminescence imaging. Hybrid field methods for stability assessment are generally based on this very common assumption. Experiments with a premixed swirl flame were made which show that the density fluctuation and the OH*-chemiluminescence fields are entirely different, because a number of other sources for the

generation of density fluctuations exist, which are not linked to heat release. Periodic motion of the interfaces between reactants and products generated by the acoustic field was observed. This motion is recorded by the vibrometer in addition to the density fluctuations from combustion. Although that effect may dominate the structure of the density field, it does not necessarily produce large errors after spatial integration.

For the PPM, the calculated fluctuations of the heat release were consistent with all three diagnostic techniques when the data were compared on the global level. In the case with equivalence ratio fluctuations (TPM), the global OH*-chemiluminescence fluctuations were significantly higher than the heat release fluctuations. This is due to the well-known sensitivity of OH* on temperature. This was found for the photomultiplier and also for the integrated high-speed camera data. In the investigated case, OH*-chemiluminescence intensity was dominated by the equivalence ratio wave which was measured using the OH*/CH*-ratio. The LV reproduced the fluctuation amplitudes expected from the measurements with the multimicrophone method for perfectly premixed and technically premixed operation as well with reasonable quality.

For perfectly premixed flames (PPM), planar OH*-chemiluminescence imaging data are better suited for the interpretation of FTF data than the LV data. Deconvolution of the line-of-sight data is required before the convection of the zones with periodic heat release can be studied in detail.

On the other hand, the LV data deliver interesting information on the dynamics of the interface between the reactants and the products which is not visible in the OH*-chemiluminescence image sequences.

This leads to the final conclusion that both methods complement each other.

Acknowledgment

This research was funded by the Austrian Science Fund FWF within Grant No. FWF-24096-N24 "Interferometric Detection of Thermoacoustic Oscillations in Flames" and by the Bavarian research program on "Flexible Power Plants."

Nomenclature

BFTM = burner and flame transfer matrix
BTM = burner transfer matrix
c = speed of sound (m/s)
c_p = constant pressure specific heat (J/kg/K)
f = frequency (Hz)
FTF = flame transfer function
FTM = flame transfer matrix
G = Gladstone–Dale constant (m^3 /kg)
h = specific heat (J/kg)
I_{CH} = CH*-intensity (AU)
I_{OH} = OH*-intensity (AU)
k_{vib} = calibration factor of LV (mm/s/V)
L = optical path length (m)
LV = laser vibrometer
p = pressure (Pa)
PPM = perfectly premixed mode
q = specific heat release (W/kg)
$\dot{Q}$ = heat release (W)
q_v = volumetric heat release (W/ m^3)
R = gas constant (J/kg/K)
t = time (s)
T = temperature (K)
T_c = temperature of reactants (K)
T_h = temperature of products (K)
TPM = technically premixed mode
U = vibrometer signal (V)
x, y, z = coordinates (m)
α = phase angle (deg)
κ = ratio of specific heats
ρ = density (kg/ m^3)
τ = phase angle at 200 Hz (deg)
ϕ = equivalence ratio
$\underline{\phi}$ = phase angle (rad)
$\bar{\phi}$ = equivalence ratio (mean)
ϕ' = equivalence ratio (fluctuations)
ω = angular frequency (rad/s)

References

[1] Rayleigh, 1878, "The Explanation of Certain Acoustical Phenomena," Nature, **18**(4), pp. 319–321.
[2] Paschereit, C. O., Schuermans, B., Polifke, W., and Mattson, O., 2002, "Measurement of Transfer Matrices and Source Terms of Premixed Flames," ASME J. Eng. Gas Turbines Power, **124**(2), p. 239.
[3] Munjal, M. L., and Doige, A. G., 1990, "Theory of a Two Source-Location Method for Direct Experimental Evaluation of the Four-Pole Parameters of an Aeroacoustic Element," J. Sound Vib., **141**(2), pp. 323–333.
[4] Lauer, M. R. W., 2011, "*Determination of the Heat Release Distribution in Turbulent Flames by Chemiluminescence Imaging*," Technische Universität München, Munich, Germany.
[5] Schuermans, B., Guethe, F., Pennell, D., Guyot, D., and Paschereit, C. O., 2010, "Thermoacoustic Modeling of a Gas Turbine Using Transfer Functions Measured Under Full Engine Pressure," ASME J. Eng. Gas Turbines Power, **132**(11), p. 111503.
[6] Schuermans, B., 2003, "Modeling and Control of Thermoacoustic Instabilities," Ph.D.thesis, École Polytechnique Fédérale de Lausanne, Lausanne, Switzerland.
[7] Freitag, E., 2009, "*On the Measurement and Modelling of Flame Transfer Functions at Elevated Pressure*," Technische Universität München, Munich, Germany.
[8] Bade, S., Wagner, M., Hirsch, C., and Sattelmayer, T., 2014, "Influence of Fuel-Air Mixing on Flame Dynamics of Premixed Swirl Burners," ASME Paper No. GT2014-25381.
[9] Bade, S., Wagner, M., Hirsch, C., Sattelmayer, T., and Schuermans, B., 2013, "Design for Thermo-Acoustic Stability: Procedure and Data Base," ASME Paper No.GT2013-94131
[10] Haber, L. C., 2000, "An Investigation Into the Origin, Measurement and Application of Chemiluminescent Light Emissions From Premixed Flames," Master's thesis, Virginia Polytechnic Institute and State University, Blacksburg, VA.
[11] Hipp, M., Woisetschläger, J., Reiterer, P., and Neger, T., 2004, "Digital Evaluation of Interferograms," Measurement, **36**(1), pp. 53–66.
[12] Hipp, M., Reiterer, P., Woisetschlaeger, J., Philipp, H., Pretzler, G., Fliesser, W., and Neger, T., 1999, "Application of Interferometric Fringe Evaluation Software at Technical University Graz," Proc. SPIE, **3745**, pp. 281–292.
[13] Pretzler, G., Jäger, H., Neger, T., Philipp, H., and Woisetschläger, J., 1992, "Comparison of Different Methods of Abel Inversion Using Computer Simulated and Experimental Side-on-Data," Z. Naturforsch., A, (J. Phys. Sci.), **47**(9), pp. 955–970.
[14] Pankiewitz, C., 2004, "*Hybrides Berechnungsverfahren für thermoakustische Instabilitäten von Mehrbrennersystemen*," Technische Universität München, Munich, Germany.
[15] Pieringer, J., Sattelmayer, T., and Fassl, F., 2009, "Simulation of Combustion Instabilities in Liquid Rocket Engines With Acoustic Perturbation Equations," J. Propul. Power, **25**(5), pp. 1020–1031.
[16] Gikadi, J., 2013, "*Prediction of Acoustic Modes in Combustors Using Linearized Navier-Stokes Equations in Frequency Space*," Technische Universität München, Munich, Germany.
[17] Dowling, A. P., and Morgans, A. S., 2005, "Feedback Control of Combustion Oscillations," Annu. Rev. Fluid Mech., **37**, pp. 151–182.
[18] Dowling, A. P., 1995, "The Calculation of Thermo-Acoustic Oscillations," J. Sound Vib., **180**(4), pp. 557–581.
[19] Leitgeb, T., Schuller, T., Durox, D., Giuliani, F., Köberl, S., and Woisetschläger, J., 2013, "Interferometric Determination of Heat Release Rate in a Pulsated Flame," Combust. Flame, **160**(3), pp. 589–600.
[20] Sangl, J., 2012, "Erhöhung der Brennstoffflexibilität von Vormischbrennern durch Beeinflussung der Wirbeldynamik," Ph.D. thesis, Technische Universität München, Munich, Germany.

3.2 Application and Advantages of LIV in Combustion

3.2.1 Experimental Burner

An experimental burner, designed by T. Leitgeb [45], was used for a comprehensive analysis of the LIV combustion-measurement tool. In order to facilitate the laser-optical investigation of thermo-acoustic oscillations, a variable geometry premixed methane/air burner was combined with in an optically accessible liner at atmospheric pressure. In such a burner an actuator alters a geometric parameter. This and previous work [30, 32, 46] used a burner where stability ranges can be extended with a variable nozzle geometry. Additionally, the flame can be independently adjusted in terms of rotation or swirl of the fluid. All parameters of the flame can be set continuously and independently during operation with such a concept. The variable geometry burner is shown in Figure 43 with the most important parts indexed. The burner was operated vertically for all of the tests. The center body (f) is moveable in axial direction. It varies the exit area (e) and consequently the exit momentum by moving a cone in and out of the exit nozzle. The swirl strength is set by the ratio between axial (c) and tangential (b) air, while keeping the overall air- and methane-flows (a) constant. Therefore the flame can be altered from a center-body-anchored flame to a swirl stabilized one. The axial air flow is forced into a purely axial direction by means of a stratifier. Methane was used as a fuel and was premixed with the tangential air in a mixing chamber (d) in the outer bushing. A total of 32 tangential bores in a four row arrangement were used to inject the tangential air-methane mixture, in contrast to previous

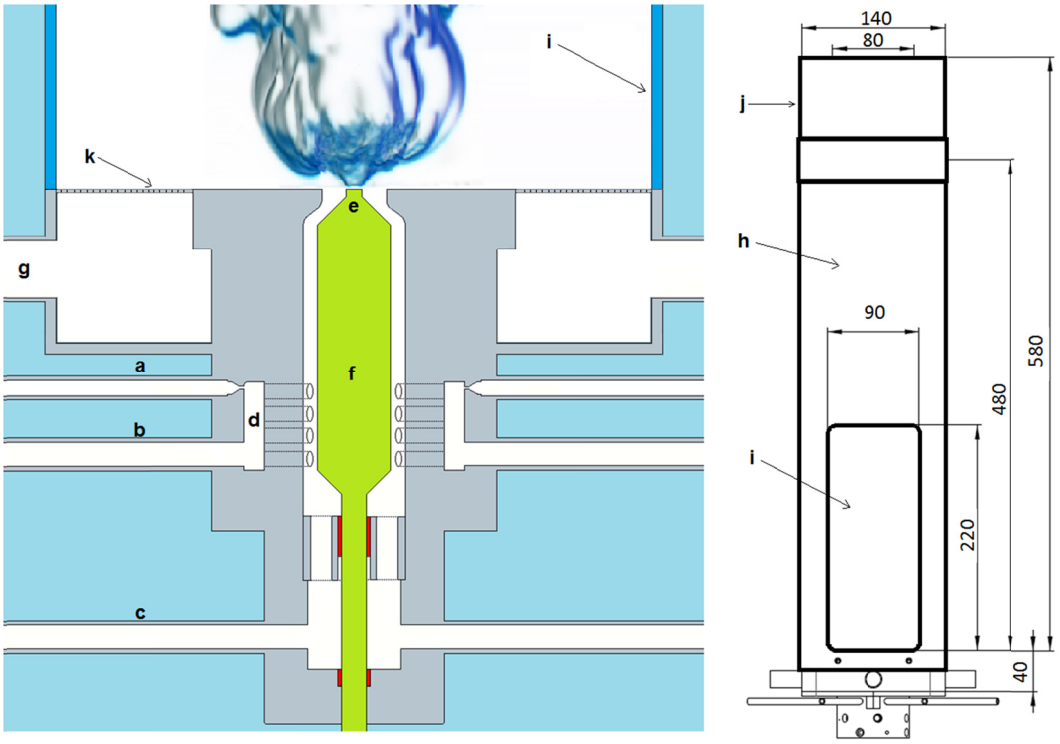

Figure 43: Variable geometry burner (VGB) with liner mounted on burner (right).

investigations, where only a total of four tangential bores provided the tangential gas mixture. This alteration in the design guaranteed a rotational symmetric flame for the investigations presented. In contrast to this, the previous design had a structure of four clearly visible flame-prongs. Additional cooling air (g) was provided through a settling chamber mounted underneath a perforated metal plate (k) with a hole diameter of 5mm and a distance between holes of 5mm. This air served as a coolant for the glass plates (i) in the liner. In the previous work by Giuliani et al. [46] all details on control and fuel supply including the metering and remote control were presented. A detailed design drawing is added to this thesis. Together with a siren in upstream flow [67] and a chamber section shown in Figure 43 this burner formed the test rig and the points of operation. The detailed combustion behavior was characterized in Peterleithner et al. 2015 C. This characterization was achieved by several measurement techniques. This also proved to be useful for plausibility check. The mean flow field in the flame and in the plenum was analyzed by particle image velocimetry and computational fluid dynamics respectively. The combustion process was characterized by means of schlieren, chemiluminescence and LIV. The microphones were used for consistency checks and as a trigger. In the unconfined flame a convective fluctuation was identified above 200 Hz. This could be explained by vortex shedding in the plenum found by means of numeric analysis of the flow field. A cavity resonance at 200 Hz was found when the flame was operated in the combustion chamber. It was particularly violent because of the heavy excitation by the convective effect. The convective effect itself was not found in the acoustics detected by the microphone while the cavity resonance caused heavy pressure fluctuations.

3.2.2 Global Heat Release

In industrial applications of gas turbine combustion, the fundamental mechanisms of thermo-acoustics are often not of primary concern. When the stability of a combustion process is of interest, a quick acquisition of significant parameters of the flame is more important than the mechanisms leading to stable or unstable regimes. The parameters significant to combustion are usually particle velocity, pressure, temperature and heat. In the worst case pressure fluctuations can destroy the combustor [68], Fluctuations of temperature affect the first turbine stage. The first turbine stage can withstand a certain temperature. This temperature is limited due to material properties. At the same time it is desired to capitalize this allowable temperature in order to gain maximum thermal efficiency. The smaller the fluctuations are and the more homogenous the temperature field is, the better. Then the mean temperature can be closer to the allowed temperature. Although those two parameters are the ones which directly affect the engine reliability and efficiency, the heat release of the flame is usually the source of temperature fluctuations and can be the source or driver of amplification of pressure fluctuations. Therefore this parameter is usually chosen by engineers in order to assess the stability of a combustor. The upstream velocity fluctuation generally influences the heat release somehow. It can be considered the major input parameter of a reduced model of flame dynamics. Therefore a very popular description of flame stability is to provide the heat release rate fluctuation, normalized by the velocity fluctuation at the burner exit. This way an amplification factor can be given for different frequencies.

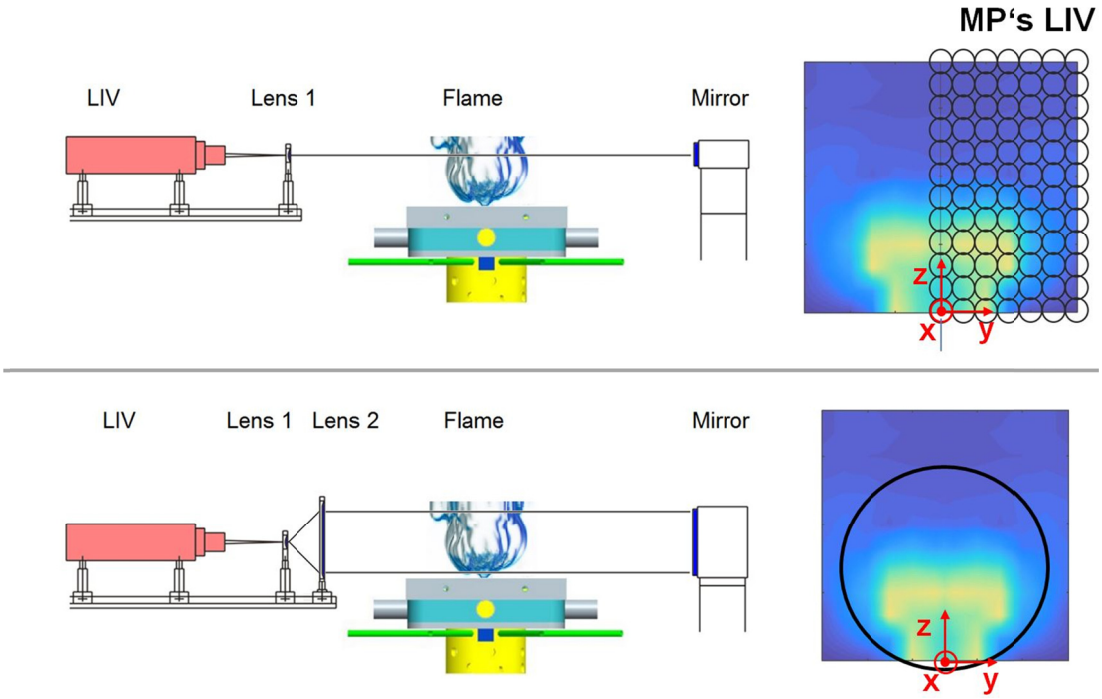

Figure 44: Conventional LIV setup for 2D-traversing (top) with measurement positions (MP) right, and setup for global heat release measurements (bottom) with measurement cross-section as used in .

These so called flame transfer functions (FTF) are defined using global (or total) heat release of the flame rather than local distributions of heat release rates. Linearity is assumed. In case of non-linear analysis the so called Flame describing function (FDF) can be measured by providing amplification as a function of frequency and amplitude of input velocity fluctuation. In order to reduce measurement

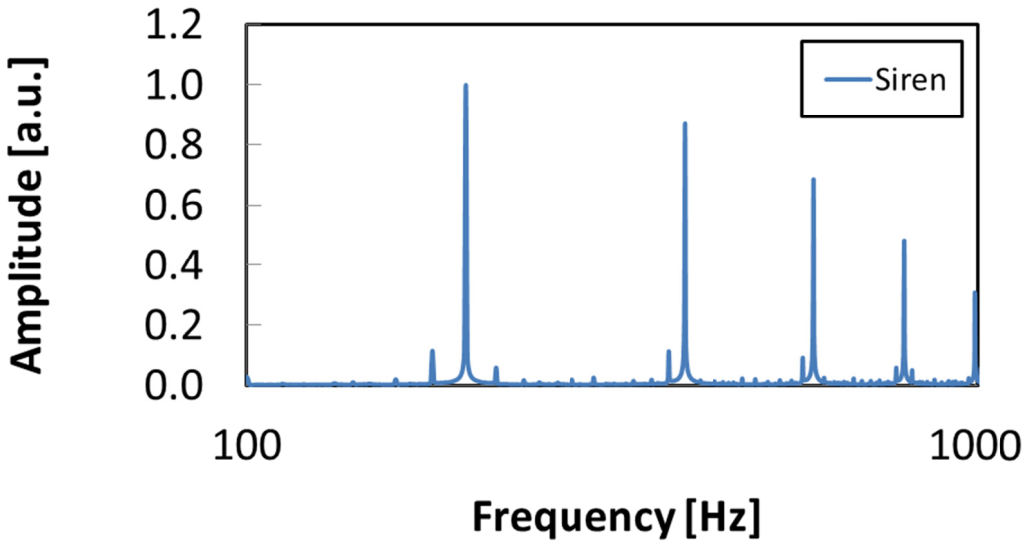

Figure 45: Spectrum of the Siren-trigger, when excited at 200 Hz (highest Amplitude).

time the LIV optics can be expanded to detect the entire heat release at once (Figure 44). This saves traversing time and thus reduces acquisition time considerably. To do so, it is necessary to ensure a homogenous illumination by the laser. For small diameters of the laser beam, the Gaussian beam intensity distribution can be neglected, but as soon as large diameters are used, this influence must be compensated because of the intensity variations. The bordering regions of the laser beam would then be underrepresented. The setup of LIV with an expanded beam was investigated and benchmarked against OH*-chemiluminescence acquired with a photomultiplier. The results are presented in PETERLEITHNER ET AL. 2016 A for the small experimental burner at TU Graz. For the measurements, excitation was carried out with a siren characterized in [67] at frequencies from zero to 600 Hz in 25 Hz steps with an additional frequency at 212 Hz. The post processing was carried out twofold. In a first step, a Fourier transform with a rectangular window was used to verify that the correct frequency was excited by the siren. This was necessary, because the sirens clutch sometimes slipped, particularly when acceleration from one point of operation to the next was steep.

In a second step, the exact amplitude was identified using a flat-top window. This windowing function is known for maximum accuracy in terms of amplitude. It successfully counterfeits the scalloping loss, which occurs when the measured frequency is between two bins of the spectrum derived by Fourier transform. As a drawback, the flat top window lacks frequency resolution. The resulting spectra are characteristic for particularly broad peaks - an originally defined peak can now spread over several bins in the spectrum. Two peaks close together cannot be separated anymore. This window is therefore particularly useful when a monofrequent signal is investigated or the frequency can be previously identified using a rectangular window.

For the above reasons, it is necessary to clarify the frequencies excited. The excitation-signal of the siren was characterized by not only one frequency and its higher harmonics, but also side lobes. Figure 45 shows the trigger signal of the siren with its side lobes and higher harmonics.

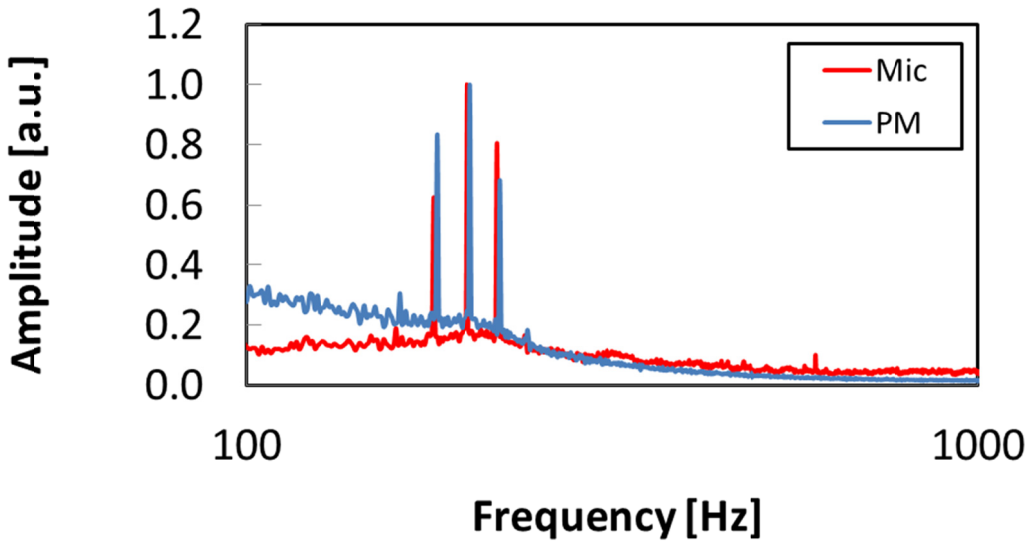

Figure 46: Spectrum of the photomultiplier signal (red) and the sound pressure in the cooling-plenum (blue), for excitation at 200 Hz (middle-lobe).

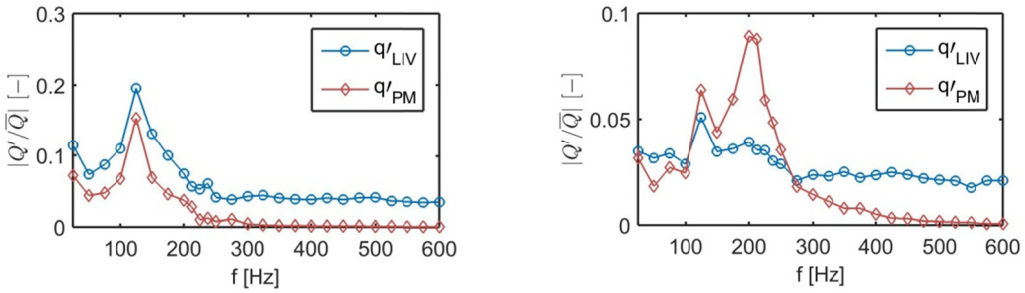

Figure 47: Heat release fluctuations detected by OH*-chemiluminescence and LIV. On the left for the perfectly premixed configuration and on the right for the technically premixed configuration.

Although these side lobes do not seem to be significant in the trigger-spectrum, higher receptivity of the combustor at certain frequencies can generate large amplitudes at these side lobes. In (Figure 46) sound pressure, integral chemiluminescence and density fluctuations directly at the burner exit are shown for the detached flame. The fluctuations of density are proportional to pressure fluctuations and consequently - according to acoustic theory - particle velocity. Isolating the main frequency ensured that the assumption of linearity be maintained.

The results of this investigation are presented below. Similar to Peterleithner et al. 2015 B, where a large scale burner was investigated at TU Munich for perfectly premixed flames, the global heat release rate measured by integral LIV and integral OH*-chemiluminescence matched very well. The overall level of heat release detected by the vibrometer was slightly higher throughout the spectrum due to the noise level caused by a short measurement time of only 15 seconds (Figure 47). Considering monofrequent excitation, both techniques found a strong amplitude at 125 Hz and a gradual decrease of amplification with higher frequencies.

This is in agreement with theory, since integral chemiluminescence should be proportional to heat release in absence of equivalence ratio waves as long as the strain rate is low [18]. Considering the technically premixed configuration, the overall amplification due to the siren is smaller. One reason for this is the fact that the mass flow through the siren is less than in the perfectly premixed configuration, since fuel is not split between the air streams anymore but injected in the burner directly. Never the less, the distinct peak at 125 Hz can be found with both techniques. The agreement of both measurement techniques is very good at this frequency. In contrast to this, the recordings at 212 Hz showed a strong deviation between measurement techniques. The amplitude is a local maximum for both but recorded with LIV, it had a similar order of magnitude as the neighboring excitation frequencies, chemiluminescence on the other hand suggested a severe amplification, exceeding neighboring frequencies by far. This was assumed to be caused by equivalence ratio waves. Such equivalence ratio waves can be detected by OH*/CH*-chemiluminescence ratio measurements.

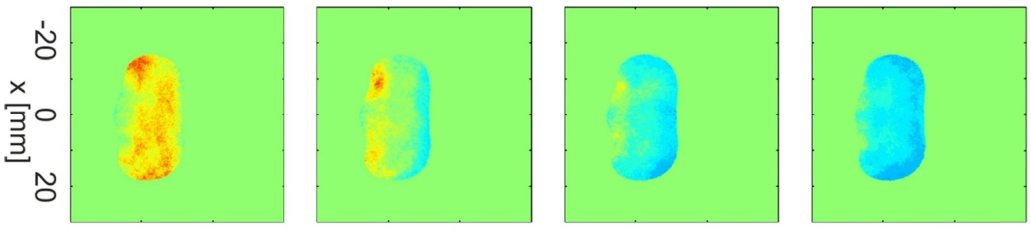

Figure 48: Equivalence ratio waves detected by measuring the OH*/CH*-ratio.

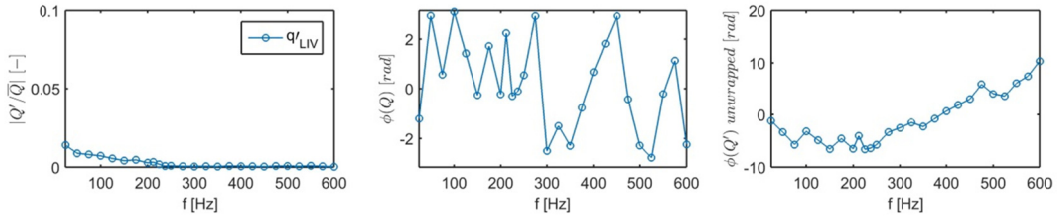

Figure 49: Heat release fluctuation-error due to pressure waves. Density fluctuations detected by the vibrometer with fluid flow but without reaction.

When measuring this ratio, the existence of a significant wave was proven for the 212 Hz case (Figure 48). For further reading, a detailed investigation of the properties of chemiluminescence is discussed in the Dissertation of Lauer [18].

Another possibility is that the vibrometer signal is corrupted by an increased sound pressure level at 212 Hz, which would reduce the detected amplitude since in the coupling equation **(**25**)** sound pressure has an opposite sign. However, the perfectly premixed setup does not show any sign of such a dampening. Additionally the density fluctuations measured by LIV without reaction (Figure 49) show very low amplitude as well. These two reasons make the case of sound waves significantly dampening the vibrometer signal not likely. The spectrum below shows density fluctuations due to pressure waves for the non-reacting case. To make an order of magnitude comparison possible they have been processed as if they were heat release fluctuations according to Equation **(**27**)** . One can see that other than for very low frequencies the amplitude of the LIV-sensor is close to zero.

One additional finding for the line-of-sight vibrometry measurements with an extended beam is an intensity variation along the lateral direction of the laser beam due to the Gaussian intensity profile. However, in this work, the influence of this non-uniform illumination did not have significant impact for the following reasons: The beam was expanded to 81 mm FWHM, however, as can be seen in the OH*-chemiluminescence measurement (Fig. 3) and the FM-DGV data (Fig. 9), the oscillations occur mainly within a zone with a radius of 20 mm around the flame center. Hence, the intensity dropped to 84 % due to the Gaussian shape for the outer regions of the probe beam. This results in a reduction of the detector signal by about 8 % for the outer region. Those outer regions have a lower influence on the FTF, because the flame extension along the line-of-sight is smaller at the outer region than at the

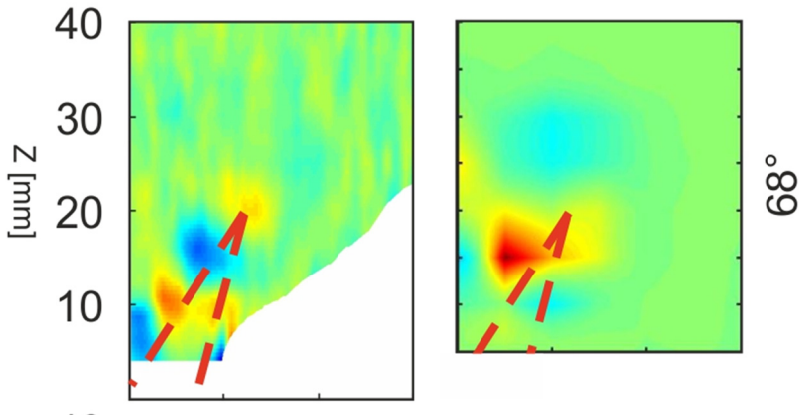

Figure 50: Phase resolved vorticity (left) and heat release rate (right) at a phase angle of 68°.

flame center due to rotationally symmetrical shape of the flame. This effect reduces the resulting error further. For accurate measurements, it is necessary to ensure a homogenous illumination by the laser. For small diameters of the laser beam, this influence is small and can be neglected, but as soon as large diameters are used, this influence should be compensated because the intensity variation would then under-represent the bordering regions of the laser beam. In PETERLEITHNER ET AL. 2016 A the approach was to widen the beam more than necessary for the diameter desired. Then only the core of the beam was sent through the collimating lens of diameter 81mm. In the same publication integral heat release with linear excitation as well as local heat release for the natural flame was shown. The latter was then compared with the velocity field of the reaction zone. During characterization of the combustor (Peterleithner et al. 2015 C), the flame showed a natural excitation frequency above 200 Hz, which was present both with and without the chamber. This excitation was caused by vortex separation in the plenum of the burner, as shown by numerical simulations using ANSYS CFD software. Under correct conditions it excited the cavity resonance of the combustor. In the chamber, at resonant conditions the phase resolved heat release detected by LIV is always difficult to interpret. In Peterleithner et al. 2016 A, it was possible to combine the LIF measurement with a FM-DGV velocity recording at TU Dresden (without chamber) to clarify the source of local phase changes of heat release in the swirl stabilized flame. Vorticity was calculated from the velocity field and compared to heat release. Matching the spatial distributions at the same frequency for both LIV and FM-DGV data sets, heat and vorticity revealed the source of instability to be vortex shedding from upstream the nozzle. Periodic vortex shedding modulates the flame surface. This variation in flame surface typically causes a fluctuation of heat release, vorticity outside the reaction zone does not cause fluctuations in heat release.

3.2.3 Reviewed Articles on the Application of LIV in combustion:

- PETERLEITHNER ET AL. 2015 C

J. Peterleithner, A. Marn and J. Woisetschläger, "Interferometric In estigation of the thermo-acoustics in a swirl stabilized Methane flame," in Proceedings of the ASME Turbo Expo, 2015.

- PETERLEITHNER ET AL. 2016 A

J. Peterleithner, R. Basso, F. Heitmeir, J. Woisetschläger, S. R., C. J. and A. Fischer, "COMPARISON OF FLAME TRANSFER FUNCTIONS ACQUIRED BY CHEMILUMINESCENCE AND DENSITY FLUCTUATION," in Proc. ASME Turbo Expo, 2016.

Proceedings of the ASME Turbo Expo 2015
GT2015
June 15-19, 2015, Montreal, Canada

GT2015-42743

INTERFEROMETRIC INVESTIGATION OF THE THERMOACOUSTICS IN A SWIRL STABILIZED METHANE FLAME

Johannes Peterleithner, Andreas Marn & Jakob Woisetschläger

Institute for Thermal Turbomachinery and Machine Dynamics, Graz University of Technology
8010 Graz, Austria
johannes.peterleithner@tugraz.at

ABSTRACT

In this work, an atmospheric model combustion chamber was characterized employing Laser Vibrometry, chemiluminescence and Particle Image Velocimetry. The test object was a variable geometry burner enclosed with a liner, with the flame optically accessible through four fused silica windows. In this burner with adjustable flame conditions the cavity of the atmospheric model combustion chamber was excited at a frequency around 200Hz. Resonant and non-resonant flame conditions were investigated and compared by laser vibrometer interferometry, schlieren visualization and OH*/CH* chemiluminescence. Additionally, the velocity field was recorded with Particle Image Velocimetry, while the aerodynamics of the burner plenum was analyzed with Computational Fluid Dynamics.

NOMENCLATURE

c	[m/s]	Speed of sound
f	[Hz]	Frequency
G	[m^3/kg]	Gladstone-Dale constant
k	[mm/s/V]	Calibration factor of LV
LV	-	Laser Vibrometer
n	-	Refractive index
$\dot{m}_{tan}/\dot{m}_{ax}$	[-]	mass ratio of tangential and axial air
OPL	[m]	Optical path length
p	[Pa]	Pressure fluctuation
P_{th}	[kW]	Thermal Power
$\dot{q}_V$	[W]	Volumetric heat release
S	-	Simplified Swirl number [1]
t	[s]	Time
U	[V]	Voltage
x, y, z,	[m]	Geometrical coordinates
u,v,w,	[m/s]	Velocities, in coordinate direct.
γ	[-]	Ratio of specific heats
ρ	[kg/m^3]	Density
Φ_{core}, Φ_{glob}	[-]	Equivalence ratio without / with Cooling air

INTRODUCTION

The thermoacoustic behavior of gas turbine combustors is critical for the reliability and performance of the whole engine. With increasing demand of part load capability, the topic is as important as ever. Nowadays low-NOx strategies include lean combustion in order to reduce the flame temperature. Consequently the combustor wall has less cooling holes and therefore less damping. Inside the combustor, interactions between fluctuations of heat release and pressure can occur periodically. With less damping, the effect of thermo-acoustic coupling is more severe. Thermoacoustics is a highly dynamic process which calls for time resolved methods of analysis. Due to the hot environment in a combustor, only few measurement techniques can be applied in order to provide local information of state variables. Laser Vibrometry (LV) is one of them. It is capable of time resolved recording of density fluctuations (dρ'/dt) which are linked to pressure and heat release fluctuations by equation [1]. In case of small pressure fluctuations, this is also a measure of local heat release rate[2],

$$\frac{d\rho}{dt} = \frac{1}{c^2}\frac{dp}{dt} - \frac{\gamma - 1}{c^2}\dot{q}_V \qquad (1)$$

Here, absence of heat release gives access to density fluctuations, but more interestingly, if heat release is present, the density fluctuations due to heat release are by orders of

magnitude higher than the ones due to pressure fluctuations. Only when cavity resonance is observed, interpretation of results must be carried out with care as pressure fluctuations can no longer be neglected. Therefore, in flames, the density gradient is also a measure of local heat release rate as shown by Leitgeb et al [3]. Laser Vibrometers were initially developed to detect vibrations of solid structures in machine dynamics employing the Doppler effect in a laser beam. By keeping the object (i.e. then a mirror) fixed, the LV detects the time derivative of the density of the gas within the cylindrical volume of the Laser beam. Local information can be obtained by a correlation technique using 2 Vibrometers, or in case of rotational symmetry by computing an inverse Abel-Transformation.

In this study, a swirl-stabilized Methane-air combustor was investigated at atmospheric conditions with and without resonance. The goal of this study was to identify regions of acoustic amplification in contrast to regions of damping.

The flame dynamics were visualized using the Laser Vibrometer combined with PIV data. The flow field in the combustor is compared to a CFD calculation employing commercial software, in order to identify sources of periodic noise.

EXPERIMENTAL SETUP

Combustor and the thermoacoustic laboratory

For laser optical investigations of flame dynamics, an atmospheric combustor with 4 quarz windows, mounted on a variable geometry burner is used. The combustor shown in FIGURE 1 is fed by fuel (a) tangential air (b), axial air (c), and cooling air (g). The axial air is forced through a stratifier in order to ensure purely axial flow. In contrast to this the tangential air passes the outer mixing chamber (d) and from there, enters the plenum through 32 cylindrical bores aligned tangentially and symmetrically around the burner axis. Methane is injected into the tangential air in the outer chamber, guaranteeing well premixed combustion.

The initial design was used in earlier publications [4]. It consisted of four tangential bores forcing swirl onto the fluid, then the flame shape had four clearly visible prongs, making tomographic methods very time consuming. The alteration in the design using 32 bores guaranteed a cylinder symmetric flame for the investigations, and dramatically simplified post-processing.

The center cone (f) of the burner can be moved axially in order to constrict the flow through the burner exit nozzle (e) and consequently maintaining the right velocity at part-load. The swirl can be adjusted by changing the mass-flow ratio of axial(c) and tangential (b) air.

For our investigations the center cone was set to 1mm above the exit-plane while changing the points of operation by changing the swirl-number, as well as total mass-flow. While the burner has been documented in detail in the work of

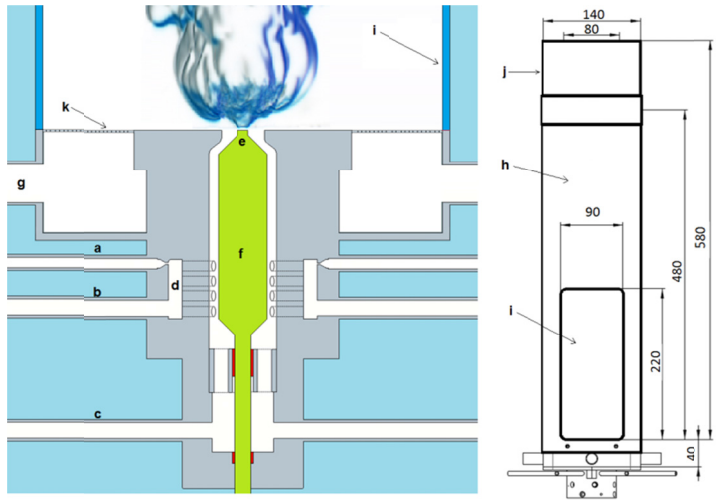

FIGURE 1: VARIABLE GEOMETRY BURNER (LEFT) WITH LINER, MOUNTED ON BURNER (RIGHT).

Giuliani et al [3], the flow-field within the liner will be discussed in this work. The liner (h) has an optical access on four sides (i), an exit constriction of 80mm in diameter at the hood (j) and is supplied with additional cooling air (g). The cooling air was provided through a settling chamber mounted underneath a perforated metal plate (k).

TABLE 1: POINTS OF OPERATION

Point of operation	$\dot{m}_{tan}/\dot{m}_{ax}$ [-]	P_{th} [kW]	ϕ_{core} [-]	ϕ_{glob} [-]	S [-]
resonant	0.9	3.37	1.49	0.68	0.65
stable	1.76	4.24	1.92	0.87	0.98

The variable geometry combustor was placed in a liner of quadratic shape with cross-section. Its dimensions can be found in FIGURE 1.

The test rig was set up in a thermoacoustic laboratory within a 3x3x2.5m^3 box with two layers of low reflective curtains and a sound absorbing ceiling.

Throughout all investigations, two points of operation are compared. The 'stable' one serves as reference, while the resonant one is of more interest for time resolved measurement techniques. Their specific properties can be found in TABLE 1. The simplified Swirl number was measured from z=8.5mm to z=17mm which 0.5 times and 1 time the burner exit diameter respectively.

NUMERICAL SETUP

Calculations were performed with Fluent in ANSYS 15 package with a pressure based solver, employing standard k-epsilon turbulence model with standard wall functions (y^+=30) and a Turbulence model with boundary conditions of velocity-

inlet, pressure-outlet, and no combustion. As operating pressure 97000Pa was set, and as a Medium air was used.

MEASUREMENT TECHNIQUES

Stereoscopic Particle Image Velocimetry

Particle Image Velocimetry (PIV, [5]) measures the velocity of particles seeded into a fluid. The measurement area is defined by the light-sheet from a double pulse laser. The displacement of particles illuminated by the laser light-sheet is captured by a camera triggered by the two laser pulses. With the time between pulses known, the velocity within the measurement plane can be calculated. By employing a second camera observing the measurement plane at a different angle, the out of plane component of velocity can be derived. (stereo-PIV).

The result is a three dimensional flow-field. In order to measure quantities such as the swirl-number S, measurement of the tangential velocity, or out-of-plane component is required.

For measurements without the liner, the stereo-PIV system at the Institute had both cameras aligned symmetrically around the y-axis and tilted 45° off the y-axis, with a distance of 660mm away from the burner axis. When measuring within the combustor, and due to restricted optical access (corner walls of the liner), a different setup had to be chosen. Camera one was aligned with the y-axis at a distance of 660mm. Camera two had an angle of 23° towards the the y-axis. In order to receive an image of the whole combustor cross-section, camera two firstly focused on one side of the combustion chamber, then the burner was rotated by 180° and the other half-plane was recorded. In this manner, all images from within the liner are stitched together from two measurements.

The laser system consists of a double-cavity Nd:YAG-Laser (from New Wave GEMINI, Sunnyvale, California, 532nm - green light, 120mJ per pulse, pulse duration 3-5ns, 15Hz), two cameras model DANTEC 80C60 HiSense (1280x1024 pixels, 12bit greyscale), and a PIV Processor model DANTEC FLOWMap 1500 (Dantec Dynamics, Skovlunde,Denmark). The raw images are processed with the DANTEC FlowManager PIV-software (v4.60.28). The field of view common to both cameras covers 70*90mm. For every point of operation, 1300 double frames for each camera were recorded. To generate vector plots out of the double images interrogation areas of 64x64 pixels size with an overlap of 50% in both horizontal and vertical directions were used. The air flow is seeded with titan dioxide (1µm diameter) for the burner and an aerosol of DEHS particles (Di-Ethyl-Hexyl-Sebacat, specific particle size 0.3-1µm) for the cooling air. Time between pulses was set to 80µs for burner investigations and 1500µs for cooling air measurements. Because of the high background illumination of titan dioxide glowing within the flame, the use of narrowband filters (532nm) and a back ground subtraction were necessary. The mass flow of injected seeding is small compared to the methane mass flow (mass ratio less than 1%), thus its effect on combustion can be neglected. For both setups calibration was performed by positioning a target in the lasersheet and traversing it perpendicular to the laser sheet. All together 5 images were acquired, (1mm; 0,5mm; 0mm; -0,5mm; and -1mm). The Dantec Software then computes a calibration polynomial for in- and out-of-plane velocities. For the given measurements, an error of +-0.5m/s was conservatively estimated, following Willert and Gharib [6].

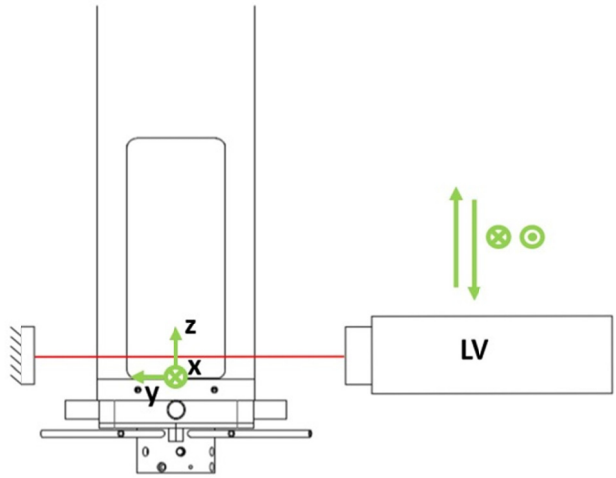

FIGURE 2: SETUP WITH BURNER, LINER, LASER VIBROMETER, COORDINATE SYSTEM, AND TRAVERSING DIRECTIONS

Laser Vibrometry

The Laser Vibrometer was the main measurement device for dynamic measurements within this investigation. The core part of the system is a Mach-Zehnder interferometer. The device utilizes the Doppler-shift which changes the frequency of the laser beam when it is reflected by a moving object to increase sensitivity. Therefore the Laser Vibrometer is widely used for detection of surface vibration of machinery. With the help of an acoustic-optical modulator these interferometers record vibration velocity rather than surface amplitude, which provides a spectral signal increased by a factor of $2\pi f$, with f the frequency of the oscillation.

In all types of interferometers the change of optical path length (OPL) is recorded rather than solely the geometrical path. This means that according to equation (2) any change of geometrical path (y) matters, as well as, changes of the refractive index (n)

$$OPL = n \times y \tag{2}$$

and consequently, changes of density along the optical path, since the refractive index is directly linked to the density (ρ) via the Gladstone-Dale constant (G) by

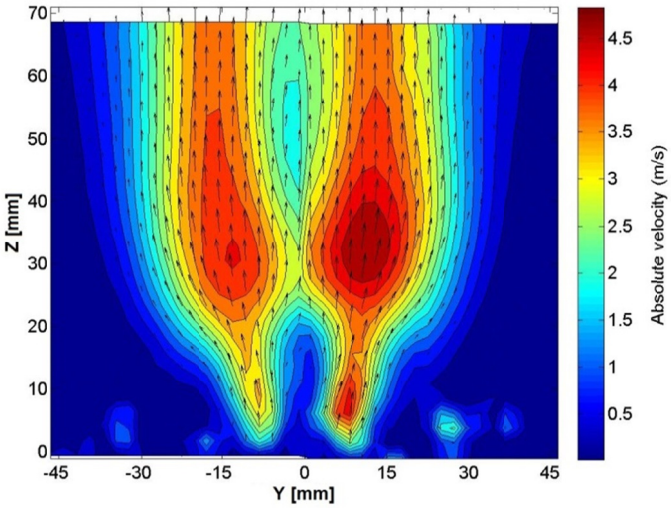

FIGURE 3: ABSOLUTE VELOCITY OF RESONANT OPERATION, MEASURED BY STEREO-PIV IN THE COMBUSTOR

$$n - 1 = G \times \rho \tag{3}$$

Employing equations (2) and (3), the laser-vibrometer detects changes of density if the beam is reflected by a rigidly fixed mirror, as the geometrical path then does not change anymore. The output voltage of the LV-processor represents the integral value of all density fluctuations along the beam path. The voltage output of the velocity decoder is given by:

$$U(t) = \frac{2G}{k} \int_y \frac{d\rho}{dt}\, dy \tag{4}$$

with the voltage U, the time t, the calibration factor k, the Gladstone Dale constant G, the coordinate in the laser light beam direction and the density ρ. The Gladstone Dale constant relates the gas density and refractive index. The density consists

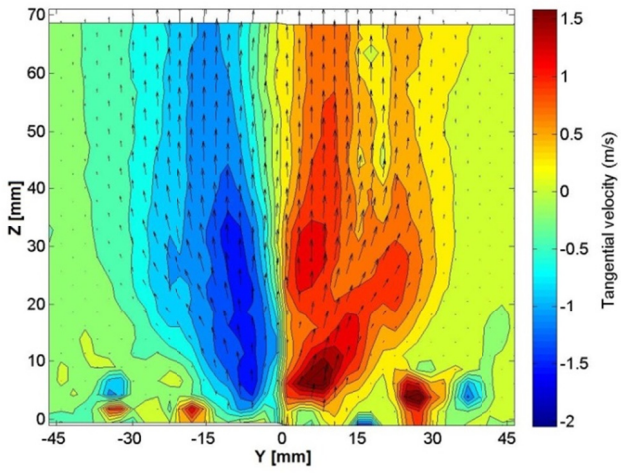

FIGURE 5: TANGENTIAL VELOCITY OF TANGENTIAL VELOCITY OF RESONANT OPERATION, MEASURED BY STEREO-PIV IN THE COMBUSTOR

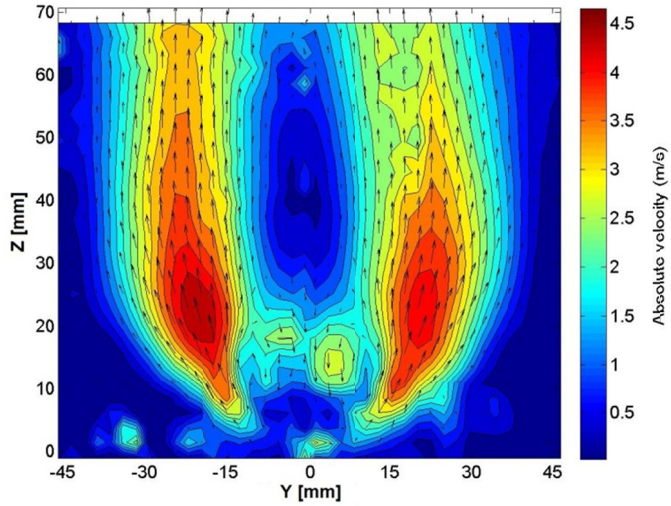

FIGURE 4: ABSOLUTE VELOCITY OF STABLE, NON RESONANT OPERATION, MEASURED BY STEREO-PIV IN THE COMBUSTOR

of a time averaged mean value and a fluctuating value ($\rho(t) = \rho_{mean} + \rho'$). Only the signal changing in time contributes to the voltage signal provided by the velocity decoder. Detailed information can be found in [3,7,8]. Turbulent flows have been investigated in [9,10,11]. During all investigations, the vibrometer was used in velocity decoder mode, with the calibration factor 5 mm/s/V for highest sensibility. For most of the measurements a single laser vibrometer was used (interferometer head OFV-353, velocity decoder OFV-3001, calibration factor 5mm/s/V, 20kHz bandwidth, no filters, Polytec, Waldbronn, Germany).

-40mm lenses were used to collimate the beam to 1.5-2mm diameter. To scan the field, the combustor was mounted on a DANTEC lightweight traverse (DANTEC Dynamics, Roskilde, Denmark), while the vibrometer was fixed. The field was traversed in the x-z plane with 25*15 positions, resolving the whole optically accessible area of the combustor.

Data acquisition was performed with analog input modules

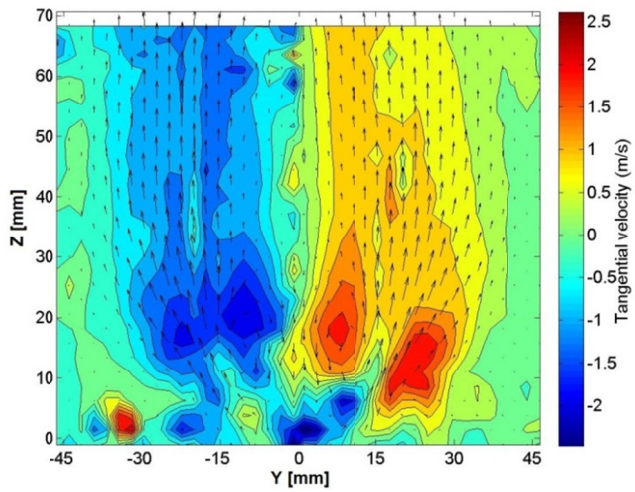

FIGURE 6: NON RESONANT OPERATION, MEASURED BY STEREO-PIV IN THE COMBUSTOR

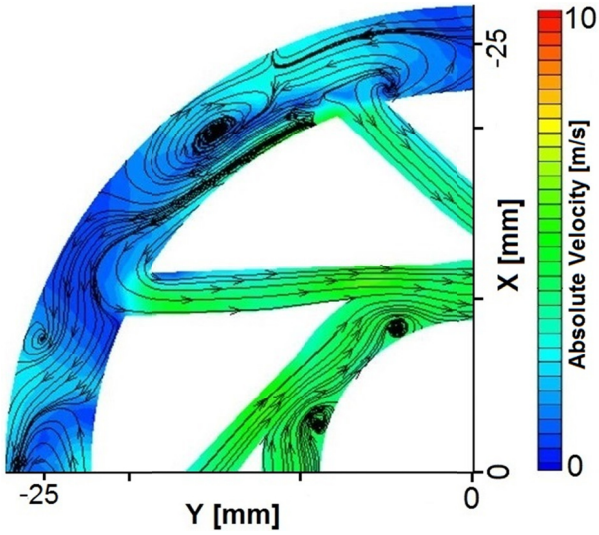

FIGURE 7: CROSS-SECTION OF THE FLOW-FIELD IN HIGHT OF TANGENTIAL SWIRLER-BORES FOR RESONANT OPERATION.

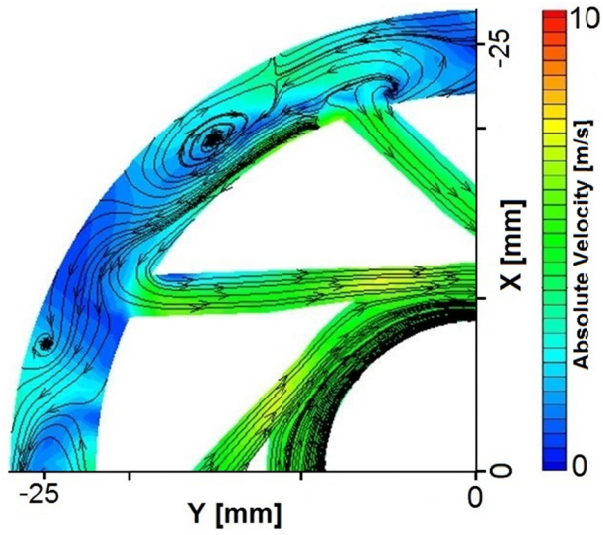

FIGURE 8: CROSS-SECTION OF FLOWFIELD WITH ABSOLUTE VELOCITY IN THE TANGENTIAL SWIRLER-BORES FOR, NON RESONANT OPERATION

NI-91215 (National Instruments, Austin, Texas) and Labview 8.6 software. For each position scanned 245760 samples were taken with a sample rate of 4096S/s. Together with the vibrometer voltage, a reference microphone signal was recorded in position x=-140mm, y=150mm, z=150mm (MIC1) and another one (MIC2) was recorded in the cooling air plenum (KECG2738PBJ-A, miniature electret condenser microphone, omni-directional, -40dB, 2.8mm diameter, Kingstate Electronics Corp, New Taipei City, Taiwan). All cross-correlations and Fourier transforms were done by a Matlab (2009b) routine using a sample length of 2048, providing frequency spectra (power, amplitude and phase) for each position scanned.

For the time series of density-fluctuation gradients, amplitude and phase were calculated by Fast Fourier transform, with the microphone as reference. For each position scanned, this provides a full frequency spectrum of fluctuations at all frequencies. After Abel-inversion of single projection lines for the frequencies of interest, this provides access to local density fluctuations at a certain frequency. Inverting integral data from a time series also provides discrete phase-angles for local data. Furthermore, origins of disturbances can be localized within single time-series.

FLOW FIELD

Experimental data

PIV-Data (Figs. 3-6) shows a maximum absolute velocity of approximately 5 m/s for both configurations. Due to higher axial momentum in the resonant case, the peak of total velocity is just above the flame when compared to chemiluminescence images below. The stable, non-resonant case establishes its peak velocity further downstream, but also sitting right on top of the flame, the wider expansion is clearly due to a higher swirl number. The arrows indicate that this high swirl number leads to a well-defined inner recirculation zone, reigniting the fresh reactants. In the resonant case, this recirculation zone cannot clearly be identified. Due to less swirl, the flame is of smaller radial expansion, and considering an interrogation area size of roughly 5mm for PIV post processing, this velocity gradient is likely not resolved. Looking at tangential velocities (FIGURE 5 and FIGURE 6), the stable non-resonant mode shows a clear recirculation zone, thus the tangential velocity is of greater radial expansion, with a low value just inside the jet, above the nozzle (z=10, x=+-15).

Numerical data

For the stable point of operation, a homogenous flow field was assumed. In FIGURE 7 and FIGURE 8 the cross-section of the critical joint of tangential air and axial air is plotted. Streamlines for the tangential air can be seen, forcing axial air towards the center rod. Major recirculation appears only in the outer chamber, improving mixing in this area. The resonant case shows several zones of recirculation in the outer mixing chamber as well. But in contrast to the non-resonant case, eight vortices establish along the center rod at the end of each tangential jet. Since the momentum of the jet is increased by almost 50%, a stronger disruption of the axial air is guaranteed. But this could also be sensitive to triggered separation of vortices. During operation, it became evident, that variation in tangential air, enables or suppresses flame oscillations, On the other side, changing axial air, slightly alters the resonance.

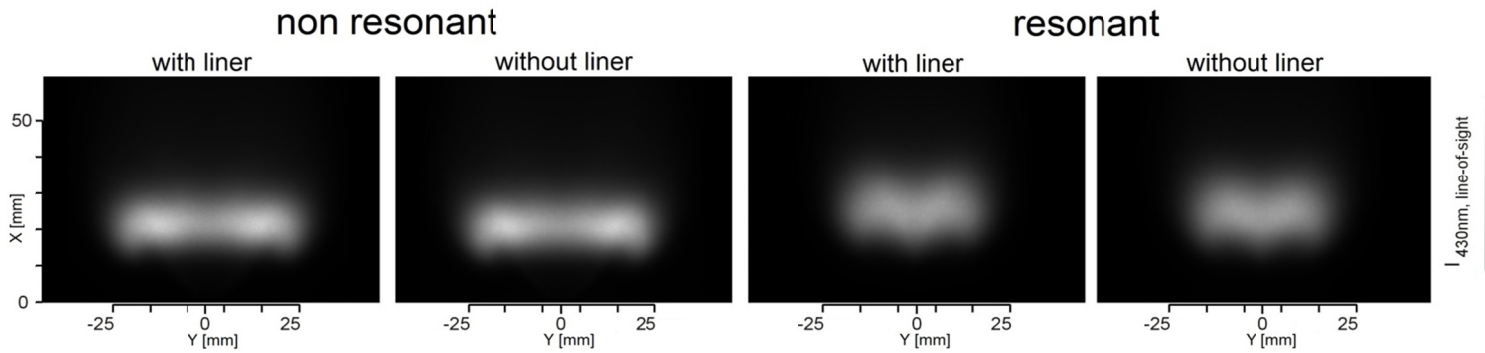

FIGURE 9: OH-CHEMILUMINESCENCE MEASUREMENTS FOR BOTH OPERATING POINTS

COMBUSTION DYNAMICS

Flame Behavior

Depending on the swirl, the Flame shows considerably different shapes. In FIGURE 9, integral OH-Chemiluminescence is shown for resonant and non-resonant points of operation, once within the liner and once without. Both points of operation are typically M-shaped, which means that reaction takes place not only in the inner shear layer but also in the outer one. The resonant flame is a lot more compact with a radial extension of 40mm while the non-resonant case the reaches 50mm in diameter. The flame is pulled apart and although these images show line of sight integrated data, one can see that less OH-chemiluminescence in the core, indicates that combustion dos not take place in the very core, but in a ring around the z-coordinate. In contrast to this, the resonant flame with higher axial momentum burns in the middle as well.

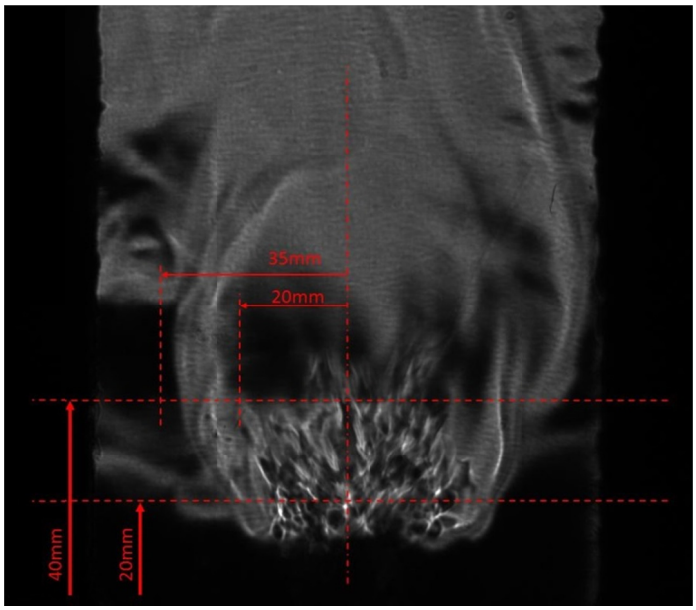

FIGURE 10: SCHLIEREN IMAGE OF THE RESONANT POINT OF OPERATOIN WITHIN THE LINER, WITH LASER VIBROMETER SCANNING POSITIONS.

Exemplarily, for the resonant case, the schlieren-image of FIGURE 10 nicely visualizes strong density gradients in the core of the flame indicating small strucutres in the combustion region, while on the sides, smooth density gradients show convective heat rising at larger diameters. Due to the size of those structures and the local flow velocity, one can estimate the frequency of these structures.

Intrinsic instability

To investigate the thermo-acoustic oscillation, the laser vibrometers measurement beam was aligned through position z=10mm, x=3mm, tangentially to the flame. In FIGURE 11, the frequency spectra of the resonant configuration are shown. The red curve is the non-reacting flow of fuel-air mixture at the given operating conditions. The spectrum is typical for a turbulent jet with a rise in amplitude for low frequencies followed by a gentle descent of amplitude towards high frequencies. As reference, the signal without flow is plotted in the same diagram (blue). Both signals are corrupted with electronic noise at 925Hz and 940Hz which disappear at higher

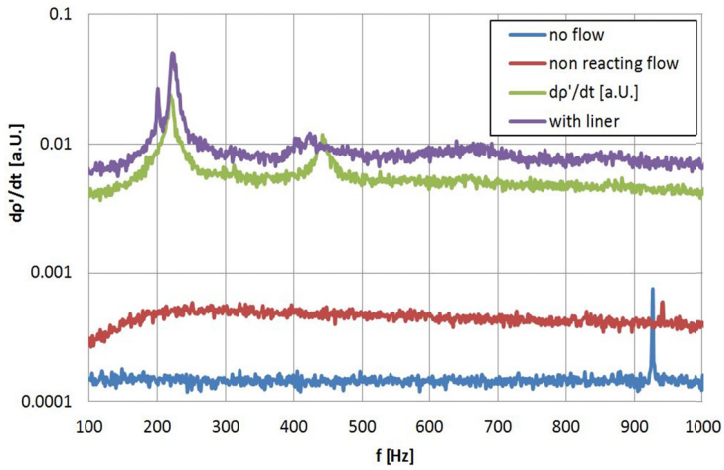

FIGURE 11: AMPLITUDE OF DENSITY FLUCTUATIONS, MEASURED BY THE LASERVIBROMETER AT Z=10MM, X=3MM FOR RESONANT OPERATION WITHOUT FLOW (BLUE), WITH NON-REACTING FLOW (RED), WITH COMBUSTION WITHOUT LINER (GREEN) AND WITH LINER(PURPLE).

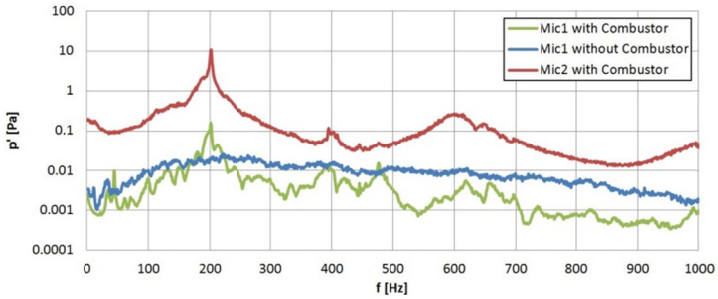

FIGURE 13: AMPLITUDE OF PRESSURE FOR RESONANT POINT OF OPERATION, WITH AND WITHOUT THE LINER IN PLACE. OUTSIDE (MIC1) AND INSIDE (MIC2) THE COMBUSTOR.

overall amplitudes at combustion. When igniting the gas, even without the liner in place, a periodic instability of the flame is visible in the spectrum.

The amplitude of the periodic phenomenon at 230Hz is approximately five times higher than the broad banded turbulent combustion with a higher harmonic at 460Hz, suggesting a non-sinusoidal signal. Although those kind of instabilities are not expected in a nearly anechoic environment such as an open flame in an acoustic laboratory, the phenomenon of intrinsic instability has been observed by a group in Holland [12,13] and recently has been analytically described by [14]. With the liner in place, the signal level is increased even further. But now, combustion excites an acoustic wave at 200Hz which can be identified by its very distinct peak.

This resonance is also observed in the microphone spectrum (FIGURE 13). For the resonant case without liner, the reference microphone (MIC1) does not detect a monofrequent pressure wave. In contrast to this, with the liner in place, significant pressure fluctuations become visible. This becomes even more evident, looking at the microphone situated in the cooling air plenum (MIC2). Here the sound pressure level reaches a maximum of 10.7Pa, which is about 15% of the burner pressure drop, from axial air inlet to flame region.

Thermo-acoustic oscillations have been observed in this model combustor, and documented in earlier works [15]. However it was assumed that the feedback loop of the resonance was closed only by the liner, meaning that the pressure wave modulates the flow conditions in the plenum. In fact, this instability occurs even without the liner, but is amplified by it. As shown in the spectrum in FIGURE 12 (left plot) the periodic phenomenon is very developed at x = +-6mm. Amplitude due to turbulent combustion expands further to x = + -15mm. The frequency spectrum for combustion within the liner (FIGURE 12 center plot) shows very similar features, but now, the periodic phenomenon excites a pressure wave in the combustor. Strong amplitude is seen at 200Hz within the region of heat release, and considerably lower amplitude at this frequency is observed in the non-reacting area. Looking at the power spectrum just above the flame at z=40mm (FIGURE 12 right plot) it is evident that the amplitude of 200Hz has a maximum beyond +-20mm radial extent. Comparison with the flow field in the section above shows that in this position the velocity is parallel to the burner axis. This and the Schlieren image in FIGURE 10 show that outside the flame radius but within the region where products rise convectively, mixing with colder cooling air takes place. This suggests that this outer region is slightly colder than the region at the center-axis, where solely the hot combustion products flow downstream. Since this flame seems to burn only in the inner shear layer, the structures on the outside seem to have just the right temperature to particularly enable the standing wave, thus the higher

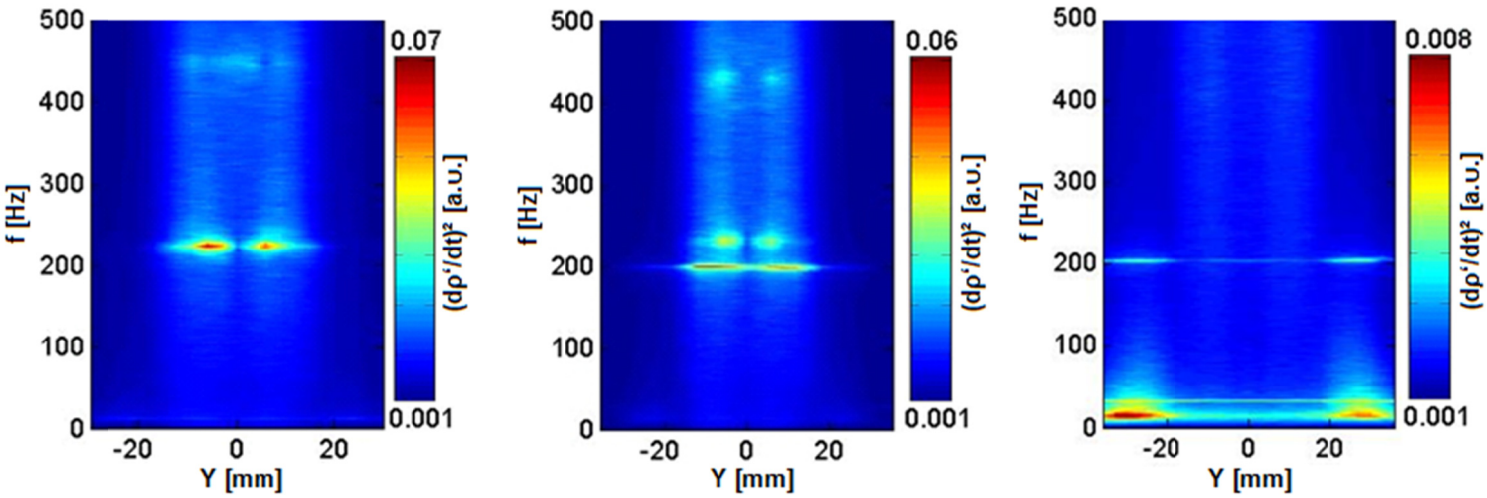

FIGURE 12: POWER SPECRUM OF THE LASER VIBROMETER IN A HORIZONTAL SCAN FOR THE RESONANT OPERATION MODE WITHOUT LINER AT Z=20MM (LEFT), WITH LINER AT Z=20MM (CENTER) AND WITH LINER ABOVE THE FLAME AT Z=40MM (RIGHT). ALL THREE ARE RESONANT FLOW CONDITIONS.

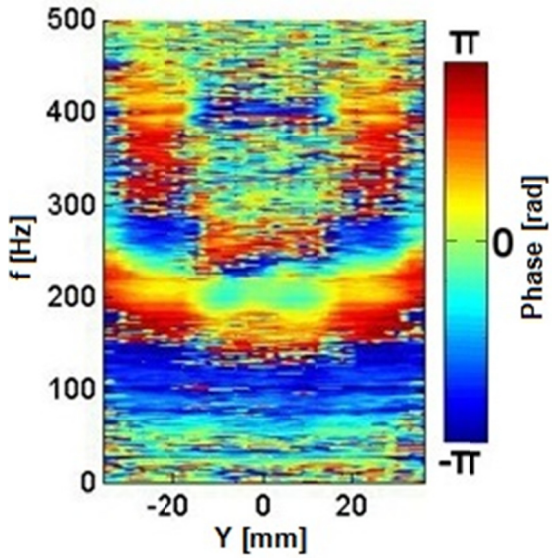

FIGURE 14: PHASE BETWEEN THE LASER VIBROMETER AND THE MICROPHONE IN A HORIZONTAL SCAN FOR THE RESONANT OPERATION, INSIDE THE LINER IN THE FLAME AT Z=20MM.

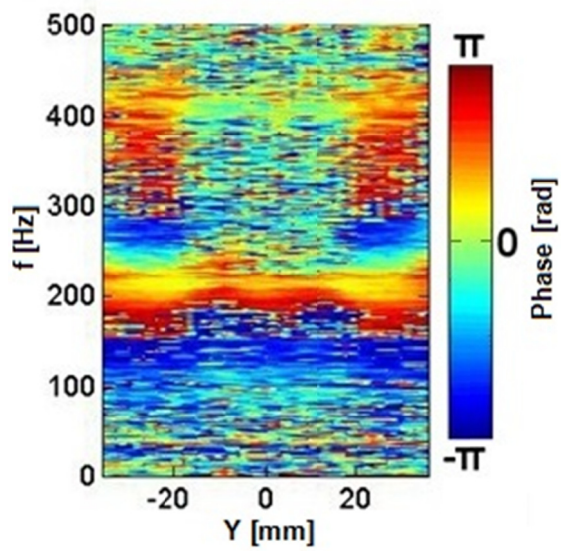

FIGURE 15: PHASE BETWEEN THE LASER VIBROMETER AND THE MICROPHONE IN A HORIZONTAL SCAN FOR THE RESONANT OPERATION, INSIDE THE LINER ABOVE THE FLAME AT Z=40MM.

oscillation amplitude in this region. In contrast to this, hot products rise within the diameter of the flame. Mixing of core flow and cooling air thus has not happened then. A scan along the radius of the exit plane revealed a peak total temperature of 520°C at the center axis, smoothly descending to 280°C at y=40mm, indicating, that cold cooling air is still escaping the constriction on the edges, therefore a homogenous temperature field can neither be assumed at this level, nor further upstream.

The exit temperature has been checked for feasibility by a heat balance. Assuming methane to fully react, a heat input of 3.365kW can be specified. Reduced by a heat loss through convection on the liner surface of 2.4kW gives an exit heat of 1.04kW. For this we measured the liner surface temperature with a thermal camera and quantified the heat loss according to the chart from Wrede for natural-convection [16]).With an entrance temperature of 20°C the exiting heat gives an exit temperature of 510°C calculated via specific heat capacity. This is above the mean exit temperature but shows the feasibility of the Temperature level.

On the bottom of FIGURE 12 (RIGHT), high oscillation amplitudes are detected at 15Hz and at 30Hz across the whole section of the burner. The 30Hz wave is constant over the whole burner, indicating a structural vibration of the test rig, and has been identified as the flexural mode of the burner mounted on the traverse. This has also been shown in [5] where the setup of test rig and measurement equipment was tuned in order to keep the region in the spectrum around the resonance free of structural vibrations. In contrast to this, the 15Hz is not of mono frequent character but decays towards higher frequencies, indicating a convective-aerodynamic effect. In this region hot strains from the flame rise with about 3m/s (FIGURE 3) next to cooling air at velocities close to 0.1m/s along the windows. This convective transport of heat was already expected by analyzing the Schlieren image in FIGURE 10.

The phase recorded from the correlation spectra LV-microphone discussed earlier, are found in FIGURE 14 and FIGURE 15. All are referenced to the microphone. Within the flame at the exciting frequency of 200 Hz (shown in FIGURE 12), a phase jump can be observed, when comparing the positions within the flame with the ones just outside. In the flame heat fluctuation dominate and as soon as the vibrometer passes the flame-edge, from within the combustion zone to the outer pressure field, a phase shift between heat release rate and pressure derivative is observed close to or at resonance. Barely visible in the amplitude, those pressure waves or convective structures can still be detected by a correlated phase. Focusing on FIGURE 15 which represents a scan across the liner in 40mm height (just above the flame) the phase-jump cannot be detected anymore, no heat release is observed, pressure is the dominant contributor to the density fluctuation.

Using the phase from LV-microphone correlations and integral line-of-sight amplitudes, a time-series of integral data can be plotted, when scanning the whole 2-dimentional field. From such integral time series (0 – 2π) local data can be calculated using Abel inversion under the assumption of radial symmetry, shown in FIGURE 16.

Harmonic Time Series

For a flame of radial symmetry after Abel-inversion, the plots in FIGURE 16 show the local density fluctuations. The

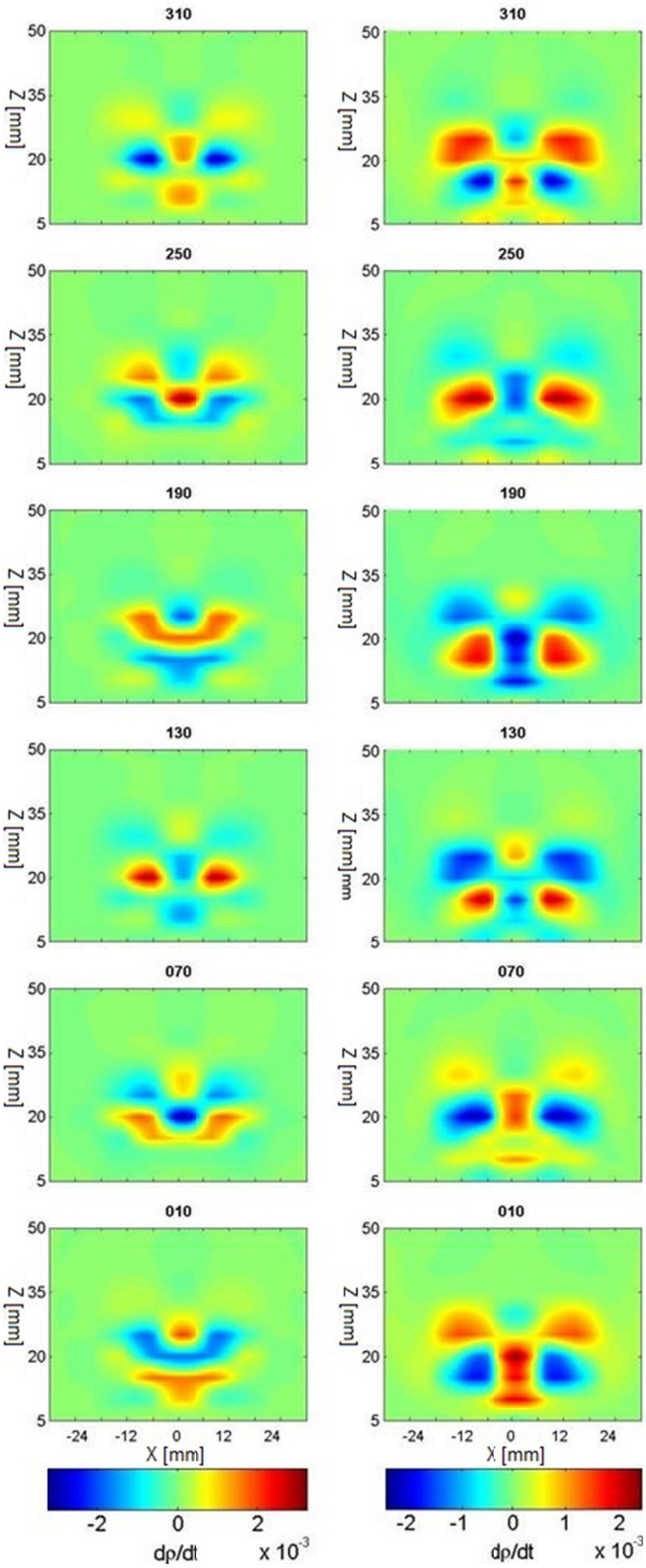

FIGURE 16: TIME SERIES OF LOCAL AMPLITUDES OF DENSITY FLUCTUATIONS (ABEL-INVERTED DATA), FOR RESONANT OPERATION, AT 232±8HZ (LEFT) AND AT 200±5HZ (RIGHT). ON TOP OF EACH PICTURE THE PHASE IS PLOTTED IN DEGREE.

two fluctuation frequencies observed in the spectra, are of different nature. The oscillation frequency at 232HZ (left in FIGURE 12) is caused by the assumed 'burner instability'. Very compact within the flame, the fluctuations decay quickly outside the main flow. The instability does not really recirculate, but rather progress through the flame. The down-streaming structures also seem to come directly from the burner orifice indicating changes in heat release, likely to be caused by periodic fuel oscillations.

In contrast to this, the 200Hz disturbance, which is also the frequency of the sound wave within the combustion chamber, has a stronger standing wave pattern, where positive structures flow around the recirculation area, and then follow back into the flame - moving in circles. Comparing the 190° image of the left time series (232HZ) in FIGURE 12 with the 310° image of the right one (200HZ) supports this impression. For the 232Hz oscillation a general impression of a mean flow direction parallel to the burner axis appears from the time-series.

CONCLUSION

In this paper, a variable geometry burner was investigated by time resolving laser vibrometry and Particle image Velocimetry, with the goal to identify and characterize the source of instability. It was shown, that the periodic phenomenon likely is an Intrinsic instability recoupling at the exit of the Tangential air-bores. The circular row of vortices at the end of those bores shown in numeric simulations, can be a very susceptible point to periodic acoustic perturbation, causing eddies to detach, which feeds flame periodically and causes the system to oscillate. A cross-check using the distance 8.5mm between those vortices (λ) and the tangential velocity of 2m/s at this point (v_{tan}) as the speed of convection results in a frequency f=235Hz. This assumption is set on the basis of numeric calculations for the burner plenum, and the results of optical measurements within the flame.

ACKNOWLEDGMENTS

This research was funded by the Austrian Science Fund FWF within grant FWF-24096-N24 "Interferometric Detection of Thermoacoustic Oscillations in Flames".

REFERENCES

Put references here.

[1] Beér, J. M., and Chigier, N. A., 1972. Combustion Aerodynamics,
1st ed. Applied Science Publishers Ltd., Barking.

[2] Dowling, A.P., "The calculation of thermoacoustic oscillations," Journal of Sound and Vibration, Vol. 180, No.
4, 1995, pp. 557-581.

[3] Leitgeb, T., Schuller, T., Durox, D., Giuliani, F., Köberl, S., Woisetschläger, J.,"Interferometric determination of heat release rate in a pulsated flame," Combustion and Flame, Vol. 160, No. 3, 2013, pp. 589-600.
[4] Giuliani, F., Woisetschläger, J., and Leitgeb, T., "Design and Validation of a Burner With Variable Geometry for Extended Combustion Range," ASME Turbo Expo 2012: Turbine Technical Conference and Exposition, Vol.
[5] von Karman Institute, 1994, Measurement Techniques in Fluid Dynamics—An Introduction _Lecture Series of the von Karman Institute, Rhode-St-Genèse, VKI LS 1994-01.
[6] Willert, C.E., Gharib, M. "Digital particle image velocimetry" Exp. Fluids, Vol. 10 No.4, 1991 pp. 181-193.
[7] Peterleithner, J., Salcher, F., Woisetschläger, J , 2013. "Frequency resolved interferometric detection of local density fluctuations in flames" in Proceedings of International Symposium on Applications of Laser Techniques to Fluid Mechanics, Lisbon, Portugal
[8] Zipser L, Franke HH (2008) Refracto-vibrometry – a novel method for visualizing sound waves in transparent media, Acoustics'08, Paris 29 June – 4 July2008
[9] Woisetschläger J, Lang H, Hampel B, Göttlich E, Heitmeir F (2003a) Influence of blade passing on the stator wake in a transonic turbine stage investigated by particle image velocimetry and laser vibrometry Proc. Inst. Mech. Eng. A 217:385–91
[10] Woisetschläger J, Mayerhofer N, Hampel B, Lang H, Sanz W (2003b) Laser-optical investigation of turbine wake flow Exp. Fluids 34:371–8
[11] Mayrhofer N, Lang H, Woisetschläger J (2000) Experimental investigation of turbine wake flow by interferometrically triggered LDV-measurements, Proc.10th Int. Symp. on Application of Laser Techniques to Fluid Mechanics (Instituto Superior Tecnico, Lisboa), paper 28-1
[12] P. G. M. Hoeijmakers, *Flame–acoustic coupling in combustion instabilities*, Ph.D. thesis, Technische Universiteit Eindhoven, Eindhoven, The Netherlands, 2014.
[13] M. Hoeijmakers, V. Kornilov, I. Lopez Arteaga, P. de Goey, H. Nijmeijer, Combust Flame, in press, http://dx.doi.org/10.1016/j.combustflame.2014.05.009.
[14] Emmert, T., Bomberg, S., Polifke, W. Intrinsic thermoacoustic instability of premixed flames (2014) Combustion and Flame, Article in Press.
[15] Peterleithner JJ, Marn A, Leitgeb T, Woisetschläger J (2013) Frequency Resolved Density Fluctuation Measurements of Combustion Oscillations in a Model Combustor, 49th AIAA/ASME/SAE/ASEE Joint Propulsion Conference & Exhibit, 15 - 17 Jul 2013, San Jose, CA , Paper No.: 1589261
[16] Gesellschaft, VDI: VDI-Wärmeatlas. 10. Aufl. 2006. Berlin, Heidelberg: Springer.

Proceedings of ASME Turbo Expo 2016: Turbine Technical Conference and Exposition
GT2016
June 13-17, 2016, Seoul, South Korea

GT2016-57485

COMPARISON OF FLAME TRANSFER FUNCTIONS ACQUIRED BY CHEMILUMINESCENCE AND DENSITY FLUCTUATION

Johannes Peterleithner, Riccardo Basso, Franz Heitmeir, Jakob Woisetschläger
Institute for Thermal Turbomachinery and Machine Dynamics, Graz University of Technology
8010 Graz, Austria

Raimund Schlüßler, Jürgen Czarske, Andreas Fischer
Chair of Measurement and Sensor System Techniques
Technische Universität Dresden
01062 Dresden, Germany

ABSTRACT

The goal of this study was to measure the Flame Transfer Function of a perfectly and a partially premixed turbulent flame by means of Laser Interferometric Vibrometry. For the first time, this technique is used to detect integral heat release fluctuations. The results were compared to classical OH-chemiluminescence measurements. Effects of equivalence ratio waves and vortex rollup were found within those flames and were then investigated by means of time resolved planar CH*/OH*-chemiluminescence and Frequency modulated Doppler global velocimetry. This work is motivated by the difficulties chemiluminescence encounters when faced with partially premixed flames including equivalence ratio waves and flame stretching. LIV, recording the time derivative of the density fluctuations as line-of-sight data, is not affected by these flame properties.*

NOMENCLATURE

c	[m/s]	speed of sound
D_{exit}	[mm]	burner exit diameter
f_D	[Hz]	Doppler shift of laser light
FTF	[-]	flame transfer function
G	[m³/kg]	Gladstone-Dale constant
$\vec{i}$	[-]	Laser incidence direction
I_{OH*} I_{CH*}	[-]	light intensity of OH* and CH*
k_{vib}	[mm/s/V]	vibrometer calibration constant
LIV		laser interferometric vibrometry
LDA		laser Doppler interferometry
i-OH*-CL		integral OH* Chemiluminescence
$\vec{o}$	[-]	observation direction
PPM		perfectly premixed
Q',	[W]	fluctuation of heat release
q_v'	[W/m³]	fluctuation of heat release
$\vec{s}$	[-]	sensitivity vector
TPM		technically premixed
u'	[m/s]	fluctuation of Axial velocity
U	[V]	voltage
$\vec{v}$	[m/s]	velocity vector
x, y, z	[mm]	coordinates
Φ	[-]	equivalence ratio
α	[°]	phase angle
ζ	[m]	length of measurement volume
K	[-]	ratio of specific heats
λ	[nm]	laser wave length
ρ	[kg/mm³]	density

INTRODUCTION

Modern gas turbines for power generation rely on premixed combustion systems to achieve high combustion efficiency and low emissions. As a drawback, high power densities and reduced damping capabilities of the combustor increase the susceptibility to thermoacoustic oscillations. These instabilities arise from the positive coupling between the fluctuations of pressure and heat release [1]. Prediction of gas turbine stability is often achieved by network models, originally used in system dynamics analysis. Within the model the flame remains a 'black box'. The flame is described as a single input single output block. Usually the data for this block comes from

flame transfer functions, which relate the unsteady heat release of the flame to perturbations of acoustic velocity at the burner exit [2, 3]. In the past, a variety of methods for the measurement of flame transfer functions in research combustors have been published. A method widely used for determining the FTF is measuring the chemiluminescence from OH* within the flame as the measure for heat release. Velocity fluctuations at the burner exit are obtained either directly from hot wire anemometry or laser Doppler anemometry. Whereas approaches relying on chemiluminescence are only applicable for adiabatic flames with low strain rates and constant equivalence ratio [4, 5], this method is not applicable to technically premixed combustion systems.

As an alternative Interferometric techniques like laser interferometric vibrometry (LIV) are not affected by this. They can detect heat release without the restriction of perfect mixing [6, 7]. The advantage of this technique is that it measures the time derivative of density fluctuations directly. With the absence of pressure fluctuations, this is a measure of heat release rate [8]. The link between those quantities has been exploited before, but this is the first time, integral heat release is recorded. As a benefit, it overcomes the time consuming process of traversing the whole field. In this study the technique is applied to a swirl stabilized burner configuration with a known flow field and well defined operating conditions. The flow is excited using a siren in the main air supply, where the perturbation level is measured with laser Doppler anemometry (LDA) in the burner exit nozzle. Secondly, integral Heat release is discussed for excitation frequencies from 0 Hz to 600 Hz. As a result from both, the flame transfer function can be calculated. This was done for a perfectly premixed flame, where chemiluminescence should provide a reliable result due to the absence of equivalence ratio waves. Then a technically premixed configuration more relevant to industrial applications is investigated. Differences in heat release are further analyzed by means of planar time resolved equivalence ratio measurements. To interpret the natural heat release spectrum of the flame, a Doppler global velocimeter with laser frequency modulation (FM-DGV) was used to compare the time resolved velocity field with line-of-sight-integrated heat release rate.

EXPERIMENTAL SETUP

For the investigations presented in this paper, a variable geometry burner was used and the flow was excited with a siren, mounted into the axial air-feedline. The burner has been documented in detail in the work of Giuliani et al [9], the flow-field and characteristics have been published recently [10] and the siren has been characterized in [11]. In Fig. 1 the burner is shown with the standard configuration - technically premixed (TPM) - to the left and the reference configuration - perfectly premixed (PPM) - to the right of the setup.

In the TPM configuration, the combustor is fed by fuel (a) tangential air (b) and axial air (c). The axial air is forced through a stratifier in order to ensure purely axial flow. In

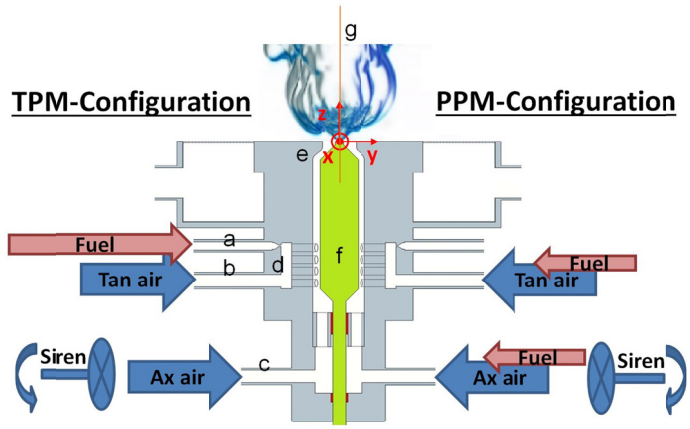

FIGURE 1: THE EXPERIMENTAL SETUP WITH THE TPM CONFIGURATION TO THE LEFT AND THE PPM CONFIGURATION TO THE RIGHT

contrast to this the tangential air passes the outer mixing chamber (d) and from there, enters the plenum through 32 cylindrical bores aligned tangentially and symmetrically around the burner axis. Methane is injected into the tangential air in the outer chamber. The siren modulates the axial air flow only.

In case of perfect mixing (PPM), the methane was injected into the air supply far upstream before tangential and axial air split. As shown in Fig. 1, the fuel is injected through small bores of a diameter of 0.5 mm. At those injectors a large pressure drop is present. Therefore, they are assumed to be acoustically stiff and the acoustics of the plenum would only slightly alter the fuel flow. Then equivalence ratio waves are enabled without necessarily generating large amplitudes of heat release.

TABLE 1: FLOW PROPERTIES

Axial air [g/s]	Tangential air [g/s]	Fuel [g/s]	Swirl Number [-]
0.422	0.397	0.0683	0.54

The movable center cone (f) of the burner was set to 1 mm above the exit in order to constrict the flow through the burner exit nozzle (e) and consequently ensure correct momentum for the point of operation. The test rig was set up in a thermoacoustic laboratory within a 3x3x2.5 m3 box with two layers of low reflective curtains and a sound absorbing ceiling. The mass flow, which was the same for both points of operation, can be found in Table 1. The simplified Swirl number, according to [2] neglecting the pressure term, was measured using a burner exit radius of 8 mm averaging over a height of z = 8.5 mm to z = 17 mm which is 0.5 times and 1 time the burner exit diameter respectively. The coordinate system for all measurements originates at the burner exit and the measurement plane (g) is defined by the x and z-axis.

Measuring Techniques

Heat release fluctuations for the FTF were acquired by means of LIV and OH*-chemiluminescense using a photomultiplier with a filter. Velocity fluctuations for the FTF were acquired by means of laser Doppler anemometry. For planar time resolved velocity fields, FM-DGV was employed, and finally the phase averaged planar CH*/OH*-chemiluminescence measurements were used to visualize equivalence ratio waves. Below the different measurement techniques are explained in detail.

Laser interferometric vibrometry (LIV) detects the line of sight (ζ) integrated density fluctuations of gasses by means of interferometry. This is shown in detail in [12] and applied in [13, 14]. Using a Polytec laser vibrometer (interferometer head OFV-353, velocity decoder OFV-3001, calibration factor 5mm/s/V, 200kHz bandwidth, no filters, Polytec, Waldbronn, Germany), the measured voltage (U) is linked to the derivative of the density fluctuation (ρ) by the Gladstone-Dale constant (G) which is 2.59e-4 m³/kg for the present points of operation and the calibration factor (k) which was set to 5 mm/s:

$$\int \frac{d}{dt}\rho(t)\, d\zeta = \frac{2 * k_{vib}}{G} U(t) \tag{1}$$

The link between density fluctuations and heat release fluctuations has been derived and extensively discussed by **[8, 6, 7]**. Neglecting pressure fluctuations which - for unconfined flames - are low compared to volumetric heat release rate q_v, the following equation applies:

$$\frac{d\rho}{dt} = -\frac{\kappa - 1}{c^2}\frac{dq_V}{dt} \tag{2}$$

With the ratio of specific heats (κ) and the speed of sound (c). In combustion application LIV is used to locally or globally detect heat release fluctuations. In order to locally resolve the heat release fluctuations, the vibrometer must be traversed in a two dimensional field **[14]**. Since for FTFs, only the space integrated information of the flame is relevant, the laser beam of the vibrometer was expanded to and collimated at a diameter of 81 mm and centered at a height of 40 mm above the burner exit plane in order to acquire the entire combustion fluctuations at once. For the comparison with vorticity, the vibrometers beam was narrowed down to 5 mm in diameter and traversed in two directions with increments of 5mm. The result was interpolated in order to provide more readable plots. Areas of uncertainty of the LIV technique include the varying Gladstone-Dale constant discussed in **[6]**, dependency on temperature discussed in **[12]** and a varying intensity of the laser beam over the beam diameter due to a Gaussian distribution of the laser light. Since only the central part of the beam covered the test section, the accuracy of the LIV detector signal is less than +/- 4 %, this can be further reduced, using a sufficiently strong light source.

Alternatively, for the FTF, the integral **OH*-chemiluminescence** (i-OH*-CL) intensity emitted by the flame was acquired using an UV filtered photomultiplier (PMM01, Thorlabs Inc., Newton, New Jersey, USA). On the photomultiplier a narrow band OH* interference filter (310 nm CWL, FWHM 10±2 nm Bandwidth, 50mm Mounted Diameter, 18 % Transmission, Edmund Optics, Barrington, NJ, USA) was mounted.

The processing of LIV and the i-OH*-CL signal were acquired with 100 kilosamples per second using a data acquisition with analog input modules NI-91215 (National Instruments, Austin, Texas) and Labview 8.6 software. The spectral analysis was performed using a fast fourier transform (FFT) based on Matlab routines. In order to tackle the scalloping loss of Fourier transforms, a Matlab 2015a implementation of a Flattop filter was used, which is valid if frequencies are known in advance, ensuring a high signal to noise ratio.

To record the velocities for the FTF a classical **laser Doppler anemometer** (LDA) was used to measure the axial velocity at the burner exit at z=2 mm x=r= 5.5 mm. (FibreFlow, DANTEC Dynamics, Roskilde, Denmark). Since LDA does not provide frequency spectra per se, with the help of a siren trigger the result was phase averaged and then divided into 64 bins. A FFT was performed on the phase averaged result and the base-frequency was used for the FTF.

A **particle image velocimetry** (PIV) was used as reference. The PIV setup was the same as in **[10]** with 1200 averaged images and two cameras set up at an angle of 45°.

A **Doppler global velocimetry** measurement system with laser frequency modulation (FM-DGV) was employed to assess the flame dynamics of the non-excited flame in part two of this article. The FM-DGV technique relies on measuring the Doppler frequency shift f_D of laser light, which is scattered by seeding particles moving with the flow:

$$f_D = \vec{v}\,\frac{|\vec{o} - \vec{\imath}|}{\lambda} * \frac{(\vec{o} - \vec{\imath})}{|\vec{o} - \vec{\imath}|} \;\; with \;\; \frac{(\vec{o} - \vec{\imath})}{|\vec{o} - \vec{\imath}|} = \vec{s} \tag{3}$$

with λ as laser wavelength, $\vec{o}$ as observation direction and $\vec{\imath}$ as laser incidence direction. Hence, the velocity component $v_{oi} = \vec{v} * \vec{s}$ along the direction of the sensitivity vector $\vec{s}$ (i.e., along the bisecting line of $\vec{o}$ and $-\vec{\imath}$) can be derived from the measured Doppler frequency. For determining the Doppler frequency shift, a frequency stabilized laser source in combination with a molecular cesium absorption cell with frequency dependent transmission was used. The frequency

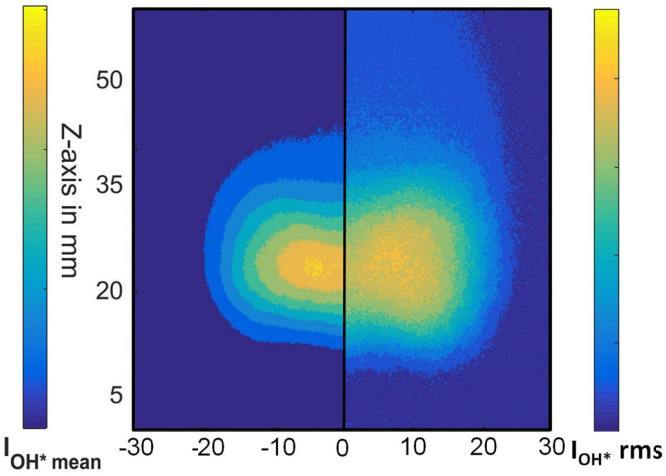

FIGURE 2: OH*-CHEMILUMINESCENCE OF THE TPM FLAME. MEAN (LEFT) AND RMS OF FLUCTUATION (RIGHT)

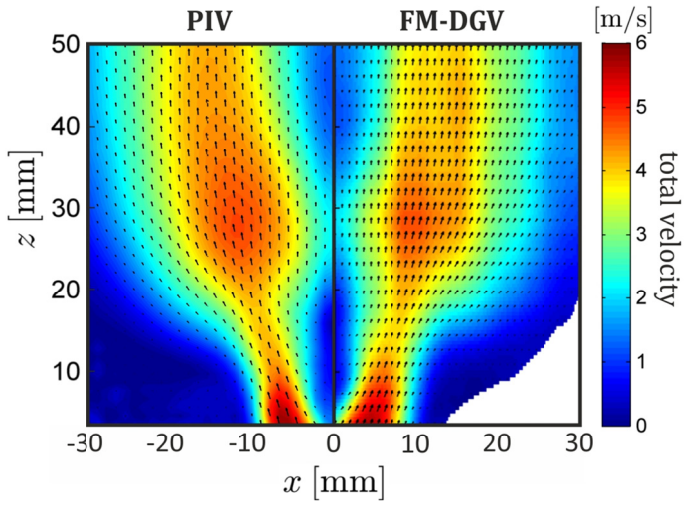

FIGURE 3: PIV (LEFT) AND FM-DGV (RIGHT) RESULTS OF THE MEAN VELOCITY FIELD.

shift can then be evaluated by measuring the intensity variation of the scattered light behind the absorption cell [15].

The applied FM-DGV system was described in more detail in [16]. It features a high-power continuous laser illumination with a maximum output power of 1 W at 895 nm (Toptica Photonics AG) for achieving a high signal-to-noise ratio. Also three observation directions were used, enabling simultaneous, three component measurements with a spatial resolution of 1 mm and a maximum measurement rate of 100 kHz. Hence, velocity spectra with up to a maximum frequency of 50 kHz can be resolved. A temporal averaging was applied for reducing the measurement uncertainty, resulting in a cut-off frequency for the velocity spectra of 2 kHz, which is sufficiently high to resolve expected flow structures.

The OH* and CH* acquisition providing the equivalence ratio waves were measured with a light-intensified camera (NanoStar, 1280x1024 Pixel, photocathode radiant sensitivity 310 nm/430 nm = 65 %, DaVis 7.6 Software, LaVision, Göttingen, Germany) and a OH* (above) or a CH* interference filter (430±2 nm CWL, FWHM 10±2 nm Bandwidth, 50 mm Mounted Diameter, 98 % Transmission, Edmund Optics, Barrington, NJ, USA). The camera was triggered by the siren with the images recorded phase resolved and then phase averaged. For phase steps α of 45° one hundred images were averaged according to:

$$\frac{\phi'(\alpha)_{xz}}{\bar{\phi}^{\,}_{\alpha xz}} = \frac{\frac{I_{CH*}(\alpha)_{xz}}{I_{OH*}(\alpha)_{xz}} - \overline{\left(\frac{I_{CH*xz}}{I_{OH*xz}}\right)}^{\alpha}}{\overline{\left(\frac{I_{CH*}}{I_{OH*}}\right)}^{\alpha xz}} \qquad (4)$$

RESULTS

Stationary Flame Properties and Flow Field

The mean flame behavior and flow field will be discussed below on the example of the TPM case. The distribution of reacting gasses measured by OH*-chemiluminescence (Fig. 2 left) shows the main reaction zone just after 2xDexit downstream of the burner exit extending to a maximum of 2.5Dexit. The typical V-shape flame indicates that the reaction takes place in the inner shear layer of the jet only, while the reaction is quenched in the outer shear layer by heat loss and strain.

In this flame the fluid flow of the reacting gasses is dominated by the axial component (Fig 3). From half the burner exit diameter (D_{exit}) after the burner exit nozzle, the velocity decreases slightly due to swirl induced jet opening, which is caused by the sudden area change at the burner exit. At around $2xD_{exit}$ or 30 mm downstream the fluid starts to accelerate driven by expansion of the hot gases in the reaction zone, and from $2.5xD_{exit}$ gradually decelerates due to mixing with the ambient gasses. The mean velocity field for reacting gasses was acquired by FM-DGV and stereo-PIV. As shown in (Fig. 3) the agreement between the two different measurement techniques, FM-DGV and stereo-PIV is very good. This confidence check shows the reliability of the novel FM-DGV which was used to record velocity spectra as discussed below.

Flame Dynamics

Premixed swirl stabilized combustion is a highly dynamic process. Fig. 2 (right) shows the RMS value of OH*-chemiluminescence fluctuations. Comparison with the mean value (left) shows that the highest amplitudes of fluctuation are around the position of mean heat release. Below the fluctuations are more extended than above the flame. Looking at the spatially integrated heat release recorded by the photomultiplier (Fig. 4), the spectra for both operating points (TPM and PPM) look quite different. Both flame spectra show the typical features of a turbulent process. They peak at frequencies below 200 Hz and gently decrease towards higher frequencies. This is expected due to the comparably low velocities within the flame of around 5m/s (Fig. 3). The PPM's

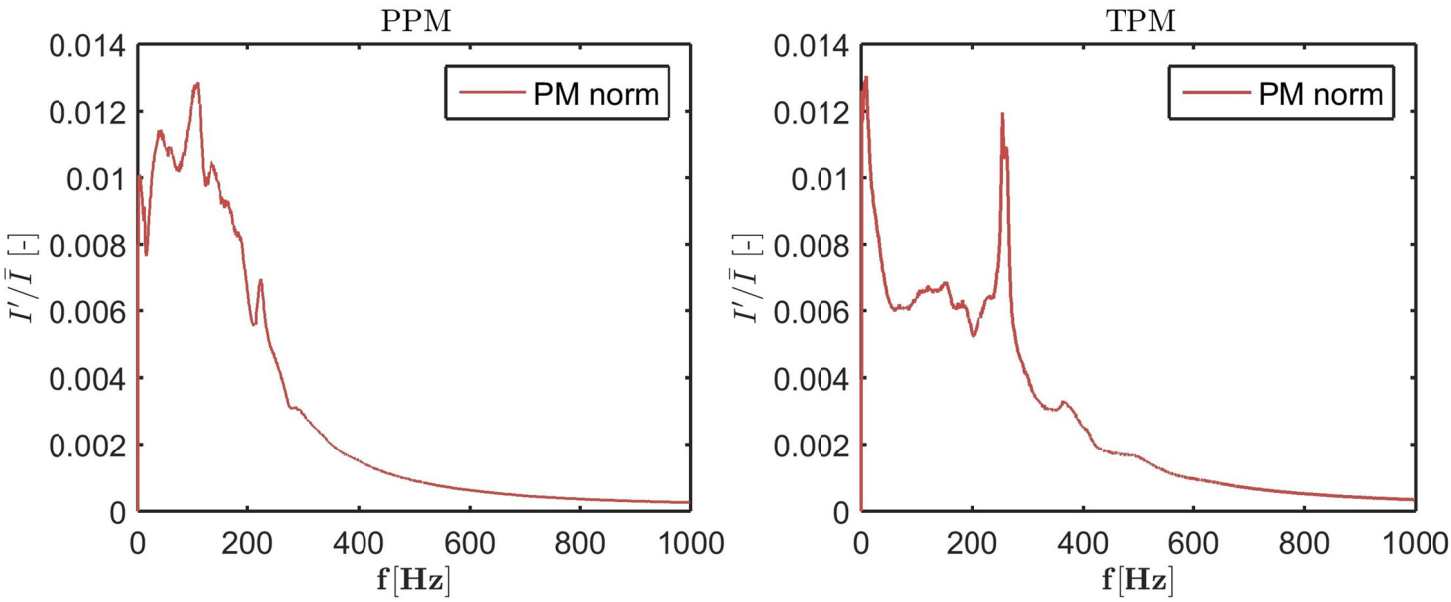

FIGURE 4: NATURAL SPECTRUM OF OH*-CHEMILUMINENCE FOR THE PPM (LEFT) AND TPM (RIGHT) TEST CASE.

broadband background peaks at around 125 Hz, which is considerably lower than the one of the TPM test case. Additionally the perfectly premixed flame shows a distinct peak at around 125 Hz, sitting on top of the smooth underground signal.

In contrast to this, the TPM case shows a lower overall fluctuation in the low frequencies. Secondly a very distinct peak at 250 Hz is recorded which is about twice as high as the broad band spectrum. This effect will be further discussed below.

Recording the Flame Transfer Function

In the folowing, the linear response of the flame to upstream excitation is investigated. By means of LIV and i-OH*-CL flame transfer functions (FTF) under TPM and PPM conditions are recorded. A comparison between both approaches is performed.

To investigate thermoacoustic stability of flames, recording the FTF is a common tool. FTF reduces the complex dynamic behavior of combustion to an amplitude and a phase plot. This information can be used for network models, where the flame is generally treated as a 'black box'. This model includes one input which is the fluctuation of velocity upstream of the flame, and one output which is the heat release fluctuation

$$\mathrm{FTF} = \frac{\dot{Q}'/\bar{\dot{Q}}}{u'/\bar{u}} \tag{5}$$

with the heat release fluctuation $\dot{Q}'$ mormalized by the mean heat release $\bar{\dot{Q}}$. This is then divided by the axial velocity fluctuation u', again normalized by its mean counterpart $\bar{u}$. There are several methods to acquire the FTF, most commonly from experiments. While [17, 18] have developed a purely acoustic method, called multi microphone method (MMM), still the most widely used approach is to measure the dynamic velocity just upstream of the flame and the heat release rate with i-OH*-CL.

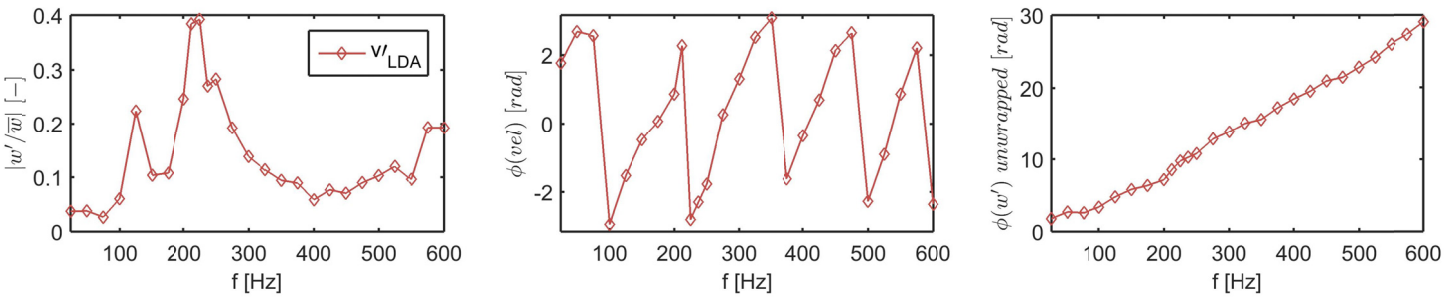

FIGURE 5: BURNER EXIT VELOCITY SPECTRA OF THE NON-REACTING FLOW.

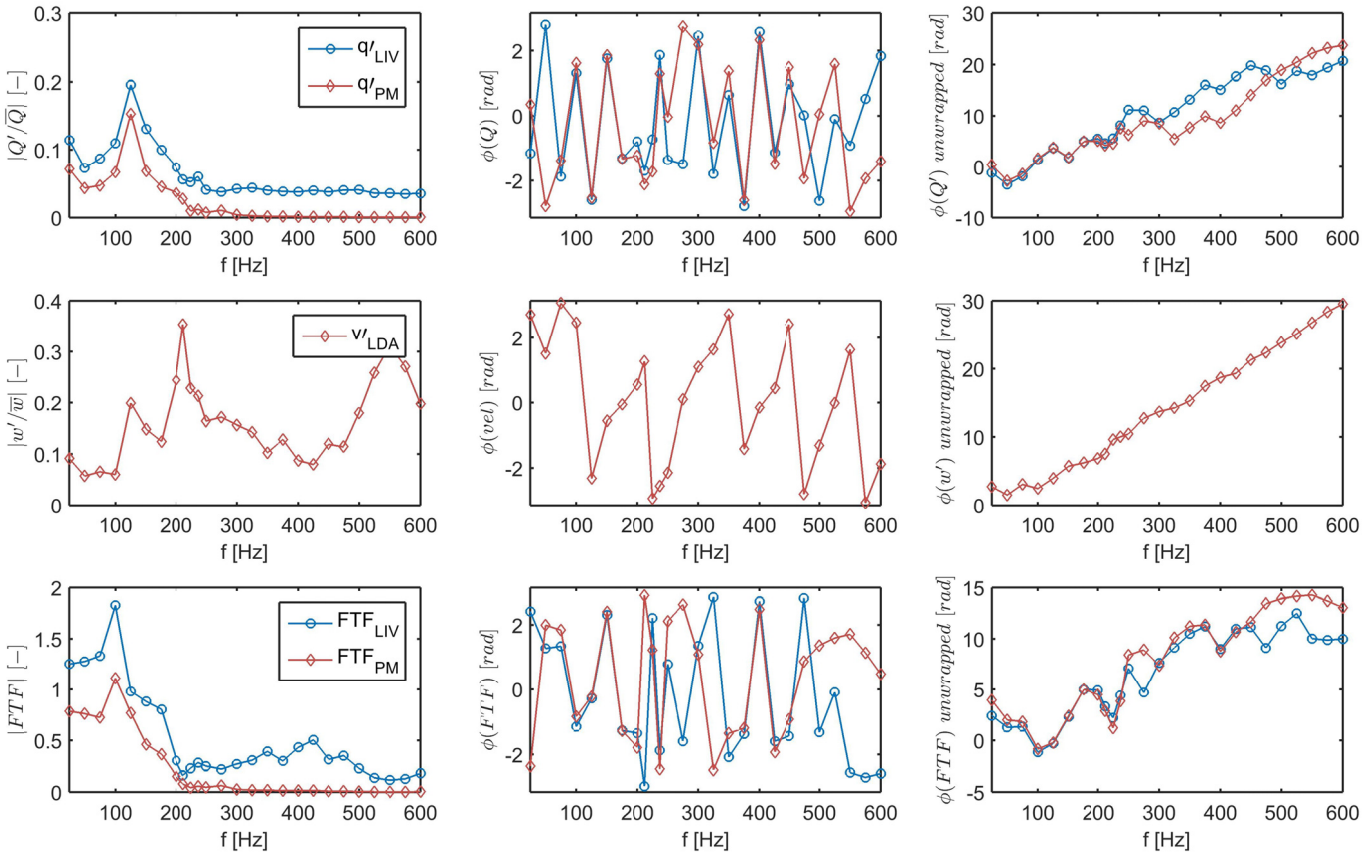

FIGURE 6: FLUCTUATIONS OF HEAT RELEASE, VELOCITY AND THE FTF FOR THE PPM TEST CASE WITH THEIR AMPLITUDE, PHASE AND UNWRAPPED PHASE RESPECTIVELY.

While it is a simple task to record the upstream velocity fluctuations causing the flame perturbations, unfortunately it is not so easy to acquire the heat release fluctuations quantitatively. I-OH*-CL is a commonly used optical measurement tool to assess the dynamics and heat distribution of flames. Mostly the OH*-radical emission is recorded by using an appropriate narrow band filter. Generally it is a comparably easy to use and low cost measurement technique. For perfect premixing where the equivalence ratio does not change with time, it is the most preferred tool for stability analysis. For a constant equivalence ratio the light intensity of the OH* radical is proportional to the heat release [19]. By normalizing the intensity by the mean value even the calibration factor can be avoided. The major drawback is its dependency on the equivalence ratio and the strain rate. This comes into play when partly premixed, so called 'technically premixed' flames are investigated. Then fluctuations of equivalence ratio can cause an overestimation of heat release fluctuations when measuring the OH*-chemiluminescence only [4]. Unfortunately most industrial combustion applications are not perfectly premixed, and therefore an alternative technique to measure heat release fluctuations is needed. LIV is a technique not significantly affected by equivalence ratio fluctuations.

LIV has proven to measure heat release in laminar flames and turbulent flames [6, 7, 20]. For technically premixed flames the technique is capable of recording the overall heat release fluctuations better than chemiluminescence techniques, since it is barely affected by equivalence ratio waves. Only a minor influence is present due to a change in the Gladstone-Dale constant. Following the above equations, the LIV measures the heat release not only qualitatively but also quantitatively. For the FTF the result was normalized by the mean power of the flame (3,4 kW) assuming a combustion efficiency of 100 %. The mean temperature of the flame was set to 1200 °C due to prior temperature measurements [21] and a cross-sectional flame area of 1000 mm^2 was used.

The **fluctuations of velocity** measured by LDA are shown in (Fig. 5) recorded without the reacting flame (flow only). The amplitude spectrum is plotted from 25 Hz up to 600 Hz. A strong overall modulation level of the bulk velocity of more than 5 percent of the mean flow proves that the siren modulation is strong enough to vary the velocity at the burner exit. Three significant peaks can be found in the spectrum, one minor peak at 125 Hz with about 20 percent fluctuation and one at 550Hz. The strongest fluctuation is however at 212 Hz with alsmost 40 percent fluctuation. The phase (Fig. 5 right) shows an increasing lag with increasing frequency.

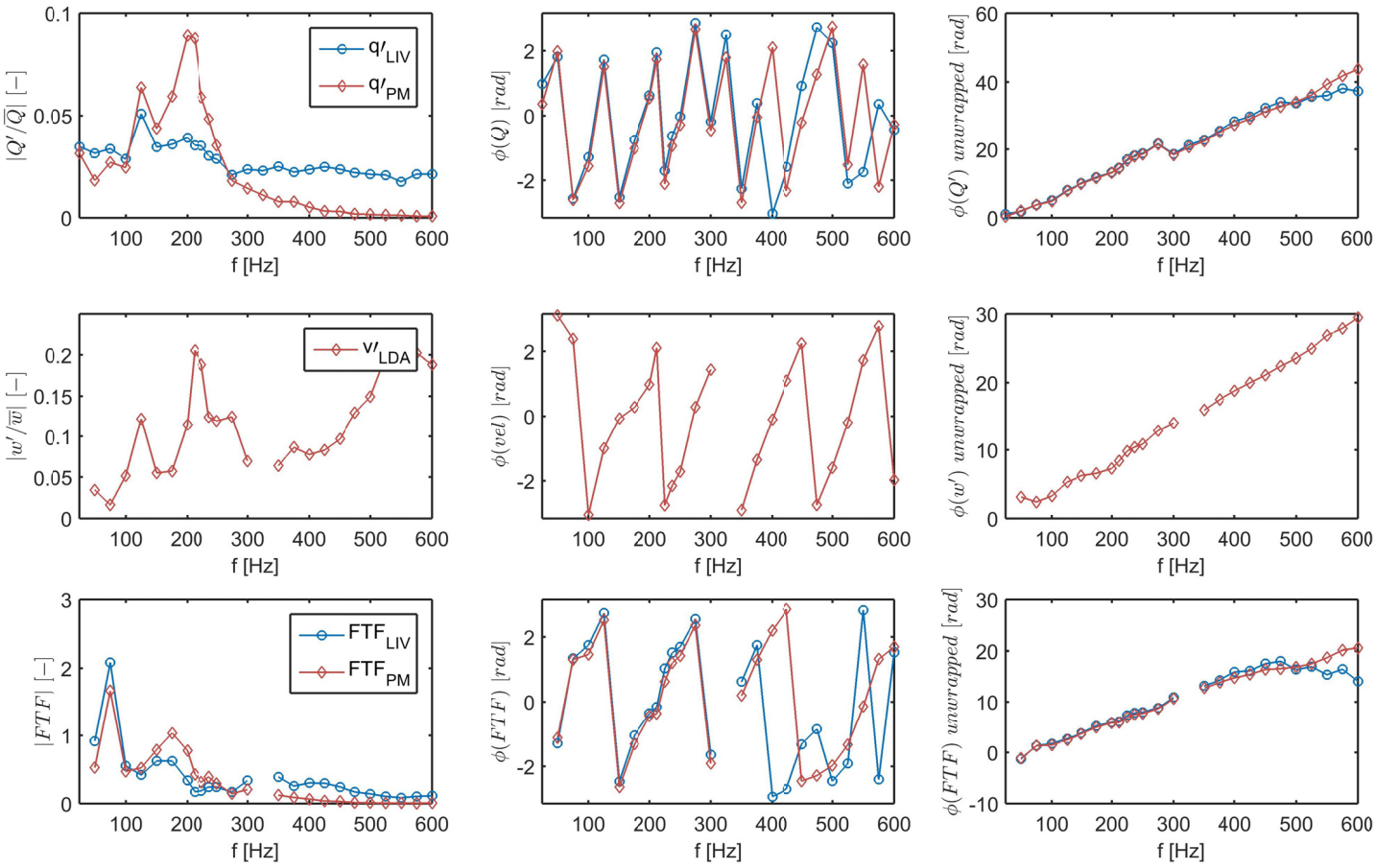

FIGURE 7: FLUCTUATIONS OF HEAT RELEASE, VELOCITY AND THE FTF FOR THE TPM TEST CASE WITH THEIR AMPLITUDE, PHASE AND UNWRAPPED PHASE RESPECTIVELY.

In Fig. 6 and Fig. 7 the relative heat release, the velocity and the FTF calculated from both, is shown for the test cases PPM and TPM. For both reacting cases, the velocity shows a similar trend as seen in the non-reacting flow (Fig. 5). This supports the expectation, that the flow field in the plenum upstream of the flame is not significantly changed by the different injection setups for TPM and PPM or the reaction itself.

Considering **heat release rate**, the typical behavior of flames acting as a low-pass filter is observed. Starting with PPM, the spectra of the photomultiplier and LIV match very well. The velocity-fluctuations discussed earlier, manifest themselves in the heat release causing a strong peak at 125 Hz. Other frequencies are widely suppressed, only minor fluctuations can be found due to the intense velocity fluctuation at 212 Hz. Over the whole spectrum, both measurement techniques match very well. The phase generally also matches over the whole frequency band.

When discussing the TPM test case (Fig. 7) a similar trend as for PPM can be found. Again at 125 Hz the flame clearly responds to the velocity fluctuations and again the 550 Hz peak is dampened due to the low-pass-filter characteristic of the flame but now the fluctuation at 212 Hz also affects the flame behavior. Although the LIV clearly detects increased fluctuations of heat release, it does not show a significant deflection compared to neighboring frequencies. In contrast to this, i-OH*-CL senses high amplitude at 212 Hz, which is more than 30 % higher than the fluctuation at 125 Hz. Thus, the assumption is that i-OH*-CL overestimates the heat release compared to the LIV. This strong overshoot in company of small heat release fluctuations can arise in configurations with large pressure drops over the injector. Then fluctuations of air flow hardly affect the fuel mass flow.

Although the amplitude values of i-OH*-CL and LIV do differ, the phase between both measurement systems matches very well. This means that the additional effect recorded by i-OH*-CL is roughly in phase with the heat fluctuations. Such an overestimation is expected for chemiluminescence measurements when equivalence ratio waves are present, which is possible in partially premixed flames and has been documented for example by [7].

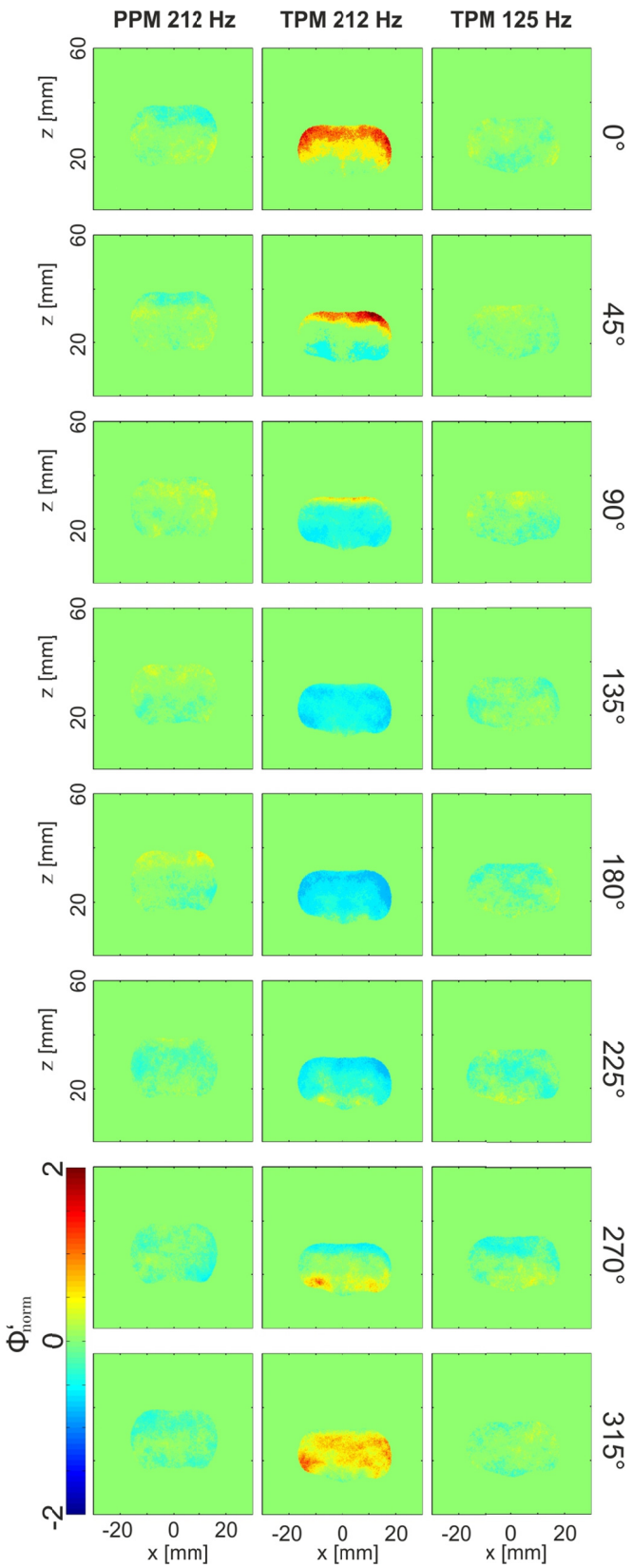

FIGURE 8: EQUIVALENCE RATIO WAVES AT DIFFERENT FREQUENCIES FOR BOTH TEST CASES.

The **flame transfer functions** of the PPM case shown in the last line of plots in Fig. 7 indicate similar trends for both measurement techniques. Since the same set of LDA velocity measurements was used for the FTF (i-OH*-CL and LIV), the difference is only caused by different recordings of heat release fluctuations. The stronger amplification at the LIV-FTF is because the LIV predicts a higher overall heat release fluctuation. Apparently, for both systems the major amplification is not at 125 Hz where both velocity and heat are high, but at around 100 Hz where heat fluctuation is high in spite of low velocity fluctuations. The phase for both measurement techniques matches well at regions where the amplitude is high and a good correlation is possible. The flame transfer function of the TPM case also shows the interesting result of high amplifications where velocity is low.

Equivalence Ratio Waves

Although heat release fluctuations are generally recorded correctly by both measurement techniques, a strong deviation in the heat release recordings by i-OH*-CL and LIV exists at 212 Hz for the TPM case. The hypothesis is that the chemiluminescence intensity recorded by the photomultiplier overestimates the heat release of the flame at 212 Hz due to an equivalence ratio wave being present. This assumption needs to be validated in order to correctly identify the influence of such an effect.

Chemiluminescence might not always represent heat release reliably, but it is a very good tool to measure changes in equivalence ratio [4]. Fig. 8 shows one cycle of equivalence ratio fluctuations ϕ' acquired by means of OH*/CH*-ratio measurements, following equation 4. For eight phase steps the normalized ϕ'-distribution across the flame is plotted. Regions of low signal-to-noise-ratio were masked. For the PPM test case at 212 Hz, the variations of ϕ are close to zero. Due to the mixing far upstream of the source of excitation for the PPM case, changes in equivalence ratio cannot appear. They are not exactly zero, because ambient air can mix with the swirled jet of reactants due to the unconfined flame setup. This however is a minor order effect compared to possible changes in equivalence ratio within the bulk flow. With regard to the uncertainty of such measurements it can be seen that wherever the signal is low (e.g. at the edges of the flame) measurement uncertainty increases. Therefore values in the center of the flame - where the signal-to-noise-ratio is high - are more reliable.

Considering TPM, the variations in ϕ are also close to zero for the 125 Hz case. This is expected, because there the agreement of both measurement techniques is good. However, at 212 Hz the TPM case exhibits violent oscillations in ϕ. This is exactly where the i-OH*-CL signal overshoots significantly compared to the LIV recordings. This measurement provides strong evidence that the OH*-Intensity overestimates the true heat release fluctuations of the flame.

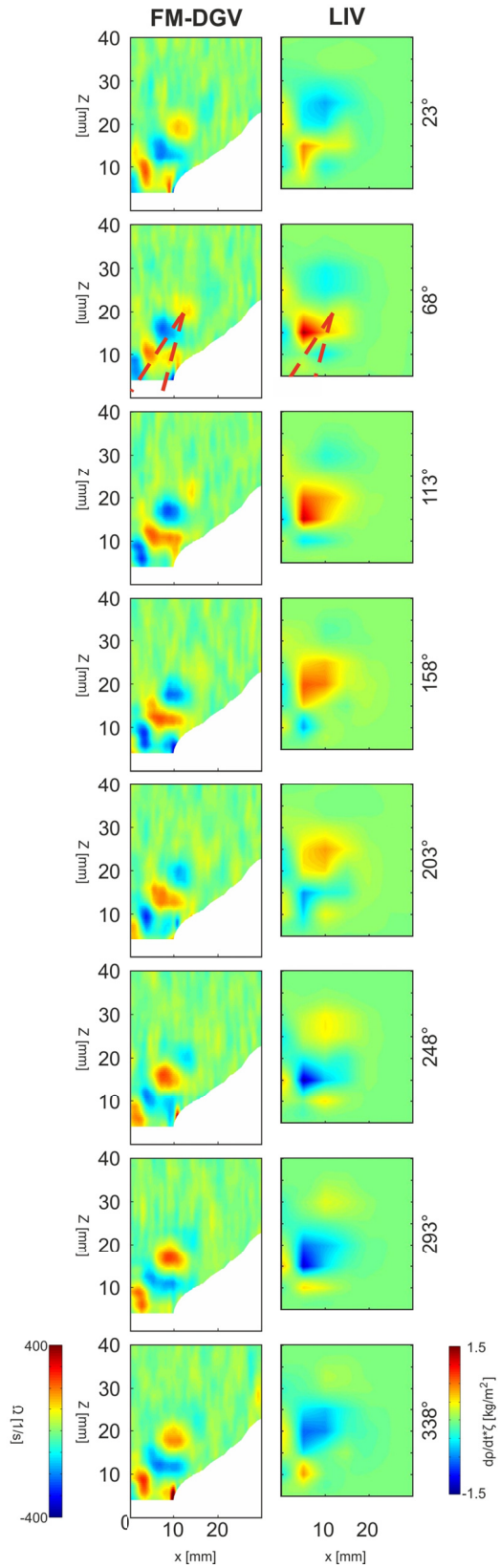

FIGURE 9: VORTICITY (LEFT, FM-DGV) AND HEAT RELEASE FLUCTUATIONS (RIGHT, LIV) FOR THE PULSATION AT 250HZ.

Comparison of Heat Release Fluctuations and Velocity Fluctuations

In the previous chapter, an overshoot of the i-OH*-CL signal in the FTF was shown at 212 Hz for linear excitation. It was identified as an equivalence ratio wave. This, however raises the question about the natural spectrum of i-OH*-CL at the TPM case where the most obvious effect can be found at 250 Hz. To identify the formation of this peak, the heat release is relevant, not only as integral data but also spatially resolved. In this chapter the heat release distribution (LIV) is investigated to trace the origin of this instability and compare it to vorticity fluctuations (FM-DGV) which are expected to interact with the flame front. The velocity signal from FM-DGV and the heat release signal from the LIV also identify the oscillation at around 250 Hz with several higher harmonics in the velocity spectrum.

For the dominant frequency of around 250 Hz a two dimensional cross-section of the flame was analyzed. A phase resolved evolution of heat and vorticity at this frequency is presented in Fig. 9. The photomultiplier signal served as phase-reference.

Comparing the **vorticity fluctuation** in Fig. 9 (left) with the mean flow and the mean heat distribution in Fig. 2 reveals that the vorticity is most dominant along the inner shear layer of the conical swirl-jet (illustrated in the second phase plot). It rises to a height of approximately 3 x D_{exit}. A second vortex can be found on the outer shear layer. It is less developed and starts in counterphase to the inner shear layer vortex. Both are caused by the velocity fluctuation coming from the plenum generating two counter rotating vortices, both veering off the center axis of the conical jet (right side of the flame). The swirl bends the jet and its shear layers outwards, away from the burner axis. Therefore the inner shear layer is longer than the outer one. As the undisturbed jet thins towards the tip of the cone, the vortices on both sides merge. However, quickly after detaching from the corner of the burner exit, the

outer vortex merges with the co-rotating one which detached 180° earlier. Looking at the time step 23° a positive vortex is about to detach from the outer corner of the burner (x = 10 mm, z = 5 mm) and a negative vortex is about to detach from the center body at (x = 0), but already at timestep 113° the outer vortex has reached the closest inner co-rotating one. By this the inner vortex street is amplified. Since it is the one which interacts with the flame, this could be the reason why exactly at this point of operation, the amplification is so strong. It seems that at this point of operation, velocity and swirl are just right to enable this merge of correlated swirls. Although the mean velocity remains high above the flame, no correlated vortices can be found.

The **heat release fluctuations** show pulsations in the same region as the mean heat release of the flame (Fig. 2). The strong pulsations are closer to the burner axis and just below the peak of mean heat release. While there is no pulsation below z = 10 mm (68° - 113°), the strongest amplitudes of heat release are reached at x = 5 mm and z = 15 mm, slowly decreasing towards higher levels. Due to lower measurement resolution less

obvious but still distinct, the fluctuations in heat release start at x = 5 mm, z = 10 mm and float down- and outwards following the inner shear layer of the right-side jet. For interpretation of the results, it is important to keep in mind that the measurement resolution is only 5 mm in comparison to 1 mm for velocity measurements.

Comparison of results from two measurement techniques shows that both fluctuations occur within the upper inner shear layer of the jet, which is also the lower part of the main heat release, and the region where the flame is anchored. Looking at the phase evolution, it shows that negative vorticity leads to positive heat release, which means that a vortex veering away from the jet curls up the surface of the flame. This leads to an increased surface area and consequently to an increased burn rate. At x = 5 mm and z = 15 mm the heat release is highest and this is also the region where the vortex fully hits the flame just after it merged and grew in strength. Here both measurement techniques acomplish each other, in order to gain insight into the flame dynamics.

CONCLUSION

The focus of this study was to discuss an alternative way of recording heat release rate and the FTF. It was the first time integral LIV was used for this application. The technique is promising of a better prediction of heat release in partially premixed (technically premixed) flames, where it is less receptive to equivalence ratio waves than the classical i-OH*-CL method.

Heat release spectra and FTF's for both perfectly premixed and technically premixed flames were analyzed. The trend of both systems correlated very well for the perfectly premixed flame as the literature suggests. While for the technically premixed case the agreement of the overall trends were good as well, a strong overshoot at one peak in the spectra of the i-OH*-CL signal was found. This was related to the known dependency of OH*-emission on equivalence ratio and correctly identified as such by visualizing the ratio between OH* and CH* fluctuations. A significant overshoot of OH*-CL without a considerable fluctuation of heat release can occur when the system features a high pressure drop over the injector. This acoustically stiff fuel line is then less sensitive to fluctuations of air flow. In the special case of this swirl-stabilized flame, the overshoot of the photomultiplier signal does not affect the FTF significantly because the trend of the FTF is mainly dominated by velocity fluctuations. Therefore the LIV method is an interesting alternative to i-OH*-CL in order to measure and quantify heat release fluctuations in perfectly as well as partially premixed flames. Secondly, naturally excited frequencies of the technically premixed flame were investigated, since the LIV technique clearly identified this effect as a heat release fluctuation. Time resolved velocity was an obvious quantity to investigate, in order to identify the root of these fluctuations. By means of FM-DGV the heat release fluctuation was tracked back to flame front roll up and consequently vorticity. Pulsations of heat release can be observed in the shear layer where the flame is anchored and where vortices hit the flame, heat release is in phase with the vortices. Detailed analysis of the plots identifies the vortices as the source of the heat release pulsations. This leads to the final conclusion that LIV is a promising technique for full field heat release measurements. It has been shown, that it is possible to measure the heat release rate of an unconfined flame. Similar to chemiluminescence, it is not free of restrictions. These include sensitivity of the Gladstone-Dale constant to mixture fluctuations, and sensitivity to temperature. Additionallly, care must be taken when adjusting the laser beam in order to maintain a homogenous illumination of the measurement volume.

ACKNOWLEDGEMENT

This research was partially funded by the Austrian Science Fund FWF within grant FWF-24096-N24 "Interferometric Detection of Thermoacoustic Oscillations in Flames". The authors would like to thank Prof. Thomas Sattelmayer, TU Munich for the fruitful discussions and all the support during this work.

References

[1] Rayleigh, "The explanation of certain acoustical phenomena," *Nature,* vol. 18, no. 455, pp. 319-321, 1878.

[2] S. Candel, D. Durox, T. Schuller, J. .. Bourgouin and J. P. Moeck, Dynamics of swirling flames, vol. 46, 2014, pp. 147-173.

[3] T. Sattelmayer and W. Polifke, "Assessment of methods for the computation of the linear stability of combustors," *Combustion Science and Technology,* vol. 175, no. 3, pp. 453-476, 2003.

[4] M. R. W. Lauer, Determination of the Heat Release Distribution in Turbulent Flames by Chemi-luminescence Imaging, Technische Universität München, 2011, pp. 147-173.

[5] B. Schuermans, F. Guethe, D. Pennell, D. Guyot and C. O. Paschereit, "Thermoacoustic modeling of a gas turbine using transfer functions measured under full engine pressure," *Journal of Engineering for Gas Turbines and Power,* vol. 132, no. 11, 2010.

[6] T. Leitgeb, T. Schuller, D. Durox, F. Giuliani, S. Köberl and J. Woisetschläger, "Interferometric determination of heat release rate in a pulsated flame," *Combustion and Flame,* vol. 160, no. 3, pp. 589-600, 2013.

[7] J. Peterleithner, N. V. Stadlmair, J. Woisetschläger and T. Sattelmayer, "Analysis of measured flame transfer functions with locally resolved density fluctuation and OH-Chemiluminescence Data," *Journal of Engineering for Gas Turbines and Power,* vol. 138, no. 3, 2016.

[8] A. P. Dowling and A. S. Morgans, "Feedback Control of Combustion Oscillations," *Annu. Rev. Fluid Mech.,* vol.

37, pp. 151-182, 2005.

[9] F. Giuliani, J. W. Woisetschläger and T. Leitgeb, "Design and validation of a burner with variable geometry for extended combustion range," in *Proceedings of the ASME Turbo Expo*, 2012.

[10] J. Peterleithner, A. Marn and J. Woisetschläger, "Interferometric In estigation of the thermo-acoustics in a swirl stabilized Methane flame," in *Proceedings of the ASME Turbo Expo*, 2015.

[11] F. Giuliani, A. Lang, K. Johannes Gradl, P. Siebenhofer and J. Fritzer, "Air flow modulation for refined control of the combustion dynamics using a novel actuator," *Journal of Engineering for Gas Turbines and Power,* vol. 134, no. 2, 2012.

[12] J. Peterleithner and J. Woisetschläger, "Laser vibrometry for combustion diagnostics in thermoacoustic research," *Technisches Messen,* vol. 82, no. 11, pp. 549-555, 2015.

[13] N. Mayrhofer and J. Woisetschlaeger, "Frequency analysis of turbulent compressible flows by laser vibrometry," *Experiments in Fluids,* vol. 21, pp. 153-161, 2001.

[14] B. Hampel and J. Woisetschläger, "Frequency- and space-resolved measurement of local density fluctuations in air by laser vibrometry," *Measurement Science and Technology,* vol. 17, pp. 2835-2842, 2006.

[15] A. Fischer, J. König, J. Czarske, J. Peterleithner, J. Woisetschläger and T. Leitgeb, "Analysis of flow and density oscillations in a swirl-stabilized flame employing highly resolving optical measurement techniques," *Experiments in Fluids,* vol. 54, no. 12, 2013.

[16] R. Schlueßler, M. Bermuske, J. Czarske and A. Fischer, "Simultaneous three-component velocity measurements in a swirl-stabilized flame," *Experiments in Fluids,* vol. 56, no. 10, 2015.

[17] C. O. Paschereit, B. Schuermans, W. Polifke and O. Mattson, "Measurement of transfer matrices and source terms of premixed flames," *Journal of Engineering for Gas Turbines and Power,* vol. 124, no. 2, pp. 239-247, 2002.

[18] M. L. Munjal and A. G. Doige, "Theory of a two source-location method for direct experimental evaluation of the four-pole parameters of an aeroacoustic element," *Journal of Sound and Vibration,* vol. 141, no. 2, pp. 323-333, 1990.

[19] C. S. Panoutsos, Y. Hardalupas and A. M. K. P. Taylor, "Numerical evaluation of equivalence ratio measurement using OH* and CH* chemiluminescence in premixed and non-premixed methane-air flames," *Combustion and Flame,* vol. 156, no. 2, pp. 273-291, 2009.

[20] J. Li, D. Durox, F. Richecoeur and T. Schuller, "Analysis of chemiluminescence, density and heat release rate fluctuations in acoustically perturbed laminar premixed flames," *Combustion and Flame,* vol. 162, no. 10, pp. 3934-3945, 2015.

[21] T. Leitgeb, "On the Design and Validation of a Variable Geometry Burner Concept," Graz, 2012.

3.3 Combustion Noise Prediction by LIV

Since low Mach numbers and high Reynolds numbers are typically encountered in combustion, the dominant noise source is commonly associated with fluctuations in the heat release rate q´ [44, 57, 69, 70]. Under the assumption that the wavelength of sound is large compared to the combustion field, we learn from [44] that the pressure fluctuation in the far-field p'_{∞} is related to the density fluctuations by the following equation:

$$P_{far} \propto -\int_V \frac{\partial^2 \rho'}{\partial t^2} \tag{43}$$

It is seen from Strahle's discussion [44] that the radiated sound from the combustion volume V depends on the second time derivative of the density fluctuations. With the recorded acoustic pressure distribution in the far-field of the unconfined flame, equation (43) can be tested, when the density fluctuations are recorded. Such, a recording of the density fluctuations with the help of laser-vibrometers in the flame volume should enable an analysis of the acoustic field around the flame with

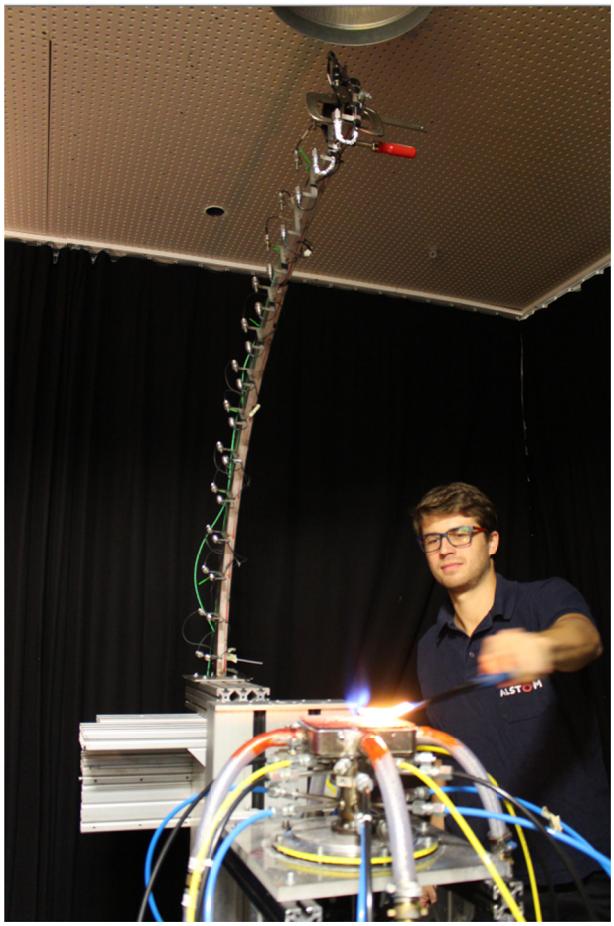

Figure 51: Sound intensity measurement setup with the experimental burner in front.

respect to total amplitude and frequency behavior. This provides an innovative aspect for experimental thermoacoustic research. Thus, a correlation between laser vibrometer density data and acoustic pressure data was performed to verify this hypothesis. Sound emitted by a flame can be predicted by measured density fluctuations (above equation) as derived by Strahle [44]. This, an old theory, has never been experimentally validated. To prove this, a microphone array was arranged in an arch to detect the spherical sound radiated. The arch configuration is shown in Figure 51.

The setup included 14 pairs of microphones in order to detect the sound power rather than only the sound pressure. The entire field was recorded by rotating the burner. Then a comparison was drawn with the vibrometer measurements. Traversing in latitudinal direction was necessary, due to the arch configuration. During measurements it turned out that due to the short measurement time, low (sub-Hertz) frequency fluctuations of the combustion process produced a considerable fluctuation in amplitude. To compensate this, a reference microphone was traversed with the burner. The sound field was rotationally symmetric after normalization by the reference microphone, as assumed on the basis of optical recordings (Figure 52).

In this paper three different configurations of mixing and flame stabilization were investigated. All three had major combustion noise radiation at around 45° downstream, as literature suggested [71]. In contrast to the attached flame however, the two detached flames showed a higher level of combustion noise in downstream direction (i.e. at higher angles.) and low levels of noise towards the sides - independent of their mixing configuration (Figure 53). One possible reason for this phenomenon lies in the aerodynamic stabilization of the detached flames, which is purely accomplished by the recirculation into the low pressure zone in the center of the flame, caused by the swirl of the inlet velocity field. The region of major volume expansion may move up and down due to fluctuations of inlet velocity. The flame front can then act as a membrane vibrating in axial direction. In contrast to this the attached flame is stabilized by a mixture of swirl induced recirculation and stabilization in the wake of the center cone. This generates a V-shaped flame. The reaction region cannot move as freely in axial direction due to this anchoring. Here a variation in axial velocity influences the swirl number, causing the sidewalls of the V-shape to expand and contract. This vibration of the sidewalls causes additional noise towards the sides, but suppresses parts of the downstream vibration of the flame. This explains that on the one side, the combustion noise of the v-shaped flame is not focused towards the exit as much and on the other hand shows a lower overall noise. This is due to the fact that the attached flame cannot be modulated as freely by an incoming disturbance due to its anchoring to the burner center cone.

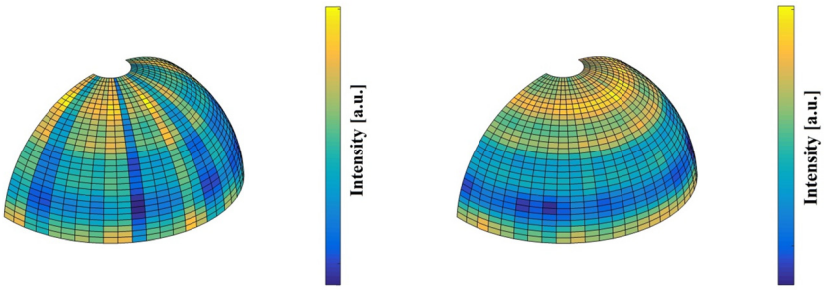

Figure 52: Sphere of sound intensity of PPM det, before (left) and after (right) correction by reference microphone

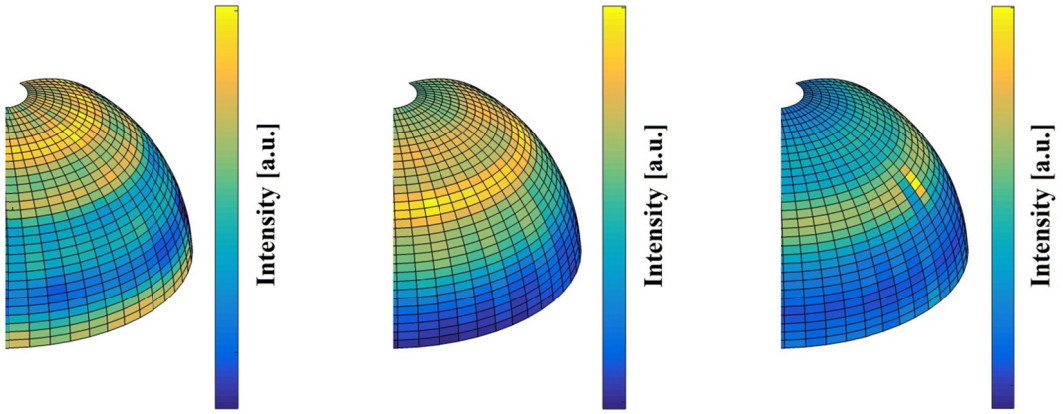

Figure 53: Sphere of sound intensity of PPM det (left), TPM det (middle) and TPM att (right).

In order to compare the sound field to density fluctuations, the entire combustion field was scanned by means of LIV. The system was two-dimensionally traversed and the fluctuations were integrated over the whole field. LIV measures the time derivative of density fluctuations $\partial\rho/\partial t$. According to [44] the sound power however is proportional to the second time derivative of density fluctuations ($\partial^2\rho/\partial t^2$,). Differentiation of the LIV signal gives the sound power, in the frequency domain. This is accomplished by a multiplication with $2\,\pi\,f$. This emphasizes high frequencies in the spectrum dramatically. This is a problem with respect to the signal-to-noise level because premixed flames typically have a low pass filter behavior. It is challenging to compare the natural spectrum of the two techniques, since

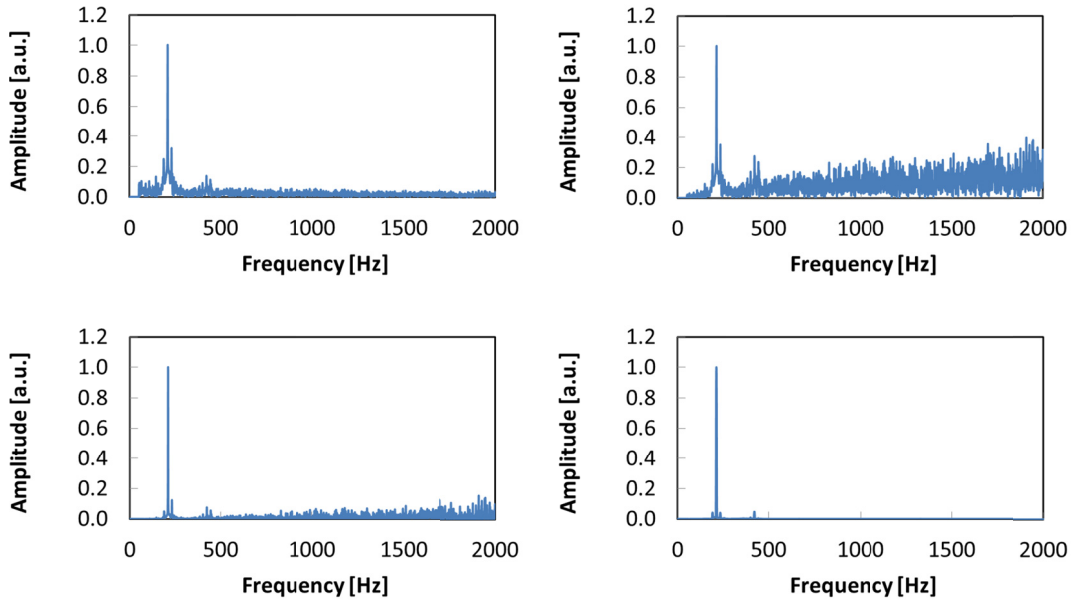

Figure 54: Time derivative of density fluctuations (top left), second time derivative of density fluctuations (top right), sound power derived from density fluctuations (bottom right) all measured by LIV and the actual sound power measured by microphones (bottom right).

a certain level of noise is inevitable with this measurement technique. The high frequency noise will eventually overpower the actual signal due to the multiplication of the frequency, as shown in Figure 54.

In order to solve the problem of high frequency noise it is possible to excite the feedline flow of the flame artificially by means of a siren and evaluate this frequency only. A comparison of amplitudes can then be drawn more accurately due to a more favorable signal to noise ratio.

The comparison of the two measurement techniques is shown below for one of the three test cases (Figure 55). Excitation with a siren showed a good agreement for values of the phase and the frequency. The trend is similar, starting off with low values at 125 Hz, highest amplitude at 212 Hz which then again decreases towards higher frequencies.

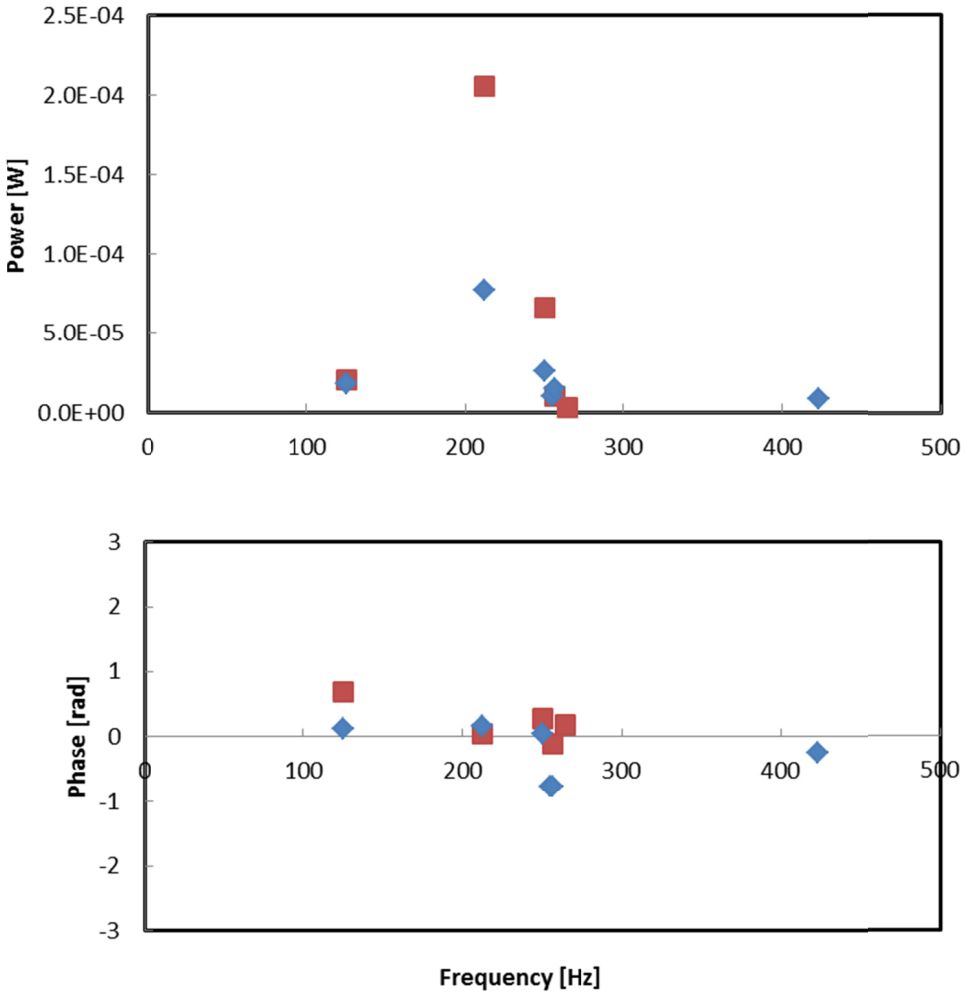

Figure 55: Sound power and phase measured by a Microphone array and LIV.

In terms of absolute amplitude, the vibrometer and microphone values match very well. Keeping in mind that for turbulent flames, the sound power emitted is in the range of 10^-8-10^-6 of the thermal power and the excitation level is in the range of 10-30% of the mean thermal power, the deviation found represents a very good agreement. The vibrometer mostly underestimates the microphone results by less than 70% of the microphone sound power. This is shown in Table 4. N/A marks frequencies where either only microphone or only vibrometer results are available. Only operating points where the amplitude is very low show a considerable over estimation by the vibrometer. This is a result of noise measured by the technique. In order to avoid arbitrary manipulations of the data, there has not been any 'noise' filtering of the LIV system but for low amplitudes the noise can contribute to the predicted sound power.

Table 4: Deviation of the sound power measured by LIV compared to microphone measurements in percent, for different frequencies and points of operation.

f [Hz]	TPM att	TPM det	PPM det
125	11.82%	-12.10%	-3.38%
212	-70.21%	-62.42%	-47.70%
225	n/a	n/a	176.12%
250	-36.72%	-60.69%	-38.37%
255	n/a	n/a	n/a
256	n/a	53.14%	n/a
264	n/a	n/a	n/a
423	-68.03%	n/a	32.18%

Aside from the mentioned noise, an additional source of error lies in the implementation of Strahles equation **(**31**)**. Strahle assumed that only the density fluctuations in the flame front contribute to the radiated sound. This is intuitive because the reaction only takes place in the flame front, hence only there, combustion can be the source of sound.

The vibrometer on the other hand integrates fluctuations of density along the line of sight. Due to this, it also takes into account fluctuations outside of the flame front. Those fluctuations can be considered small, as shown by [24] but never the less may slightly alter the resulting fluctuations.

Further slight uncertainties could be caused by the low frequency combustion fluctuations observed or by the normalization process of the microphone array which was necessary because of the low frequency combustion fluctuations. Acoustic intensity fluctuations were observed when traversing the microphone array tangentially. Those fluctuations were suppressed by normalizing the microphone signals by a reference microphone which was traversed with the burner. It is however possible, that the measured mean value of sound power does not represent the actual mean value. A measurement time of 20 seconds and 30 measurement points however gives a total of 10 minutes to average for the reference microphones. Therefore, this influence can only be small.

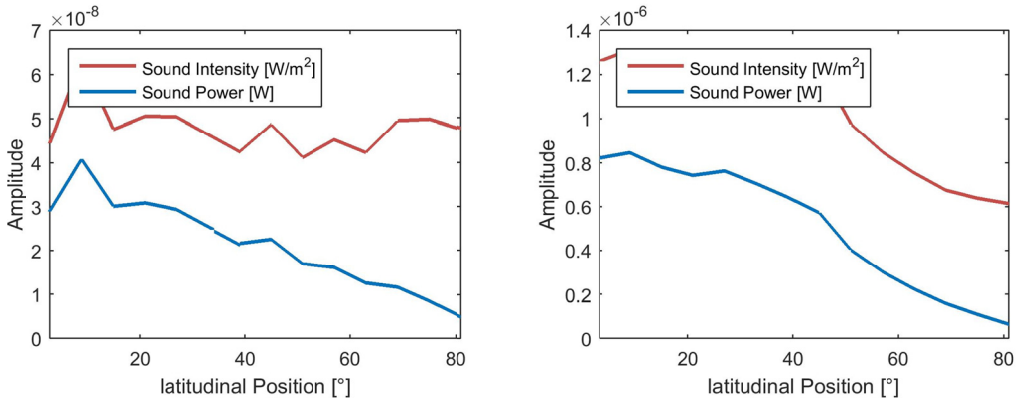

Figure 56: Sound Intensity and Power measured along the microphone arch for the non-reacting flow. The flow was excited with a siren at 125 Hz (left) and 212 Hz (right). The plots were acquired and processed similar to Figure 6 of Publication [64].

For this study the sound radiation downwards was assumed to be reflected by the heat shield, the top surface of the traverse and the aluminum bar the microphone arch was mounted on. Therefore the entire density fluctuations were compared to the sound intensity integrated over a hemisphere. Ideally the space between flame and Microphone arch should however be covered by a perfectly reflecting shield. This assumption could cause an additional small error.

The Laboratory ceiling and walls are low reflective as described in appendix D. For the post processing, no reflection from the walls was considered therefore. To further improve the accuracy of the measurements, the reflection could be subtracted from the measured sound intensity.

Finally, the background noise of the cold flow without the combustion showed very low amplitudes (Figure 56) and was therefore not subtracted. Comparing the amplitudes in Figure 56 with the ones in Figure 6 of Publication [64] shows that the level of the combustion noise exceeds the level of the non-reacting case by a factor of 300 and 250 for the 125 Hz and 212 Hz excitation respectively.

This shows that the theoretical analysis proposed by Strahle can predict combustion noise with good accuracy. The combination of measuring the density fluctuations in a flame and the theory provided by Strahle can replace far-field measurements.

Editorial Note:

During the processing computed for the presented paper a wrong equation was employed. A source [72] suggested to use the imaginary part of the cross power spectrum CPS in order to calculate the sound power. This gives correct results if the frequency resolution Δf is unity and no window function is applied. As a general solution for the sound power though, it is necessary to use the imaginary part of the cross power spectral density (CPSD) instead of the cross power spectrum (CPS) [73].

$$I = pv = -\frac{1}{\rho_0 2\pi f \Delta r} Im(CPSD) \tag{44}$$

The difference lies in the equivalent noise band width (ENBW):

$$CPSD = \frac{CPS}{ENBW} \quad (45)$$

The ENBW depends on the frequency resolution (Δf) and the window function applied [51]. Without a window function and for Δf being unity, ENBW is zero. Otherwise it differs from one. The measurement- and processing parameters used in this paper resulted in an ENBW is 3.7702. In the paper PETERLEITHNER ET AL. 2016 B, dividing the microphone measurements by a factor of 6 produced matching frequency spectra, but the reason for this discrepancy was unknown. Now with the correct computation of the sound power, there is still some variation as shown in Table 4, but the results are very close and in the expected error of such a comparison as discussed above.

3.3.1 Reviewed articles on Combustion Noise:

- PETERLEITHNER ET AL. 2016 B:

J. Peterleithner, S. Zerobin and Woisetschläger, "ANALYSIS OF COMBUSTION NOISE USING LOCALLY RESOLVED DENSITY FLUCTUATIONS AND A MICROPHONE ARRAY," in Proc. ASME Turbo Expo, 2016.

Proceedings of ASME Turbo Expo 2016: Turbine Technical Conference and Exposition
GT2016
June 13-17, 2016, Seoul, South Korea

GT2016-57490

ANALYSIS OF COMBUSTION NOISE USING LOCALLY RESOLVED DENSITY FLUCTUATIONS AND A MICROPHONE ARRAY

Johannes Peterleithner, Stefan Zerobin, Jakob Woisetschläger
Institute for Thermal Turbomachinery and Machine Dynamics, Graz University of Technology
8010 Graz, Austria

ABSTRACT

For turbulent swirl-stabilized flames combustion noise can be directly calculated, if density fluctuations as a function of time and space are known. It is however not easily possible to assess the density fluctuations directly. Therefore, in the past, combustion noise has been expressed as a function of chemiluminescence, an approach bringing in more assumptions. Now, by using interferometry, density fluctuations in the flame can be measured quantitatively. The advantage of this technique is that it measures the time derivative of density fluctuations directly. In this work laser interferometric vibrometry (LIV) was used to scan a two dimensional field in the flame in order to calculate the sound power emitted by the flame. Sound intensity was measured in a half-hemisphere by pressure-pressure-probes in order to record the total sound power of the direct combustion noise emitted by the unconfined flame. The goal of this study was to compare the measured sound power exhibited by the flame with the sound power predicted due to fluctuations of density within the flame. By using a siren to generate linear excitation, it was possible to qualitatively predict combustion noise with good agreement in trend. A quantitative comparison between both measurement techniques showed a deviation of a factor of six.

NOMENCLATURE

A_{meas}	[m^2]	cross-sectional area of the laser vibrometer beam
A_{surf}	[m^2]	surface area of microphone hemisphere
c_0	[m/s]	speed of sound
f	[Hz]	frequency
FFT		fast Fourier transform
G	[m3/kg]	Gladstone-Dale constant
I_r	[W/m^2]	radial component of sound intensity
Im		Imaginary part
k	[mm/s/V]	vibrometer calibration constant
LIV		laser interferometric vibrometry
lat		latitudinal coordinate
lng		longitudinal coordinate
MP		measurement point
natural spectrum		spectrum of flame without excitation
P_{far}, P	[W]	sound power
pp-probe		pressure-pressure probe
p’	[Pa]	sound Pressure
PPM det		detached perfectly premixed
r	[m]	radial distance of observer
r_0	[m]	radius of flame
t	[s]	time
TPM att		attached technically premixed
TPM det		detached technically premixed
U	[V]	voltage
v_r	[m/s]	radial component of particle velocity
V_{Fl}	[m^3]	volume of the flame
Δr	[m]	Distance between microphones of pp-probe
ρ_0	[kg/m^3]	mean density outside of the flame
ρ'_T	[kg/m^3]	density fluctuation within flame
$\rho'(r)$	[kg/m^3]	density fluctuation at radius of observer
ζ	[m]	length of laser vibrometer beam

INTRODUCTION

Combustion generated noise has been a topic for many years in industrial applications where reacting flows are predominantly turbulent. Especially the prediction, and consequently the reduction of correlated and stochastic sound radiation of flames has been investigated intensively [1, 2]. Early theories as well as experimental validations suggest that the far field sound pressure is proportional to fluctuations of heat release within the flame [3]. For measurability, many publications supported the use of the time derivative of OH*-Chemiluminescence [4]. However, the density distribution within the flame had to be assumed. Progress in combustion noise theory made it possible to predict sound emission directly as a function of heat release without the need of the mean density field [5], but it remains a difficult task to acquire the heat release acurately. Alternatively, early work [6] suggested the use the density fluctuations within the flame ρ'_T in order to estimate density fluctuations in the far field ρ' and consequently combustion noise:

$$\rho'(r) = \frac{1}{4\pi c_0^2 r}\frac{\partial^2}{\partial t^2}\int_V \rho'_T\left(r_0, t - \frac{r}{c_0}\right) dV(r_0) \qquad (1)$$

with c_0 speed of sound, r radial distance of observer, volume V and radius r_0 of the flame. Since time resolved density fluctuations were difficult to measure, an adaption of the equation with application of OH*-chemiluminescence estimating the mean density within the flame was often preferred [2], Recent development and experimental work enabled accurate measurements of time resolved line-of-sight and local density fluctuations in turbulent jets [7, 8] and in laminar [9] and turbulent flames [10, 11]. Therefore, it is now possible to prove Strahle's assumption directly. For the research presented herein, a novel technique recording the time derivative of the density fluctuation was used. The measurement device, a laser interferometric vibrometer (LIV), integrates along the laser beam path and scans the two dimensional field of the flame. In the standard application of vibrometers the motion of an object is measured. If that object is a fixed mirror the interferometer in the instrument measures the time derivative of the density fluctuations along the laser beam path.

THEORETICAL BACKGROUND

In the following paragraph the calculation of sound power from $\int_\zeta \partial\rho'_T/\partial t$ directly measured by LIV and from microphone measurements are presented. Comparing sound power has the advantage that this number does not dependent on the distance of the observer (microphone) and it is easier to measure if the far field condition is not met [12]. It has the same significance as comparing density fluctuations since in the far field sound power is a direct function of the density fluctuation. Flames have a low pass characteristic and in a laboratory environment the far field condition for low frequencies is usually not fulfilled. Therefore, it is more convenient to calculate and compare sound power, which is not a function of the radial distance to the flame.

Prediction of Sound Power from $\int_\zeta \partial\rho'_T/\partial t$

In the far field where sound pressure p' and particle velocity are in phase sound power P_{far} can be calculated from density fluctuations as follows.

$$P_{far} = 4\pi r^2 \frac{p'(r)^2}{\rho_0 c_0} = 4\pi r^2 \frac{(c_0^2\rho'(r))^2}{\rho_0 c_0} \qquad (2)$$

Here, a sphere is defined as detection surface. Combining Equation 1 and Equation 2 results in the sound power as a function of density fluctuations:

$$P_{far} = \frac{1}{4\pi\rho_0 c_0}\left(\frac{\partial^2}{\partial t^2}\int_{V_{Fl}} \rho'_T\left(r_0, t - \frac{r}{c_0}\right) dV(r_0)\right)^2 \qquad (3)$$

After performing a fast Fourier transform (FFT) - now in the frequency domain - the time derivative of a variable is simply the variable times the angular frequency with a time lag of pi/2 :

$$FFT\left(\frac{\partial\rho'_T}{\partial t}\right) = 2\pi f * FFT(\rho'_T, angle - 90°) \qquad (4)$$

Now, in frequency domain, the acoustic power in the far field $P_{far(f)}$ can be calculated for each frequency f from Equation 3.

$$\mathrm{P_{far}(f)} = \frac{1}{4\pi\rho_0 c_0}\left((2\pi\mathrm{f})(2\pi\mathrm{f})\int_{V_{Fl}} \rho'_{\mathrm{T}}(\mathrm{phase} - 180°)\left(\mathrm{r_0, t} - \frac{\mathrm{r}}{\mathrm{c_0}}, \mathrm{f}\right)\right)^2 \qquad (5)$$

The integral density fluctuation over the flame volume $\int_{V_{Fl}} \rho'_T$ is equal to the sum of all fluctuations in the vibrometer grid, when the density fluctuations outside the flame are low compared to the ones within the flame. That this is the case, has been shown by [13].

$$(2\pi\mathrm{f})(2\pi\mathrm{f})\int_{V_{Fl}} \rho'_{\mathrm{T}}(\mathrm{phase} - 180°)\left(\mathrm{r_0, t} - \frac{\mathrm{r}}{\mathrm{c_0}}, \mathrm{f}\right) = (2\pi\mathrm{f})\sum_{\mathrm{MP}=1}^{\mathrm{n}} \frac{4}{\pi}\mathrm{A_{meas}}\int_\zeta \frac{\partial\rho'_{\mathrm{T}}}{\partial \mathrm{t}}(\mathrm{phase} - 90°)\left(\mathrm{r_0, t} - \frac{\mathrm{r}}{\mathrm{c_0}}, \mathrm{f}\right) \qquad (6)$$

with A_{meas}, the cross-sectional area of the laser vibrometer beam and ζ the measurement length of the vibrometers laser beam between optics and mirror. The factor $4/\pi$ corrects for a circular laser beam in a rectangular measurement grid. In this grid, the fluctuations outside of the circular beam cross-section would otherwise not be accounted for.

Combining Equation 5 and 6 yields the total sound power as the sum over all frequencies:

$$\sum_f P_{far}(f) = \sum_f \frac{1}{4\pi\rho_0 c_0}\left(2\pi f \sum_{MP=1}^{n} \frac{4}{\pi} A_{meas} \int_\zeta \frac{\partial \rho'_T}{\partial t}(phase - 90°)\left(r_0, t - \frac{r}{c_0}\right)\right)^2 \quad (7)$$

Equation 7 holds true if the flame diameter is small compared to the wavelength and distance to the observer. Then the space distribution of heat release can be neglected [6]. This is the case in our setup. If the flame diameter would be large, the spatial distribution of coherent heat release could not be neglected anymore. Extinction and amplification of pressure waves from local heat release (density) fluctuations would depend on the position of the source within the flame.

Calculation of Sound Power from PP-Probe

In the near field where sound pressure p' and the radial component of the particle velocity v_r are not in phase, sound power can be calculated via the radial component of sound intensity I_r which is perpendicular to the surface of the hemisphere A_{surf}:

$$P = \int_A I_r dA_{surf} = \int_A p' v_r dA_{surf} \quad (8)$$

Pressure is far easier to measure than particle velocity, therefore, the Euler equation is often used to estimate the particle velocity [12]:

$$\frac{\partial v_r}{\partial t} = -\frac{1}{\rho_0}\frac{\partial p}{\partial r} \quad (9)$$

The velocity along one dimension can then be expressed as a function of the pressure at two different positions:

$$v_r = -\frac{1}{\rho_0}\int_t \frac{p_{r+\Delta r} - p_r}{\Delta r} dt \quad (10)$$

As a consequence, the sound intensity in radial direction can be calculated by

$$I_r = p v_r = -\frac{p_{r+\Delta r} + p_r}{2}\frac{1}{\rho_0}\int_t \frac{p_{r+\Delta r} - p_r}{\Delta r} dt \quad (11)$$

For spectral analysis sound intensity can be expressed as a function of the imaginary part of the cross product of the complex pressures:

$$\vec{I}(f) = p\vec{v} = -\frac{1}{\rho_0 2\pi f \Delta r} Im(FFT(p_{r+\Delta r}) \times FFT(p_r)) \quad (12)$$

The cross product in the frequency domain can then be calculated by complex conjugated multiplication:

$$FFT(p_{r+\Delta r}) \times FFT(p_r) = FFT(p_{r+\Delta r}) * FFT(p_r)^* \quad (13)$$

EXPERIMENTAL SETUP

Test Rig

For the investigations presented in this paper, a variable geometry burner was used and the flow was excited with a siren which was mounted into the axial air-feed-line. The working principle of the burner has been documented in detail [14], the flow-field and characteristics of the - for rotational symmetry adapted - design have been published recently [15]. The siren was equipped with a sonic nozzle which had 1 mm in diameter, followed by a rotating cogwheel, blocking the crossectional area of the nozzle by 100%. Details about the siren can be found in [16]. In Figure 1 the burner is shown with the standard configuration - technically premixed (TPM) - to the left and the reference configuration - perfectly premixed (PPM) - to the right of the setup.

In the TPM configuration, the combustor is fed by fuel (a) tangential air (b), and axial air (c). The axial air is forced through a stratifier in order to ensure purely axial flow. In

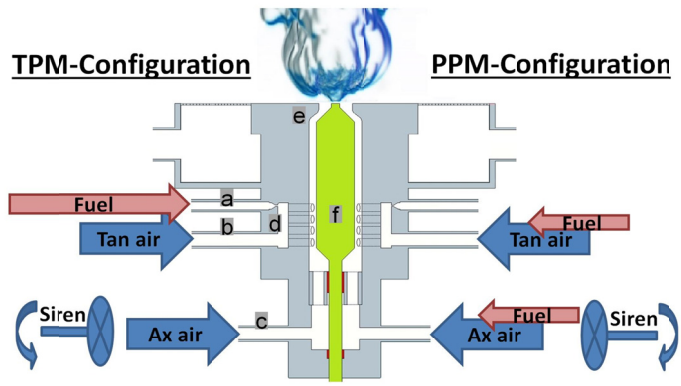

FIGURE 1: THE EXPERIMENTAL SETUP WITH THE TPM CONFIGURATION TO THE LEFT AND THE PPM CONFIGURATION TO THE RIGHT

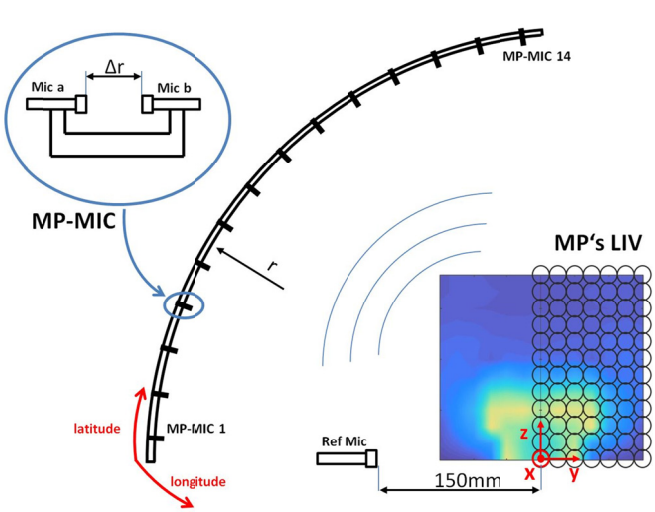

FIGURE 2: PP-PROBE-SETUP WITH TWO MICROPHONES (TOP LEFT), PP-PROBE MP'S ONE TO FOURTEEN IN ARCH-CONFIGURATION AND LONGITUDINAL TRAVERSING DIRECTION (MIDDLE) AND 2D-MEASUREMENT GRID OF LIV (BOTTOM-RIGHT).

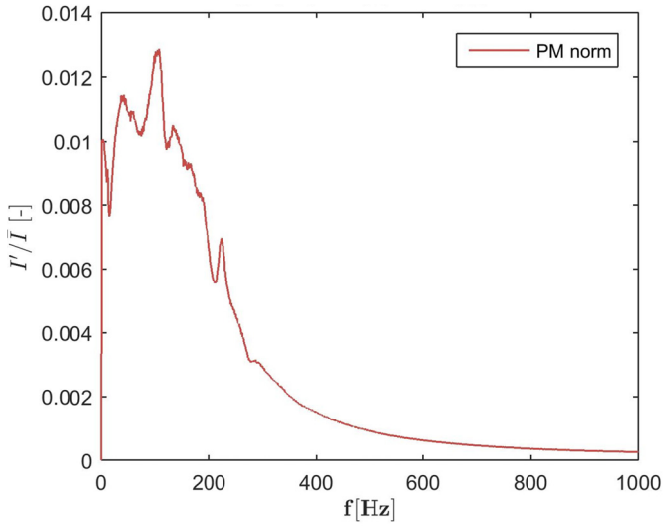

FIGURE 3: NATURAL OH*-CHEMILUMINESCENSE SPECTRUM OF PPM DET.

contrast to this the tangential air passes the outer mixing chamber (d) and from there, enters the plenum through 32 cylindrical bores aligned tangentially and symmetrically around the burner axis. Methane is injected into the tangential air in the outer chamber. The siren modulates the axial gas flow only.

In case of perfect mixing, the methane was injected into the air supply far upstream before tangential and axial air split. The movable center cone (f) of the burner was set to 1 mm above the exit in order to constrict the flow through the burner exit nozzle (e) and consequently ensure correct momentum for the point of operation. Mass flow was measured using caloric mass flow meters of the EL-FLOW series from Bronkhorst, Netherlands, with an accuracy of 0.6 % FSC. The test rig was set up in a thermoacoustic laboratory within a 3x3x2.5m3 box with two layers of low reflective curtains and a sound absorbing ceiling. The specific mass flows of the points of operation can be found in Table 1. The simplified swirl number was measured according to [17], neglecting the pressure term, using a burner exit radius of 8 mm averaging over a height of z=8.5 mm to z=17 mm which is 0.5 times and 1 time the burner exit diameter respectively.

For this investigation three points of operation were examined. In the technically premixed setup two flame shapes are stable. Generally, the flame is attached to the center rod of the burner. Once the flame detaches the flame stays detached in a stable way. In the perfectly premixed setup the flame was detached all the time - the flame cannot anchor at the bluff body of the burner-center-rod.

MEASURING TECHNIQUES

Microphone Array

For the acoustic measurements, a custom built microphone array, with 14 measurement positions aligned in an arch of one meter radius, was built (Figure 2). At those 14 measurement points in latitudinal direction, acquisition was performed simultaneously. The setup covered 90° in 6° steps of the downstream area of the flame. In longitudinal direction (around the positive z-axis), the burner was rotated in 6°steps to cover a semicircle. At each of the measurement positions two microphones where set up facing each other. With this configuration, also known as pp-probe [18], acoustic pressure was measured directly and particle velocity was derived. From that configuration the sound intensity can be calculated, as well as, the total sound power without a need to fulfill the far-field assumption.

The distance between two opposing microphones was 56 mm. This provides accurate measurements for the frequency spectrum between 50 and 1000 Hz, which covers the spectrum of the flame investigated [18]. Additionally, two microphones were rotated with the burner in order to provide a reference signal. They were used to normalize the sound intensity signal

Table 1: Flow properties

Axial air [g/s]	Tangential air [g/s]	Fuel [g/s]	Swirl Number [-]
0.422	0.397	0.0683	0.54

in order to account for slight variations in the point of operation of the burner. The photomultiplier (PMM01, Thorlabs Inc., Newton, New Jersey, USA with OH* filter 310 nm CWL,

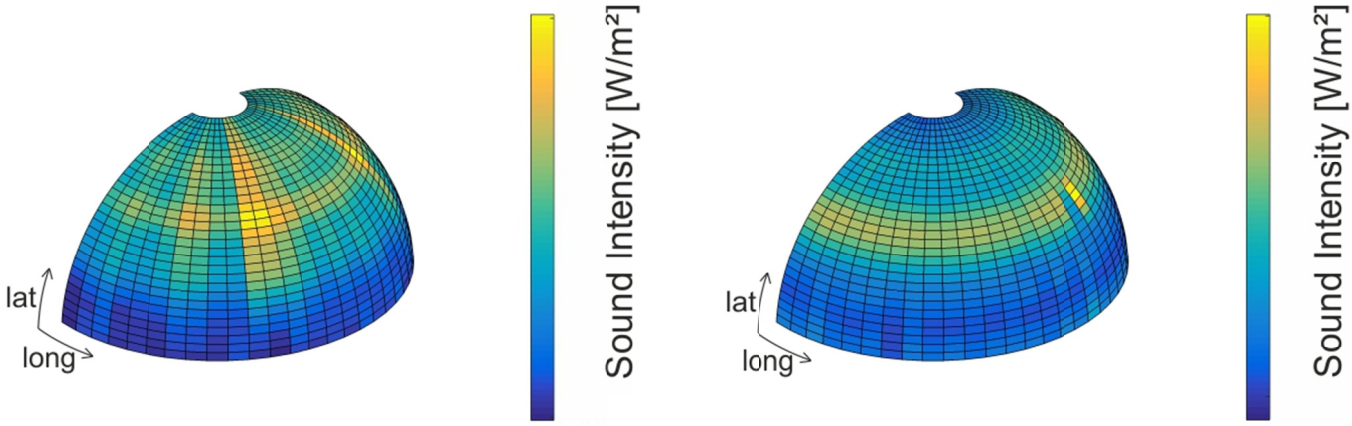

FIGURE 4: SOUND INTENSITY DISTRIBUTION BEFORE (LEFT) AND AFTER (RIGHT) NORMALISATION BY THE REFERENCE MICROPHOHNE.

FWHM 10 ±2 nm Bandwidth, Edmund Optics, Barrington, NJ, USA) and the siren signal were acquired as well. This gives a total of 32 channels which were recorded with a PXI-module and Labview 8.6 software, both from National Instruments, Austin, Texas, USA. The sample rate of was 100 kilo samples per second.

Laser Interferometric Vibrometry

Here, laser interferometric vibrometry (LIV) detects the time derivative of line-of-sight integrated density fluctuations in a gas by interferometric principles [19, 7, 8, 9, 11]. Using a Polytec laser vibrometer (interferometer head OFV-353, velocity decoder OFV-3001, calibration factor 5mm/s/V, 200 kHz bandwidth, no filters, Polytec, Waldbronn, Germany) the measured voltage (U) is linked to the derivative of the density fluctuation by the Gladstone-Dale constant (G) and the calibration factor (k). G and k were set to 2.59e-4 m^3/kg and 5 mm/s respectively for all points of operation:

$$\int_{\zeta} \frac{\partial \rho'_T}{\partial t}(A_{meas}, \zeta, t) d\zeta = \frac{k}{2G} U(t) \qquad (14)$$

In velocity mode the output voltage U(t) is linked to the line of sight integrated derivative of the density fluctuation in the flame $d\rho'_T/dt$ per measurement area A. A factor of two is due to the laser beam passing the cylindrical measurement volume twice. The beam diameter was set to 5mm. The field was scanned from z = 5 mm to 60 mm and from y = 0 to 30 mm with 5 mm increment (Figure 2). The beam direction with integration length ζ is parallel to y coordinate.

Processing

Evaluation of both data sets, LIV and microphone, was performed in Matlab 2015a using Welch's periodogram [20] and the analogous cross product function with a sample length of 100,000. The built in flattop window was applied for all single frequency investigations, in order to face the scalloping loss of FFT. For the spectrum-integrated data, a rectangular window was used.

Schlieren

For visualization of density gradients in space, a schlieren technique [21] was applied. The same setup as in [15] was used, but now the camera was triggered with the siren signal, and one hundred images were acquired and averaged.

RESULTS AND DISCUSSION

Below, the acoustic behavior of the flame in the three different configurations is discussed. In a first step, the natural sound spectrum (no siren) and the radiation behavior will be analyzed. Then, by excitation with a siren, the linear behavior of the flame at a single frequency is discussed. A quantitative benchmark with the sound power, calculated from heat release using Strahle's Equation 1, should deliver a similar result. This is only possible by a high enough signal to noise ratio, necessary to ensure comparability between the two different measurement techniques, and is achieved by linear excitation with a siren. Finally, the schlieren technique is used to discuss different trends of noise levels between points of operation for the natural spectrum and mono frequent excitation.

Acoustics

Since the typical hydrocarbon flame acts as a low pass filter, the spectrum of the heat release is usually characterized first by a rapid increase of amplitude with increasing frequency that tops out on a smooth peak and is followed by a gentle slope towards higher frequencies. This typical behavior is shown in the OH*-chemiluminescence image in Figure 3.

In a first step, **the natural spectra** of the flames were recorded. In Figure 4 the sound intensity calculated from

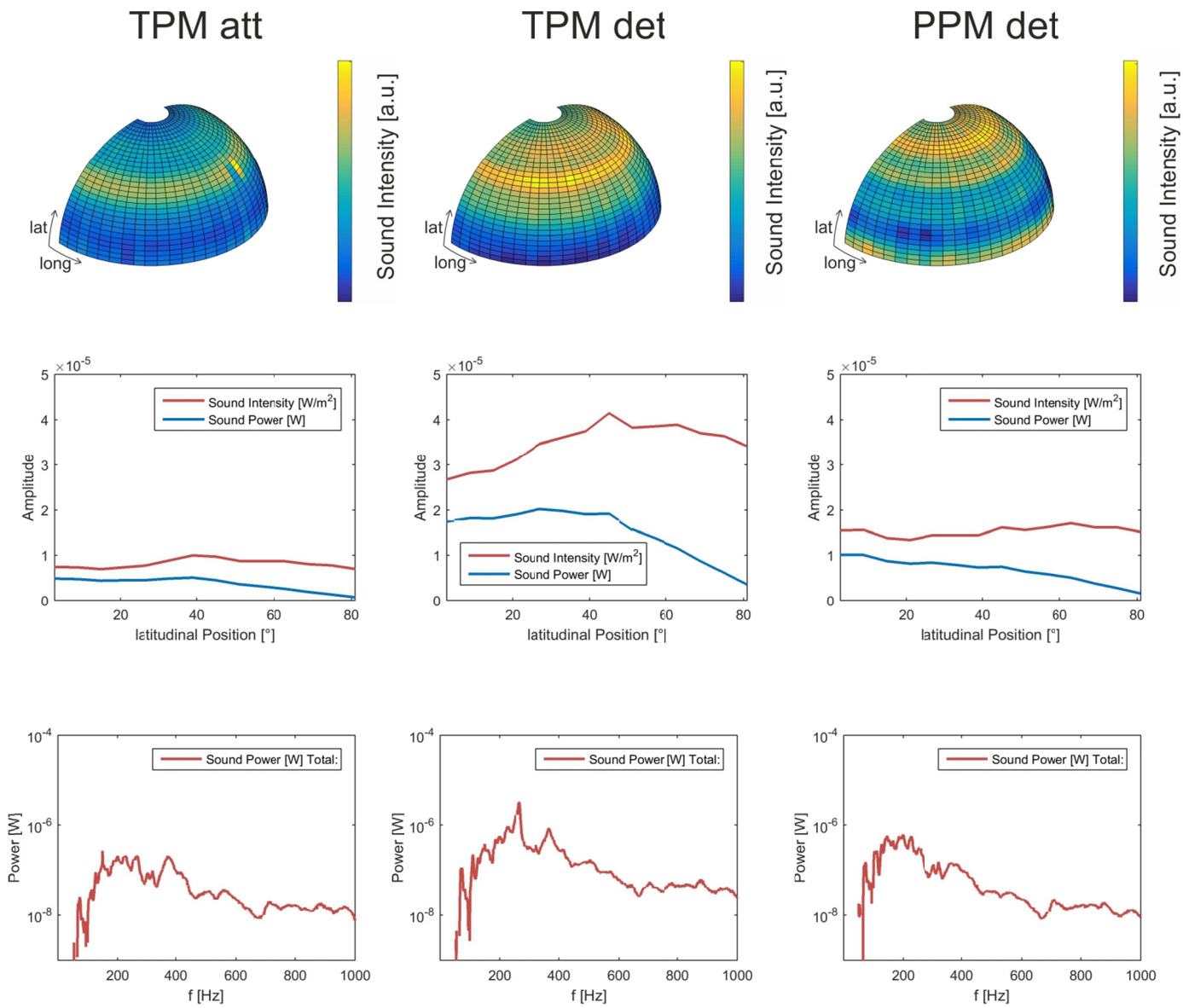

FIGURE 5: SOUND INTENSITY DISTRIBUTION (TOP), INTENSITY AND POWER ALONG LATITUDINAL POSITIONS (MIDDLE) AND TOTAL SOUND POWER SPECRUM (BOTTOM) FOR ALL THREE POINTS OF OPERATION.

Equation 12 integrated over all frequencies is plotted in half a hemisphere, as a function of longitudinal and latitudinal coordinates. The latitudinal measurement points were acquired simultaneaously, while the longitudinal measurement points were acquired one after the other, by rotating the burner. Before normalization (Figure 4 left), two trends are obvious. Firstly, the sequential measurement method introduces a fluctuation of sound intensity (longitudinal direction). Secondly, sound intensity also depends on latitudinal position. In order to interpret the result properly, the measurement of half the hemisphere was normalized by a reference microphone, which was traversed with the burner. The pressure signals used for the calculation were normalized for each frequency in the spectrum and each latitudinal (lat) and longitudinal (long) position individually according to:

$$p'^2{}_{norm}(lng, lat, f) = \frac{p'^2(lng, lat, f)}{p'^2{}_{ref}(lng, f)} * \overline{p'^2{}_{ref}(f)}^{lng} \qquad (15)$$

with the normalized pressure signal p'_{norm} calculated from the original signal p' and the reference signal p'_{ref}. This linear normalization of the square of the pressure is equivalent to normalization of the sound power. This simple correction results in a nearly perfect rotationally symmetric distribution of sound intensity (Figure 4 left) and confirms the assumption of an axis symmetric flame [22]. Consequently it was not

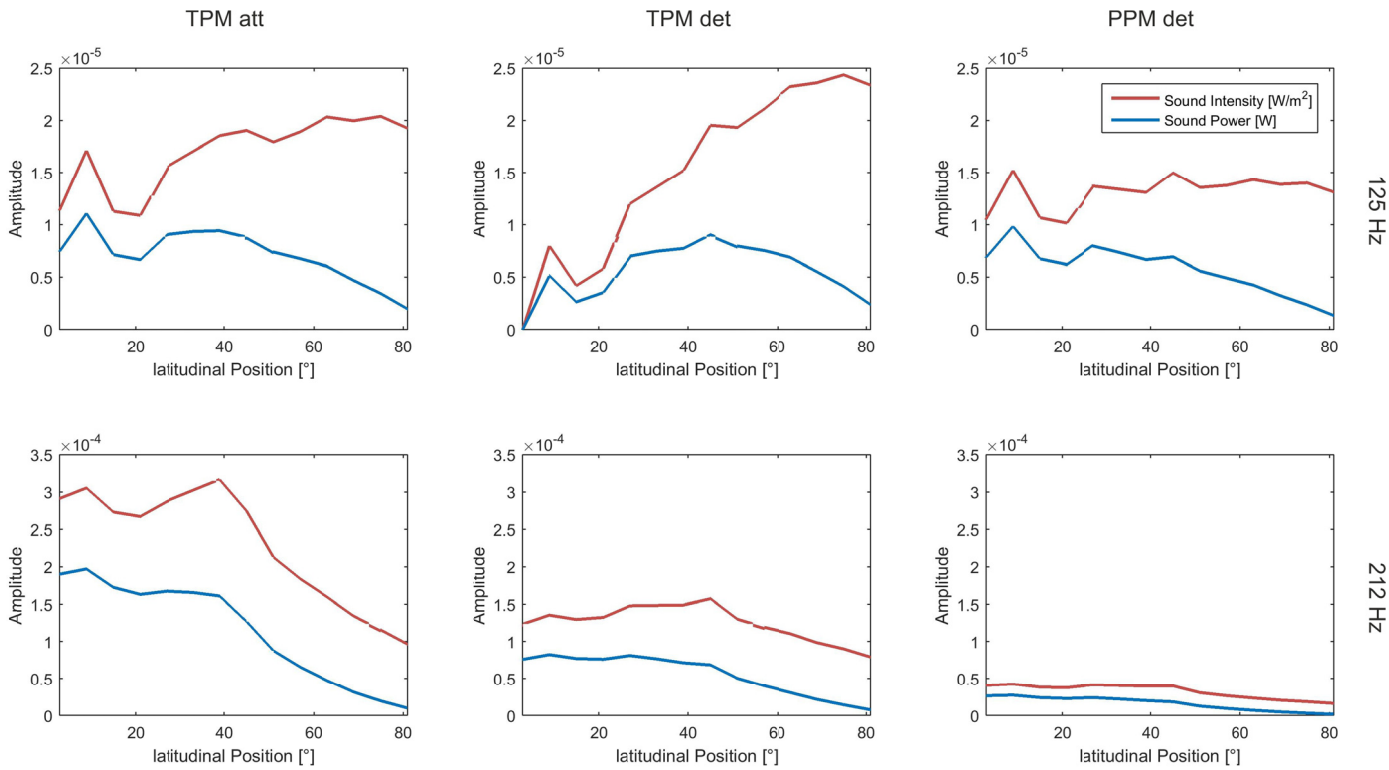

FIGURE 6: SOUND INTENSITY (TOP) AND POWER (BOTTOM) FOR LINEAR EXCITATION AT 125 HZ AND 212 HZ FOR ALL THREE POINTS OF OPERATION.

necessary to measure the whole field of half a hemisphere. To double-check the results and due to the short acquisition time of 20 seconds per measurement point this task was performed, since small variations in burner operation are inevitable. Therefore, for all results presented in this work, the 30 longitudinal measurement points were averaged in order to provide repeatable results.

The sound intensities for all three points of operation normalized by the reference microphone are presented in Figure 5 (top). Averaging over longitudinal measurement points gives sound intensity and derived from that, sound power as a function of latitude (Figure 5 middle). Finally a spectrum of total sound power / Hz is shown (Figure 5 bottom).

For all points of operation, a weak directionality can be found, as literature has suggested [23]. The attached TPM flame shows its highest amplitude of sound intensity at 45° downstream, falling off in amplitude towards higher as well as lower angles. The overall sound power is lowest for this configuration. Similar results can be found for the detached TPM configuration, the peak amplitude is located at the same latitude of about 45°, but now sound intensity stays high towards higher frequencies. The overall sound power is highest for this configuration. Finally, the detached PPM case shows a local peak sound intensity at 45°, but now it is topped by the noise in downstream direction. The overall noise level is in-between the noise of the other two points of operation.

The reason that the attached flame was the quietest one can be found in the flame stabilization process. The flame is anchored in the wake of the center cone of the burner which is a stable point in space. This makes the flame less receptive to small turbulent fluctuations from upstream. In contrast to this - in the detached configuration - the flame is stabilized solely by the swirl induced recirculation zone, which generally makes the flame much more receptive to flow field disturbances such as vortex shedding and other fluctuations. In the frequency spectra of the sound power (Figure 5 bottom), this can be seen as well.

The detached TPM case shows a mono-frequent effect at around 250 Hz, which has been identified in previous work as vortex shedding at the burner exit [24]. The vortices follow the conical jet of the swirl outwards and interact with the recirculated reactants. The angular direction of the swirl jet roughly meets the latitudinal angle of highest amplitude in sound intensity distribution. PPM det and TPM att have a less mono-frequent pattern in spectrum, explaining a lower overall sound emission. All three operation points have in common that in their spectra, hardly any combustion noise is present above 500 Hz. This fact is not surprising when comparing with the OH* emission in Figure 3. Integrating over the whole spectrum of sound power gives a total sound power of 5.06*10-5 W, 2.1*10-4 W and 9.34*10-5 W for TPM att, TPM det, and PPM det respectively. With a thermal power of the flame of 3.4 kW this gives thermal efficiencies of 1.5*10-8, 0.6*10-7 and

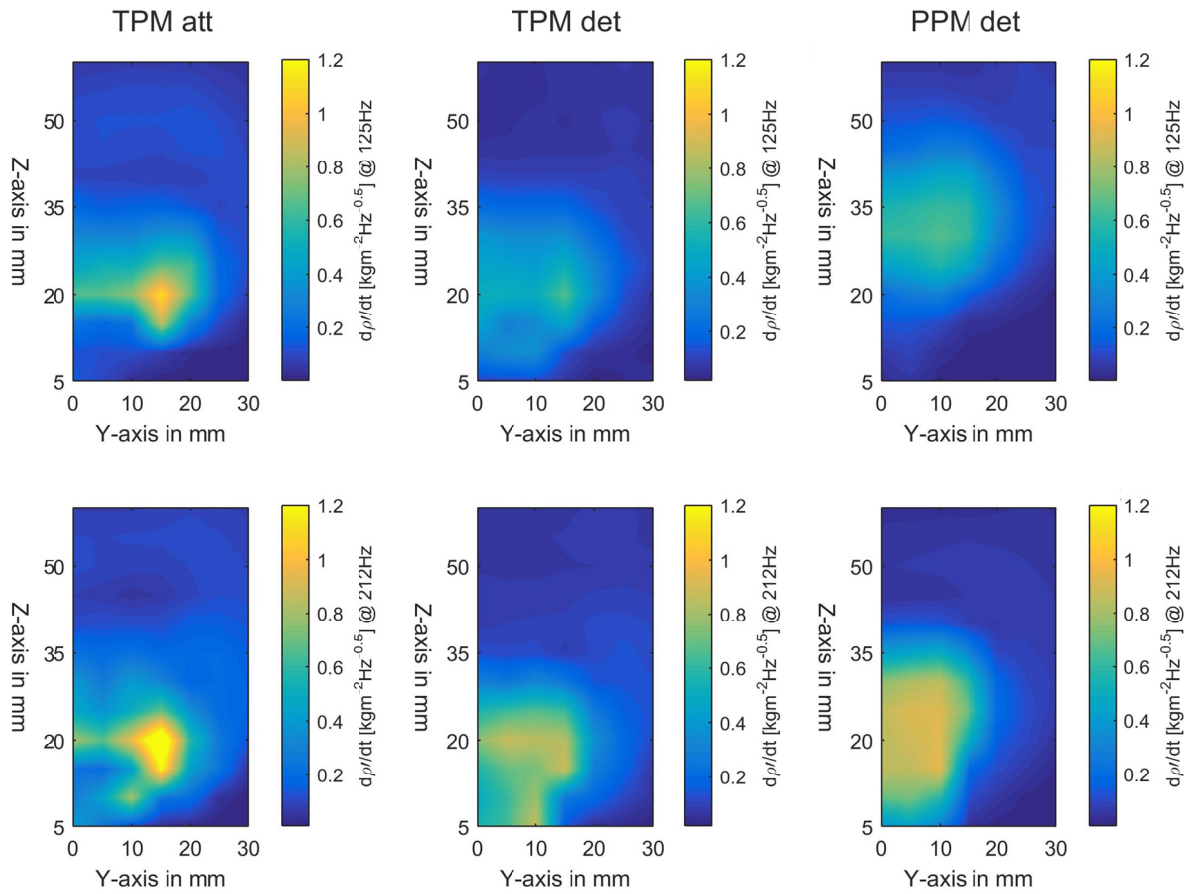

FIGURE 7: TIME DERIVATIVE OF LINE-OF-SIGHT-INTEGRATED DENSITY FLUCTUATIONS MEASURED BY LIV FOR 125 HZ AND 212 HZ EXCITATION. THE PLOTTED VALUE IS THE AMPLITUDE RESULTING FROM FFT.

2.8*10-8. This lies in the range of 10-8 to 10-7 which is consistent with other research [25, 23].

In a second step, the flame was **excited by a siren**. All parameters were kept constant, only the excitation frequency was altered. Sound intensities were averaged for half the hemisphere. Power and sound intensity can be found in Figure 6 for 125 Hz and 212 Hz. The trend for 125 Hz along the height is very similar to the natural spectrum discussed above. At both TPM cases the noise level increases with latitude. Except now for TPM det the sound intensity is close to zero at the bottom of the microphone array. In contrast to this, the excitation at 212 Hz shows an entirely different behavior. Now the amplitude is high at low measurement positions and gradually decreases with increasing latitude.

Sound Prediction by LIV

The time derivative of density fluctuations were measured by means of LIV. With some assumptions, this quantity is proportional to the heat release rate fluctuations in the flame [9, 11]. In Figure 7 the amplitude distributions for siren excitation at 125 Hz (top) and at 212 Hz (bottom) are shown. For all points of operation, the total fluctuation of density stretches widely in radial as well as in axial direction. For PPM the fluctuations are further downstream in comparison to the technically premixed flame. This can be explained by an increased axial momentum at perfect mixing, where half of the fuel is injected into the axial flow. In contrast to this, in case of technical mixing, the entire fuel is injected tangentially. Looking at the excitation at 125 Hz it is obvious that the major fluctuations are within the core of the flame, which is at around z = 20 mm for the TPM cases and at around z = 30 mm for the PPM case. In contrast to this, at 212 Hz the major fluctuations of the detached configurations are smaller in amplitude. The flame seems to be strongly excited by incoming perturbations at this frequency. Especially the detached flames change the position of main oscillations. Comparing the density fluctuations at 212 Hz with the sound power measured by the microphone array as shown in Figure 6, one could explain the trend of the flame to radiate more in horizontal direction (side-wise) at this frequency. Generally a greater surface of heat release fluctuations will lead to higher noise radiation as long as those zones are correlated in phase.

For the comparison of sound power calculated from the density fluctuations within the flame and the sound power

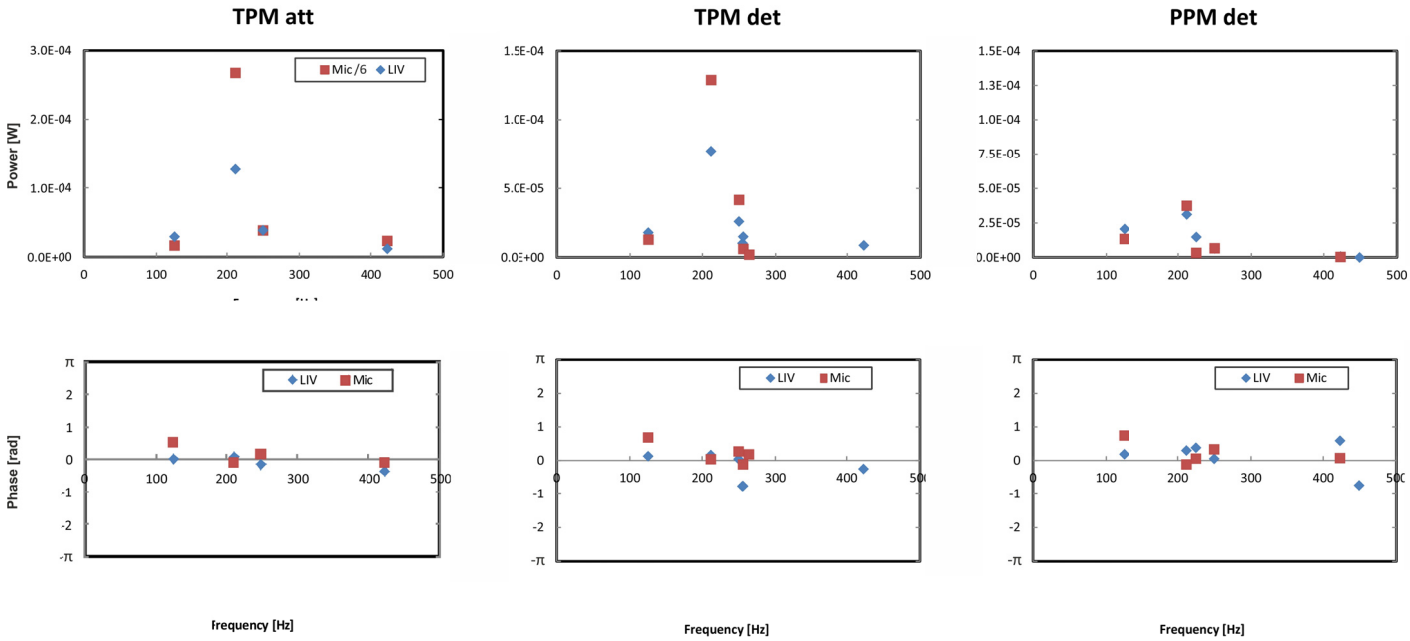

FIGURE 8: AMPLITUDE AND PHASE OF SOUND POWER MEASURED BY MICROPHONES AND LIV, WITH PM AS REFERENCE FOR THREE POINTS OF OPERATION, EXCITATION BY SIREN.

measured by the microphone array, linear excitation by a siren was done. The amplitude of sound pressure measured by microphones and prognosed due to the heat release from LIV are in a comparable range. For the microphone measurements sound power lies between 2e-3 mW for the PPM flame at 423 Hz and 1.6 mW for the attached TPM flame at 212 Hz.

For the same measurement points vibrometry prognosed a sound power level of 0.7e-3 mW and 0.13 mW respectively. This is less than one order of magnitude in difference. The comparison of trends over frequencies is shown in Figure 8. For the sake of visualization in Figure 8, the microphone results were divided by a factor of six. This makes it possible to see the matching trend over frequencies for both measurement techniques (Figure 8 top). For both, the attached TPM flame (Figure 8 left) shows highest fluctuations over the whole band of frequencies, followed by TPM det (Figure 8 middle), which is consistently quieter. Finally, the PPM det flame (Figure 8 right) is the quietest one throughout the spectrum. Considering the individual frequencies, similar trends can be found for all points of operation. At 125 Hz low sound pressure is measured, with good consistency of both measurement techniques for all points of operation. Moving on to 212 Hz the acoustic sound due to combustion is highest, and at the same time the prediction of sound by LIV slightly underestimates the actual

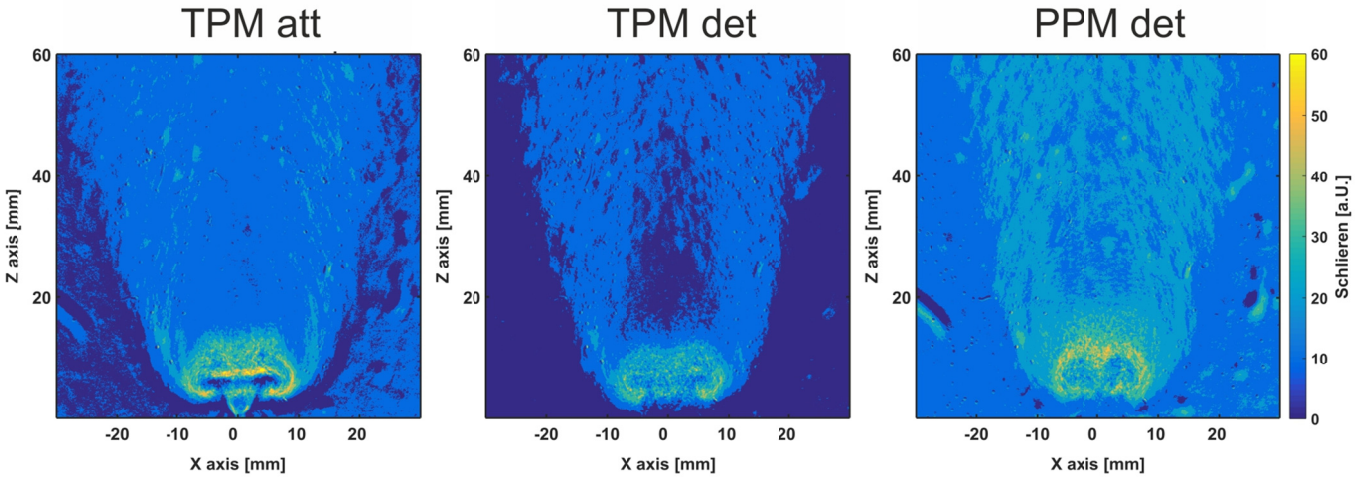

FIGURE 9: DENSITY GRADIENTS IN SPACE OF ALL POINTS OF OPERATION AT 212 HZ AND 315° PHASE ANGLE VISUALIZED USING SCHLIEREN TECHNIQUE.

sound power. From higher frequencies onward, the consistency of trends for both techniques is again very good.

For linear excitation, the phase of the sound power derived from LIV and the microphone array is plotted in Figure 8 (bottom). Measurements show that for all frequencies tested the phase of the LIV is very close to the photomultiplier signal. A low deviation of no more than 30 degrees (mostly below 10 degrees) is expected, since both techniques represent the heat release of the flame. In order to compare the phase of the microphone with the phase of heat release recorded by LIV, firstly, one has to account for the time delay, the acoustic wave needs for the distance between the flame and the microphones. Secondly, the vibrometer signal is proportional to $\partial\rho/\partial t$, but the resulting sound is proportional to the second time derivative of density. 90° phase shift have to be accounted for when the time derivative of a signal is calculated in the frequency domain. Therefore, the phase of the acoustics was corrected by adding a phase shift which is a function of the distance between flame and measurement position as well as the frequency. Then $\pi/2$ was subtracted to correct for the time derivative in frequency domain.

Analysis of Specific Sound Levels

When comparing the natural spectrum and the amplitudes of linear excitation for the sound power measured by microphones, it can be found that the PPM detached flame is consistently quieter than the TPM det flame. However, the TPM att case is the quietest one for the natural spectrum but with excitation, all of a sudden, it becomes the noisiest flame. The reason for the natural spectrum to be of lowest amplitude has been identified to lie in the stabilization process of the anchored flame. But then, with siren excitation, the fluctuations of heat release get so violent that the flame anchoring region behind the bluff body is heavily disrupted. In Figure 9 left density gradients in space at one frequency and one phase angle are shown. The surface of the attached flame is heavily disrupted. At the end of the flame cone vortex an induced flame roll up is observed. This process enlarges the flame surface and coherent fluctuations in heat and consequently in noise can be observed. The attached V-cone flame almost acts like a rubber band, trying to keep the vortex attached to the flame, and then suddenly snaps back. In comparison to this, the other points of operation are purely dynamically stabilized. Therefore, those flames can, within limits, travel up and downstream of the flow, dampening the process. Vortex rollup, which introduces shear stress in the flow, is more suppressed by this flame motion. The vortex rollup in the flame can still be found in the detached flames (Figure 9 middle and right), but the density gradients are more smeared.

CONCLUSION

Strahle postulated that the sound of a flame in the far field is a function of density fluctuations within the flame. The focus of this study was to prove Strahle's assumption by comparison between the predicted noise measured with LIV and a microphone array. In the first part, the acoustic field of the flame was analyzed. Normalization by the reference microphone corrected for sub-Hz frequency fluctuations during operation, results in an almost perfectly symmetrical sound field. In latitudinal direction, a slight dependency on angle was found as detected by other authors [23]. Overall sound power is in agreement with experience of former work as well. For the level of noise, the stabilization process was found to be the dominant factor. For siren excitation, the angular variation of sound intensity was traced back to the distribution of combustion fluctuations, which were particularly intense at the root of the flame.

Considering sound prediction by heat release fluctuations qualitatively, both measurement techniques lie in the same order of magnitude. In this study LIV underestimated the actual sound level by a factor of six. A very good agreement in trend over the range of investigated frequencies was shown. Some factors of influence lie within the equation of sound power due to density fluctuations. First, the assumption of a monopole, second, in the equation the diameter of the laser beam raised to the fourth is considered. Therefore, it is critical to accurately determine the diameter when the system is set up.

Finally, the behavior of the TPM att was explained by means of the schlieren technique. This operation point initially was the quietest. However, once excited by the siren, it consistently had the highest amplitude.

This leads to the final conclusion, that it is possible to predict combustion noise qualitatively due to density gradients within the flame. On the basis of direct physical quantities a comparison of both techniques revealed a deviation by a factor of six.

ACKNOWLEDGEMENT

This research was funded by the Austrian Science Fund (FWF) within grant FWF-24096-N24 "Interferometric Detection of Thermoacoustic Oscillations in Flames".

References

[1] W. C. Strahle, "Combustion noise," *Progress in Energy and Combustion Science,* vol. 4, no. 3, pp. 157-176, 1978.

[2] T. Schuller, D. Durox and S. Candel, "Dynamics of and Noise Radiated by a Perturbed Impinging Premixed Jet Flame," *Combustion and Flame,* vol. 128, pp. 88-110, 2002.

[3] R. B. Price, I. R. Huerle and T. M. Sudgen, "Optical studies of generation of noise in turbulent fames," *Twelfth Symposium (International) on Combustion,* 1969.

[4] I. R. Huerle, R. B. Price, T. M. Sudgen and A. Thomas, "Sound emission from open turbulent flames," *Proc. R. Soc. A,,* 1968.

[5] A. P. Dowling and Y. Mahmoudi, "Combustion noise," *Proceedings of the Combustion Institute,* vol. 35, no. 1, pp.

65-100, 2015.

[6] W. C. Strahle, "On combustion generated noise," *Journal of Fluid Mechanics,* vol. 49, no. 02, pp. 399-414, 1971.

[7] B. Hampel and J. Woisetschläger, "Frequency- and space-resolved measurement of local density fluctuations in air by laser vibrometry," *Measurement Science and Technology,* vol. 17, pp. 2835-2842, 2006.

[8] N. Mayrhofer and J. Woisetschlaeger, "Frequency analysis of turbulent compressible flows by laser vibrometry," *Experiments in Fluids,* vol. 21, pp. 153-161, 2001.

[9] T. Leitgeb, T. Schuller, D. Durox, F. Giuliani, S. Köberl and J. Woisetschläger, "Interferometric determination of heat release rate in a pulsated flame," *Combustion and Flame,* vol. 160, no. 3, pp. 589-600, 2013.

[10] J. Li, D. Durox, F. Richecoeur and T. Schuller, "Analysis of chemiluminescence, density and heat release rate fluctuations in acoustically perturbed laminar premixed flames," *Combustion and Flame,* vol. 162, no. 10, pp. 3934-3945, 2015.

[11] J. Peterleithner, N. V. Stadlmair, J. Woisetschläger and T. Sattelmayer, "Analysis of measured flame transfer functions with locally resolved density fluctuation and OH-Chemiluminescence Data," *Journal of Engineering for Gas Turbines and Power,* vol. 138, no. 3, 2016.

[12] M. Möser, Engineering Acoustics, Vienna, New York, Heidelberg, 2014, p. 552.

[13] A. P. Dowling and A. S. Morgans, "Feedback Control of Combustion Oscillations," *Annu. Rev. Fluid Mech.,* vol. 37, pp. 151-182, 2005.

[14] F. Giuliani, J. W. Woisetschläger and T. Leitgeb, "Design and validation of a burner with variable geometry for extended combustion range," in *Proceedings of the ASME Turbo Expo*, 2012.

[15] J. Peterleithner, F. Salcher and J. Woisetschläger, "Frequency resol ed interferometric detection of local density fluctuations in flames," *Proc. 17th International Symposium on Application of Laser Techniques to Fluid Mechanics, Lisbon,,* 2014.

[16] F. Giuliani, A. Lang, K. Johannes Gradl, P. Siebenhofer and J. Fritzer, "Air flow modulation for refined control of the combustion dynamics using a novel actuator," *Journal of Engineering for Gas Turbines and Power,* vol. 134, no. 2, 2012.

[17] S. Candel, D. Durox, T. Schuller, J. .. Bourgouin and J. P. Moeck, Dynamics of swirling flames, vol. 46, 2014, pp. 147-173.

[18] Brüel and Kjaer, *Sound intensity,* 1993.

[19] J. Peterleithner and J. Woisetschläger, "Laser vibrometry for combustion diagnostics in thermoacoustic research," *Technisches Messen,* vol. 82, no. 11, pp. 549-555, 2015.

[20] A. V. Oppenheim and R. W. Schafer, Digital signal processing, Englewood Cliffs, N.J.: Prentice-Hall., 1975.

[21] G. Settles, Schlieren and Shadowgraph Techniques, Springer, Wien Heidelberg New York, 2006.

[22] J. Peterleithner, A. Marn and J. Woisetschläger, "Interferometric In estigation of the thermo-acoustics in a swirl stabilized Methane flame," in *Proceedings of the ASME Turbo Expo*, 2015.

[23] T. J. B. Smith and J. K. Kilham, "Noise Generation by Open Turbulent Flames," *Journal of Acoustical Society of America,* vol. 35, no. 05, pp. 715-724, 1963.

[24] J. Peterleithner, R. Basso, F. Heitmeir, J. Woisetschläger, S. R., C. J. and A. Fischer, "COMPARISON OF FLAME TRANSFER FUNCTIONS ACQUIRED BY CHEMILUMINESCENCE AND DENSITY FLUCTUATION," in *Proc. ASME Turbo Expo*, 2016.

[25] J. Wäsle, A. Winkler and S. T., "Spatial Coherence of the Heat Release Fluctuations in Turbulent Jet and Swirl Flames," *Flow, Turbulence and Combustion,* vol. 75, pp. 29-50, 2005.

4 Conclusion and Outlook

The LIV technique is comparably straight forward when used for the detection of density fluctuations. The influence of refractive index and the Gladstone-Dale constant is low for the participants of typical natural gas-air combustion in the lean regime. With increasing equivalence ratio beyond 1.16 the variation of the Gladstone-Dale constant considerably increases and is no longer neglect able. This however is not a significant limitation, since modern combustion systems mostly rely on lean combustion systems [13]. Changing from perfectly premixed systems (laboratory setups) to partially premixed systems (industry setups) increases the uncertainty. This influence however is small.

If pressure fluctuations are low, detection of the time derivative of density fluctuations via LIV is also a good alternative measurement technique in order to gain information about the heat release rate. This has been shown to be valid for laminar and turbulent flames between 4 kW and 50 kW in confined and unconfined configuration.

Then, an influence of the speed of sound is present. This influence is due to the speed of sound being dependent on the local temperature in the flame. The detection of the temperature field in a reactive environment is however challenging. It was shown in this thesis, that by detecting the absolute density field in addition to the fluctuations, this influence can be compensated as well. Shearography was used for measurements of absolute values of density. The prefect gas equation was employed and pressure fluctuations assumed to be small. Shearography is based on the relative change in density from pixel to pixel (gradient detection).

A drawback of the LIV system is the time consuming traversing. To reduce measurement time, in a first step, the laser beam was expanded to and collimated at a diameter where the whole flame is captured at once. For detection, the laser beam is then focused again onto the single photo cell in the sensing head of the vibrometer. This technique was compared to OH*-chemiluminescence and proven to work. As a drawback, with this procedure geometrical resolution is sacrificed.

Optionally, measurement time can be reduced in the same way without losing space resolution. The laser beam must again be expanded and collimated, but instead of collecting the information on one photocell, mounting a two dimensional array of receptors now gives local information. Detection of the whole field at once, including the undisturbed environment, gives the ability of not only detecting fluctuations in time but also performing spatial correlations. These spatial correlations will provide integral length scales in the flame, in addition to line-of-sight averaged flow velocities.

A full-field laser vibrometer with an array of laser beams detecting density fluctuations could perform this task by the relative phase lags from pixel to pixel. Thus, such a future system would record temperature field and density fluctuations as line-of-sight data for the same pixel-array.

The most important tasks on the way towards a full-field LIV will then be to maintain a good level of signal-to-noise ratio in all pixels and an approach to limit the deflection of light rays. A strong deviation would otherwise produce ghost images in neighboring measurement cells.

Conclusively, this thesis proved the hypothesis that LIV is a good alternative tool to record heat release fluctuations. It also shows the error margins for different types of flames.

Finally, the assumption that sound emission can be predicted by measuring density fluctuations proved to be correct. By comparing acoustic pressure data and heat release data it was shown that this procedure can replace acoustic far-field measurement.

5 References

[1] C. Soares, Gas Turbines - A Handbook of Air, Land, and Sea Applications, Elsevier Inc., 2008.

[2] W. J. Fischer and P. Nag, "H-Class High Performance Siemens Gas Turbine SGT-8000H series," *Proc. Power Gen International 2011, Nevada,* 2011.

[3] L. Balling, "Fast-cycling and Starting Combined Cycle Power Palants to Backup Fluctuating Renewable Power," *Industrial Fuels and Power,* vol. August 27, 2010.

[4] ICAO, Global Air Transport Outlook to 2030 and Trends to 2040, ICAO, 2013, p. 152 S..

[5] EU, EU transport in figures, Publications Office of the European Union, 2014, p. 152 S..

[6] D. S. Lee, D. W. Fahey, P. M. Forster, P. J. Newton, R. C. N. Wit, L. L. Lim, B. Owen and R. Sausen, "Aviation and global climate change in the 21st century," *Atmospheric Environment,* vol. 43, no. 22-23, pp. 3520-3537, 2009.

[7] IPCC, *CLIMATE CHANGE 2014: Synthesis Report. Summary for Policymakers,* 2014.

[8] National_Research_Council, Advancing the Science of Climate Change, Washington, DC: The National Academies Press, 2010.

[9] IPCC, *IPCC SPECIAL REPORT AVIATION AND THE GLOBAL ATMOSPHERE,* 1999.

[10] J. E. Penner, Aviation and the global atmosphere: a special report of the Intergovernmental Panel on Climate Change, Cambridge University Press, 1999.

[11] US_Environmental_Protection_Agency, "Nitrogen Dioxide Health," 2016. [Online]. Available: https://www3.epa.gov/airquality/nitrogenoxides/health.html. [Accessed 19 7 2016].

[12] US_Environmental_Protection_Agency, "Unburned Hydro Carbons," 1994. [Online]. Available: https://www3.epa.gov/otaq/consumer/05-autos.txt. [Accessed 19 7 2016].

[13] C. Lieuwen and V. Yang, Gas Turbine Emissions, Cambridge: Cambridge Univ. Press, 2013.

[14] ICAO, ICAO Annex 16 Volume II, ICAO, 2008, p. 99 S..

[15] T. –. Environmental_Protection, "ANNEX III CO2," 2016. [Online]. Available: http://www.icao.int/secretariat/postalhistory/annex_16_environmental_protection.htm. [Accessed 19 7 2016].

[16] P. P. Walsh and P. Fletcher, Gas turbine performance, John Wiley \& Sons, 2004.

[17] Norris, Guy - Aviation Week & Space Technology , "Rolls-Royce Details Advance And UltraFan Test Plan," 2014. [Online]. Available: http://aviationweek.com/commercial-aviation/rolls-royce-details-advance-and-ultrafan-test-plan.

[18] M. R. W. Lauer, Determination of the Heat Release Distribution in Turbulent Flames by Chemi-luminescence Imaging, Technische Universität München, 2011, pp. 147-173.

[19] A. Lewin, M. F. and S. H., "Heterodyn-Interferometer zur Vibrationsanalyse / Heterodyne interferometers for vibration analysis," *Technisches Messen,* vol. 57, no. JG, p. 335–345, 1990.

[20] W. Gardiner, Y. Hidaka and T. Tanzawa, "Refractivity of Combustion Gases," *Combustion and Flame,* vol. 40, pp. 213-219, 1981.

[21] N. Mayrhofer and J. Woisetschläger, "Frequency analysis of turbulent compressible flows by laser vibrometry," *Experiments in Fluids,* vol. 31, no. 2, pp. 153-161, 2001.

[22] Rayleigh, "The explanation of certain acoustical phenomena," *Nature,* vol. 18, no. 455, pp. 319-321, 1878.

[23] S. Candel, D. Durox, T. Schuller, J. .. Bourgouin and J. P. Moeck, "Dynamics of swirling flames," vol. 46, pp. 147-173, 2014.

[24] A. P. Dowling and A. S. Morgans, "Feedback Control of Combustion Oscillations," *Annu. Rev. Fluid Mech.,* vol. 37, pp. 151-182, 2005.

[25] J. Woisetschläger, H. Lang, B. Hampel, E. Goettlich and F. Heitmeir, "Influence of blade passing on the stator wake in a transonic turbine stage investigated by particle image velocimetry and laser vibrometry," *Proceedings of the Institution of Mechanical Engineers, Part A: Journal of Power and Energy,* vol. 217, no. 4, pp. 385-392, 2003.

[26] J. Woisetschläger, N. Mayrhofer, B. Hampel, H. Lang and W. Sanz, "Laser-optical investigation of turbine wake flow," *Experiments in Fluids,* vol. 34, no. 3, pp. 371-378, 2003.

[27] N. Mayrhofer, H. Lang and J. Woisetschlaeger, "Experimental investigation of turbine wake flow by interferometrically triggered LDV-measurements," in *International Symposium on Application of Laser Techniques to Fluid Mechanics*, 2000.

[28] D. Lengani, R. Spataro, J. Peterleithner and E. Göttlich, "Unsteady flow evolution through a turning midturbine frame Part 2: Spectral analysis," *Journal of Propulsion and Power,* vol. 31, no. 6, pp. 1597-1606, 2015.

[29] T. Leitgeb, T. Schuller, D. Durox, F. Giuliani, S. Koeberl and J. Woisetschläger, "Interferometric determination of heat release rate in a pulsated flame," *Combustion and Flame,* vol. 160, no. 3, pp. 589-600, 2013.

[30] J. Peterleithner, N. V. Stadlmair, J. Woisetschläger and T. Sattelmayer, "Analysis of measured flame transfer functions with locally resolved density

fluctuation and OH-Chemiluminescence Data," *Journal of Engineering for Gas Turbines and Power,* vol. 138, no. 3, 2016.

[31] J. Li, D. Durox, F. Richecoeur and T. Schuller, "Analysis of chemiluminescence, density and heat release rate fluctuations in acoustically perturbed laminar premixed flames," *Combustion and Flame,* vol. 162, no. 10, pp. 3934-3945, 2015.

[32] A. Fischer, J. König, J. Czarske, J. Peterleithner, J. Woisetschläger and T. Leitgeb, "Analysis of flow and density oscillations in a swirl-stabilized flame employing highly resolving optical measurement techniques," *Experiments in Fluids,* vol. 54, no. 12, 2013.

[33] S. Köberl, F. Fontaneto, F. Giuliani and J. Woisetschläger, "Frequency-resolved interferometric measurement of local density fluctuations for turbulent combustion analysis," *Measurement Science and Technology,* vol. 21, no. 3, 2010.

[34] F. Giuliani, T. Leitgeb, A. Lang and J. Woisetschläger, "Mapping the density fluctuations in a pulsed air-methane flame using laser-vibrometry," *Journal of Engineering for Gas Turbines and Power,* vol. 132, no. 3, 2010.

[35] M. Martarelli, P. Castellini and E. P. Tomasini, "Subsonic jet pressure fluctuation characterization by tomographic laser interferometry," *Experiments in Fluids,* vol. 54, no. 12, 2013.

[36] L. Zipser, S. Lindner and R. Behrendt, "Interferometric Measurement and Visualisation of Acoustic Waves and Vortexes," *Technisches Messen,* vol. 69, no. 6, pp. 275-281, 2002.

[37] A. R. Harland, J. N. Petzing and J. R. Tyrer, "Visualising scattering underwater acoustic fields using laser Doppler vibrometry," *Journal of Sound and Vibration,* vol. 305, no. 4-5, pp. 659-671, 2007.

[38] A. R. Harland, J. N. Petzing, J. R. Tyrer, C. J. Bickley, S. P. Robinson and R. C. Preston, "Application and assessment of laser Doppler velocimetry for underwater acoustic measurements," *Journal of Sound and Vibration,* vol. 265, no. 3, pp. 627-645, 2003.

[39] P. Gren, K. Tatar, J. Granström, N.-E. Molin and E. V. Jansson, "Laser vibrometry measurements of vibration and sound fields of a bowed violin," *Measurement Science and Technology,* vol. 17, pp. 635-644, 2006.

[40] J. M. Buick, J. A. Cosgrove, P. .. Douissard, C. A. Greated and B. Gilabert, "Application of the acousto-optic effect to pressure measurements in ultrasound fields in water using a laser vibrometer," *Review of Scientific Instruments,* vol. 75, no. 10 I, pp. 3203-3207, 2004.

[41] L. Zipser and H. H. Franke, "Refracto-vibrometry - A novel method for visualizing sound waves in transparent media," pp. 1997-2001, 2008.

[42] B. Hampel and J. Woisetschläger, "Frequency- and space-resolved measurement of local density fluctuations in air by laser vibrometry," *Measurement Science and Technology,* vol. 17, pp. 2835-2842, 2006.

[43] F. Giuliani, B. Wagner, J. Woisetschlaeger and F. Heitmeir, "Laser vibrometry

for real-time combustion instability diagnostics," in *Proc. ASME Turbo Expo*, 2006.

[44] W. C. Strahle, "On combustion generated noise," *Journal of Fluid Mechanics,* vol. 49, no. 02, pp. 399-414, 1971.

[45] T. Leitgeb, "On the Design and Validation of a Variable Geometry Burner Concept," Graz, 2012.

[46] F. Giuliani, J. W. Woisetschläger and T. Leitgeb, "Design and validation of a burner with variable geometry for extended combustion range," in *Proceedings of the ASME Turbo Expo*, 2012.

[47] F. Giuliani, *Habilitation: Advanced Gas Turbine Combustion Management,* Graz, Austria, 2010.

[48] M. Alonso and E. J. Finn, Fundamental University Physics - II Fields and Waves, Addison-Wesley Publishing Company, Inc., 1967.

[49] J. O. Smith III, Spectral Audio Signal Processing, W3K Publishing, 2011.

[50] S. W. Smith, The Scientist and Engineer's Guide to Digital Signal Processing, California Technical Pub, 1997.

[51] G. Heinzel, A. Rüdiger and R. Schilling, "Spectrum and spectral density estimation by the Discrete Fouriertransform (DFT), including a comprehensive list of window functions and some new flat-top windows," Germany, Max-Planck-Institut für Gravitationsphysik (Albert-Einstein-Institut) Teilinstitut Hannover, 2002.

[52] C. S. Panoutsos, Y. Hardalupas and A. M. K. P. Taylor, "Numerical evaluation of equivalence ratio measurement using OH* and CH* chemiluminescence in premixed and non-premixed methane-air flames," *Combustion and Flame,* vol. 156, no. 2, pp. 273-291, 2009.

[53] C. Pankiewitz, "Hybrides Berechnungsverfahren f€ur thermoakustische Instabilit€aten von Mehrbrennersystemen," Munich, Germany., 2004.

[54] J. Pieringer, T. Sattelmayer and F. Fassl, "Simulation of Combustion Instabilities in Liquid Rocket Engines With Acoustic Perturbation Equations," *J. Propul. Power,* 2009 25(5), pp. 1020–1031.

[55] J. Gikadi, "Prediction of Acoustic Modes in Combustors Using Linearized Navier-Stokes Equations in Frequency Space," Munich, Germany, 2013.

[56] A. P. Dowling, "The calculation of thermoacoustic oscillations," *Journal of Sound and Vibration,* vol. 180, no. 4, pp. 557-581, 1995.

[57] W. C. Strahle, "Combustion noise," *Progress in Energy and Combustion Science,* vol. 4, no. 3, pp. 157-176, 1978.

[58] T. Schuller, D. Durox and S. Candel, "Dynamics of and Noise Radiated by a Perturbed Impinging Premixed Jet Flame," *Combustion and Flame,* vol. 128, pp. 88-110, 2002.

[59] R. B. Price, I. R. Huerle and T. M. Sudgen, "Optical studies of generation of noise in turbulent fames," *Twelfth Symposium (International) on Combustion,* 1969.

[60] I. R. Huerle, R. B. Price, T. M. Sudgen and A. Thomas, "Sound emission from open turbulent flames," *Proc. R. Soc. A,,* 1968.

[61] J. Peterleithner and J. Woisetschläger, "Laser vibrometry for combustion diagnostics in thermoacoustic research," *Technisches Messen,* vol. 82, no. 11, pp. 549-555, 2015.

[62] J. Peterleithner, A. Marn and J. Woisetschläger, "Interferometric In estigation of the thermo-acoustics in a swirl stabilized Methane flame," in *Proceedings of the ASME Turbo Expo*, 2015.

[63] J. Peterleithner, R. Basso, F. Heitmeir, J. Woisetschläger, S. R., C. J. and A. Fischer, "COMPARISON OF FLAME TRANSFER FUNCTIONS ACQUIRED BY CHEMILUMINESCENCE AND DENSITY FLUCTUATION," in *Proc. ASME Turbo Expo*, 2016.

[64] J. Peterleithner, S. Zerobin and Woisetschläger, "ANALYSIS OF COMBUSTION NOISE USING LOCALLY RESOLVED DENSITY FLUCTUATIONS AND A MICROPHONE ARRAY," in *Proc. ASME Turbo Expo*, 2016.

[65] S. Loria, "Über die Dispersion des Lichtes in gasförmigen Kohlenwasserstoffen," *Annalen der Physik,* vol. 334, no. 8, pp. 605-622, 1909.

[66] J. Peterleithner, F. Salcher and J. Woisetschläger, "Frequency resol ed interferometric detection of local density fluctuations in flames," *Proc. 17th International Symposium on Application of Laser Techniques to Fluid Mechanics, Lisbon,,* 2014.

[67] F. Giuliani, A. Lang, K. Gradl, P. Siebenhofer and J. Fritzer, "Air flow modulation for refined control of the combustion dynamics using a novel actuator," *Journal of Engineering for Gas Turbines and Power,* vol. 134, no. 2, 2012.

[68] T. C. Lieuwen and V. Yang, Combustion Instabilities in Gas Turbine Engines - Operational Experience, Fundamental Mechanisms, and Modeling, vol. 210, American Institute of Aeronautics and Astronautics, 2005.

[69] S. Candel, D. Durox, S. Ducruix, A.-L. Birbaud, N. Noiray and T. Schuller, "Flame Dynamics and Combustion Noise: Progress and Challenges," *International Journal of Aeroacoustics,* vol. 8, no. 1, pp. 1-56, 2009.

[70] T. Schuller, N. Noiray, D. Durox and S. Candel, "On mechanisms of intense combustion noise emission," vol. 1, pp. 596-605, 2006.

[71] T. J. B. Smith and J. K. Kilham, "Noise Generation by Open Turbulent Flames," *Journal of Acoustical Society of America,* vol. 35, no. 05, pp. 715-724, 1963.

[72] B. &. Kjaer, "Sound intensity," 1993. [Online]. Available: http://www.bksv.com/doc/br0476.pdf. [Accessed 21 11 2015].

[73] F. Fahy, Foundations of Engineering Acoustics, Elsevier Science, 2000.

[74] L. Zipser, S. Lindner and R. Behrendt, "Interferometrische MEssung und Visualisierung von Schallwellen und Trubulenzen," *Technisches Messen,* vol. 69, no. 3, pp. 275-281, 2002.

[75] A. P. Dowling and Y. Mahmoudi, "Combustion noise," *Proceedings of the*

Combustion Institute, vol. 35, no. 1, pp. 65-100, 2015.

[76] T. e. a. Stocker, Climate Change 2013 - The Physical Science Basis, CAMBRIDGE UNIVERSITY PRESS, 2013.

[77] V. N. Nori and J. M. Seitzman, "CH* chemiluminescence modeling for combustion diagnostics," *Proceedings of the Combustion Institute,* vol. 32, pp. 895-903, 2009.

Appendix A – List of Publications

The project FWF-24096-N24 “Interferometric Detection of Thermoacoustic Oscillations in Flames” which funded the present work, resulted in a total of 13 publications. The complete list of publications is shown below.

Table 5: Complete list of publications, resulting from project FWF-24096-N24.

Title	Journal/Conference	Year
ANALYSIS OF FLOW AND DENSITY OSCILLATIONS IN A SWIRL-STABILIZED FLAME EMPLOYING HIGHLY RESOLVING OPTICAL MEASUREMENT TECHNIQUES	A. Fischer, J. König, J. Czarske, J. Peterleithner, J. Woisetschläger and T. Leitgeb, Experiments in Fluids, vol. 54, no. 12, 2013.	2013
FREQUENCY RESOLVED DENSITY FLUCTUATION MEASUREMENTS OF COMBUSTION OSCILLATIONS IN A MODEL COMBUSTOR	Peterleithner JJ, Marn A, Leitgeb T, Woisetschläger J (2013), 49th AIAA/ASME/SAE/ASEE Joint Propulsion Conference & Exhibit, 15 - 17 Jul 2013, San Jose, CA , Paper No.: 1589261	2013
FREQUENCY RESOLVED INTERFEROMETRIC DETECTION OF LOCAL DENSITY FLUCTUATIONS IN FLAMES	Peterleithner, J., Salcher, F., Woisetschläger, J , 2014. in Proceedings of International Symposium on Applications of Laser Techniques to Fluid Mechanics, Lisbon, Portugal	2014
LASER VIBROMETRY FOR COMBUSTION DIAGNOSTICS IN THERMOACOUSTIC RESEARCH	Peterleithner J, Woisetschläger J, in Fachtagung “Lasermethoden in der Strömungsmesstechnik” (GALA), 2015	2015
LASER VIBROMETRY FOR COMBUSTION DIAGNOSTICS IN THERMOACOUSTIC RESEARCH	J. Peterleithner and J. Woisetschläger, Technisches Messen, vol. 82, no. 11, pp. 549-555, 2015.	2015
Unsteady Flow Evolution Through a Turning Midturbine Frame Part 2: Spectral Analysis	Lengani, D. and Spataro, R. and Peterleithner, J. and Göttlich, E. Journal of Propulsion and Power vol. 31, no. 6, 2015.	2015
ANALYSIS OF MEASURED FLAME TRANSFER FUNCTIONS WITH LOCALLY RESOLVED DENSITY FLUCTUATION AND OH-CHEMILUMINESCENCE DATA	Peterleithner, J. and Stadlmair, N.V. and Woisetschläger, J. and Sattelmayer, T. in Proceedings of the ASME Turbo Expo, 2015.	2015

ANALYSIS OF MEASURED FLAME TRANSFER FUNCTIONS WITH LOCALLY RESOLVED DENSITY FLUCTUATION AND OH-CHEMILUMINESCENCE DATA	J. Peterleithner, N. V. Stadlmair, J. Woisetschläger and T. Sattelmayer, Journal of Engineering for Gas Turbines and Power, vol. 138, no. 3, 2016.	2015
INTERFEROMETRIC INVESTIGATION OF THE THERMO-ACOUSTICS IN A SWIRL STABILIZED METHANE FLAME	J. Peterleithner, A. Marn and J. Woisetschläger, in Proceedings of the ASME Turbo Expo, 2015.	2015
COMPARISON OF FLAME TRANSFER FUNCTIONS ACQUIRED BY CHEMILUMINESCENCE AND DENSITY FLUCTUATION	J. Peterleithner, R. Basso, F. Heitmeir, J. Woisetschläger, S. R., C. J. and A. Fischer, in Proc. ASME Turbo Expo, 2016.	2016
ANALYSIS OF COMBUSTION NOISE USING LOCALLY RESOLVED DENSITY FLUCTUATIONS AND A MICROPHONE ARRAY	Johannes Peterleithner, Stefan Zerobin, Jakob Woisetschläger in Proc. ASME Turbo Expo, 2016.	2016
Introduction of a Project-Based-Course in Turbine Stage Design for Undergraduate Students at Graz University of Technology	Marn A, Schönleitner F, Peterleithner J, Woisetschläger J, Heitmeir F, in Proceedings of the ASME Turbo Expo, 2016.	2016
DETECTING TRANSITION IN FLAT PLATE FLOW WITH LASER INTERFEROMETRIC VIBROMETRY (LIV)	Bader P, Sanz W, Peterleithner J,Woisetschläager J, Heitmeir F, Meile W Brenn G, in Proceedings of the ASME Turbo Expo, 2016.	2016

Appendix B –Variable Geometry Burner 2.0

The variable geometry burner was originally designed by Thomas Leitgeb [45]. The intent of his work was the design and characterization of an extended stability- and operation-map. This burner was used for the majority of the present work because the variable geometry enables the user to find a point of instability due to a higher number of parameters to be varied. Instead of fuel and air mass flow only, here additionally the ratio between axial and tangential air can be varied, as well as the axial position of the center cone. Design changes have been made to the burner in comparison to the Leitgeb version [45]. Firstly, the center swirler has been adjusted. Initially it featured four slots (Figure B.1) which had the advantage of easy and cheap manufacturing and a low pressure drop. When the focus lies on the measurement technique, for line of sight integrating techniques a rotationally symmetric flame is favorable in order to reduce measurement time. Therefore a new swirler was designed. With 32 bores evenly distributed around the circumference (Figure B.2), the new design enabled a perfectly rotationally symmetric flame Figure B.3) in contrast to a flame with four prongs (Figure B.4). This drastically reduced the measurement time, since now local effects can be assessed simply by performing an inverse Abel reconstruction from one projection. With a non-rotationally symmetric flame, tomography is necessary to assess local effects. This technique however relies on several measurement projection-directions.

Additionally, the heat shield of the burner was replaced with a perforated plate on top of a cooling air plenum (Figure B.5). This was necessary for measurements with liner (Figure B.6). The setup ensured a smooth and gradual cooling air supply, avoiding a significant aerodynamic influence onto the flame of the cooling air due to low velocities.

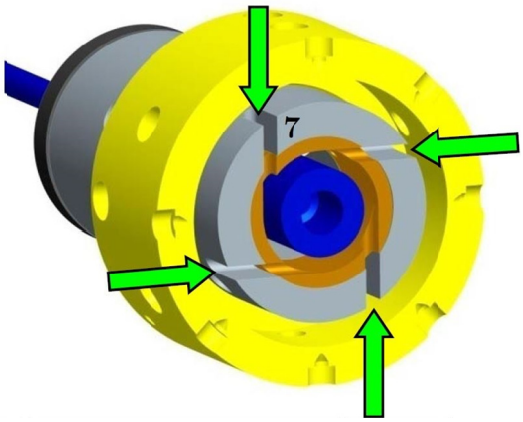

Figure B.1: Initial swirler design (orange part) with 4 slotted holes, generating a four prong-flame (Image courtesy Leitgeb [46]).

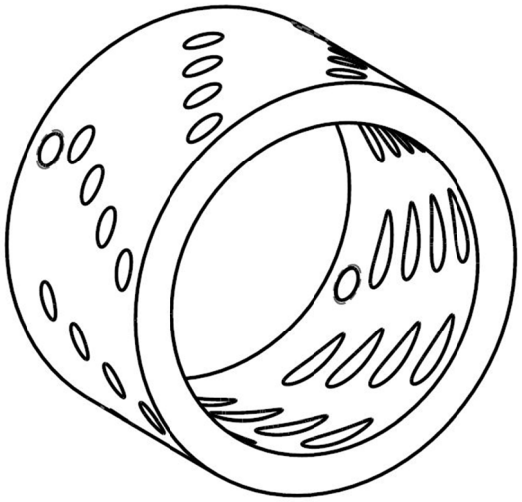

Figure B.2: New swirler design with 32 tangential bores.

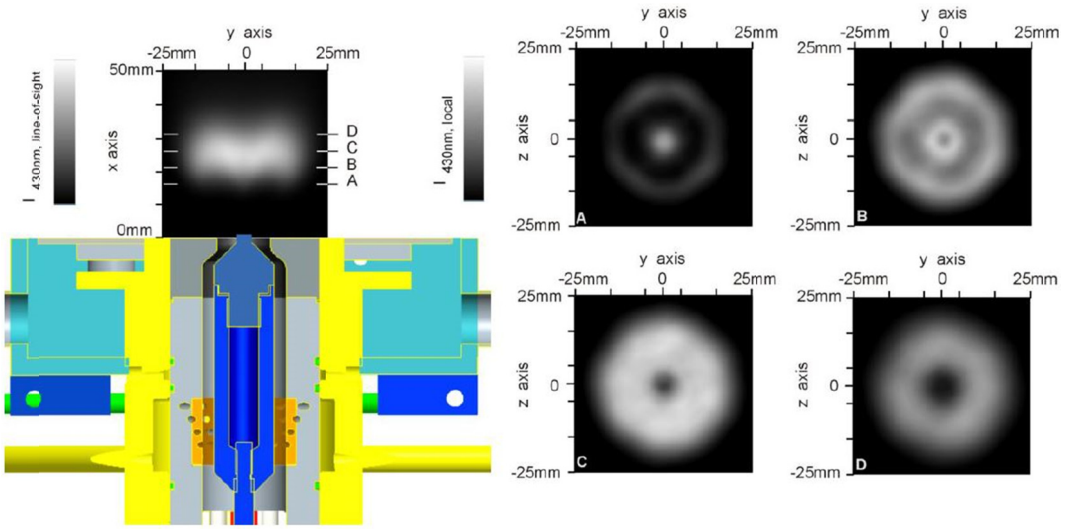

Figure B.3: New burner Design: Tomographic reconstruction of the flame shape from the spectral emittance I at 430nm (CH*) for $\phi = 1.1$ at mass ratio 0.89 ('resonant' flame). The flame was unconfined. 18 projections were recorded to verify the rotational symmetry which is within 10% with respect to the local intensity values in section C. Left is a single projection perpendicular to the observation direction (z-axis) together with the burner, right are four reconstructed planes perpendicular to the flame axis x. The planes are labeled from A–D (Data taken from [66]).

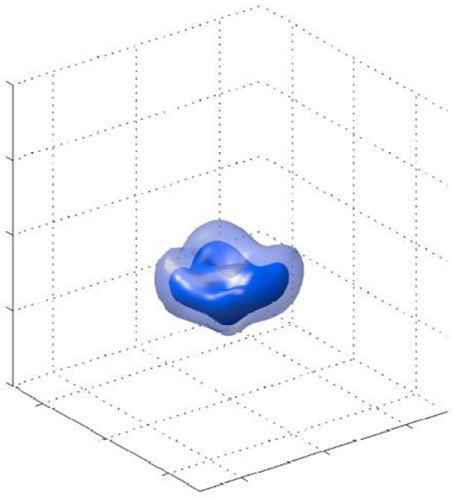

Figure B.4: Initial Design: Tomographic reconstruction of the flame shape from the spectral emittance I at 430nm (CH*) with the initial burner design featuring four prongs (Data taken from [45]).

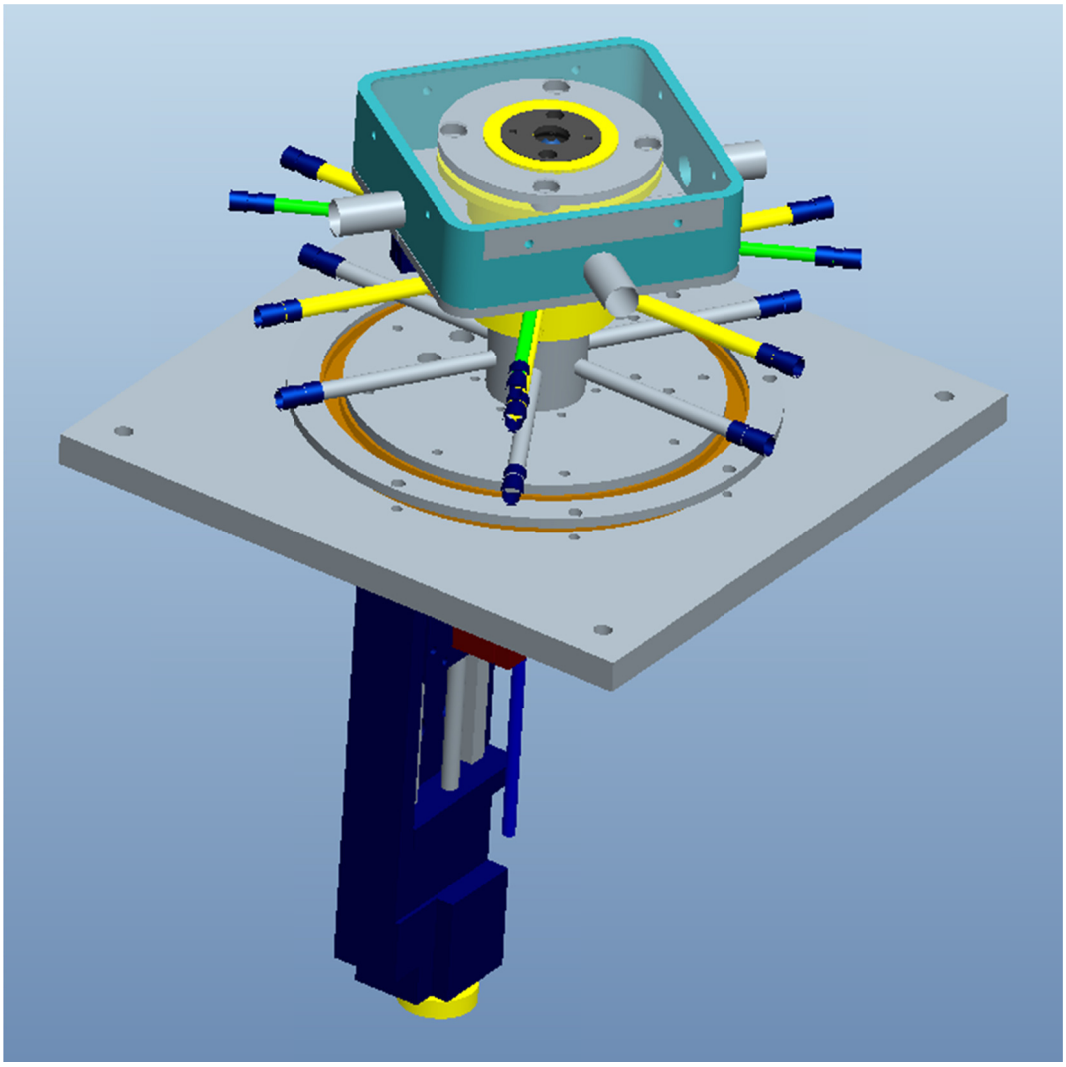

Figure B.5: Three dimensional sketch of the new Burner with cooling air plenum (turquoise) an ball bearing support for 360° rotation of the burner (grey).

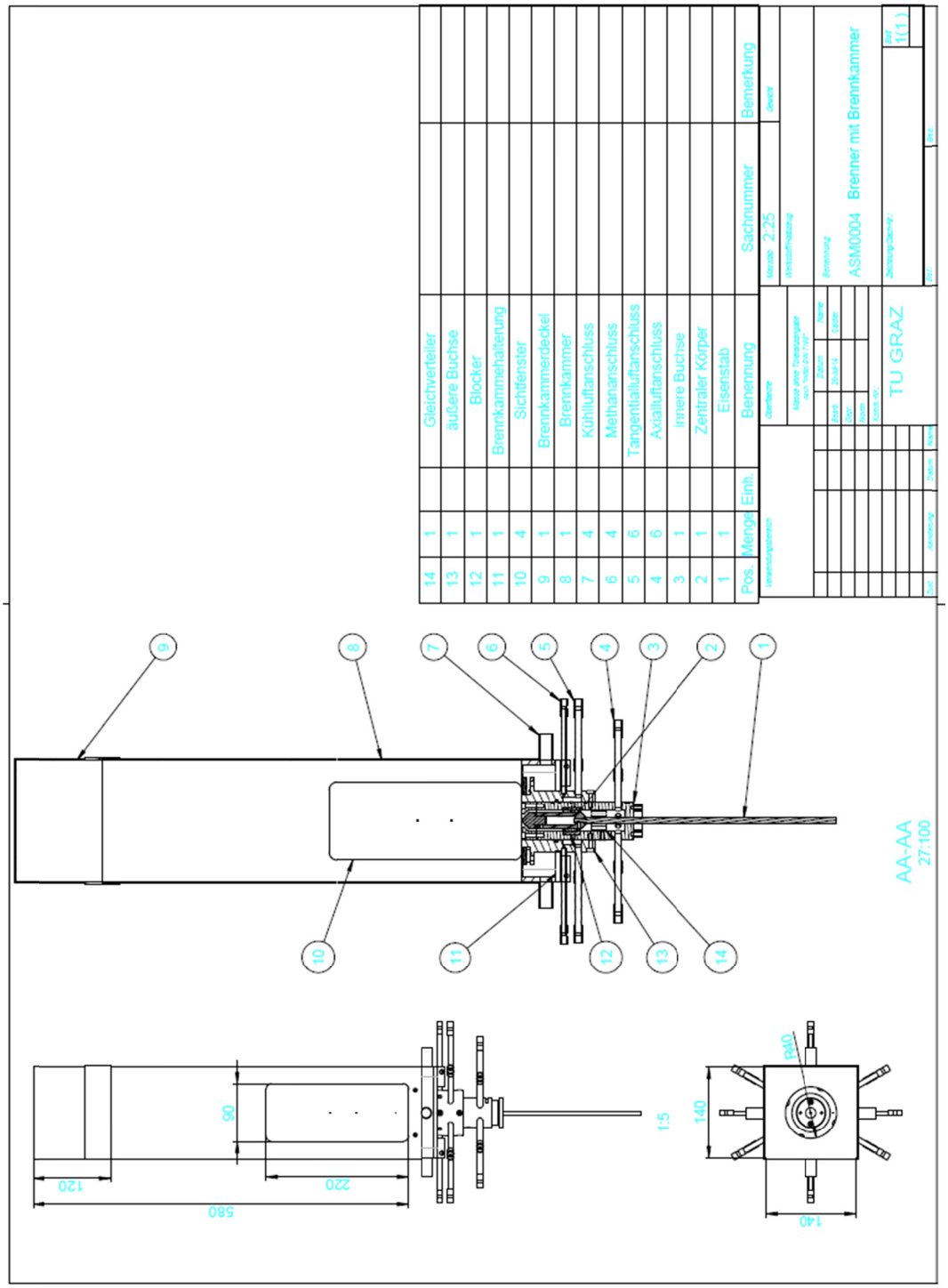

Figure B.6: Assembly of the burner with liner.

Appendix C – pp-Probe

As derived in the theory part, sound power is generally a function of the complex values of sound pressure and particle velocity. Those two values may not be in phase in the near field and the transitional region of a point source, which makes it necessary to measure both values in order to compute sound power. They are in phase in the far-field. There it is possible to express the particle velocity as a function of the sound pressure. Consequently sound power can be expressed as a function of one parameter only.

For low frequencies as common in combustion, it is practically impossible to fulfill the far-field requirement in confined spaces such as a laboratory. Therefore it is necessary to measure both, p' and v'. Alternatively measuring sound pressure at two positions using a pp-probe and approximating the particle velocity by employing the Euler equation provides sound intensity. Integration of the sound intensity over a surface area enveloping the sound source gives the sound power. The first law of thermodynamics demands energy conservation, consequently neglecting losses, sound power must stay constant with increasing radial distance to the sound source. Assuming a spherical enveloping surface, this area increases with increasing diameter. Looking at equation **(**37**)** it becomes clear that sound intensity must then decrease with increasing radius, since power stays constant. When comparing acoustics in one single laboratory setup, using sound intensity is legitimate, however comparing sound power is more universal and should therefore be preferred for acoustic analysis. Here the distance between the two microphones is critical and must be adjusted according to the expected sound frequency. If the distance is too high, a phase jump could provide wrong results. If the distance between the two microphones is too short, the SNR of the microphones will become a problem (Figure C.1).

For the presented measurements, a distance of 53mm between the microphone membranes was chosen, in order to provide maximum accuracy in the low frequency region up to a maximum of 1250 Hz (Figure C.2). This, because the siren used, can modulate the feed line flow up to a maximum frequency of 1000 Hz. The arch designed to hold the microphones in place is shown in Figure C.3. The pp-probe configuration and arch-setup is shown in Figure C.4. A maximum of 28 microphones was – in pairs - evenly distributed along the arch.

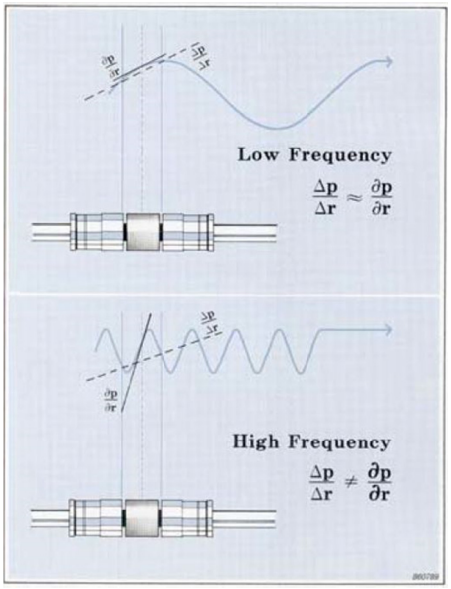

Figure C.1: correct distance between microphones (top) and wrong distance (to short) between microphones (Data taken from [72]).

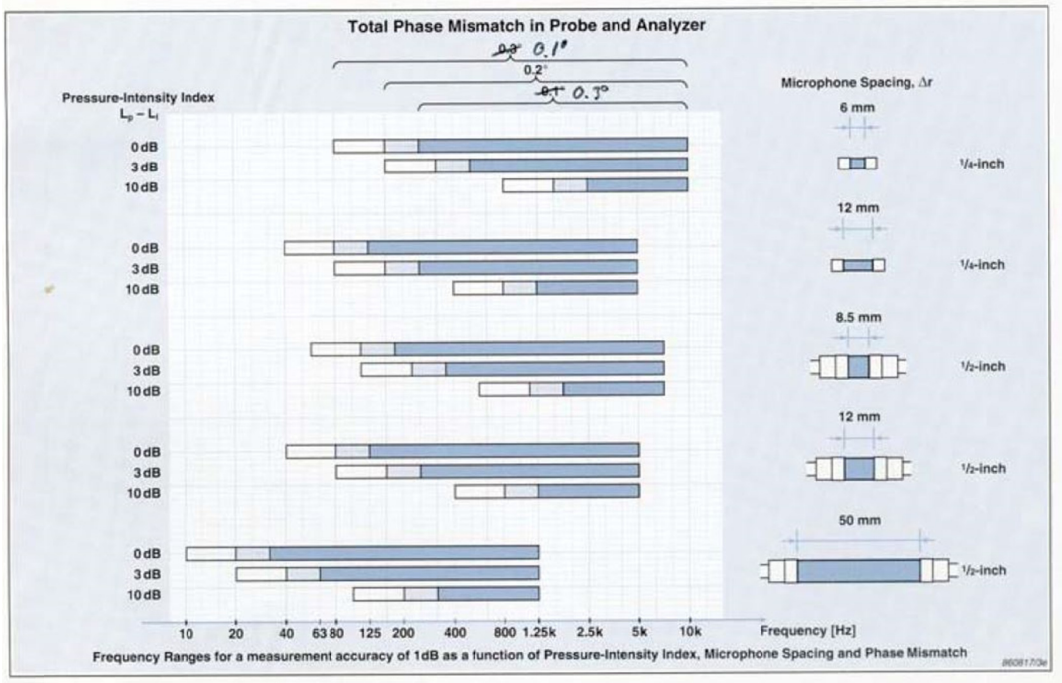

Figure C.2: Error in pressure intensity and phase as a function of frequency bands for different microphone distances [72].

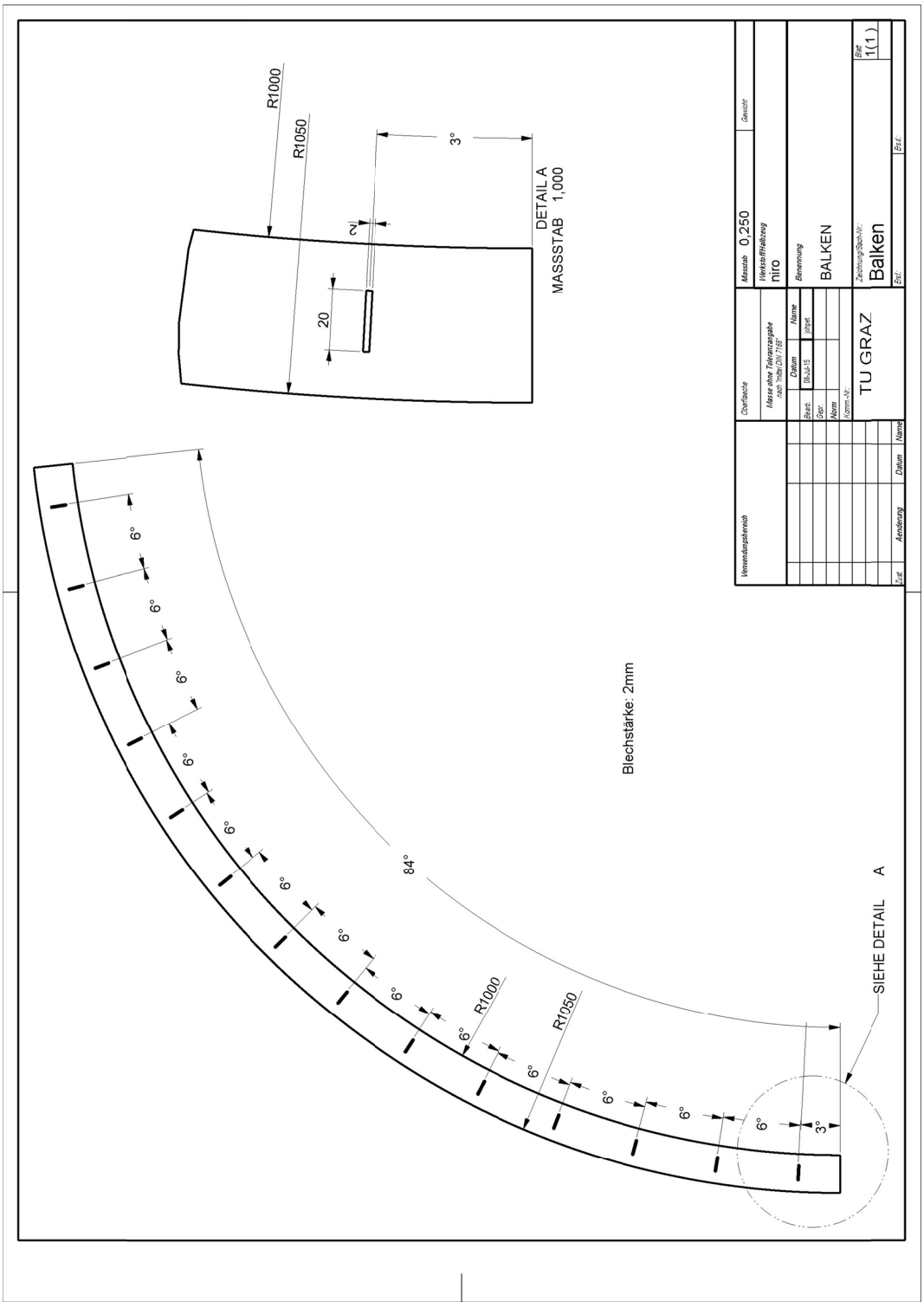

Figure C.3: Dimensioning of the microphone arch.

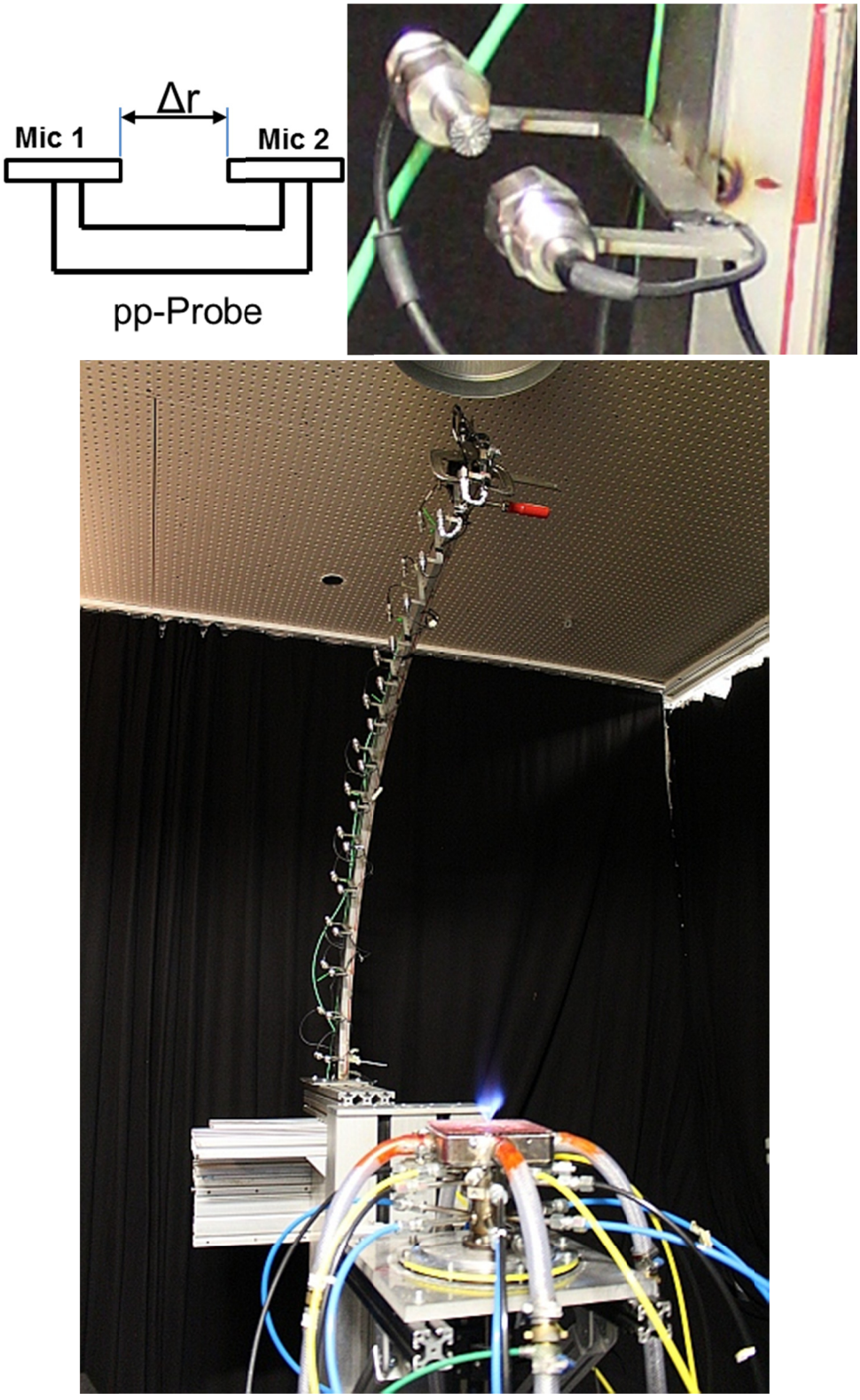

Figure C.4: pp-probe with two microphones (Mic 1 and Mic 2) and a distance Δr of 53mm (top left and right). Microphone arch with 14 pp-probes behind burner (bottom).

Appendix D – Acoustic Laboratory

All measurements but the ones for [30] were carried out in the 'Thermoakustik-Messraum' in the basement of the Institute for Thermal Turbomachinery and Machine Dynamics at TU Graz. The Laboratory features a low reflective ceiling and heavy acoustic curtains (320g/m²) which are flame resistant according to DIN 4102 B 1 both are shown in Figure B.3 in the background. The structural improvements reduced the reverberation time from 44 ms to less than 12 ms. Values were calculated with measured data shown in Figure D.1 for a decrease in amplitude of 60 db.

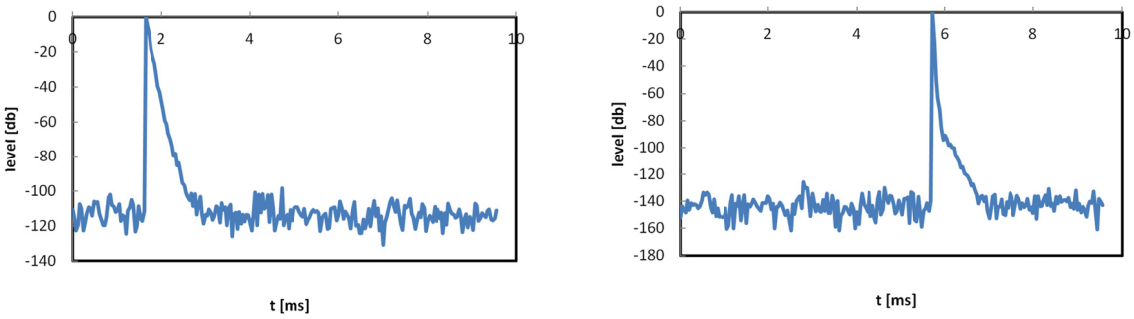

Figure D.1: reverberation time before (left) and after (right) the acoustic improvements of the laboratory.

Appendix E – Definitions of Error Analysis

Reliability is the degree to which an assessment tool produces stable and consistent results.

Validity refers to how well a test measures what it is intended to measure.

Sensitivity (also called the true positive rate, or the recall in some fields) measures the proportion of positives that are correctly identified as such (e.g., the percentage of sick people who are correctly identified as having the condition).

Specificity (also called the true negative rate) measures the proportion of negatives that are correctly identified as such (e.g., the percentage of healthy people who are correctly identified as not having the condition). Thus sensitivity quantifies the avoiding of false negatives, as specificity does for false positives.

Sensitivity analysis is the study of how the uncertainty in the output of a mathematical model or system (numerical or otherwise) can be apportioned to different sources of uncertainty in its inputs. A related practice is uncertainty analysis, which has a greater focus on uncertainty quantification and propagation of uncertainty. Ideally, uncertainty and sensitivity analysis should be run in tandem.

Uncertainty: A set of possible states or outcomes where probabilities are assigned to each possible state or outcome – this also includes the application of a probability density function to continuous variables.

In physical experiments uncertainty analysis, or experimental uncertainty assessment, deals with assessing the uncertainty in a measurement. An experiment designed to determine an effect, demonstrate a law, or estimate the numerical value of a physical variable will be affected by errors due to instrumentation, methodology, presence of confounding effects and so on. Experimental uncertainty estimates are needed to assess the confidence in the results. A related field is design of experiments.

Precision is a description of a level of measurement that yields consistent results when repeated. It is associated with the concept of "random error", a form of observational error that leads to measurable values being inconsistent when repeated.

Accuracy: The ISO definition is that accuracy is a level of measurement that yields true (no systematic errors) and consistent (no random errors) results